Ollscoil na hÉireann, Corcaigh

National University of Ireland, Cork

CHARACTERISATION AND MONITORING OF FOREST DISTURBANCES IN IRELAND USING ACTIVE MICROWAVE SATELLITE PLATFORMS

Thesis presented by

PREETHI MALUR BALAJI, B.E., M.Sc.

for the degree of

Doctor of Philosophy

University College Cork

DEPARTMENT OF GEOGRAPHY

Head of School/Department: Kieran Hickey

Supervisors: Dr. Fiona Cawkwell

Dr. Ned Dwyer

2020

Research funded by Department of Agriculture, Food and the Marine

DEDICATED TO MY AWE-INSPIRING PARENTS, TO THE COVID FRONTLINERS AND TO ALL THE COVID-19 VICTIMS WHO LOST THEIR LIVES DURING THE PANDEMIC 2020!

Contents

List of Figures

List of Tables

ACRONYMS

ALOS – Advanced Land Observing Satellite
CORINE – Co-Ordinated Information on the Environment
CLC – CORINE Land Cover
DAFM – Department of Food, Agriculture and the Marine
DEM – Digital Elevation Model
DN – Digital Number
ECV – Essential Climate Variable
EO – Earth Observation
ESA – European Space Agency
EU – European Union
FAO – Food and Agricultural Organization
FBD – Fine Beam Dual Polarisation Mode
FIPS – Forest Inventory and Planning System
GHG – Green House Gas
GLCM – Grey-Level Co-occurrence Matrix
HH – Horizontal Transmit Horizontal Receive
HV – Horizontal Transmit Vertical Receive
IPCC – Intergovernmental Panel on Climate Change
ISODATA – Iterative Self Organizing Data Analysis
ITM – Irish Transverse Mercator
JAXA – Japan Aerospace Exploration Agency
MDA – Mean Decrease Accuracy
MDG – Mean Decrease Gini
NFI – National Forest Inventory
OSi – Ordnance Survey of Ireland
PALSAR – Phased Array L-band Synthetic Aperture Radar
RADAR – Radio Detection and Ranging
RF – Random Forests
SAR – Synthetic Aperture Radar
UNFCCC – United Nations Framework Convention on Climate Change

Declaration

This is to certify that the work I am submitting is my own and has not been submitted for another degree, either at University College Cork or elsewhere. All external references and sources are clearly acknowledged and identified within the contents. I have read and understood the regulations of University College Cork concerning plagiarism.

.....

Preethi Malur Balaji

ABSTRACT

Forests are one of the major carbon sinks that significantly contribute towards achieving targets of the Kyoto Protocol, and its successors, in reducing greenhouse (GHG) emissions. In order to contribute to regular National Inventory Reporting, and as part of the on-going development of the Irish national GHG reporting system (CARBWARE), improvements in characterisation of changes in forest carbon stocks have been recommended to provide a comprehensive information flow into CARBWARE. The Irish National Forest Inventory (NFI) is updated once every six years, thus there is a need for an enhanced forest monitoring system to obtain annual forest updates to support government agencies and forest management companies in their strategic decision making and to comply with international GHG reporting standards. Sustainable forest management is imperative to promote net carbon absorption from forests. Based on the NFI data, Irish forests have removed or sequestered an average of 3.8 Mt of atmospheric CO_2 per year between 2007 and 2016. However, unmanaged and degraded forests become a net emitter of carbon. Disturbances from human induced activities such as clear felling, thinning and deforestation results in carbon emissions back into the atmosphere. Funded by the Department of Agriculture, Food and the Marine (DAFM, Ireland), this PhD study focuses on exploring the potential of data from L-band Synthetic Aperture Radar (SAR) satellite based sensors for monitoring changes in the small stand forests of Ireland.

Historic data from ALOS PALSAR in the late 2000s and more recent data from ALOS-2 PALSAR-2 sensors have been used to map forest areas and characterise the different disturbances observed within three different regions of Ireland. Forest mapping and disturbance characterisation was achieved by combining the machine learning supervised Random Forests (RF) and unsupervised Iterative Self-Organizing Data Analysis (ISODATA) classification techniques. The lack of availability of ground truth data supported use of this unsupervised approach which forms natural clusters based on their multi-temporal signatures, with divergence statistics used to select the optimal number of clusters to represent different forest classes. This approach to forest monitoring using SAR

imagery has not been reported in the peer-review literature and is particularly beneficial where there is a dearth of ground-based information. When applied to the forests, mapped with an accuracy of up to 97% by RF, the ISODATA technique successfully identified the unique multi-temporal pattern associated with clear-fells which exhibited a decrease of 4 to 5 decibels (dB) between the images acquired before and after the event. The clustering algorithm effectively highlighted the occurrence of other disturbance events within forests with a decrease of 2±0.5dB between two consecutive years, as well as areas of tree growth and afforestation.

A highlight of the work is the successful transferability of the algorithm, developed using ALOS PALSAR, to ALOS-2 PALSAR-2 data thereby demonstrating the potential continuity of annual forest monitoring. The higher spatial and radiometric resolutions of ALOS-2 PALSAR-2 data have shown improvements in forest mapping compared to ALOS PALSAR data. From mapping a minimum forest size of 1.8 ha with ALOS PALSAR, a minimum area of 1.1 ha was achieved with the ALOS-2 PALSAR-2 images. Moreover, even with some different backscatter characteristics of images acquired in different seasons, similar signature patterns between the sensors were retrieved that helped to define the cluster groups, thus demonstrating the robustness of the algorithm and its successful transferability.

Having proven the potential to monitor forest disturbances, the results from both the sensors were used to detect deforestation over the time period 2007-2016. Permanent land-use changes pertaining to conversion of forests to agricultural lands and windfarms were identified which are important with respect to forest monitoring and carbon reporting in Ireland.

Overall, this work has presented a viable approach to support forest monitoring operations in Ireland. By providing disturbance information from SAR, it can supplement projects working with optical images which are generally limited by cloud cover, particularly in parts of northern, western and upland Ireland. This approach adds value to ground based forest monitoring by mapping distinct forests over large areas on an annual basis. This study has demonstrated the ability to apply the algorithm to three different study areas, with a vision to operationalise the algorithm on a national scale. The main limitations

experienced in this study were the lack of L-band SAR data availability and reference datasets. With typically only one image acquired per year, and discrepancies and omissions existing within reference datasets, understanding the behaviour of certain cluster groups representing disturbances was challenging. However, this approach has addressed some issues within the reference datasets, for example locating areas for which a felling licence was granted but where trees were never cut, by providing detailed systematic mapping of forests. Future satellites such as Tandem-L, SAOCOM-2A and 2B, P-band BIOMASS mission and ALOS-4 PALSAR-3 may overcome the issue of limited SAR image acquisitions provided more images per year are available, especially during the summer months.

ACKNOWLEDGMENTS

"Let us be grateful to people who make us happy; they are the charming gardeners who make our souls blossom."--Marcel Proust

This thesis is a product of the help and support of many people. Firstly, I am indebted to my supervisors Dr. Fiona Cawkwell and Dr. Ned Dwyer for believing in me and being my biggest support through all these years. Your inputs and advice have made me grow and become a stronger person. I have learnt a lot from you and my confidence has boosted up in becoming an independent researcher. I must say that I am very lucky to have you both as my supervisors. Thank you!!! I am deeply grateful to the Department of Agriculture, Food and the Marine for funding my research.

I am very thankful to Dr. Brian Barrett who during the initial days of my PhD provided me valuable inputs that helped me build a foundation to the project. I thank Dr. John Devaney for providing insights on the study areas selected for the project. I would like to thank Ned Horning (Director of Applied Biodiversity Informatics) for answering many of my queries related to Machine Learning classifiers.

Next I would like to express my special thanks to Dr. Daniel McInerney, Forest Scientist at Coillte Teoranta who offered me an internship at Coillte. The knowledge that I have gained from him during my tenure as a Remote Sensing Analyst Intern is priceless and is for a lifetime. Thanks to Coillte Teoranta for providing the reference datasets that were really importanat to the research. Special thanks to Dylan Walsh, PhD student at Coillte. Thanks Dylan for being immensely supportive and I learned so much from you! Cannot thank you enough!!!Huge thanks to my ex-colleague and housemate Ana De Miguel Munoz for sharing her field knowledge on forestry and being the best housemate and friend that I needed back then!!!Thanks to John Le Gear and Brandon and all the staff at Coillte for taking me on field visits and sharing their knowledge with me.

Huge thanks to Rory Scarrott for guiding me with the clustering algorithm and building up my confidence. Thanks so much Rory for your time!! Thanks to Gourav Mishra for the timely guidance.

I would like to thank my ex-colleagues and manager from Mallon Technology for being extremely supportive and providing me all the resources that I needed to learn and apply my skills and work for the Department of Agriculture, Food and the Marine (DAFM). I thank them for providing me the opportunity to work for them and help me grow as a Remote Sensing Analyst.

Huge shout out to my friends at the Department of Geography, UCC. Thanks guys for keeping me sane. Special thanks to Agnes and Mary for the administrative and technical support. Thanks to the entire department and UCC for providing me a prestigious platform to learn and flourish as a researcher.

My family like friends! You added a lot more fun and colour to my PhD days and I made a lifetime memories with you all! Loads of love to you all!I cannot afford to miss mentioning Anjena Daswani and Shatabdi Choudhury – I don't know what I would do without you two. Thank you girls for everything!!!

Special mention of Sourabh Pargal and Tanvi Rajput for being there whenever I needed. Thank you for the timely inputs and help on software related issues. Thanks to Dr. Vishnu Nandan for providing me insights on radar remote sensing during the initial days of my PhD. I must mention Mr. Shashi Kumar, my Master's supervisor from Indian Institute of Remote Sensing, Dehradun, India. Thank you Sir for always answering my queries and encouraging me to do a PhD.

I thank my sister Jyothi and brother-in-law Shankar, cousins and relatives for always checking on me and caring for me! Thanks to my in-laws for being very supportive and understanding throughout! Thanks for always being there!Ranjitha, Shreya, Supriya, Sahana, Sumana aunty, Vandana, Shubha, Varsha, Sreedevi, Kannu, Lakshmi aunty, Narsimha mama, Vatsala aunty and Kanna mama– thank you for being there– the moral support means a lot!!! I feel so grateful to have the blessings and support of some incredible people in my life- Pammu aunty, Sampath uncle, Prasad mama, Nagu aunty, Shubha aunty, Vinutha aunty, Atti and Atti mama, Satyanarayan uncle, Chaya aunty and Jai aunty. Thank you all!

Finally and the most important, to my parents - M.N.Balaji and M.B.Janaki – my world, my support system! This work has been possible only because of your support and all the sacrifices you made! You mean the world to me! Thanks to my dear husband Karthik for being immensely supportive and encouraging!! Thank you for bearing with me through the stress times! I cannot imagine a word of this thesis without your love and support. I am tremendously grateful to you all, You are the Best!!

Part I

PROJECT BACKGROUND, LITERATURE REVIEW, STUDY AREAS AND DATASETS

Chapter 1

General Introduction

"I walked among the seven woods of Coole: Shan-walla, where a willow-bordered pond Gathers the wild duck from the winter dawn; Shady Kyle-dortha; sunnier Kyle-na-no, Where many hundred squirrels are as happy As though they had been hidden by green boughs Where old age cannot find them; Pairc-na-lee, Where hazel and ash and privet blind the paths..." – W.B.Yeats

1.1 Forests

Forests are undoubtedly one of the most valuable resources on Earth covering one third of the land surface. Our planet is covered by 4 billion hectares of forests *(Martone et al., 2018)*. The importance of forests cannot be underestimated. In terms of economic, social, ecological, environmental and aesthetic aspects, the services that forests provide to humankind are manifold and they also regulate the overall health of the planet. Being the most important part of the ecological cycle, forests are one of the natural carbon sinks, are havens for biodiversity, provide food, medicinal and forest products, regulate the hydrological cycle, protect soil resources, provide recreational uses, spiritual needs and aesthetic values.

To emphasise the importance of forests to our planet, three inspiring quotes about forests by renowned personalities have been presented below:

"The clearest way into the universe is through a forest wilderness" – **John Muir**

"A nation that destroys its soils destroys itself. Forests are the lungs of our land, purifying the air and giving fresh strength to our people" – **Franklin D. Roosevelt**

"The forest is a peculiar organism of unlimited kindness and benevolence that makes no demands for its sustenance and extends generously the products of its life activity; it affords protection to all beings, offering shade even to the axe-man who destroys it" – **Gautama Buddha**

The majority of the world's forests belong to tropical (comprising 50% of the world's forests, occuring in areas where temperatures are relatively high), boreal (occuring exclusively in the Northern Hemisphere) and temperate biomes (occuring in the cool temperate regions of the Earth) *(Abramovitz et al., 1998; Landsberg and Waring, 2014*). According to the Food and Agricultural Organisation (FAO), in the global context, forest is defined as "Land spanning more than 0.5 hectares with trees higher than 5 meters and a canopy cover of more than 10 percent, or trees able to reach these thresholds *in situ*. It does not include land that is predominantly under agricultural or urban land use" *(FAO, 2018)*. Forests are complex ecosystems that undergo human induced and natural changes which influence their interaction with the surroundings.

This PhD study focuses on monitoring and understanding the kind of changes the forests in Ireland undergo using satellite imaging technologies. This chapter provides context on how these changes influence climate change and on the carbon reporting system in Ireland.

1.2 Climate change and role of forests as a carbon sink

Climate change has been a major concern for a number of decades. Global warming is one of the most evident aspects of climate change which has caused many negative consquences on physical, biological, human and other systems on Earth. Global warming is the gradual increase in the temperature of the Earth's atmosphere attributed to the enhanced greenhouse effect caused by the increased levels of greenhouse gases (GHGs) in the atmosphere which are mainly Carbon Dioxide (CO_2), Methane (CH_4), Nitrous Oxide (N_2O) and Ozone (O_3). In the report on understanding global warming by the Intergovernmental Panel on Climate Change (IPCC) *(Intergovernmental Panel on Climate Change, 2018)*, it has been reported that as of 2017 human activities have caused approximately 1.0°C of global warming compared to pre-industrial levels. It has also been estimated that global warming is likely to reach 1.5°C between 2030 and 2052 if the current trend continues. In the fourth assessment report of the IPCC Working Group II *(Solomon et al., 2007)*, it has been declared that CO_2 is the most important anthropogenic GHG. The atmospheric CO_2 concentration was 411.0 ± 0.1 parts per million (ppm) in October 2019 and has increased from 277 ppm in 1750, the beginning of the industrial era *(Le Quéré et al., 2018)*. Since 2000, there has been a 20 ppm rise in CO_2 per decade, which has been the fastest rise during the past 800,000 years *(Intergovernmental Panel on Climate Change, 2018)*. The primary reasons for the increase of CO_2 in the atmosphere above pre-industrial levels is the release of carbon from fossil-fuel burning, cement production, deforestation and other land-use change activities *(Philippe et al., 2013)*. According to the State of the World's forest 2018 report by FAO *(FAO, 2018)*, the world's forest area decreased from 31.6% of global land area to 30.6% between 1990 and 2015. This 1% comprises of a loss of 129 million hectares of trees (about the size of South Africa) with an annual net loss rate of 0.13% *(Food and Agriculture Organization of the United Nations, 2016)*. This has caused a decrease of 11 gigatonnes (Gt) of global carbon stocks in forest biomass which is a threat to global climate.

The IPCC states *"Taken as a whole, the range of published evidence indicates that the net damage costs of climate change are likely to be significant and to increase over time".* Some of the main findings from the fourth assessment report of the IPCC *(Solomon et al., 2007)* have been presented here to get an understanding of the impacts of climate change on Earth.

"Observational evidence from all continents and most oceans shows that many natural systems are being affected by regional climate changes, particularly temperature increases" *(Solomon et al., 2007 pg.no.8)*

"A global assessment of data since 1970 has shown it is likely that anthropogenic warming has had a discernible influence on many physical and biological systems" (Solomon et al., 2007 pg.no.9)

"Some large-scale climate events have the potential to cause very large impacts, especially after the 21st century" (Solomon et al., 2007 pg.no.17)

Melting of glaciers at the poles and sea water thermal expansion in turn causing rise in the sea levels, extreme and violent weather conditions such as hurricanes, floods, tsunamis, drought, fires, extinction of flora and fauna, disruption and cause of catostrophic effects on human lives, destruction of food chain and economic resources are some of the worst climate change impacts the world is facing today.

1.2.1 Tackling climate change – global context

Tackling climate change is a challenge and many efforts are being taken to reduce carbon emissions by up to 50% by 2050 compared to 1990 levels. In 2007, the European Commission issued a communication *(Commission of the European communities, 2007)* stating that the European Union's (EU) objective is to limit global average temperatures to less than 2°C compared to pre-industrial levels. The European Council came to an agreement that developed countries will have to take the lead to reduce their emission between 15 to 30% by 2020. It also emphasises that many developing countries will need to take efforts to reduce their emissions significantly *(Weaver et al., 2007)*. International agreements on climate action were started to bring countries to work together to limit GHG emissions and thus mitigate climate change. The main international agreement on climate action is the United Nations Framework Convention on Climate Change (UNFCCC) which was adopted at the Rio Summit in

1992. The Kyoto Protocol to the UNFCCC was agreed in 1997 to set out GHG emission reduction targets for each developed country. During the first commitment period of the Kyoto Protocol (2008-2012), participating countries were committed to reduce emissions by an average of 5% below 1990 levels. Ireland's target under EU burden-sharing is to limit emissions to no more than 13% from the 1990 baseline year *(European Commission, 2012).* The second commitment period of the Kyoto Protocol started in January 2013 and will end in 2020. The participating countries have comitted to reducing emissions by atleast 18% below 1990 levels. Under the UNFCCC, the Paris Agreement entered into force in November 2016 with an action plan to limit global warming below 2°C. Signatory countries have committed to reducing carbon emissions to achieve the assigned temperature target.

To assess the regular status of global climate observations and provide guidance for it, the World Meteorological Organisation (WMO), Intergovernmental Oceanographic Commission of UNESCO (IOC-UNESCO), United Nations Environment Programme (UN Environment) and International Science Council (ISC) have co-sponsored the Global Climate Observing System (GCOS) programme. GCOS defines Essential Climate Variables (ECVs) that characterize Earth's climate. Three main categories of ECVs are defined – Atmosphere, Land and Ocean. The Land category includes aboveground biomass and land cover variables which are crucial for understanding the changes in the greenhouse gas sinks and the climate system. Vegetation systems have the potential to sequester large amounts of carbon and have a direct influence on the local, regional and global climate. Being ECVs, global assessment of forests and land cover changes are essential inputs to climate models that guide mitigation and adaptation strategies. The programme by the European Space Agency (ESA) called the Global Monitoring of ECVs (also known as ESA Climate Change Initiative) is an initiative started by ESA to respond to the climate change challenge. The Integrated Carbon Observing System (ICOS) is another system developed to quantify and understand greehouse gas balance in Europe and neighbouring regions. ICOS data are openly available at the ICOS Carbon Portal that provides data on natural and human emissions and uptake of greenhouse gases from ocean, land and atmosphere. ICOS is an international organisation of 12 European member countries and 130 greehouse gas measurement stations *("ICOS - Integrated Carbon Observation System," 2020)*.

Globally, people, especially youth, are becoming more aware of the climate change threats to the planet and are contributing in their own ways to put pressure on world leaders to take actions to address climate change. The massive wildfires faced by the Amazon forests in 2019 raised an alarm, compared to recent years, starkly highlighted the issue of global change and ecosystem destruction *("Amazon fires," 2019)*. A global climate strike took place from 20-27 September 2019 where 7.6 million people took to the streets and demanded climate action. In parallel to these strikes, the climate action summit of the UN general assembly on 23rd September 2019 showcased new initiatives by government, business and civil society to increase the commitments to achieve the goals of the Paris agreement and work towards reducing net emissions to zero by mid-century.

1.2.2 Importance of forests as carbon sinks

One of the pathways to achieve the Kyoto Protocol emission reduction target is through sustainable management of forests as they play key roles as carbon sinks. Climate change and Irish forestry by *Hendrick and Black, (2009)* states

"Unlike many other sectors, forestry can contribute both to reducing emission sources and to increasing sinks. Due to the direct link between land-use decisions and sustainable development, forestry plays a key role when addressing the climate change problem in the broader context of global change and sustainable development" (Hendrick and Black, 2009, pg.no.2)

A sink is defined as a storage reservoir that is increasing in size *(Cannell, 1996)*. A carbon sink is anything that absorbs more carbon than it releases. The carbon cycle is an ongoing process in which the carbon circulates between the reservoirs in a continous cycle- the main reservoirs being forests, soils, oceans and the atmosphere. Forests can play the role of a sink or a source (anything that releases more carbon than it absorbs) of carbon at different times *(FAO, 2015)*. According to the findings from FAO[1], forests have been a carbon sink by storing an average of 2.1 Gt of CO_2 annually between 2011-2015 *(FAO, 2015)*. In forests, carbon is stored in several pools such as vegetation (the above-ground and below-ground biomass – wood and non-wood

[1] FAO forest assessment involves people with local field knowledge of the vegetation and land use, this contributing to enhanced quality of the data collected. Considering FAO as one of the rigorous methodologies, it has been referenced here.

material and the root-system); dead-wood and litter (dead plant biomass/plant debris) and soil. In all forests, tropical, temperate and boreal together, 31% of carbon is stored in the biomass and 69% in the soil *(FAO, 2001)*.

1.3 Forests in Ireland

According to the National Forest Inventory (NFI), *(Forest Service, 2013)* forest in Ireland is defined as "Land with minimum area of 0.1 ha, a minimum width of 20 m, trees higher than 5 m and a canopy cover of more than 20% within the forest boundary, or trees able to reach these thresholds *in situ*". Irish forests belong to the category of temperate forest biome which is situated in areas with relatively milder winter seasons in comparison with boreal forests *(Grebner et al., 2013)*. By the beginning of 20th century, only about 1% of the country was covered in forests *(Cross, 2012)*. Ireland experienced mass destruction of forests due to human activities. To reverse deforestation, the Irish state carried out afforestation programmes which continue today. Ireland has the lowest forest cover of all European Union – 11% of the total land area of the Republic of Ireland.

To manage the State's commercial forests, the Irish Government established a new state body, Coillte Teoranta. Under the Forestry Act 1988, Coillte was established as a private limited company. A State grant scheme was introduced to encourage private landowners to plant forests. At present, the national forest estate is managed by three forest owners (i) Public: State Owned (Mainly Coillte); (ii) Private (grant-aided); (iii) Private (non grant-aided). Table 1.1 shows the forest ownership in Ireland.

Table 1.1: Forest ownership in Ireland (Department of Agriculture, Food and the Marine, 2018)

Ownership	Area (ha)	Percentage (%)
Public	391,357	50.8
Private (grant-aided)	268,100	34.8
Private (non-grant-aided)	110,563	14.4
Total	770,020	100

The Forest Service is responsible for setting national forest policy, control of tree felling, promotion of forest research and development and promotion of private forestry and administration of the State forestry grant schemes. The increase in grant-aided privately owned land parcels has resulted in a highly fragmented forest landscape with privately owned forests being on average <11 ha in size *(Devaney et al., 2015).* However, the target set by the government to expand the forest estate to 18% by 2050 may help reduce the fragmentation *(COFORD, 2014).* Changes in forest area in Ireland since 1656 are indicated in table 1.2. The forest estimates presented in table 1.2 have been collected from various reports such as *Aalen et al., (1997); Department of Fisheries and Forestry, (1973)* and others by *Department of Agriculture, Food and the Marine, (2018)*. For further details of the reports, *Department of Agriculture, Food and the Marine, (2018), pg. no. 6* can be referred.

Table 1.2: Forest area in Ireland (Department of Agriculture, Food and the Marine, 2018)

Year	Area (ha)	% Total Land Area
1656	170,000	2.5
1841	140,000	2.0
1908	125,200	1.8
1918	100,717	1.4
1928	89,000	1.2
1949	144,000	2.1
1965	254,350	3.7
1973	323,654	4.6
1985	411,529	5.9
2006	697,730	10.1
2012	731,650	10.5
2017	770,020	11

Table 1.2 shows how after Ireland's independence in 1922 forest area has grown from just over 1% to the current 11% of the total land area. The first statistical and multi-resource inventory (NFI) carried out on the national forest estate took place between 2004 and 2006. The NFI was established to record and access the extent and nature of Irish forests (both public and private). The NFI is a detailed timely survey of forest sample plots based on a randomised systematic grid of 2km × 2km. The NFI records

information on forest area and species composition, health and carbon content, biodiversity and growing stock volume for the entire national forest estate. The second NFI cycle began in 2009 and was completed in 2012. The third cycle began in 2015 and was completed in 2017.

1.3.1 Forest species in Ireland

Much of the forest expansion in Ireland since the early 20th century has been with non-native species. Because the native tree resources such as oak, ash, Scots pine and willow were depleted, the Irish State's forestry programme decided to introduce non-native trees that would supply Ireland's timber needs and to develop a sustainable forest industry *(Cross, 2012)*. The prominent non-native trees that were brought are Sitka spruce, Norway spruce, beech, sycamore and larch. These trees host a lot of benefits - due to their fast growing nature, they provide great financial returns to forest owners, they provide an efficient method of sequestering atmospheric CO_2. Inspite of the benefits they provide, these trees are posing a major threat to biodiversity and ecosystems. They drive out endangered animal species by transforming their habitats. Irish sitka spruce monocultures require pesticides and fertilizers and when these are harvested through clear-felling process, acid sulphate is generated, affecting waterways *(Murphy, 2020)*.

The national forest estate is comprised of 479,530 ha (71.2%) conifers and 193,580 ha (28.7%) broadleaves. The conifer – Sitka spruce is the most common species found in Ireland (51.1% of forest area) *(Department of Agriculture, Food and the Marine, 2019)*. Many forests also contain a mixture of species. The age of these trees is ownership dependant. Quantitative information based on forest age and ownership is given in table 1.3.

Table 1.3: Quantitative information on forest age and ownership (Department of Agriculture, Food and the Marine, 2019)

Age <30	
Ownership	**Forest area (ha)**
Public	235,000
Private (grant aided)	225,000
Private (non-grant aided)	37,000

Age >51	
Ownership	**Forest area (ha)**
Public	25,000
Private (grant aided)	5,000
Private (non-grant aided)	25,000

The rotation of forests depends on the quality of timber, some of which take more than 50 years to meet the harvest standards. Usually in Ireland, conifers have a shorter rotation period than broadleaves.

1.4 Forest Carbon reporting system in Ireland

The NFI measures carbon stocks in the forest pools. The carbon stock present in five different forest pools as per 2017 NFI records is shown in figure 1.1.

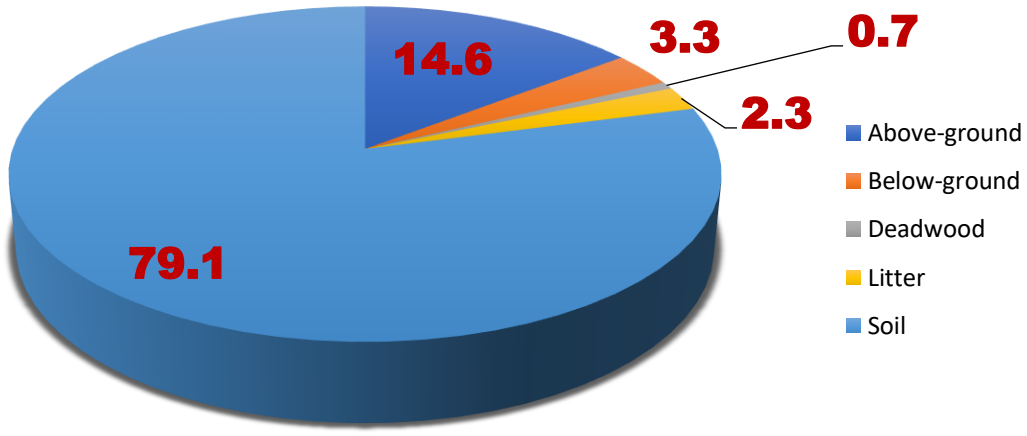

Figure 1.1: Proportionate carbon stock in the five different pools in Irish forests in 2017 (Forest Service, 2018a)

Looking at the carbon pools of Irish forests, most of the carbon is stored in the soil. According to *Forest Service,(2018a*), most of the forests in Ireland are grown on mineral soils (60.8%) and the rest 39.2% are grown on peats. This conversion of peatland into forestry and other land use has caused moderate to severe damage of

peatlands in Ireland. The drainage of peat soils for conversion to land use (forestry and agriculture) promotes increased emissions of CO_2 due to oxidation of organic matter within the aerobic layers of the peatlands (carbon emissions and removal). However, the impact of afforestation on carbon cycle in peatland ecosystems is complex and much research is being conducted in the country to understand this better. The conifer forests dominating in the country also accumulate carbon rapidly over time. The carbon stock in the above-ground biomass (stems, leaves and branches) was 45.6 million tonnes in 2017. This carbon stock and stock changes using the NFI data were calculated using a software called CARBWARE *(Black et al., 2011)* which is the national forest carbon reporting system in Ireland. The CARBWARE model estimates changes in the five forest carbon pools (figure 1.1) needed for international reporting. Forest carbon emissions and removals are recorded in the model resulting from afforestation, reforestation and deforestation.

1.5 Forest disturbances and their impact on forest carbon stock

Changes in the carbon stock arising from forest disturbances such as afforestation, deforestation and harvesting are required to be quantified to comply with the Land Use, Land Use Change and Forestry (LULUCF) reporting requirements. In Ireland, Kyoto forests were started (afforestation since 1990) to meet the reporting requirements. In Ireland, young trees grow quickly[2] and absorb large amounts of carbon dioxide. The forest management practice in Ireland includes harvesting the trees before they die naturally; this locks the carbon in the wood and wood products. Followed by almost immediate replantation this starts the carbon storage cycle again.

According to the second NFI cycle results *(Forest Service, 2018b)*, 3.6 million m^3 of mean annual standing were harvested between 2006 and 2012. Clear felling is the dominant harvest type in Ireland, accounting for 76.6% of the timber felled between these years. In Private forests (grant aided), first thinning is the dominant harvest type *(Department of Agriculture, Food and the Marine, 2018)*. Although the national forest area continues to expand, evidence from *Devaney et al., (2015)* suggests that the gross national deforestation rate is increasing. The first national deforestation map was developed by *Devaney et al.,(2016)* for the years 2000-2012 as part of the DEFORMAP project. A total of 5,457 ha of deforested land were identified in the

[2] The fast growth is related to the fast-growing nature of non-native conifer trees.

country. Apart from the human induced changes, forests in Ireland are regularly subjected to threats from natural events such as strong winds (Storm Darwin in 2014 for example), fire (Galway fire in 2018) and insect pests. Such events result in damage to forests. These changes in the forests would benefit from annual monitoring to ensure improved forest management.

1.5.1 Importance of forest monitoring in Ireland

Research has improved understanding of climate change in Ireland. Rise in sea-levels, increase in temperatures and changes in patterns of storms and precipitation are some of the negative effects of climate change reflected on the country *(Dwyer, 2013)*. This trend is projected to continue and intensify in future with Ireland's climate become warmer and drier *(European Environment Agency, 2017)*. In response to climate change mitigation, Ireland introduced the National Adaptation Framework (NAF) to provide plans for adaptation measures to reduce the negative effects of climate change on the country. The NAF has identified forestry as one of the sectors *(Department of Communications, Climate Action and Environment, 2018)* and has developed guidelines to ensure a consistent approach to adaptation planning is adopted by the forestry sector. In response to climate change, the first policy pursued address the reduction of GHG and afforestation to increase carbon sinks *(Department of Communications, Climate Action and Environment, 2018)*. Programmes such as the forestry programme 2014-2020 have been introduced to contribute to Europe 2020 objectives and targets *(European Commission, 2010)* and comply with the Kyoto Protocol emission reduction targets.

One of the targets set by the European Union is to reduce the GHG emissions by at least 20% compared to 1990 levels. To comply with these targets, DAFM has identifed specific needs in Ireland's forestry sector *(Davies and Image, 2014)*. One of them is the need to permanently increase forest cover. Afforestation to increase carbon sequestration without disturbing the natural habitats for wildlife must be a top priority of a forest management system. With the Irish forest monoculture, affecting ecosystems, Ireland is taking efforts to introduce schemes such as Native Woodland Scheme to encourage farmers to protect and expand Ireland's native woodlands and associated biodiversity.

Ireland has been involved in forest monitoring for over 20 years through collecting data and reporting on the forest condition. It is crucial to understand the role that forests play in absorbing carbon, providing natural habitats for flora and fauna and conserving soils and water. In this regard, it is therefore essential that forest monitoring continue both in Ireland and across the world.

1.6 Remote Sensing technology – potential and scope in forest change monitoring

At a global scale, forest monitoring is important to comply with the GHG emission reduction targets and to understand climate change to safeguard the planet. It is equally important to monitor forests at a regional scale to assess their health and provide maximum benefits to the forest owner and help maintain a healthy ecosystem.

Remote Sensing is defined as the art, science and technology of observing an object, scene or phenomenon by instrument-based techniques *(Tempfli et al., 2009)*. In the past, foresters would use field and aerial surveys to collect forest data. With the introduction of space-borne remote sensing around 60 years ago, the era of supplementing field data with satellite images began. The advancements in satellite remote sensing such as availability of higher spatial, temporal and spectral resolution products, are benefitting the remote sensing community immensely. Many international organizations have been established to promote Earth Observation (EO) for the benefit of the society. Missions like Global Earth Observation System of Systems (GEOSS) by Group on Earth Observations (GEO) and Copernicus previously known as Global Monitoring of Environment and Security (GMES) have been useful for forest monitoring applications. One of the important utilities of EO technologies is using them as a tool to measure and map the past and existing forests and calculate the GHG estimates. By exploiting several parts of the electromagnetic spectrum, many EO satellites have been developed for conducting space-based monitoring and forest management of the world. With the advancements in the EO technologies, faster and robust approaches have created platforms to monitor forests and extract the different forest parameters to examine the forest health.

Optical EO sensors that operate with wavelengths ranging from 0.7 to 300 μm (Infrared) and 0.4 to 0.7 μm (visible) of the electromagnetic spectrum offer many benefits for forest monitoring. The visible bands of the optical sensors are sensitive to

the photosynthetic activity of vegetation, type of forest and forest density *(Lynch et al., 2013)*. They have a vast spatial coverage along with good spatial resolution and provide frequent observations, thus delivering good annual coverage. Many optical satellites such as Landsat, RapidEye, SPOT and Sentinel-2 provide high spatial, temporal and spectral resolution supply products and services in forest cover and other land-cover mapping and in many other application areas. The Light Detection and Ranging (LiDAR) has been a powerful technique for forest monitoring. Obtaining canopy height data, observing canopy damage and other structural changes have been made possible using LiDAR which is an active sensor for capturing and analysing forest data in 3D format. Many studies *(Wulder, 1998; Banskota et al., 2014; Wulder et al., 2012; Tusa et al., 2020)* have explored the potential of multispectral optical and LiDAR sensors for forest monitoring. However, given the limitations of these satellites such as dependence on weather conditions and high cost, sensors operating within the microwave region of the electromagnetic specturm have been widely explored in recent years.

Synthetic Aperture Radar[3] (SAR) sensors using the microwave portion of the electromagnetic spectrum (wavelength: 1mm to 1m) have become an important source of EO data due to the distinct capabilities they offer over the optical and thermal infra-red regions. Especially in a country like Ireland where there is heavy cloud cover, Active SAR data (which provide their own source of illumination) are particularly of great use because of their cloud penetrating, weather independent capabilities[4].

Many civilian based space-borne imaging Radar systems have been launched since the launch of the first such system SEASAT-1 in 1978 by National Aeronautics and Space Administration (NASA). A number of radar sensors have been launched by countries such as the USA, Canada, India, Germany, Japan and others to support different applications. Few of the current missions that prioritize forest monitoring are Radarsat-2 launched by the Canadian Space Agency, TessaSAR-X and TanDEM-X by the German Aerospace Centre (Deutsches Zentrum für Luft- und Raumfahrt; DLR), Sentinel-1 by ESA, and Advanced Land Observing Satellite (ALOS and ALOS-2) Phased Array Type L-band Synthetic Aperture Radar (PALSAR and PALSAR-2) by

[3] Radar – Radio Detection and Ranging
[4] Due to the longer wavelengths compared to visible and infra-red regions, these are largely unaffected by cloud cover, rain and haze

the Japan Aerospace Exploration Agency (JAXA). BIOMASS is another satellite mission foreseen in 2021, operating at P-band, that will focus on forest studies.

To monitor global forests, many global forest maps have been developed using satellite imaging technologies. One of them is the Global Forest Watch (GFW). It is an online platform that provides tools and data necessary to monitor forests- the key focus being forest extent and change. NASA has also developed forest height maps and forest fires maps. The European Forest Fire Information System (EFFIS) managed by the European Commissions's Joint Research Centre (EC-JRC) uses the most updated satellite data to identify wildifres and forest damage in Europe *(Sedano et al., 2012)*. *Martone et al., (2018)* derived global forest/non-forest classification mosaics from Interferometric SAR data acquired by the TanDEM-X mission. The data were collected between 2011 and 2016. *Shimada et al., (2014)* generated global mosaics of ALOS PALSAR data to monitor variability in forests between regions and proved the potential of L-band ALOS PALSAR data in mapping forests.

On a national and local scale, studies such as *McInerney et al., (2016); J. Devaney et al., (2015)* and *Devaney et al., (2017)* have conducted forest monitoring in Ireland using RapidEye and aerial photography data, L-band SAR data and fusion of aerial photos and satellite imagery. LiDAR/Airborne Laser scanning is a good choice for detailed mapping of forests, but they are very expensive *(McInerney et al., 2016)*. While selecting the optimal satellite data for a particular study, factors such as cost, temporal and spatial resolution, weather conditions and the field of application must be considered.

1.7 Research Rationale

Articles 3.3 and 3.4 of the Kyoto Protocol *(Nabuurs et al., 2000)* state the following

`... direct human induced land use change and forestry activities, limited to afforestation, reforestation and deforestation since 1990, measured as verifiable changes in stocks ... shall be used ...' - Article 3.3, (Nabuurs et al., 2000, pg.no.124)

that decisions will be taken concerning inclusion of `... additional human induced activities ... by sources and removals by sinks in the agricultural soils and the land-use change and forestry (LUCF) categories' – Article 3.4, (Nabuurs et al., 2000 pg.no.124)

To provide the necessary estimates for the activities under Article 3.3 of the Kyoto Protocol, improvements to CARBWARE were necessary *(Duffy et al., 2012)*. COFORD has funded many climate change projects such as CLI-MIT programme, CARBiFOR and CARBiFOR II to facilitate improvements to CARBWARE. Although the current reporting complies with the International Panel for Climate Change Good Practice Guidance (IPCC GPG) *(IPCC et al., 2003)*, annual UNFCCC reviews for Ireland recommended improvements under three areas

1. Reassessing soil-C stock changes following land-use change and forest-management impacts
2. National tracking of annual changes in forest area from deforestation and disturbances
3. Assessing stock changes from disturbances and management interventions

This PhD study focuses on point 2 to support tracking of annual changes in Irish forests using active L-band SAR data to provide comprehensive information flow to CARBWARE.

1.7.1 Relevance of the work to End Users

- Facilitate National GHG reporting: Assessment of the forest change and extent through improved tracking of deforestation and other forest disturbances. Frequent monitoring of forest disturbances will supply relevant data to CARBWARE and therefore help making decisions compliant with Kyoto Protocol emission reduction targets
- Provide annual forest updates: As the NFI is conducted once in six years, there is information gap. Private forest owners and forest companies need annual updates to run an effective forest management industry from an economic, social and environmental perspective
- Capturing illegal deforestation and felling activities non-compliant with the felling license conditions: the forest service offers felling licenses under the Forestry Act 1946 *(Maguire and COFORD, 2001)*, but illegal felling activities are not recorded in the current system. This study has the potential to provide relevant data and enable improvement of the felling compliance verification.

1.8 Research objectives

The objectives of this study are to investigate the potential of L-band SAR sensors (ALOS PALSAR and ALOS-2 PALSAR-2) in identifying the different disturbance types in the forest areas of Ireland. In particular, the objectives are:

- Explore the potential application of microwave satellite platforms in mapping the forest fragments in Ireland using a machine learning approach
- Develop an unsupervised algorithm to characterise the different disturbance types in Irish forests and assess the type and extent of change.
- Transfer the developed algorithm for forest mapping and change monitoring to the data from the currecntly active ALOS-2 sensor and examine the robustness of the algorithm to facilitate a continuous forest monitoring operability
- Make recommendations to support the continuous operation of a forest monitoring system in Ireland to address the refinements proposed to the Irish carbon reporting system

This thesis is divided into seven chapters.

Chapter 2: This chapter entitled **"Literature review"** provides a brief survey of scholarly sources on SAR remote sensing for forest change mapping and monitoring

Chapter 3: This chapter entitled **"Study Area and Datasets"** provides a description of the areas selected for the study along with ALOS PALSAR and ALOS-2 PALSAR-2 sensors and the different data sources used for the project

Chapter 4: This chapter entitled **"Mapping the Fragmented Forest Covers of Ireland – a Systematic Approach"** investigates the potential of ALOS PALSAR data to map the forest fragments in Ireland using a machine learning approach

Chapter 5: In this chapter entitled **"Characterisation and Monitoring of Forest Disturbances in Ireland using Divergence Guided ISODATA clustering algorithm"**, an unsupervised classification algorithm has been presented to characterise and monitor the different disturbance types in Irish forests

Chapter 6: In this chapter entitled **"ALOS PALSAR Based Algorithm Transferability to ALOS-2 PALSAR-2"**, the algorithm developed in chapters 4 and

5 have been transferred to another SAR sensor to investigate the robustness of the algorithm and examine the forest monitoring operability

Chapter 7: This chapter entitled **"Conclusions and Recommendations"** summarizes the research findings and presents a general outlook for future research

Chapter 2

Monitoring and Characterizing Forest Disturbances: A review of common approaches used

"Literature is my Utopia" – Hellen Keller

2.1 Introduction

For several decades, in situ forest information has been complemented with remote sensing-based observations which provide consistent data over a large spatial extent in a cost-effective manner. Several efforts such as *Hansen et al., (2013), Shimada et al., (2014)* and *Hu et al., (2016)* have been made to map forests around the globe from regional to global scales to establish a systematic and sustainable operational monitoring system. Optical and active SAR sensors are two dominant types of sensor systems that satellite platforms have been carrying for the past few decades. The former, spanning the range of electromagnetic spectrum from 400-3000 nm, is more sensitive to tree foliage and forest biochemical properties whereas the latter, measuring the backscattered radiation at wavelengths between 1 cm and 1000 cm, provide information on woody biomass and forest structure. Microwave systems have increased the possibility of obtaining cloud-free data and hence are particularly favoured given that many forests are located at higher elevations, temperate and sub-Arctic latitudes, and tropical regions where there can be persistent cloud cover. Spaceborne SAR systems have proliferated as a result of recommendations by various studies which have demonstrated the potential of SAR systems for mapping forest cover *(Isola and Cloude, 2001; Dwyer et al., 2000; Dostálová et al., 2016; Lei et al., 2018*; *Tomppo et al., 2019).*

The purpose of this chapter is to provide a comprehensive review of SAR change detection approaches and their application to forest disturbance mapping. This chapter starts with an overview of microwave remote sensing with relevance to forests, covering the influence of different bands, polarization and incidence angle, followed by a brief discussion of speckle reduction and coregistration which are vital for change detection (section 2.2). The next part (section 2.3) of the review is focused on the different SAR change detection techniques that have been most widely evaluated in the literature. The review concludes with a summary of potential techniques which could be applied to Irish forest cover, based on an assessment of advantages and limitations of each technique.

2.2 Microwave remote sensing

Microwave remote sensing comprises both passive and active systems. Passive systems (radiometers) offer a unique view of the Earth's surface by detecting the

naturally emitted microwave radiation within their field of view, however they typically have a coarse spatial resolution (for example 25km) as the amount of emitted energy is very low so has to be resolved over a large area. Active systems on the other hand provide their own source of illumination with an additional factor – the timing of the return pulse to measure distance. Active sensors can be categorized as imaging (radar/SAR) and non-imaging sensors (scatterometers and altimeters). Active imaging radars can penetrate through cloud cover and most weather conditions and image the surface at any time, day or night. Because of these attributes, SAR has become a valuable remote sensing tool for both military and civilian users with various applications such as intelligence gathering, weapons guidance, topographic mapping, sea ice monitoring, forest monitoring, oceanography, agricultural monitoring, mining and many more. Scatterometers are mainly designed to study ocean wind speed and directions, but they have also been applied to the study of the cryosphere, vegetation and soil surface properties *(Naeimi and Wagner, 2010)*. Altimeters have been used to measure elevation profiles of the Earth's surface. Other applications in geodesy, hydrology and atmospheric sciences have also been explored.

2.2.1 Radar remote sensing of forests – basic theory

The forest canopy represents a heterogeneous volume system with structural components of varying sizes and densities. This makes the interaction of the microwaves with forests complicated. The different scattering elements of a forest are leaves (needle-like, flat-like), stems and branches as well as the soil *(Ulaby et al., 1981)*. Varying sizes of these elements in terms of diameter can be found in a large forest. In the smaller stands of forests of Ireland, mixed tree species can be found that vary in their structure, resulting in complex scattering. Given the complexity of the forest canopies, it is appropriate to model them as a random volume *(Woodhouse, 2005)*. The amount of radar backscatter received from a forest canopy is dependent on the wavelength, polarization and incidence angle of the SAR system as well as the target parameters such as forest structure and moisture. The different wavelengths of the microwave region interact with different elements of the forest. The shorter wavelengths such as the X- (2.3 - 3.75 cm) and C-bands (3.75 - 7.5 cm) are of comparatively smaller order than the canopy elements and therefore, these bands do not tend to penetrate a dense forest canopy. For longer wavelengths such as L- (15 – 30 cm) and P-bands (30 – 100 cm), the canopy elements appear smaller than the

wavelength, therefore the microwave pulses can penetrate further into the canopy. As a result, these wavelengths undergo multiple scattering between the canopy, branches and soil. It is imperative to consider the effect of soil moisture on backscatter. Water with a very high dielectric constant (80) leads to higher backscatter causing confusion with forests. In the presence of dense vegetation, L-band can retrieve soil moisture due to its deep penetrating properties. To separate the backscattering contributions from soil and vegetation, a number of SAR backscatter models have been proposed *(Li and Wang, 2018)*. The most commonly used model is the Water Cloud Model (WCM) which can relate the backscattering coefficient to soil and vegetation properties and thus separate the moisture effects from SAR backscatter. However, while assessing the performance of WCM, the surface roughness and vegetation must be taken into account.

In the absence of any P-band satellite sensors prior to the early 2020s, most studies have used L-band for forest and vegetation studies *(Fransson, 1999; Lucas et al., 2007; Almeida-Filho et al., 2007; Yu and Saatchi, 2016; Tanase et al., 2018; Belenguer-Plomer et al., 2018; Yun et al., 2019)*. In a study by *Olesk et al., (2015)*, L-band was deemed more suitable than C-band for detecting disturbances such as logging and thinning in areas smaller than 1 ha[5]. This conclusion is highly relevant to Irish forests given the presence of few forest stands of less than 1 ha. A review by Global Forest Observations Initiative *(GFOI, 2013)* which focused on improving remote sensing data inputs to enhance the forest monitoring systems, reported that L-band can be used independently, while X- and C-band SAR are not sufficient on their own due to their reduced sensitivity to forest structural parameters. A comparative study by *Haarpaintner et al., (2009*) has shown how L-band was able to detect details such as regrowth better than C-band. Another study by *Saatchi et al., (1997*) illustrates the potential of using L-band SAR for monitoring deforestation in which the accuracy increased from 87% with C-band to 92% with L-band. The most commonly used L-band SAR sensors, ALOS PALSAR (2006-2011) and ALOS-2 PALSAR-2 (2014-present) have been extensively used for forest monitoring applications *(Marshak et al., 2019; Fransson et al., 2007; Urbazaev et al., 2018; Shimada et al., 2014)*.

[5] This was because of the higher spatial resolution of the ALOS-2 L-band sensor than the Sentinel-1 C-band sensor.

As SAR is sensitive to soil moisture, care must be taken while performing change detection as variations in soil moisture can be misinterpreted as a disturbance signal. The shorter wavelength of C-band SAR primarily interacts with leaves and branches, partially penetrating the forest canopy *(Reiche et al., 2018)*. In situations where the forests are less dense, C-band is largely responsive to surface roughness and soil moisture. An increase in backscatter may be reported after heavy rain events due to an increase in the soil moisture. Lower frequencies such as L-band also provide greater sensitivity to soil moisture as they can penetrate the vegetation layer and be influenced by moisture content. At L-band, the contribution from soil is dominant for most low vegetation covers *(Woodhouse, 2005)*. Performing time-series analysis and having knowledge of weather data can help identify the effects of moisture and aid in interpreting the variations in received SAR signals.

Another factor influencing SAR backscatter from forests is the polarization. Cross-polarized data (HV/VH - Horizontal Transmit Vertical Receive/Vertical Transmit Horizontal Receive) can be more useful than co-polarized data (HH/VV - Horizontal Transmit Horizontal Receive/Vertical Transmit Vertical Receive) for forest monitoring. This is because the depolarizing effect in the cross-polarized data is related to volume scattering from forest elements than the latter which is more sensitive to surface components. *Santoro et al., (2010*) demonstrated that HV polarized data presented a strong contrast between forests and non-forests, whereas HH was more affected by environmental conditions (for example frozen, thaw or dry conditions) and was less able to discriminate between the vegetation types. Another study by *Santoro et al., (2012*) used only HV L-band data as the contribution of HH band was found to be marginal. Although these studies emphasize the use of only HV data for forest change monitoring, *Pantze et al., (2010), Almeida-Filho et al., (2009) and Watanabe et al., (2018)* stress the importance of retaining the HH band as it can contain important information related to areas of recent deforestation (e.g. surface roughness caused due to uncleared debris leads to surface scattering detected by the HH channel). *Reis et al., (2017)* also demonstrated the use of fully polarimetric L-band SAR to detect forest changes and showed that the HV band presented the best results, once again underlining the potential of this polarization in forest change detection. However, the limited availability of this polarization in certain areas is a hindrance to using the fully polarimetric data. Reflecting on the general consensus from literature,

dual polarized (HV, HH) and longer wavelength (L-band) SAR data can be considered the most suitable for forest disturbance monitoring.

Choosing the best sensor configuration for different applications is vital in order to obtain the best results. The dependence of radar backscatter on the SAR incidence angle (the angle between the Earth's surface normal and the direction of illumination by radar) should not be underestimated. A study by *Rauste, (1990*) highlighted key points about the relationship of SAR incidence angle with forested and non-forested areas.

- Thick canopies exhibit volume scattering, therefore, such targets have only a slight dependence on incidence angle
- For rough surfaces (example: clear-cut areas with debris), backscatter is more uniform for all incidence angles
- Areas that have been clear-cut and contain no debris exhibit specular scattering, thus the backscatter reduces with increasing incidence angle

For L-band instruments, at low incidence angles most of the backscatter comes from the ground (*Hoekman, 1987*) and the contribution to backscatter from the forest canopy increases with incidence angle. *Devaney et al., (2015*) performed forest mapping and change detection using L-band data of incidence angle corresponding to 38°.

Monitoring disturbances requires images before and after the disturbance has occurred. In general, change detection is the process of identifying differences in the state of an object or phenomenon by observing it at different times *(Singh, 1989)*. Change detection is more challenging in SAR systems that optical systems due to the geometric distortions and speckle involved. It is important to acknowledge the geometric distortions that SAR images are subjected to due to their side-looking geometry. The two main geometric distortions relating to SAR image acquisition and interpretation are scale distortions and relief displacement. Scale distortions are a result of the distance measured in slant range and not ground range. Due to the slant range distance, objects in near-range appear steep while in the far-range, the objects appear shallow. This can be resolved by converting the slant range distance to ground range distance – this can be achieved by calculating the true horizontal distance along the ground corresponding to each point measured in slant range *(CCRS, 2006)*. The

main geometric relief distortions are layover, foreshortening and shadowing. As the distance is measured in slant range, top of a tall feature is displaced towards the flight direction from its true position on the ground. This effect is called layover which occurs when the radar beam reaches the top of a tall feature first before illumating its base. On contrary to this effect, foreshortening occurs when the radar beam reaches the base of a tall feature such as mountain tilted towards the sensor before it reaches the top. The effects of layover and foreshortening look very similar to each other on a radar image. Layover effects are more severe for small incidence angle (for near-range) and decrease towards far range (large incidence angles). Both foreshortening and layover effects result in radar shadow. Shadow occurs behind vertical features or slopes with steep sides. These are the areas that the radar beam cannot illuminate and no signal is received in return. The shadowing effects increase from near to far range and these areas appear dark on the SAR image. These effects add bright or dark effects on the image which interfere with the change detection analysis. Therefore, it is very important to remove such terrain-induced geometric distortions before making any further processing. Using Digital Elevation Models (DEMs) can help in removing some of such effects by making the slant to ground range conversion by compensating for foreshortening.

Speckle is a common feature present in SAR images which is a multiplicative noise *(Lou et al., 2019; Ajadi et al., 2016; Shang et al., 2014)*. Speckle is generated by different scatterers within the same resolution cell behaving differently leading to constructive and destructive interference of the coherent SAR signal *(Goodman, 1976)*. Speckle can be reduced through techniques such as multi-looking and speckle filtering. Multi-looking improves the radiometric resolution but compromises the spatial resolution. Many studies *(e.g. Lee et al., 1991; Hagg and Sties, 1994; Kulkarni et al., 2018)* have documented the use of adaptive and non-adaptive filters to reduce speckle. Non-adaptive filters, based on the use of mean, median or mode, apply the same set of weights over the entire image regardless of the distribution of radar reflectivity. Although these filters are easy to implement and compute, they smooth high frequency information. Adaptive filters such as the Lee filter *(Lee, 1980)*, Frost filter *(Frost et al., 1982)*, Kuan filter *(Kuan et al., 1985)*, Gamma-Maximum-A-Posteriori (MAP) filter *(Lopes et al., 1990)*, refined Gamma-MAP (RGMAP) filter *(Nezry et al., 1991)*, Lee Sigma filter *(Lee, 1983a, 1983b)*, and Improved Lee Sigma

filter *(Jong-Sen Lee et al., 2009)* are better at preserving subtle image information *(Mather and Tso, 2016)*. Depending on the degree of speckle in the image, these filters adapt their weights accordingly, which can result in more reliable outputs but with a high computational cost. A De Grandi multi-temporal filter *(De Grandi et al., 1997)* may be applied to multi-temporal images acquired of the same track and frame, exploiting the temporal correlation of speckle among the images. Another critical step in multi-temporal image change detection is the co-registration of images *(Abdelrahman et al., 2011)*, to ensure that coincident pixels within the images correspond to the same ground area.

2.3 Change detection techniques

Various change detection approaches have been developed and applied to SAR data. This section discusses some of the commonly used methods for SAR change detection, and their relevance to forest disturbance monitoring. The methods have been categorized into different groups for convenience. The different SAR change detection approaches discussed in this chapter have been listed in table 2.1 along with their advantages and limitations.

Table 2.1: Summary of SAR change detection approaches with relevance to forest monitoring

Approach	Examples	Advantages	Disadvantages
Algebra-based: • Image Differencing • Image Ratioing	(Pantze et al., 2010) (Durieux et al., 2019)	Straight-forward approaches and easy to implement	Requires selection of threshold to separate change and no-change pixel; image ratioing assumes non-normal distribution
Principal Component Analysis (PCA)	(Yun et al., 2019)	Reduces the dimensionality of the dataset; change can be detected in new components and enhances such patterns in the data; speckle reduction in SAR images	It is scene dependent, therefore results between different dates are difficult to interpret and label. Also, assumes that multi-temporal data are highly correlated
Interferometry • Interferometric SAR (InSAR)	(Balzter, 2001) (Cloude and Papathanassiou, 1998)	Along with amplitude, phase is used which reveals information of the target	Temporal and geometric decorrelation limit this approach
• Coherence	(Wagner, 2003) (Askne et al., 1997)	Additional information complementing the information contained in the intensity of the backscatter	Several factors cause phase decorrelation; coherence values very low for forests making it unreliable.
Classification • Maximum Likelihood/Mahanalobis distance	(Wijaya et al., 2010) (Lehmann et al., 2011)	Until recently, the most widely used classifiers – works best for normally distributed datasets	Classification process is slow, not all datasets are normally distributed – leading to misclassification.
• Machine learning	(Wheeler et al., 2017) (Liesenberg and Gloaguen, 2013) (Wang and Xue, 2014) (Ghimire et al., 2010) (J. Devaney et al., 2015b)	Automatic methods that learn about the data. More accurate than the traditional methods. Robust and handle complex and large number of datasets. Non-parametric that do not assume any data distribution.	Require lot of training data to train the algorithm, requires extensive ground-truth data. Requires programming knowledge and not straight forward to implement.
• Unsupervised	(Ali et al., 2013) (Pierce et al., 1998)	No training data is required, simple and easy to implement. Clustering is purely based on pixel values and therefore it is unbiased.	Post-classification interpretation is time consuming and grouping the clusters is challenging. Difficult to apply correct labels without good in situ data.
SAR Polarimetry	(Pardini et al., 2012) (Trisasongko, 2010)	All polarizations can be used to describe the complex scattering mechanisms within a pixel. The scattering mechanisms can be separated and more information can be derived	Limited availability of fully polarimetric data in certain areas
SAR and optical data fusion	(Pourshamsi et al., 2018) (Kellndorfer et al., 2010)	Full capabilities of multi-sensor platforms can be exploited.	Scaling and validation issues

2.3.1 Algebra-based

Algebra-based approaches, which were amongst the earliest change detection algorithms to be developed, include image ratioing and image differencing. The latter is simply the pixel by pixel subtraction of DN values of two spatially registered images, while the former is the ratio of DN values of corresponding pixels on two co-registered images. The key concept behind these algorithms is the generation of a Difference Image. These algorithms are straight forward, easy to implement and widely applied, and require threshold selection to determine areas of change *(Lu et al., 2004)*. Given the speckle present in a SAR image, image ratioing is better adapted to the statistical properties of SAR image than image differencing *(Hecheltjen et al., 2014; Chen et al., 2019)* as it can decrease the influence of calibration and radiometric errors *(Lu et al., 2004; Rignot and van Zyl, 1993 ;Singh, 1989).* Studies such as those described by *Pantze et al., (2010)* and *Ban and Yousif, (2012)* have successfully applied image ratioing techniques to SAR data for change detection of forests and other features such as urban.

One common problem with both image differencing and ratioing is the selection of a threshold between Change and No-change which can be challenging, and in some instances subjective. To select these thresholds, standard deviation is often used as reference values *(THÉAU, 2007)*. Incorrect thresholds lead to unreliable results. In forest monitoring, selecting a threshold for one area may not work when applied to a different area, depending on the type and forest conditions. Selecting a common threshold that can be applied for national scale monitoring becomes laborious and unreliable. Image ratioing is also criticized because of the non-normal distribution of the resultant image which limits the validity of the threshold selection using the standard deviation of resultant pixels *(THÉAU, 2007; Lu et al., 2004 ;Singh, 1989)*.

A variation to the ratio method – the log-ratio method - has been presented for change detection on SAR images *(Bovolo and Bruzzone, 2005; Zhuang et al., 2018a; Zhuang et al., 2018b)*. This is because the logarithmic transformation can convert multiplicative noise into additive noise and compress the value range. Although many studies support the fact that the log-ratio method outperforms the ratio method, a study by *Zhuang et al., (2019), p.491* disagreed with this finding and stated the notion that "log ratio outperforms ratio is a misunderstanding in change detection of SAR

images". This experiment was conducted over three study areas in Berne, Switzerland, Ottawa, Canada and FengFeng, China using C-band SAR sensors: ERS-2, Radarsat-1 and Radarsat-2 satellites. However, the effect of this experiment on L-band sensors is unknown and requires to be examined to decide if the log-ratio method performs better than the ratio method for SAR change detection.

The ratio technique can be applied well to a pair of images, but with more than two images, several temporal ratios have to be fused to detect the changing areas. *Bujor et al., (2004)* concluded that the ratio of means was useful for step, or abrupt, changes such as deforestation which correspond to a significant modification of the land cover between two dates. *Mermoz and Le Toan, (2016)* successfully used the ratio technique to detect large changes in the tropical forests of Vietnam using ALOS PALSAR HH and HV polarization data. Most of the studies such as *Joshi et al., (2015)* and *Motohka et al., (2014)* have used SAR backscatter ratios to detect changes in tropical forests.

Image differencing and image ratioing have been widely discussed in literature to detect changes between SAR images, however, these methods do not provide a detailed change matrix from which the time and extent of change can be derived. Added to this, the challenging tasks of selecting appropriate thresholds limit the full potential of these approaches. Consequently, advances in change detection of SAR images have seen the development of more robust approaches to track and characterize the disturbances.

2.3.2 Transformation based

Principal Component Analysis (PCA) is a technique for reducing the dimensionality of a data set *(Jolliffe and Cadima, 2016)*. Also called Eigenvector analysis, it is a powerful statistical technique to generate a new reduced set of uncorrelated variables of components by transforming several correlated variables. Studies by *Baronti et al., (1994); Gimeno et al., (2003); Lee and Hoppel, (1992); Henebry, (1997)* have recognized its utility for analysis of SAR images where it has one main advantage– speckle reduction using multiple image dates, with minimal loss of spatial resolution *(Henebry, 1997)*. *Lee and Hoppel, (1992)* developed a generalized principal component transform (PCT) which maximized the signal-to-noise ratio (SNR) and was tailored to the multiplicative speckle noise characteristics of polarimetric SAR

images. It was found that PCT could compress information, reduce speckle and enhance details at the same time.

During the process, the principal components (PCs) are calculated from eigenvectors based on all pixels, including the changed pixels. The first PC contains more information and the variance of data is strongly concentrated in the first component. However, the change pixels (oriented along the second PC axis) introduce certain amount of erroneous information in the first and other PCs. To minimise this effect, *Wiemker, (1997*) developed an iterative PCA approach which calculates the covariance matrix by incorporating a weighting coefficient for all pixels that quantifies the probability of each to be a no-change pixel. This method improves the ability to extract change information and the identification of no-change pixels *(Hecheltjen et al., 2014). Yun et al., (2019*), applied the PCA technique to a time series of ALOS PALSAR imagery to screen noise components – the study was performed over the dense North and Eastern Korean forests, which are mainly boreal and cool-temperate with native conifer trees. However, even with the application of PCA transformation, a large number of errors in the time series signatures were found. These errors were associated with factors such as mis-coregistration of SAR images and weather factors such as wind and moisture. To address these issues, a kernel PCA was introduced in the study from which the noise components in the time series were eliminated and the performance was improved.

As PCA is scene dependent, the change detection results between different dates are often difficult to interpret and label. A thorough examination of the eigen structure of the data accompanied by a visual inspection of the images is required to ascertain the exact nature of the PCs derived from temporal datasets *(Coppin et al., 2004),* but uncertainty can remain. This has an impact for forest change monitoring when using multi-temporal datasets over a period when the change may arise from a variety of different sources, and can manifest in a number of different ways. *Fung and LeDrew, (1987)* state that this analysis technique should not be applied as a change detection method without a proper knowledge of the study area, which can be challenging when the ground information is lacking.

2.3.3 SAR Interferometry based

Repeat-pass SAR Interferometry (InSAR) is a technique that generates an interferogram (in which a fringe pattern appears) which is an image of the complex correlation between two image SAR images. This interferogram contains phase and coherence information which are useful in the image interpretation. The interferogram calculates the phase difference between two images which shows the difference in the two-way (satellite to target and back) travel path of the radar signal. Phase is a measure of path-length, and in a single image the exact number of complete wave cycles is unknown which makes it of no practical use *(Woodhouse, 2005)*. However, comparing phase measurements by calculating the phase differences obtained from two or more SAR images can generate topographic products such as DEMs. When the phase of the backscattered signal is affected, for example as a result of topographic change due to an earthquake, the fringe pattern and the number of fringes in the interferogram is altered.

Coherence is the degree of similarity between two SAR images ranging from 0, showing no coherence, to 1 showing perfect coherence. The success of repeat pass InSAR depends on the interferometric coherence, if the ground surface remains undisturbed between the first and second overpasses *(Zhou et al., 2009)*. Spatial baseline decorrelation (changes in the viewing geometry) and temporal decorrelation (physical changes in the surface between acquisition) are the most important factors that result in destruction of the interferometric phase *(Zebker and Villasenor, 1992)*. *Suga and Takeuchi, (2000), Askne et al., (1997), Lei et al., (2018a)* applied InSAR coherence approaches to map and monitor forest disturbances, however, they found that several issues contribute to the phase decorrelation and generate unreliable coherence results. The temporal decorrelation is high for forests *(Balzter, 2001)* due to changes in wind motion, disturbance causing loss of trees, or changes in their dielectric constant. Separating the signal caused due to a forest disturbance from other factors contributing to decorrelation is challenging. This factor is immensely reduced in single-pass interferometry when the two images are acquired simultaneously. The TanDEM-X mission comprises of bistatic SAR system with twin satellites TerraSAR-X and TanDEM-X. For forest mapping, the potentials of TanDEM-X data have been demonstrated in *Schlund et al., (2013)* and *Martone et al., (2015)*. Many studies that have used TanDEM-X for forest height and biomass estimation *(Toraño Caicoya et*

al., 2016; Schlund et al., 2015; Kugler et al., 2014; Chen et al., 2016; Lee et al., 2018). Mapping forest changes can be accomplished by using stacks of repeated acquisitions as demonstrated in *(Martone et al., 2018)*.

Differential SAR Interferometry (DInSAR) is another technique in which an interferometric pair and a DEM are used to generate a differential interferogram. In this technique, the phase changes due to topography are removed. *Tanase et al., (2015*) used a TanDEM-X DInSAR and Shuttle Radar Topography Mission (SRTM) technique to map forest changes in semi-arid and tropical forests in Australia. Being semi-arid region, the influence of a change in dielectric constant was relatively low. Forest height was calculated, and negative height was considered as a sign of forest degradation or deforestation while positive height was considered as a sign of forest growth or afforestation. The synergy between SRTM and TanDEM-X datasets allowed identifying changes in forest extent.

To summarise, although InSAR has proven to be a powerful and promising technique, it is more suitable for applications such as ground deformation monitoring, and in forestry, for canopy height estimation. Factors such as temporal and geometric decorrelation limit the use of InSAR and DInSAR approaches to analysis of forests which are areas of low coherence *(Ferretti et al., 2001)*. More on the advantages and limitations of using InSAR for forest mapping can be found in *Balzter, (2001)*. The TanDEM-X mission, which avoids temporal decorrelation, is an alternative approach however, the shorter wavelength X-band limits the canopy penetration and obtaining full-coverage height may be challenging. The L-band TanDEM-L mission planned for launch in 2022, may offer a better alternative to overcome such issues and derive more information on, not only the forest structure, but also on the level of disturbance in the forest.

2.3.4 Classification based

Image classification techniques are amongst the oldest techniques developed to generate land cover information with post-classification comparison used to analyze changes between images acquired on different dates. Most traditional classification approaches employ the image pixel as the basic unit of analysis *(Li et al., 2014; Wang et al., 2004),* and many pixel-based classification methods for forest cover mapping and change detection can be found in the literature *(Lu and Weng, 2007; Gislason et*

al., 2006; Pal and Mather, 2005; Walker et al., 2010; Pantze et al., 2014; Rignot et al., 1994; Saatchi and Rignot, 1997).

Pixel-based supervised image classification is a widely used approach and requires an analyst to build a model using labeled information of selected pixels which is generalized to the whole image. Among the various supervised classification techniques available, machine learning (ML) algorithms are gaining widespread recognition in preference to parametric methods such as maximum likelihood which operate on the assumption that the data are normally distributed *(Jawak et al., 2015)*. Moreover, the increasingly high temporal and spatial resolution nature of multitemporal datasets can be too large for these statistical classifiers to handle resulting in poor performance. ML can be broadly defined as "computational methods using experience to improve performance or to make accurate predictions" *(Mohri et al., 2018, p.1)*. Over the past decade, ML techniques have been widely adopted to provide solutions to excavate the information hidden in big datasets. The ML algorithms can handle many input variables, do not assume any data distribution, can work on different measurement scales for both categorical and numeric variables and there is no issue of over fitting. Traditional ML approaches within remote sensing involve image classification, feature selection and extraction, signal unmixing and model inversion *(Camps-Valls, 2009)*. Recent advancements in ML techniques for tackling remote sensing problems include manifold learning, semi-supervised learning, transfer learning, active learning and structured learning *(Criminisi et al., 2012)*.

ML algorithms such as Decision trees (Random Forests (RF), Extremely Randomised Trees (ERT)), Support Vector Machines (SVM) and Artificial Neural Networks (ANN) have been gaining more acceptance in forest cover mapping applications *(Wheeler et al., 2017; Liesenberg and Gloaguen, 2013; Wang and Xue, 2014; Ari Sambodo and Indriasari, 2013; Mellor et al., 2013; Mascaro et al., 2014; Krizhevsky et al., 2012; Ghimire et al., 2010; Bosch et al., 2007; Devaney et al., 2015)* because they can handle different scaled data and many input features and are effective in high dimensional spaces.

One of the ML classifiers extensively used for forest monitoring is the Random Forests (RF) classifier. First proposed by *Breiman, (2001),* it is a decision tree classifier that

builds an ensemble of individual trees and the decision from each tree is later combined to arrive at a final decision based on a voting scheme. Using a bootstrapped sample of the original data, the RF algorithm generates multiple Classification and Regression tree (CART)-like trees from two thirds of training data provided and the remaining one third are left out of the sample (Gislason et al., 2006a). These out-of-bag (OOB) samples are used to test the individual trees as well as the entire forest. The OOB error estimates the average misclassification from all trees. These classifiers are non-parametric (do not assume normal data distribution) and they deliver a variable importance plot (a graph to assess the most relevant variables to the classification). The variable importance plot derived from this algorithm provides valuable insight as the importance of each variable can be assessed, and the variables of most importance can be retained for further improving the classification. A study by *Devaney et al., (2015*) applied a RF classifier for forest cover monitoring to two test sites in Ireland and obtained 97% accuracy for forest class mapping. The performance of a supervised classifier depends on the quality of the input features and the sufficiency of information in training samples, in addition to the robustness of the classifiers *(Du et al., 2015; Rodríguez-Galiano et al., 2011). Du et al., (2015)* evaluated a RF classifier used on fully polarimetric SAR data and found that the use of spatial features such as the Gray-Level Co-occurrence Matrix (GLCM) texture measures increased the classification accuracies by at least 30%. Studies such as *Mellor et al., (2013), Gislason et al., (2006), Walker et al., (2010), Simard et al., (2000), Waske and Braun, (2009)* also evaluated the performance of RF classifier for land cover mapping and found that RF outperformed single decision tree classifiers and are less sensitive to the number of training samples. For multitemporal stacks of SAR imagery, RF are highly efficient. Although best classification accuracies were obtained for classes such as grassland and urban with completely different backscatter, in *Simard et al., (2000)* forest was found to be mixed up with swamps, temporarily flooded woody vegetation and open forests. To improve understanding of the correlation between pixels (closely located or contiguous pixels), an independent accuracy assessment of the classification is suggested by *(Mellor et al., 2013).* Further, understanding how the classifier manages noise and outliers requires research. A review by *Belgiu and Drăguț, (2016*) summarized the use of RF in remote sensing with a focus on its parameterization, the influence of changes in sampling procedures, and the size and representativeness of training sample sets. The paper emphasizes the need to set two parameters to produce

the forest trees – Ntree which is the number of trees to be generated and Mtry which is the number of variables to be selected and tested for the best split. The variable importance measurement provided by the RF classifier is one of the most useful features and has been extensively used for various applications such as reducing the number of dimensions in data and identifying the most relevant variables for classification.

Although many studies acknowledge the use of RF for SAR classification, a comparative study by *Trisasongko et al., (2017*) using a fully polarimetric (PLR) ALOS PALSAR dataset showed that SVM outperformed RF and ANNs for land cover classification. It demonstrates the importance of tuning in non-parametric classifiers – substantial improvements in classification accuracies (20%) were observed. SVM responded primarily to tuning. It was found that tuning parameters such as Ntree and Mtry were unresponsive in the case of RF. In another study by *Attarchi and Gloaguen, (2014*), both SVM and RF produced better classification values at the 95% confidence level compared to Neural Network (NN) for complex mountainous Hyrcanian forest on ALOS PALSAR imagery. There is no way to state which classifier is better in performance as it depends on the dataset and application. In general, RF can be simpler to tune than SVM and ANN, it can be faster than SVM and works well with categorical data.

Recently, Deep Learning (DL), a subset of ML algorithms which is gaining high popularity in pattern recognition, is being applied to SAR data for more robust information extraction *(Zhang et al., 2019)*. DL extracts information through multi-layer artificial neural networks, whereby each layer extracts one or more features of the image. The greater the number of layers, the better the interpretation of the images through extraction of higher-level features. *Keshk and Yin, (2019),Cui et al., (2019), L. Chen et al., (2019)* have explored the potential of DL on SAR imagery for classification and change detection of features as woods, farmland, roads and others. *Hamdi et al., (2019*) used deep convolutional neural networks (CNNs) to detect changes in forests using X-band COSMO-SkyMed Stripmap SAR images. For areas ranging between 0.1 ha and 0.5 ha, accuracies slightly above 80% were obtained, while for areas greater than 0.01 ha, accuracies of 50% were obtained. One limitation of DL in comparison to other ML methods is that it typically requires a large amount of training data as well as hardware issues related to graphics processing unit (GPU)

computing power. In remote sensing, there exists few studies for classification and mapping of forest types and disturbances using DL *(Onishi and Ise, 2018; Freudenberg et al., 2019).* More evaluation of the potential of DL is required in applied forestry as there exists a knowledge gap between deep learning and remote sensing for application areas such as forestry.

Post-classification comparison can be performed to detect changes within the mapped land covers. As none of the classified maps can be considered to have perfect accuracy, due to various factors such as the unavailability of ground truth data to derive training samples, the influence of image noise and the complex background *(Wang and Cheng, 2010),* comparing them induces classification errors from each input and decreases the overall accuracy of the final output. Using unsupervised learning provides a possible solution when the main application is change detection *(Jawak et al., 2015).* The most commonly used classifiers under the category of unsupervised clustering algorithms are the K-means and Iterative Self-Organizing Data Analysis (ISODATA) approaches. Used by *Long and Singh, (2013), Abbas et al., (2016), Rahman, (2016),* these methods exploit the spectral distance between adjacent pixels to divide the feature space by identifying natural groupings based on spectral similarities *(Tempfli et al., 2009)*. Used on multi-temporal images, various clusters are formed based on the data distribution or as defined by the user. A key step in this approach is the separability of clusters based on their mean and standard deviation. The nature of a target before and after change in temporal images can be studied using the cluster signatures. These signatures carry information on the temporal behavior of clusters and this level of detail is useful in extracting information on change – when, where and the extent of change that has occurred. While monitoring change in forests using multi-temporal images, this ability of ISODATA algorithm aids in characterizing the disturbance type. Any supervised/unsupervised algorithm can identify change within multi-temporal images, the main difference being the use of training data. The unsupervised ISODATA classifier does not require any training data to identify areas of change and is more helpful in areas where there is a lack of reference data to extract different types of changes. Most of the studies based on ISODATA clustering have used optical imagery, however a few studies such as *Pierce et al., (1998), Quegan et al., (2003) and Rignot et al., (1992)* have studied the application of ISODATA clustering on SAR datasets and found that when polarimetric classifiers such as the Wishart classifier are

combined with the ISODATA classifier, there is an increase in the overall accuracy of around 10%. A study by *Sgrenzaroli et al., (2002*) conducted on tropical forest cover in three sites – Mato Grosso, Rondonia and Colombia displayed different results to the ones that have been mentioned before. This study focused mainly on the comparison between wavelet segmentation and ISODATA techniques, with ISODATA showing poor performance in detecting clear-cuts. The performance of ISODATA depends on the input parameters such as standard deviation and minimum distance values, convergence threshold, the maximum number of iterations and the number of clusters to be used. It is important to choose all these parameters carefully to improve the classifier performance.

Due to the challenge of defining a priori the number of clusters, many cluster validity indices have been proposed in the literature *(Arbelaitz et al., 2013; Ramze Rezaee et al., 1998; Wang and Zhang, 2007)* that measure the distance between the signatures of two clusters and extract statistical separability values. Used by *Goodenough et al., (1978)* and *Swain and King, (1973),* divergence, which is computed using the mean and variance-covariance matrices of the data representing feature clusters, was one of the first separability indices applied to remote sensing imagery *(Halls, 2001). de Bie et al., (2012*) used the Divergence index to derive the optimal number of clusters for ISODATA clustering in land cover classification using hyper-temporal optical imagery. The index can be calculated on any number of image bands to represent the variability in land cover. Agricultural landscapes which were used in the study displayed a high temporal (seasonal/inter-annual) variability – the divergence indices were able to provide guidance in making the best choice in terms of the number of clusters that could be generated to represent the variability. More details on this approach can be found in *Ali et al., (2013)* and *De Bie et al., (2008)*. Other studies by *Nguyen et al., (2012) and Khan et al., (2010)* have used a similar approach for classification with an overall accuracy of approximately 94% in mapping crop patterns. To explore the usability of indices such as the divergence index on SAR for forestry applications, no relevant literature was found.

In summary, both supervised and unsupervised approaches to land cover classification of radar imagery have been used for forest monitoring, land cover mapping and change detection. Both the approaches offer advantages and limitations as listed in table 2.1. Combining both approaches to map forests and characterize and label the type of

disturbances occurring in them provides a platform to explore the utility of each approach.

2.3.5 SAR Texture

Texture is a representation of the grey-level variations and their spatial relationships in an image *(He et al., 2010)*. It is an important source of information as different surfaces have distinct textural features that help in discriminating the different land-cover types. If there is a change from one land-cover type to another, a difference in texture may be observed. There are various techniques to analyze texture features such as the GLCM (R.M. Haralick et al., 1973), Markov Random Field *(Deng and Clausi, 2005, 2004)* and Gabor filters *(Jain and Farrokhnia, 1990; Gong et al., 2014)*. Among these approaches, the GLCM based methods are the most predominant *(Baraldi and Parmiggiani, 1995; Kandaswamy et al., 2005; Shanmugan et al., 1981; Gebejes and Huertas, 2013)*. First proposed by *Haralick et al., (1973),* GLCM indicates the relationships between pixel grey levels in a particular direction or distance specified.

The textural information in a SAR image is derived from statistical measures based on the statistical dependencies between neighboring pixels. The statistical texture measures are grouped into first-, second- and higher-order statistics. The first order measures also known as the occurrence measures include elements such as mean, skewness, variance and kurtosis. These measures are derived from the histogram of pixel intensities in a given neighborhood and do not account for spatial relationships *(Jones and Vaughan, 2010)*. The second-order measures or the co-occurrence measures include elements such as contrast, correlation, dissimilarity, entropy, homogeneity and second moment. These measures describe the statistical dependencies between pixel pairs (spatial relationship of pixels) given the direction and inter-pixel distance. The second order measures are derived from the GLCM. While the second-order measures deal with the relationship between two pixels, higher-order measures analyze the properties of two or more pixels.

For forest monitoring and mapping applications, texture has been used as a valuable input to classification *(Pierce et al., 2003; Han et al., 2005; Benelcadi et al., 2014)*. *De Alban et al., (2018)* used SAR-derived GLCM textures to discriminate forest classes in the tropical biodiversity hotspot of the Tanintharyi region in Myanmar. It was found that except for contrast measures, the rest of the texture measures did not

influence the classification, potentially because of the use of the small 3x3 kernel in comparison with other studies. *Longepe et al., (2011)* used two different kernel sizes of 5×5 and 13×13 for classification of tropical rainforest in the Riau province in Sumatra using ALOS PALSAR data. The larger window size (13×13) was found to be preferable to estimate the spatial variations and the entropy was the most relevant texture measure. Care must be taken in choosing the right window size, especially where there are features such as hedgerows at the edges of forests. An inappropriate window size will blur these edges, and lead to incorrect land cover classification and change estimation. The choice of the window size therefore depends on the structure of the study area and spatial resolution of the imagery *(Chen et al., 2004)*. While texture measures are a useful input for SAR applications, their value can be affected by the selection of window size and application area.

2.3.6 Others

Additional change detection techniques include the Kittler-Illingworth threshold method *(Bazi et al., 2005; Moser and Serpico, 2006; Hu and Ban, 2014)* wavelets *(Bovolo and Bruzzone, 2005; Celik, 2010; Gong et al., 2012)*, curvelets which have shown better representation than wavelets *(Schmitt et al., 2010)*, fuzzy hidden Markov chains *(Carincotte et al., 2006)*, object-based image segmentation techniques *(Yousif and Ban, 2015)*, and SAR and optical image data fusion approach *(Lehmann et al., 2015; Hirschmugl et al., 2018; Poulain et al., 2011)*. Recent article by *Tewkesbury et al., (2015)* provides a clearer, synoptic review of change detection approaches in remote sensing. Specific to SAR, polarimetric decomposition algorithms and classifiers have been used for forest monitoring using fully polarimetric data *(Trisasongko, 2015b; Trisasongko, 2010; Pardini et al., 2012; Coulibaly et al., 2012; Park et al., 2012; Durden et al., 1989; Trisasongko et al., 2010; Trisasongko, 2015a)*.

In the light of growing volumes of remote sensing data, integrating multi-sensor frameworks have been used in applications such as urban and forest monitoring. Developing global monitoring systems that take advantage of the potential synergies and complementary nature of optical and radar datasets has been of significant interest as shown in studies by *Lehmann et al., (2012)* and *Lehmann et al., (2015)* as they provide combined benefits from both datasets to provide an effective monitoring system. Research activities combining LiDAR (Light Detection and Ranging) and

radar remote sensing have also increased in recent years. Studies such as *Pourshamsi et al., (2018) and Kaasalainen et al., (2015)* have integrated the benefits of polarimetric interferometric SAR (PolInSAR) data with LiDAR measurements to obtain improved forest canopy height estimates and retrieve above-ground biomass. Using the advantage of wide-scene coverage offered by PolInsar and the variables derived from PolInsar such as coherence, scattering from HV, HH and VV channels, more accurate results were achieved using a small Lidar sample. *Kellndorfer et al., (2010)* used LiDAR from the Laser Vegetation Imaging Sensor (LVIS), InSAR from SRTM and Landsat ETM+ data to characterize forest stand heights. The predicted map was tested against ground survey data which resulted in a correlation coefficient r = 0.83 with 9% error. Although LiDAR provides exceptional spatial detail of forest structure, it is limited in terms of complex data processing and high cost of data collection.

2.4 Concluding remarks

Given the small-scale coverage of traditional ground-based methods of forest monitoring, satellite remote sensing approaches have become significant contributors to operational studies. The preference of SAR sensors over optical sensors for forest monitoring is mainly due to their longer wavelengths and polarization capabilities and the fact that they are largely unaffected by cloud cover and haze. The variation in backscatter before and after change depends on surface roughness and dielectric properties of the target which requires knowledge of the area to label the changes.

Regarding SAR, several factors are to be considered before using the data. For forestry applications, the longer wavelengths such as the L-band have more penetrating capability and hence provide more information on the forest health, height and the disturbances. Moreover, cross polarized HV/VH data is better as it is more sensitive to volume scattering which is common within forests. The capabilities of co-polarized HH data cannot be underestimated and retaining HH data for forest monitoring will add value to the process of change detection of forests. Therefore, using dual- or quad-polarized SAR data is more useful than single-polarized data to extract their full potential in understanding the different scattering mechanisms.

The most commonly used change detection techniques are algebra-based, transformation-based, interferometry based, and classification based. Significant

progress has been made in change detection approaches which includes advanced techniques such as InSAR, machine learning classifiers and deep learning. While the usefulness of the traditional statistical classifiers cannot be underestimated, the power that advanced machine learning classifiers and the conventional unsupervised clustering algorithms provide are unique and are of great potential.

Chapter 3

Study Area and Datasets

"The goal is to turn data into information and information into insight"
– Carly Fiorina

3.1 Introduction

Selecting an optimal remotely sensed dataset is ironically a challenge as a consequence of the wide range of data currently available. The question is how to optimize the data characteristics that will effectively address the application or the research problem. For example, an issue with using multi-temporal datasets is that, with too little data, the quality of the analysis is reduced and too much detail will have a negative effect which can be burdensome leading to inaccurate results *(Warner et al., 2009)*. Keeping in mind the project budget, required spatial, temporal, spectral and radiometric resolution for the application, along with the knowledge of the study area, a decision must be made in making the right choice of data. As detailed in Chapter 2 of the thesis, for forest monitoring applications, L-band dual-/quad-polarized SAR data has shown to be a useful data source. Given the limited availability of quad-polarized data and based on the factors discussed in chapter 2, section 2.2.1 that could lead to the best results for this project, L-band dual polarized data has been selected for the present work. The only available L-band dual polarized data at the time of data order was JAXA's ALOS PALSAR data, the details of which have been given in section 3.3 of this chapter.

The focus of this chapter is to describe the study sites and datasets selected for the study. Pre-processing steps for the acquired datasets are also presented.

3.2 Description of Study Sites

"A man and his environment are more intimate than a snail and his shell" – Paul Vidal de la Blache, French geographer.

In order to select the study areas for this work, the country was assessed and the most suitable sites were chosen at a nationwide level. This assessment was based on topography, forest/land use and climate which are described in the following sections.

3.2.1 Topography

A topographical image of Ireland is presented in figure 3.1 with elevation data acquired from the Ordnance Survey of Ireland (OSi). The resolution of this DEM is 10m.

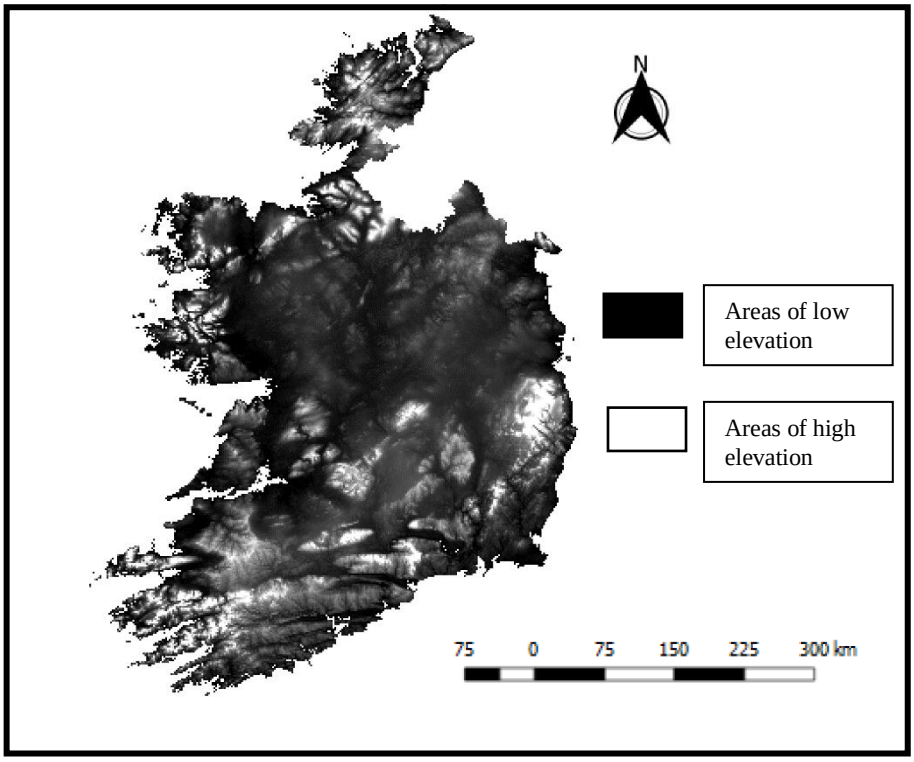

Figure 3.1: DEM from OSi of 10m resolution

A mix of these lowland and upland areas were selected for the study to incorporate the various topographical features within the algorithm which is useful for transferability. Based on this assessment, three areas from South, North and East were identified which were a mix of mountains and plainlands. This would allow consideration of interaction of different topographies with SAR backscatter and provide a fair evaluation of the algorithm developed for the study. Processing the SAR image by accounting for backscatters from targets such as steep mountains that would interefere with forest backscatter would allow in developing a robust algorithm. The three areas identified from this assessment were Cork (South), Donegal (North) and Wicklow (East). However, when the ALOS PALSAR images for these areas were explored, the images covered parts of the neighbouring areas which were then included in the study. The study areas as covered by the ALOS PALSAR images are shown in figure 3.2. The blue frames are the KML files generated from the ALOS PALSAR datasets. These areas were grouped into three main areas based on their location.

Area1: Cork, Limerick – Located in the South

Area2: Donegal, Leitrim – Located in the North

Area3: Wicklow, Meath, Kildare, Carlow, Dublin, Wexford – Located in the East

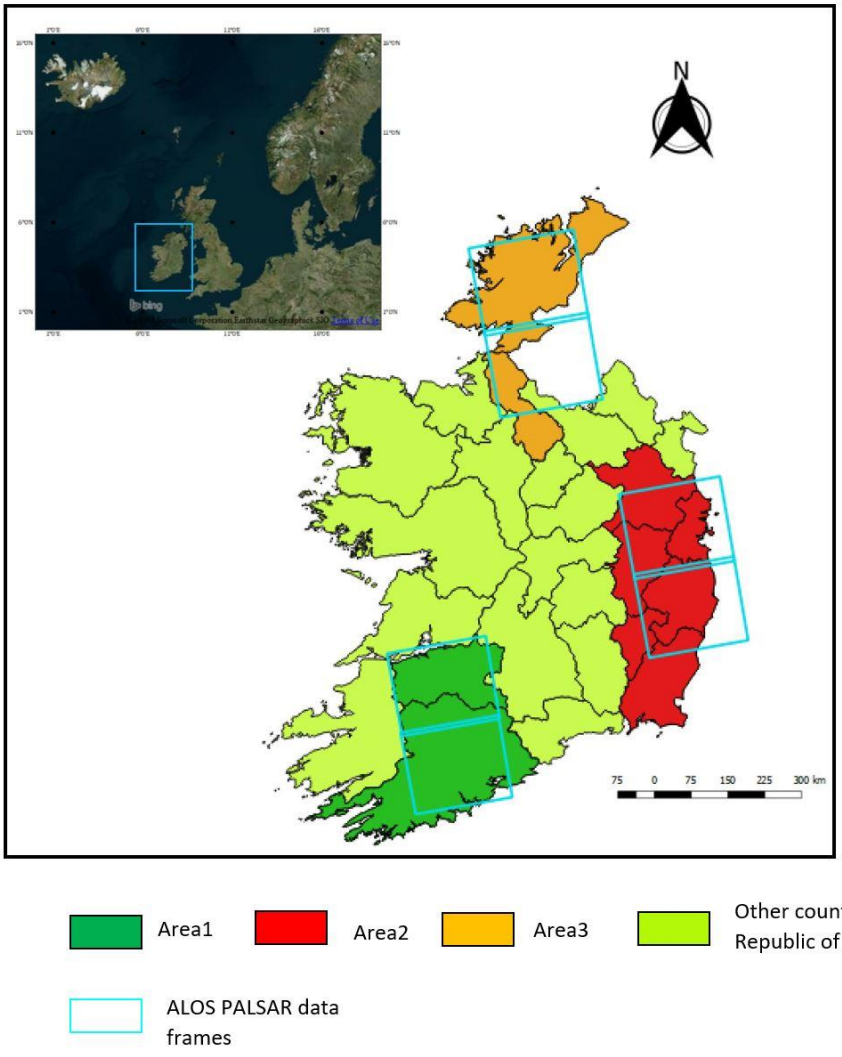

Figure 3.2:Study areas in the Republic of Ireland

3.2.2 Forest cover

The areas selected based on topography were then assessed with respect to forest cover. Relevant recent forest information from *Department of Agriculture, Food and the Marine, (2019)* has been extracted for each area; the forest area information based on ownership for each county is presented in table 3.1. According to the NFI third cycle conducted between 2015 and 2017, the area of forest in Ireland is estimated to be 770,020 ha (11% of total land area). Species information in each county is presented in table 3.2.

Table 3.1: Forest cover information for selected study areas from 2019

Study area	Counties	% Forest cover within county (forest as a proportion of total land area)	State-owned forests (%)	Private forests (grant-aided; other) (%)
Area1	Cork	12.1	52.9	47.1
	Limerick	10.4	35.7	64.3
Area2	Donegal	11.4	64.9	35.1
	Leitrim	18.9	48.6	51.4
Area3	Wicklow	17.9	62.2	37.8
	Meath	5.7	24.2	75.8
	Kildare	6.1	46.1	53.9
	Carlow	9.4	57.2	42.8
	Dublin	6.5	66.7	33.3
	Wexford	6.2	46.0	54.0

Table 3.2: Species information for each county of the study area (NFI 2017)

Study area	Counties	% Conifer forests	% Deciduous forests
Area1	Cork	73.4	26.6
	Limerick	82.9	17.1
Area2	Donegal	82.0	18.0
	Leitrim	70.0	30.0
Area3	Wicklow	71.8	28.2
	Meath	28.1	71.9
	Kildare	34.7	65.3
	Carlow	69.9	30.1
	Dublin	59.9	40.1
	Wexford	72.1	27.9

From table 3.1, Leitrim has the highest percentage of forest cover (18.9%) followed by Wicklow (17.1%) and Cork (12.1%). In the study sites, the non-native tree species

Sitka Spruce (*Picea sitchensis*) is predominant. Although Sitka Spruce is the most common tree species, other native and non-native species such as Alder (*Alnus glutinosa*), Birch (*Betula pubescens*), Oak (*Quercus*), Norway Spruce (*Picea abies*), Japanese larch (*Larix kaempferi*) and Lodgepole pine (*Pinus contorta*) are also found in the study areas – a mix of conifers and broadleaves are common in these areas. In Meath and Kildare, higher percentage of broad-leaved trees are found than the conifers (table 3.2).

There is predominance of peatbogs in Area2 particularly over the northern parts. Covered by lesser peatbogs, Area2 and Area3 are dominated by croplands and grasslands. While there is a higher concentration of settlement class in Area3 particularly over Dublin, water bodies are more prevalent in Area2. The different land cover classes present in these areas was an important factor while choosing the study areas.

3.2.3 Climate

Ireland is mostly characterized by mild, moist climate with abundant rainfall. The local climate across the country differs from place to place. The mountains face the wettest weather and counties such as Dublin and Kildare that are located on the east coast have the driest weather. The distribution of rainfall is highly variable in Ireland and therefore Met Éireann (the Irish Meteorological Service) has planted 500 rainfall recording stations across the country to acquire countrywide rainfall readings. To describe the climate of Ireland, details of two weather elements – temperature and rainfall are given below. The data for three stations within the study sites are extracted from Met Éireann; the location of the stations are shown in figure 3.3. The 30 year average annual temperature (degree celcius) and rainfall (mm) for 1981-2010 from the three meteorological stations are given in table 3.3. The data are derived from *SÉAMUS, (2012)*.

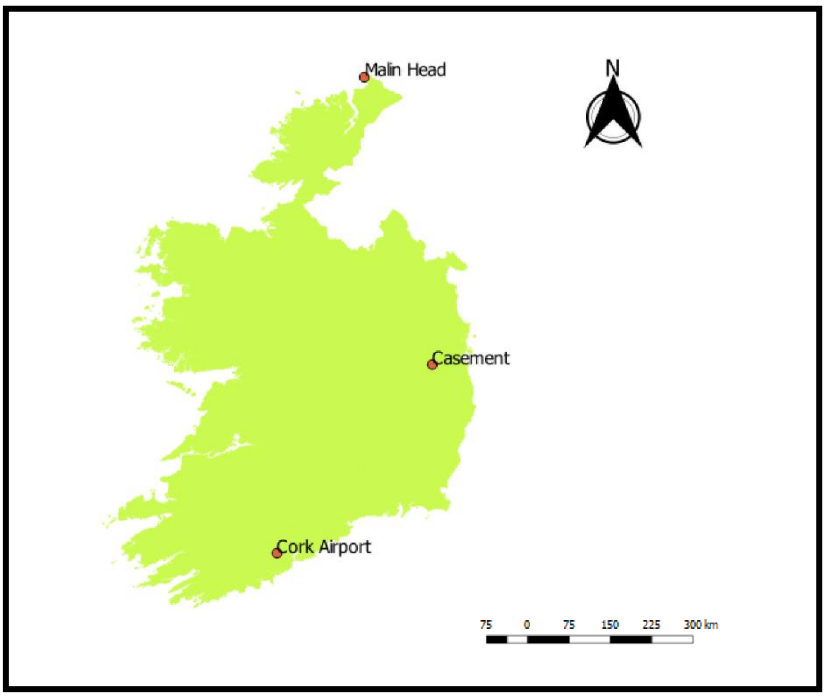

Figure 3.3: Location of three meteorological stations for which 30 year average weather data are extracted

Table 3.3: 30 year average annual Temperature and Rainfall (1981-2010) records

Station	**30 year average Temperature (degree celcius)**			**30 year average Rainfall (mm)**
	Min	**Max**	**Mean**	
Cork Airport	-8.0	28.7	9.9	1227.9
Malin Head	-6.2	25.9	9.8	1076.0
Casement	-15.7	31.0	9.7	754.2

From table 3.3, Cork Airport of Area1 has received the highest rainfall over the 30 years. Receiving the highest rainfall, Area1 also has the highest mean temperature recorded over the 30 years. The other two areas have faced relatively lesser rainfall over these years with lesser temperatures. Summer months are usually drier in Ireland compared to spring, winter and autumn.

Considering the differences in topography, forest/other land use classes and climate, Area1, Area2 and Area3 were finalised for further analysis.

3.3 SAR Data acquisition and pre-processing

3.3.1 ALOS PALSAR

The Advanced Land Observing Satellite (ALOS) was launched on 24th January 2006 and it was operational until 12th May 2011 *(Rosenqvist et al., 2007)*. This satellite carried three remote sensing instruments – Panchromatic Remote-Sensing Instrument for Stereo Mapping (PRISM), the Advanced Visible and Near-Infrared Radiometer type 2 (AVNIR-2) and the polarimetric Phased Array L-band Synthetic Aperture Radar (PALSAR). This research is focused on PALSAR data. The Equator pass time of the satellite is ~10.30 (descending) and ~22.30 (ascending) UTC with a repeat-pass cycle of 46 days. All acquisitions for the study were acquired from ascending orbits in Fine Beam Dual-Polarization (FBD) mode which comprised of both HH and HV data with a swath of 70km and an incidence angle at scene center of approximately 38° (off-nadir angle of 34°).

A total of 50 images were acquired from the European Space Agency (ESA), following the successful evaluation of a category-1 proposal (ID 17771). All data were delivered as Level 1.1 Single Look Complex (SLC) products. The characteristics of the data products acquired are given in the appendix of the thesis. Common characteristics of the data are

- Sensor: PALSAR
- Mode: FBD
- Polarization: HH, HV
- Incidence angle (Ɵ): 38°
- Wavelength: 23.6cm

The sensor mode, geographical region and time of acquisition were fixed for the ALOS satellite to support the systematic observation strategy. This therefore limits image availability. Two frames for each area were required in order to maximise coverage of the selected regions (figure 3.1). All images were acquired for the months of June with one FBD image per year.

3.3.1.1 ALOS PALSAR pre-processing

The standard SAR pre-processing steps according to *Sarmap, 2009* as shown in figure 3.4 were followed to convert the SLC data into meaningful backscatter data to enable further processing and analysis. All SAR pre-processing was carried out using the SARscape 5.0.001 software within an ENVI 4.8 environment.

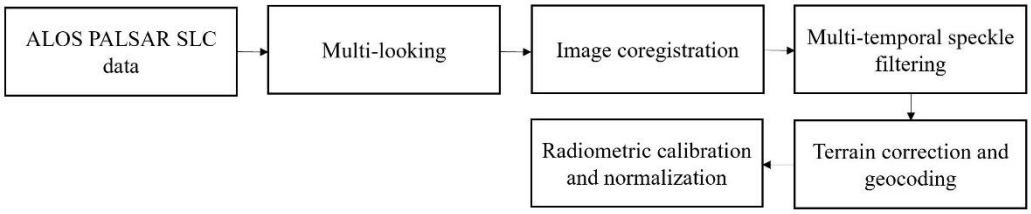

Figure 3.4: SAR pre-processing steps

The acquired SLC products were multi-looked with factors of 1 (in range) and 4 (in azimuth) to create square pixels of 15×15m. All the multi-looked images were subsequently coregistered and speckle filtered using a De Grandi multi-temporal speckle filter which preserves the structural features of the image without adding any blurring effect which is seen with other non multi-temporal speckle filters. Each element in the homogenous area is averaged with uncorrelated elements in the time-series. This multi-temporal filtering works assuming that the same resolution element on the ground is reflected in the same way and corresponds to the same co-ordinates in the image plane in all images of the time-series. The data scenes were then radiometrically and geometrically calibrated and values converted to decibels (dB) using the equation *(Shimada et al., 2014; Woodhouse, 2005)*

$$\gamma^{\circ} = \frac{\sigma^{\circ}}{cos\theta} \qquad (1)$$

Where, γ° is normalized with the cosine of the incidence angle, expressed in dB

σ° (Backscattering coefficient or differential radar cross-section) = $10*\log_{10}$ (DN); DN is the pixel digital number value in HH or HV

Θ is the local incidence angle

To ensure proper geometric correction of the SAR scenes, the OSi DEM of 10m spatial resolution and many ground control points (GCPs) were used. The scenes were

geometrically corrected to Irish Transverse Mercator (ITM) projection (EPSG:2157). Terrain-induced distortions such as layover and shadowing were masked from the images. The local incidence angle (angle between the normal to the backscattering element and the incoming radiation) generated by the DEM was used to identify the layover and shadowed areas, where negative values represented active layover areas and values greater than 90° represented active shadow areas. Finally, the two frames covering each study site were mosaicked.

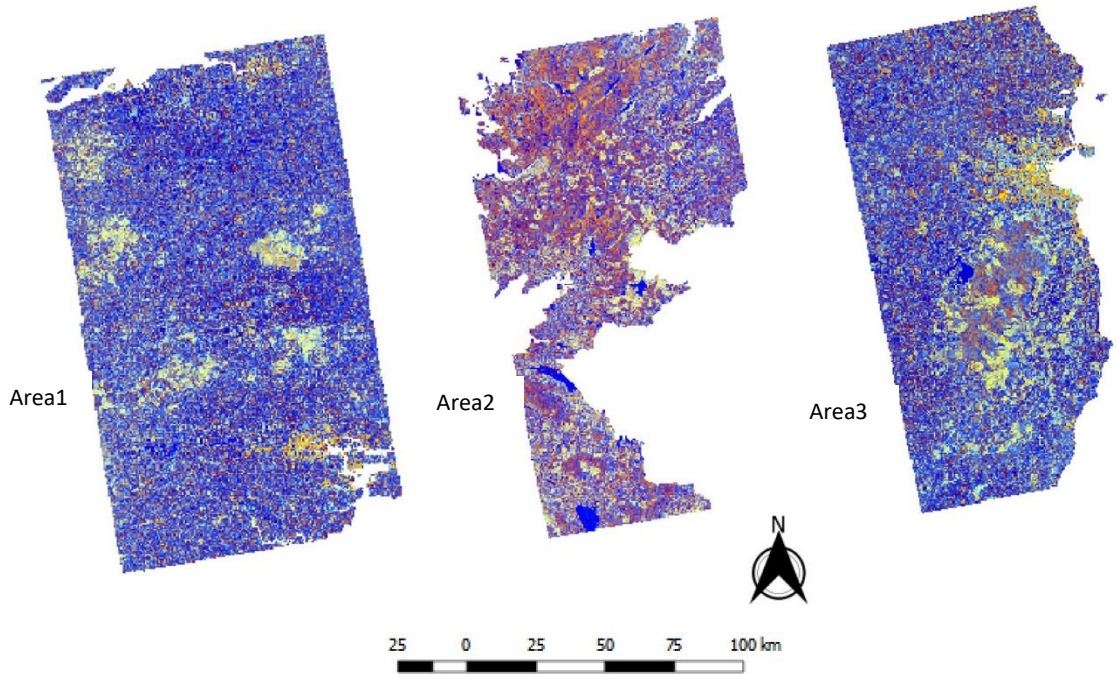

Figure 3.5*: *PALSAR false color composites with HH backscatter in red band, HV backscatter in green band and the HH/HV backscatter ratio in the blue band for all the study areas. All data are in ITM projection

The false color composites of the mosaicked backscatter images for all the areas for one year (2007) are shown in figure 3.5. Forests appear in greenish yellow color, water bodies in blue and agricultural and peatlands are in varying shades of purple – in Area2 more peatlands can be observed on the hilly terrains in shades of purple and red. Most of the agricultural activities in Ireland take place in the South Eastern parts of Ireland and hence in Area1 and Area2, more of the purple and blue shades can be observed.

3.3.2 ALOS -2 PALSAR-2

ALOS-2 was launched on May 24th, 2014 after ALOS became dysfunctional in 2011. This L-band satellite also contains three remote sensing instruments AVNIR-2,

PRISM and PALSAR-2. The PALSAR-2 sensor with a reduced revisit cycle of 14 days has three modes – Spotlight mode, Stripmap mode and ScanSAR mode. For this research, stripmap FBD mode data were used with HH+HV polarization bands with an incidence angle of 36° (off-nadir angle of 32.7°). Similar to PALSAR data, all PALSAR-2 data were acquired as level 1.1 SLC products. A total of 150 PALSAR-2 images were made available by Japan Aerospace Exploration Agency (JAXA) following the successful evaluation of the proposal submitted to the 6th Research Announcement for ALOS-2 (ID: 3342).

With the launch of this satellite in 2014, images from 2015 and 2016 were ordered over the same study areas chosen for ALOS PALSAR data processing to extend the forest monitoring algorithm to 2015 and 2016 and thereby evaluate the transferability of the algorithm to the new sensor. The available KML files covering the study areas are shown in figure 3.6.

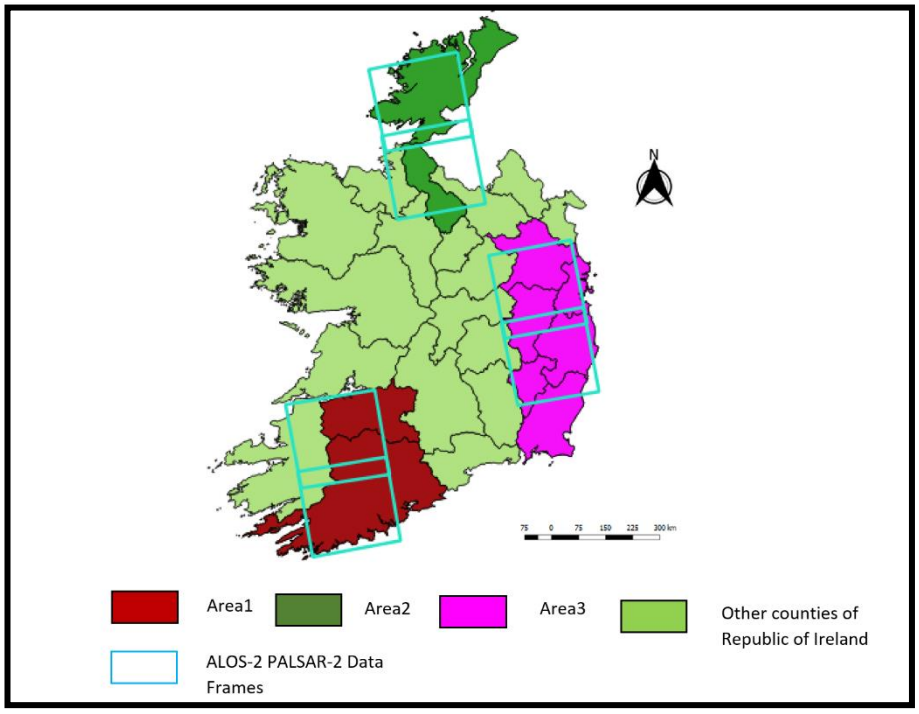

Figure 3.6: ALOS-2 PALSAR-2 data frames that were ordered; the square boxes are the data frames covering the study areas

The frames are presented in different colors to highlight the overlapping areas between them. The image dates and other characteristics are given in the Appendix.

While the FBD ALOS PALSAR datasets were available consistently over the summer months for the period 2007-2010 as discussed in section 3.3.1, the FBD mode of ALOS-2 PALSAR-2 sensor was available with infrequent acquisitions (~1-2 observations per year) over Ireland. This is because of the particular global data acquistion plan put in place by JAXA. Therefore, only winter images were available in some parts of the study areas along with autumn images in other parts of the study area.

3.3.2.1 ALOS-2 PALSAR-2 pre-processing

The PALSAR-2 datasets with dual polarization (HH, HV bands) and incidence angle of 36° were processed using the Sentinel Application Platform (SNAP) version 7.0 as the version of SARscape licensed by the Department of Geography did not support the processing of PALSAR-2. With 1 look in range and 2 looks in Azimuth, co-registered, speckle filtered, calibrated and geometrically corrected backscatter γ° images were generated using the OSi 10m DEM. The 8×8m spatial resolution images were mosaicked and clipped to the area extent corresponding to the areas of ALOS PALSAR processing for further processing and analysis. The false colour composites of the backscatter images for all areas are shown in figure 3.7.

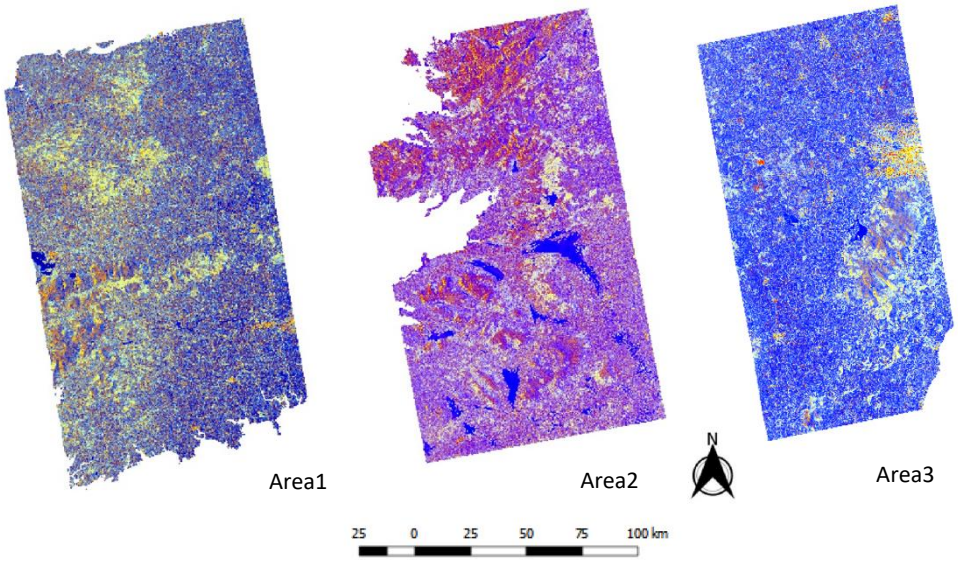

Figure 3.7: PALSAR-2 false color composites with HH backscatter in red band, HV backscatter in green band and the HH/HV backscatter ratio in the blue band for all the study areas. All data are in ITM projection

3.4 Reference datasets

To evaluate the results generated by the forest disturbance monitoring algorithm and to aid their interpretation, reference datasets were acquired from several sources.

1) **Forestry12 and PrivateForests2016 from Forest Service:** The Irish Forest Service has been providing forest datasets in Ireland since 1995 *(Gallagher et al., 1999)*. The first dataset was known as the Forest Inventory and Planning System (FIPS) and was derived for the period of 1993-1997 from automatic classification of satellite imagery and on-screen interpretation of Landsat TM imagery (1993-1997), panchromatic orthophotos (1995) and the OSi 25" map series. A new dataset (FIPS98) was generated in 1998, in which private afforestation records for plantations in receipt of grant aid were appended. The subsequent updates were made in 2007 (Forestry07) and 2016. An updated dataset Forestry12 was ordered which appended Forestry07 and afforestation records from 2008-2012. The current dataset is called PrivateForests2016 which consists of newly afforested areas (grant aided) appended to the FIPS98 dataset. The update to the FIPS forest cover which began in 2014 is the PrivateForests2016 datasets which consists a of forest cover layer for the private estate. Access to these datasets was acquired through DAFM. These datasets are used for generating forest cover maps in chapter 4 and 6 of the thesis.
2) **Felling information from Coillte:** Coillte is Ireland's semi-state forestry company owning 7% (440,000 ha) of Ireland's land which represents almost 50% of the country's forest estates. It's harvest information which comprises of spatial information on clear felling was necessary to validate the disturbance results calculated through the algorithm developed in this project. Shapefiles of felled areas for the years 2007-2010 and 2015-2016 over the study areas were acquired from Coillte following completion of a data agreement. Two main files namely MU_Felled (Minimum Unit Felled) and SUBS (sub compartments) were received for the study areas. The MU_Felled shapefile contained attribute information on the felled year and the area felled; details on the forest species and planting year could be obtained from the SUBS shapefile. These datasets are used to validate the SAR derived clear-fells in chapter 5 and 6 of the thesis.

3) **Land Parcels Identification System (LPIS) from DAFM:** The LPIS is a spatial database developed by the DAFM with more than 1.3 million land parcels. Spatial information on peatlands and croplands over the study areas were acquired to aid land cover classification. This dataset is used in chapter 4 and 6 of the thesis.
4) **The Co-Ordinated Information on the Environment (CORINE):** In Ireland, the Environmental Protection Agency (EPA) is responsible for conducting the CORINE Land Cover (CLC) mapping process. The dataset updated in 2012 (CLC2012) and 2018 (CLC2018) were used to mask urban areas from classification. This dataset was also used as reference data for water and grassland classes to aid classification. The datasets contain 44 classes with a Minimum Mapping Unit (MMU) of 25 ha. These datasets are used in chapter 4 and 6 of the thesis in which the urban areas are masked before land cover classification.

Part II

MAPPING AND CHARACTERISING FOREST DISTURBANCES USING SUPERVISED MACHINE LEARNING AND UNSUPERVISED CLASSIFIERS – TESTED AND APPLIED ON TWO SENSORS

Chapters 4 and 5 – Algorithm tested on ALOS PALSAR sensor data

Chapter 6 – Algorithm applied on ALOS-2 PALSAR-2 sensor data

Chapter 4

Mapping the Fragmented Forest Covers of Ireland – A Systematic Approach

"A breakthrough in machine learning would be worth ten Microsofts" – Bill Gates

4.1 Introduction

Large scale mapping of forests on a global level has been performed by some recent research such as *Kempeneers et al., (2013); Caccetta et al., (2012); Hansen et al., (2013); Bartholome and Belward, (2005); Hansen et al., (2010); Rosenqvist et al., (2000)*; many studies have been carried out on European forests *(Rosenqvist et al., 2004; Quegan et al., 2000; Pekkarinen et al., 2009; Wilkinson et al., 1995)*. Most forest studies using SAR have been done on dense forest covers such as the Brazilian Amazon *(Walker et al., 2010)*, dense tropical Asian forests *(Achard et al., 2001; Shimada and Isoguchi, 2002)*, Siberian forests *(Wagner et al., 2003)* and African forests *(Ryan et al., 2012)*. Relatively fewer studies have been done on fragmented and sparse forest covers existing in Ireland.

As discussed in chapter 2, the algorithm developed in the current project for mapping and monitoring forest disturbances in Ireland comprises of both supervised and unsupervised classification approaches; this chapter describes the Random Forests machine learning supervised approach to map forests in Ireland. The main objective of the present study is to investigate the potential use of dual-polarized (HH, HV) L-band SAR data in mapping the fragmented forests of Ireland. A systematic methodology was developed and implemented on Area1 and then it was transferred on the other study areas (Area2 and Area3) to evaluate the robustness of the algorithm for a possible application on a national scale.

4.2 Methodology

A systematic methodology was adopted for the present work – the end product was a forest/non-forest classification map. The approach consists of various steps such as analysis of the SAR backscatter from different targets (forests, non-forests[6] and urban), choosing the most relevant input variables, collection of training samples, RF classification and accuracy assessment. A flow diagram is shown in figure 4.1 displaying the three stages to the process chain. Each step of the algorithm is discussed in the following sections.

[6] All classes such as water, cropland, grassland and peatland excluding forests. Urban category was treated as a separate class

Process chain 1: Data preparation for classification

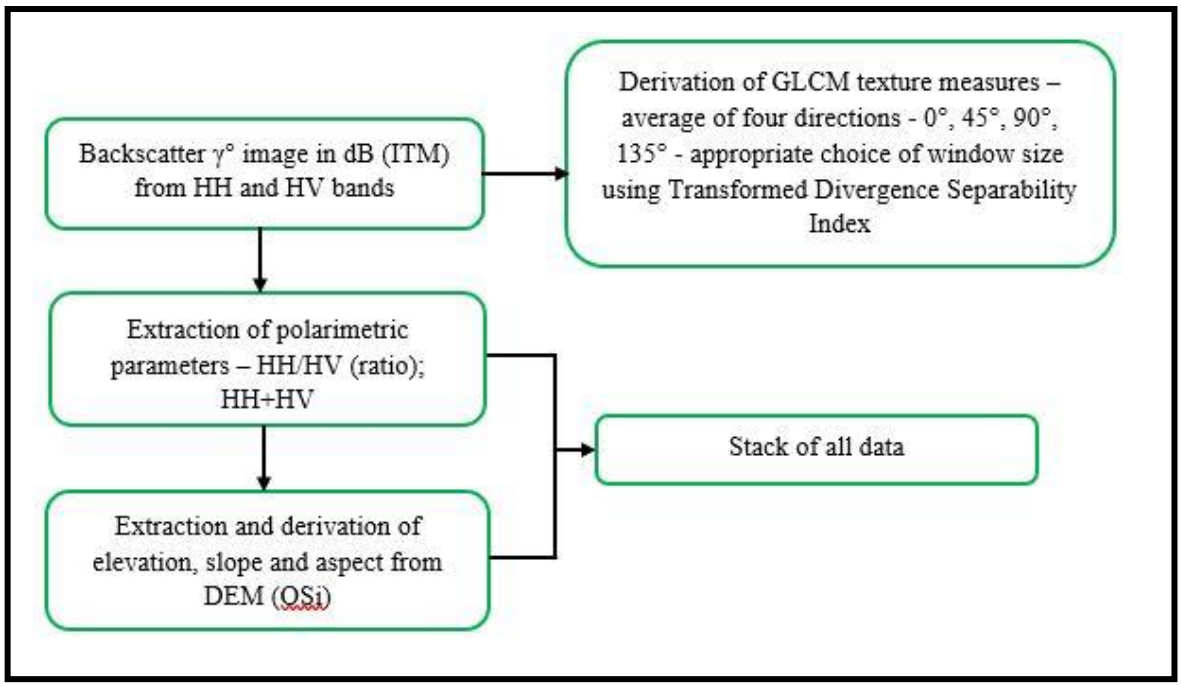

Process chain 2: Collection of Training samples

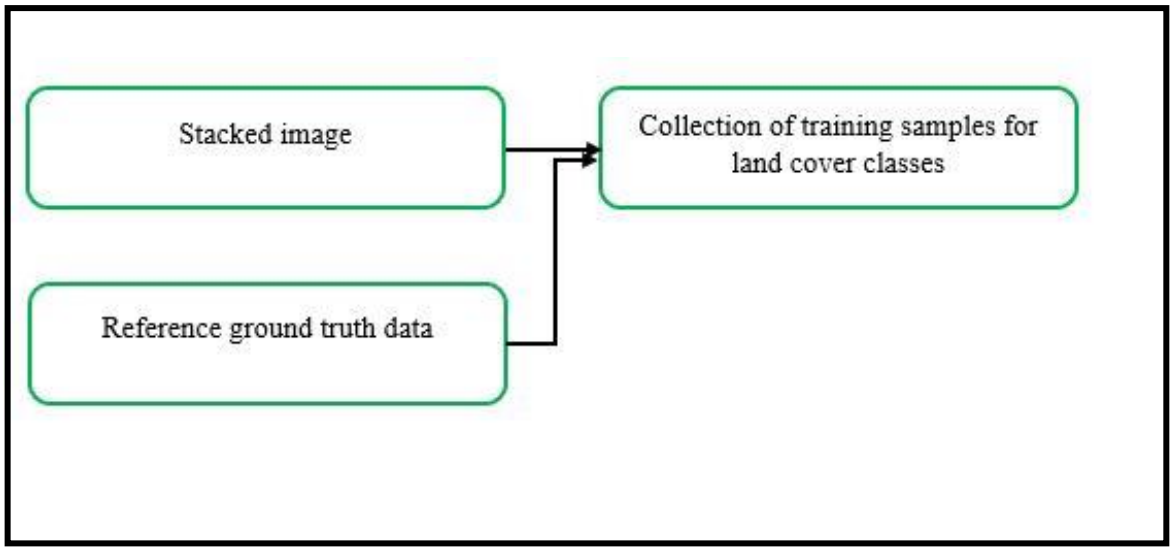

Process chain 3: Random Forests classification and generation of forest/non-forest maps

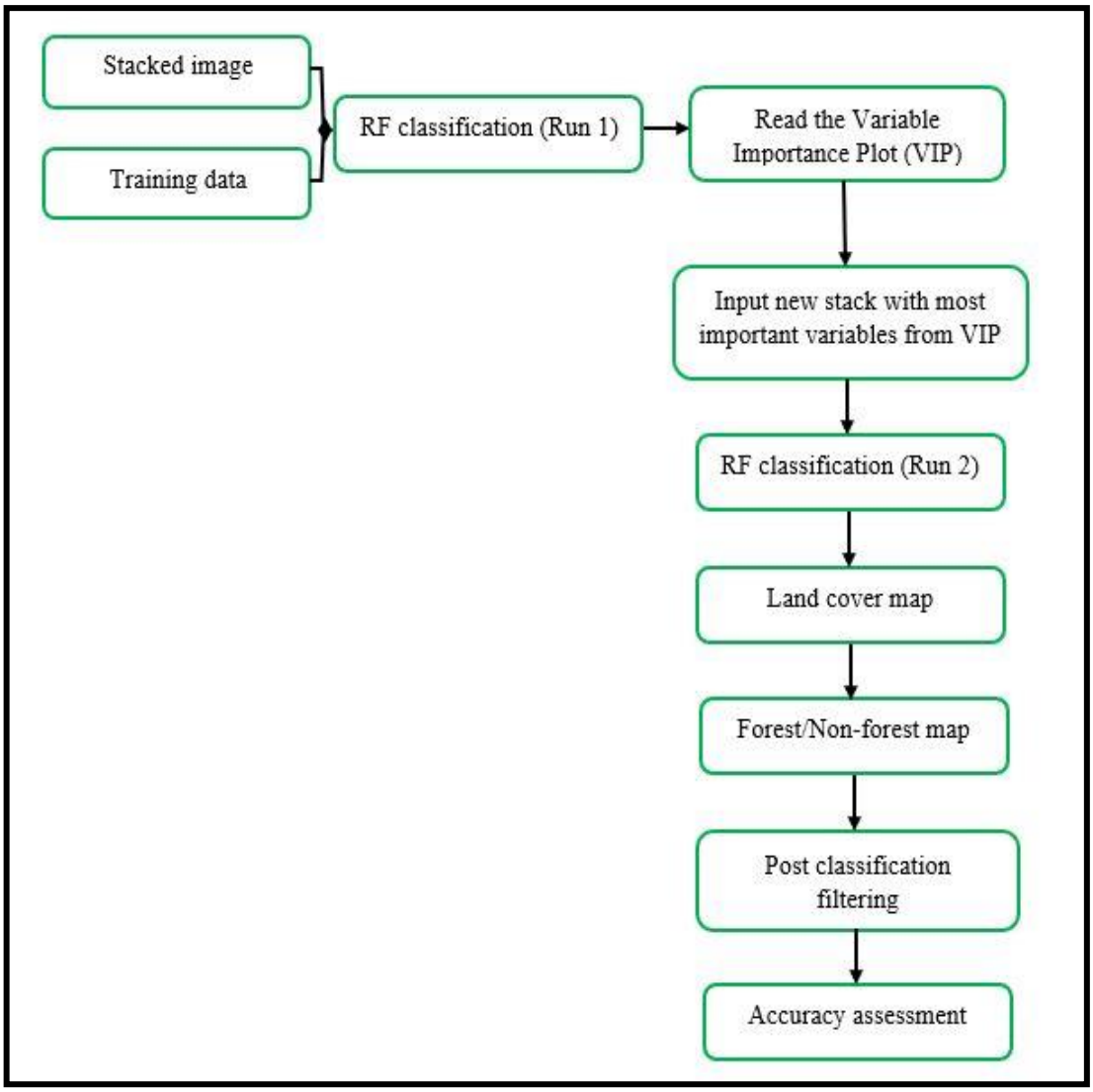

Figure 4.1: Flow diagram displaying three stages of methodology

4.2.1 Backscatter analysis of PALSAR images

The backscatter of the pre-processed PALSAR (from Chapter 3) images was analyzed to understand the reflected power obtained from forests and non-forests. This was performed as a preliminary step before classification to understand the behavior of forest and non-forest classes from L-band HH and HV PALSAR images. While HV polarisation occurs due to volume scattering from forest canopy, branches, stems and leaves leads to HV polarisation, HH polarisation is more sensitive to surface scattering observed from forest floor from which information about soil moisture can be gained. It was noted that the volume scattering from forests and double bounce and corner

reflections from urban areas give similar backscatter values and hence may lead to misclassification of forests.

Using ground truth data from Forestry12 dataset, HV and HH intensity values from 500 forest pixels were collected; 500 non-forest (excluding urban) pixels using Bing Maps and with the aid of CORINE 2012 data 500 urban pixels were extracted from both HH and HV SAR images. This collection was done in ENVI using the Region of Interest (ROI) facility available. Boxplots were plotted for all three classes and the distribution of the backscatter coefficient values for the forests, non-forests and urban classes are shown in figure 4.2. This analysis was performed for each of the three study areas. From the boxplots it is evident that forest and non-forest classes are separable from each other with an overlap between the 1st quartile of forest class and 4^{th} quartile of non-forest class, causing confusion in classification. This pattern is visible for both HH and HV bands across all study areas. More discrimination can be observed in HV polarization than HH polarization with a difference of 8dB between the two classes. Considering urban class, approximately 50% of the data lie within the second and third inter-quartile range of the forests suggesting higher level of confusion in separating these classes. The received signal gets depolarized from urban areas due to double bounce and corner reflections displaying a similar behavioral pattern to that of trees. This could lead to false classification of urban areas as forests. One possibility in avoiding such errors is to use external ancillary data such as the CORINE to mask out the urban areas *(Dostálová et al., 2016)*. This approach was adopted for the study and using the CORINE 2012 urban mask, urban areas were masked out from all the study areas. With the aid of CORINE technical guide *(Bossard et al., 2000)*, CORINE land cover classes – Continuous and Discontinuous Urban fabric, Industrial or Commercial Units, Sports and Leisure Facilities, Airports and Mineral Extraction Sites were extracted and masked out from the SAR imagery.

Nomenclature of classes within the boxplots

- For = Forests
- NF = Non-Forests
- Urban = Urban areas

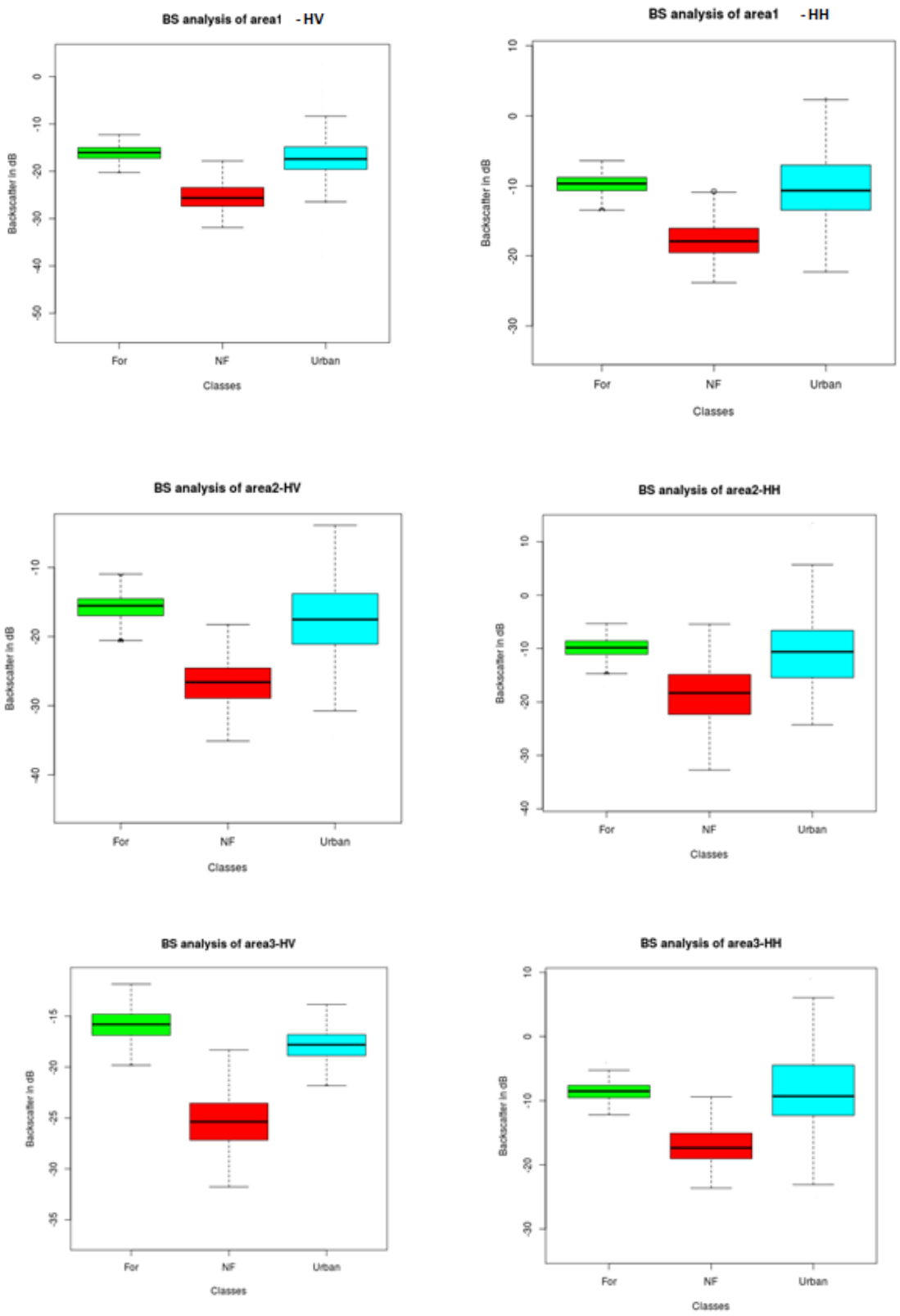

Figure 4.2: Boxplots of L-band HH and HV backscatter γ^0 for forest, non-forest and urban samples for study area1, 2 and 3

4.2.2 Data preparation for classification

Several variable bands were prepared and stacked together for classification. These variables were evaluated to determine their contribution to classification accuracies and then the most relevant variables were selected for the final run of classification. Through analysis of radar HV and HH backscatter (section 4.2.1), it was understood that cross-polarized images are better for discriminating between forests and non-forests and hence only HV backscattering coefficient was used for classification. The different variables that were prepared for initial classification were HV backscattering coefficient (γ^0), GLCM texture measures based on HV, polarimetric ratio (HH/HV) and HH+HV band, elevation from OSi DEM, and slope and aspect parameters derived from the DEM.

4.2.2.1 Introduction to non-forests classes

The focus of this study is to explore the ability of L-band SAR to distinguish between forests and non-forests on a fragmented landscape. To understand further the errors that arise in forest classification the individual classes that make up the non-forest classes (cropland, peatland, water and grassland) were also assessed in this study. The rules for forest carbon reporting are done according to the strict guidelines set out by the IPCC GPG. To adhere to the rules, the classes for classification were chosen from the IPCC guidelines *(IPCC, 2000)*. The UNFCCC invited the IPCC to produce good practice guidelines for land-use, land-use change and forestry (LULUCF) in 1998 *(IPCC et al., 2003)*. The GPG 2000 provides guidance on the selection of suitable methods to identify and represent land areas. This information on land is required for carbon-stock estimation and removal of GHGs associated with the LULUCF. Six broad categories of land have been defined by the IPCC GPG2000. The categories are (i) Forestland (ii) Cropland (iii) Grassland (iv) Wetlands (water and peatbogs) (v) Settlements and (vi) Other land – bare soil, rock, ice and unmanaged land areas. These classes are a mixture of land cover (Forestland, Grassland and Wetlands) and land use (Croplands, Settlements) categories. However, for convenience, these are referred to as land cover categories in this thesis. For this study, the classes have been slightly modified depending on the availability of reference data – Forestry12 for forestry, LPIS for Cropland, Grassland and Peatland, CORINE 2012 for water and settlements. No valid reference was available for the category (vi – other land) and also in Ireland

there is limited coverage of these classes, especially in the selected study areas. Therefore, for this study, classification was done only based on the first four categories (with settlements masked out) and the final category was amalgamated with the other non-forest classes.

4.2.2.2 GLCM Texture measures

Texture is a variation of the intensity of the surface. It is a measure to statistically quantify surface smoothness, coarseness and regularity *(Davis et al., 1979)*, and can be used to increase accuracy of classification *(Dekker, 2003)*. GLCM (R. M. Haralick et al., 1973) functions, the most common of all the texture measures *(Longepe et al., 2011; Li et al., 2012; Lu et al., 2007)*, were applied to extract textural features. The GLCM contains information about the frequency of occurrence of two neighboring pixel combinations in an image *(Gebejes and Huertas, 2013)*. Eight textural parameters (Mean, Variance, Homogeneity, Contrast, Dissimilarity, Entropy, Second Moment and Correlation) were computed using window sizes starting from 3×3 up to 19×19 in order to identify the most appropriate window to aid the classification. For a more detailed description of each of the texture measures, *Clausi and Zhao, (2002); Albregtsen, (2008)* can be referred.

Choosing suitable parameters such as direction, grey-level quantization and window size is crucial when using texture measures. The parameters chosen were

a) **Direction:** To describe the relation between neighboring pixels, four separate GLCMs in four directions - 0^0 (horizontal neighbors), 45^0 (NE-SW), 90^0 (vertical), 135^0 (NW-SE) were derived. The texture value for an individual pixel was then derived as the average of the texture values derived in all the four directions. This is done in order to derive a matrix which is independent of direction *(Albregtsen, 2008)*.

b) **Grey-level quantization:** In computing the GLCM, the number of grey levels is an important parameter. The quantization is done to merge similar grey levels in the image and thus reduce the noise to some extent. The textural information is more accurate with more quantization levels, but higher levels include more computation time and smaller levels lead to loss of information. Considering the trade-off between computation time and preservation of information, a quantization level of 64 was adopted in the present work. More

information on grey-level quantization can be found in work done by *Soh and Tsatsoulis, (1999).*

c) **Texture moving window size:** The statistical separability of classes can be used as a criterion for window size selection *(Ferro and Warner, 2002)*. To select the texture window size appropriate for the study, separability analysis was conducted using Transformed-Divergence (TD) distance as shown by *Mishra et al., (2014); Bindel et al., (2011)*. The TD distance is a measure of statistical distance between classes and varies between 0 and 2.0. Values greater than 1.9 indicate that the classes have a good separability *(Elsharkawy et al., 2012)*. From the SAR image, training samples were derived for the five classes. The TD distance was calculated between forest and non-forest classes individually for each window size to observe the distinction between forests and other classes. The window size that gave the maximum separation was chosen and used to extract GLCM measures for classification. These classes were chosen according to the IPCC GPG2000 as explained in section 4.2.2.1 using the reference data available for each class.

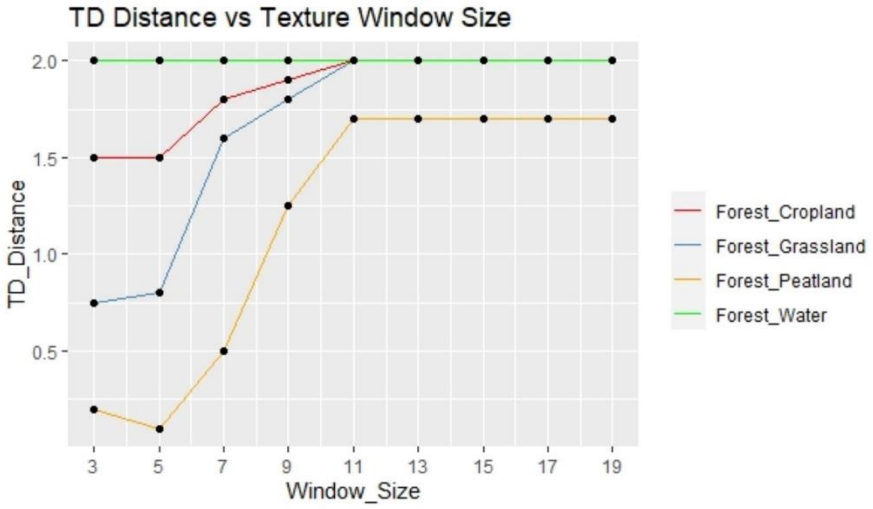

Figure 4.3: TD distance showing separability between classes for texture window

According to figure 4.3, forest is separable from water by all the window sizes with a maximum separability distance of 2 between the classes. For the separability between forest and grassland/peatland/cropland, the values become stable from window size 11. The seperability between forestland and peatland saturates at 1.75 from window size 11. This suggest that forests are not clearly separable from peatlands. The high

moisture content in peatlands leads to confusion in forest classification. Texture measures are of more use in classification if the within-class texture of each class is uniform and different from the other classes. Hence, larger windows take into account the variability of the texture elements, thus giving a stable measure, but blurred edges. Smaller windows have a reduced edge effect but they do not provide uniform or stable within-class texture values. A balance needs to be achieved between the two parameters while choosing the appropriate window size *(Wen et al., 2009)*. Based on this analysis, a texture window of size 11×11 was chosen to extract GLCM texture measures required for classification.

4.2.2.3 Polarimetric discriminators

The proportion of horizontally and vertically polarized components in the received backscatter can vary for different targets depending on the target orientation towards the radar sensor look direction and the transmitted polarization *(Patel et al., 2006)*. Studies by *Cable et al., (2014); Attarchi and Gloaguen, (2014); Turkar et al., (2012)* have shown the use of multi polarization SAR channels for effective land cover classification. Radar polarimetric information (dual or full) can be used to study land use and land cover information using polarimetric discriminators (ratio, addition, etc) which are effective in characterizing the different types of scattering mechanisms *(Dusseux et al., 2014a)*. Since these combinations carry extra information useful for decomposing the scattering mechanisms, two combinations, the ratio HH/HV and HH+HV, were calculated and added for classification.

4.2.2.4 Elevation, slope and aspect from DEM

Terrain has been found to affect the spatial and temporal vegetation distribution significantly *(Koppad and Janagoudar, 2017)* and is therefore an important factor to consider in addition to texture, especially in mountainous areas. *Dorren et al., (2003); Shrestha and Zinck, (2001); Peng et al., (2005), Albright et al., (1998)* have used terrain information such as elevation, slope and aspect for their Land-Use/Land Cover classification and have observed reduction in the confusion between different classes. Terrain parameters (elevation, slope and aspect) were generated from the OSi DEM and were added as additional bands in the classification.

4.2.3 Training data collection

A stack derived from the 2010 SAR image with the different input bands was used to train the classifier. This date was chosen because the reference for different classes were available for the year 2012, and the 2010 image was the closest to this in time. Using the training data from this image, the classifier was trained and the other images from the years 2007-2009 were classified subsequently. The training samples were collected from five different classes using the reference data available for those classes – forestland (Reference data: Forestry12), cropland and peatland (LPIS 2012), grassland and water (CORINE 2012, BING Aerial imagery).

To collect training data, the procedure requires training polygons and, based on a user-defined number of samples, pixels are randomly selected for each land cover type. The data value for that pixel is determined and these data are used to run the random forest model. A total of 5000 training samples were collected from the SAR 2010 image (forest = 3200; cropland = 300; grassland = 200; peatland = 650; water = 650). These made up a total of 3200 forest samples and 1800 non-forest samples. The location of training samples within Area1 is shown in figure 4.4. These boxes cover the five different landcover classes and user-defined number of pixels were randomly selected for each class from the boxes.

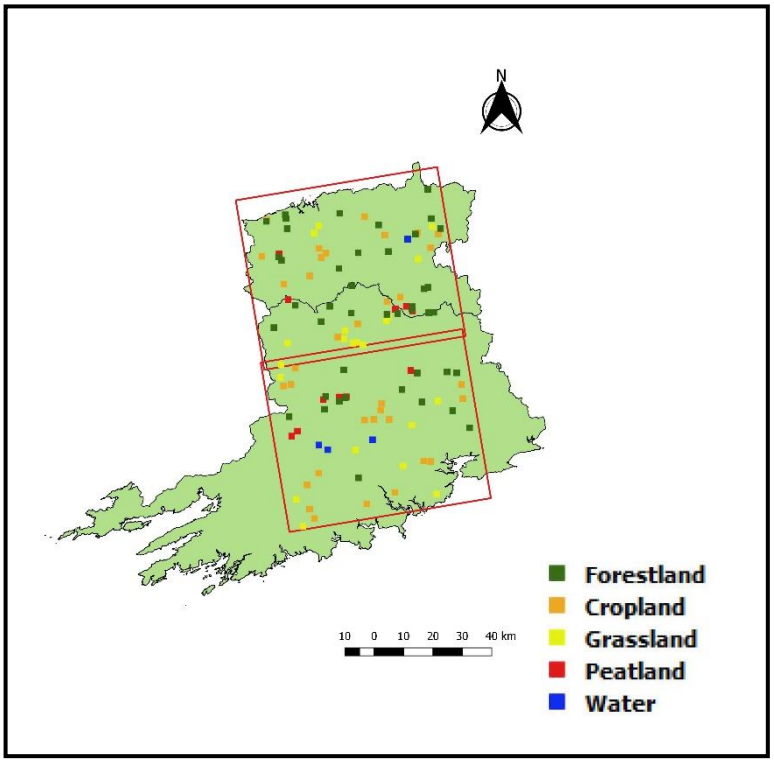

Figure 4.4: Location of training samples for Area1

4.2.4 Random Forests Classification

A Random Forests machine learning classifier was used in this study to classify the forest and non-forest classes on a SAR image. The algorithm creates a set of decision trees from a bootstrap sample of training data (randomly selected subset of training dataset). It builds a committee of a number of individual decision tree classifiers and the votes cast by each tree are later combined to make a decision based on the majority votes derived. It is a group of "weak learners" coming together to form a "strong learner". From an individual tree, when the training set is drawn by sampling with replacement, one-third of the cases are left out of the sample (this is the out-of-bag-OOB data). Estimates of variable importance plots are also derived using this OOB sample *(Brieman and Cutler, 2002).*

The main reasons why a RF classifier was chosen are

1) It can handle several input variables
2) It gives the estimate of which variables are most important to the classification via a graph which shows the strength of each variable in the model, giving a

better insight into which variables are the most relevant for the classification and reducing data redundancy *(Cutler et al., 2007)*. It is crucial not to have either too few or too many variables that will not separate the data or over explain the differences *(Zhang et al., 2017; Wang et al., 2015).*

3) There is no need for cross-validation or a separate test for validation as this is done internally through the OOB error estimate which is an estimate of the classification accuracy. When the random forests algorithm is run, about one-third of the training data are held back internally for each tree to be used for testing accuracy.
4) Robustness against over-fitting of data
5) Being non-parametric in nature, it does not assume any statistical distribution of data

RF classification was applied to the stack of radar backscatter coefficient (γ^0), GLCM texture measures (from window size 11×11), HH/HV, HH+HV, and ancillary data - elevation, slope and aspect. The variable importance plot for each year of data for Area1 is displayed in figure 4.5. Two indices to estimate the importance of the variables for classification are considered widely in literature *(Han et al., 2016; Archer and Kimes, 2008; Rodriguez-Galiano et al., 2012)* – Mean Decrease Accuracy (MDA) and Mean Decrease Gini (MDG). For this study, MDA was used as it is simpler to interpret and more robust, whereas MDG is relatively biased and unstable *(Strobl et al., 2007)* as it is a permutation based function. The MDA is calculated during the OOB estimation phase. The more the accuracy of the classification decreases due to the exclusion of a single variable, the more important is that variable for classification. To assess the importance of each variable, the algorithm removes one of the variables while keeping the rest of the input variables constant, and it estimates the decrease in accuracy that has taken place by removing that variable by calculating the OOB error. The plot in figure 4.5 shows the variables on the y-axis and their importance scores on the x-axis. The most important variables are shown starting from the top. The variables with large "MeanDecreaseAccuracy" are more important for classification of the data.

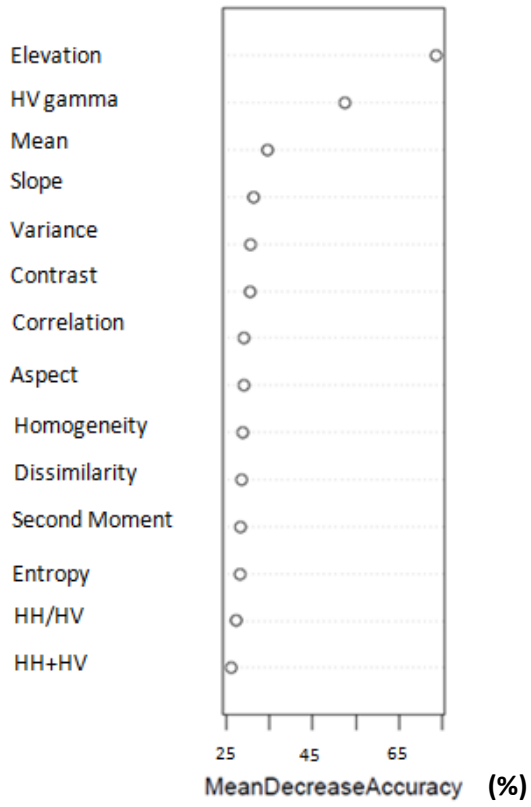

Figure 4.5: Variable Importance Plot for 2010 to select the optimal variables for classification

Elevation is the most important variable according to the plots of each year, with the classification accuracy reduced by 70% if elevation is removed. HV gamma, slope and mean GLCM measure take the next three most important positions. SAR backscatter coefficient and texture measures can be regarded as relevant to SAR image classification as they are derived from the SAR image. Variables that are correlated can be eliminated to remove data redundancy and bias in the estimation of important variables. Elevation, slope and aspect are terrain related variables that are correlated to one another and are important controls on land use and land cover. Elevation shows a dominant response in the plot and it could drive a biased classification with a disproportionate impact on the outcome. Importantly, changes in land cover between years would not necessarily be detected as the elevation remains constant, therefore, elevation was removed from the classification. *Balzter et al., (2015*) included slope and aspect from SRTM in classification and found to gain high accuracies. In order to take into account, the prevalence of forests on slopes and aspects and to incorporate the terrain element in the classification, these two variables were retained.

Considering the next most important variable – the mean texture measure, further investigation showed that it introduced an aggregating effect on classification, because of which there was an exaggeration of forest plot boundaries as shown in figure 4.6 under the red circles.

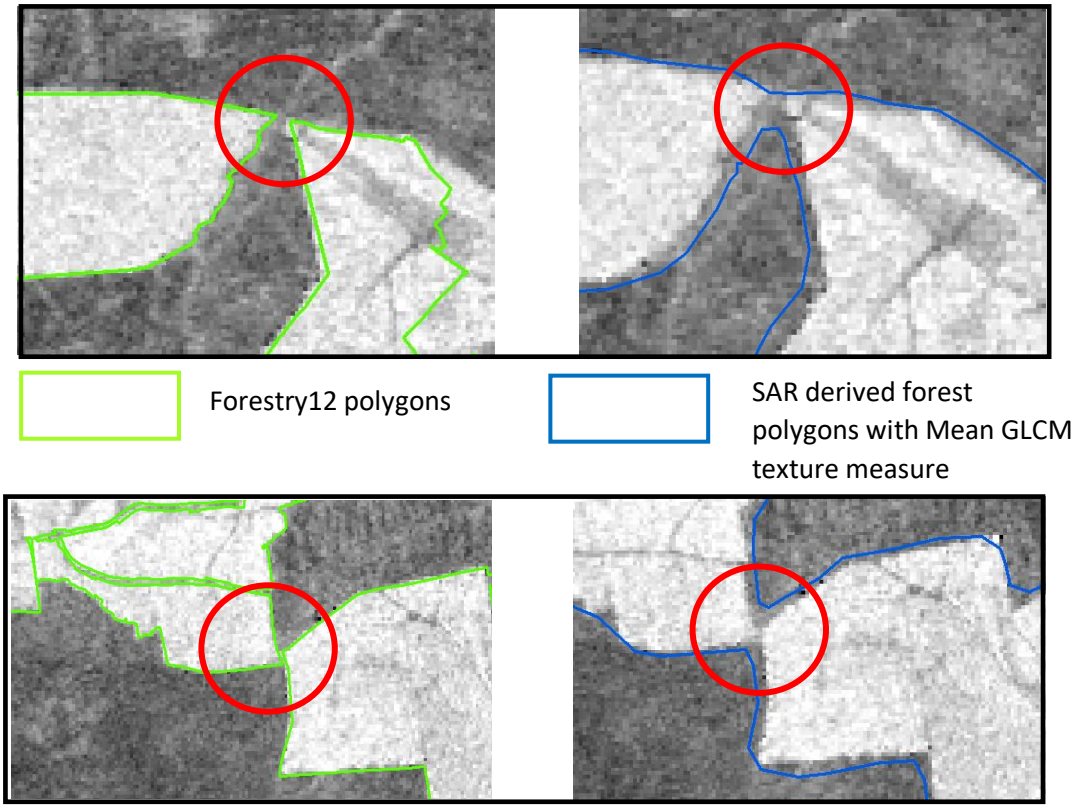

Figure 4.6: Effect of Mean GLCM texture measures on classification. The green lines indicate the forest boundaries of Forestry12 parcels (left images) and the blue lines refer to forest boundaries obtained by including the mean in RF classification (right images). The areas under the red circles show the "smoothing" effect of the mean filter.

The mean filter induces a smoothing effect by reducing the amount of intensity variation between neighboring pixels. One of the problems of including the mean filter for classification is that when the filter spans an edge, it will interpolate new values for the edge pixels, thus blurring the edge. Therefore, sharp edges or forest boundaries cannot be reliably obtained using the mean measure as part of the classification.

Texture is a measure of the variation of the surface smoothness, coarseness and regularity *(Davis et al., 1979),* in this case highlighting where there are differences in the backscatter intensity. The blurred boundaries and edges that induce error are

naturally handled by textures by detecting the various texture regions in the image and as a result forests, water bodies and urban areas are well characterized *(Kumar et al., 2015).* The variation in the image intensity levels is the primary cause of the difference in the order of texture importance in each plot, with the actual percentage values differing by only 2 to 5% between the texture variables. Due to these small differences in the percentages between the texture variables, all texture measures were included for the classification.

The last two variables (HH/HV and HH+HV), are consistently in the bottom positions in all the plots and identified as least important for classification by the RF classifier. As these have very limited impact on the accuracies, these variables were removed from further analysis.

4.2.5 Post-classification filtering

SAR backscatter images are characterized by speckle, which is not entirely removed by procedures such as multi-looking and speckle filtering, and the effect can still be seen on the further processed outputs in the form of single, or small clusters of, misclassified pixels. Therefore, it is important to perform another round of filtering on the output products. Small shrubs and hedgerows were removed by selecting a specific filter size through analyzing the connectivity of the originally classified forest pixels. As a first step, a majority filter was run on the classified map to eliminate single isolated pixels or noise. Next, seven post-classification filters were applied in ArcGIS using the nibble tool, which dissolved contiguous regions of 4 to 82 pixels, and the forest area and accuracy were calculated for each filtered map. Trial 1 started by dissolving 4 contiguous pixels, trial 2 dissolved 20 pixels followed by trail 3 with 32, trial 4 with 46, trial 5 with 59, trial 6 with 73 pixels and trial 7 with 82 pixels. Before filtering, the originally classified forest map estimated a forest area of 85,765 ha with an accuracy of 82.72% but dissolving 82 contiguous pixels gave an estimate of 81,795 ha with the highest accuracy of 87.74% compared to the other filters. In table 4.2, the impacts of different trials on the accuracy are shown.

Table 4.1: Impact of different post-classification filters on the overall accuracy

Filter Trials	Overall Accuracy
Trial1	83.91%
Trial2	84.22%
Trial3	84.80%
Trial4	85.13%
Trial5	86.11%
Trial6	86.52%
Trial7	87.74%

4.3 Classification results and discussion

4.3.1 Classification maps of area1 and visual comparison between Forestry12 and SAR derived forest polygons

The land cover map of Area1 with all classes and forest/non-forest maps for 2010 are shown in figure 4.7. Detailed analysis of the rest of the land cover classes is beyond the scope of the study. Therefore, focusing on forest and non-forest maps, a zoomed-in extent of an area on the border of counties Cork and Limerick is shown in figure 4.8. The Google Earth image of the same area is also provided for reference. The forest changes are clearly seen in each forest map under the red circles highlighting the changes in each year.

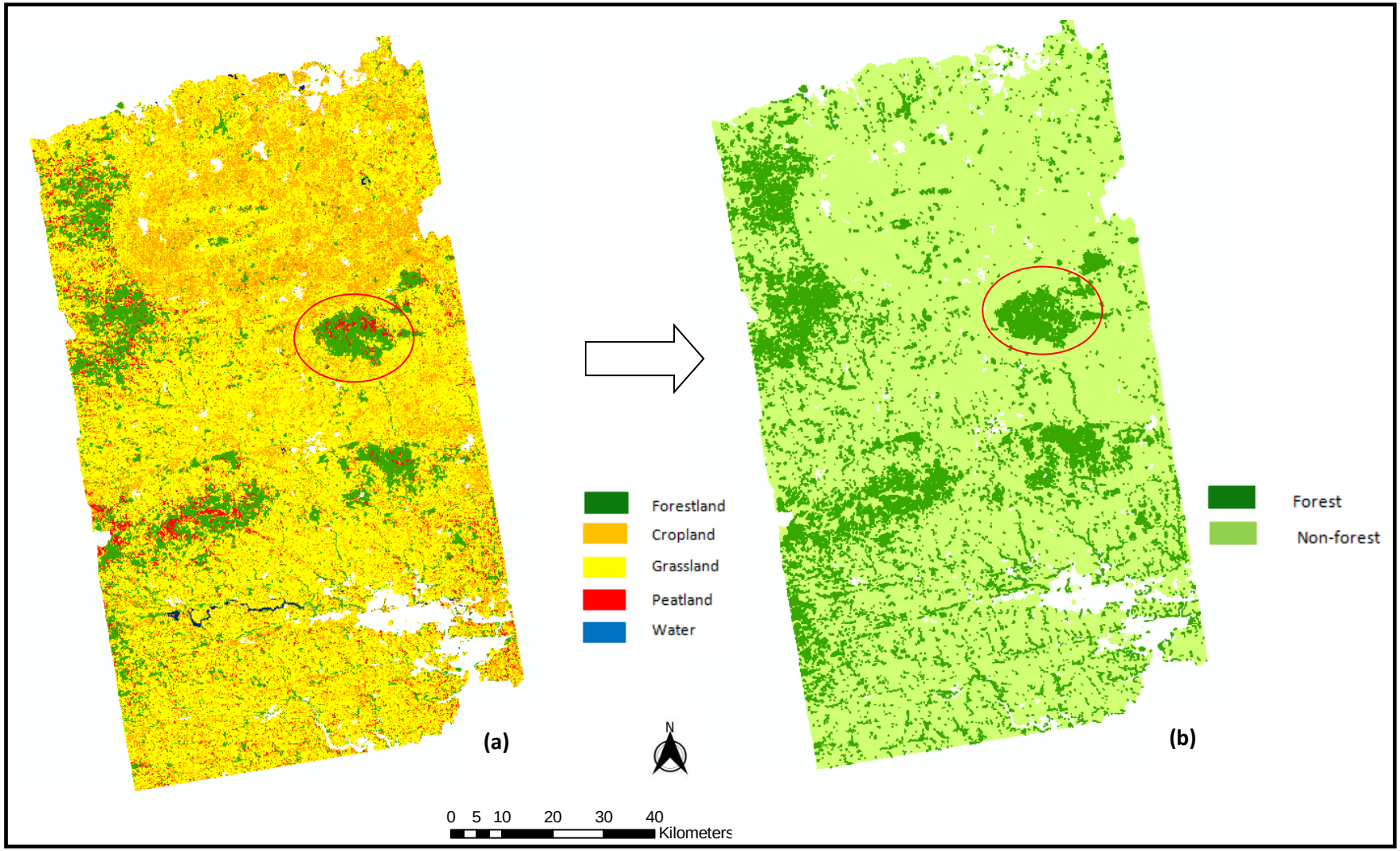

Figure 4.7: Land cover map (a) and forest/non-forest maps (b) derived from (a) from 2010 SAR image of Area1 (the red circle area is highlighted in figure 4.8)

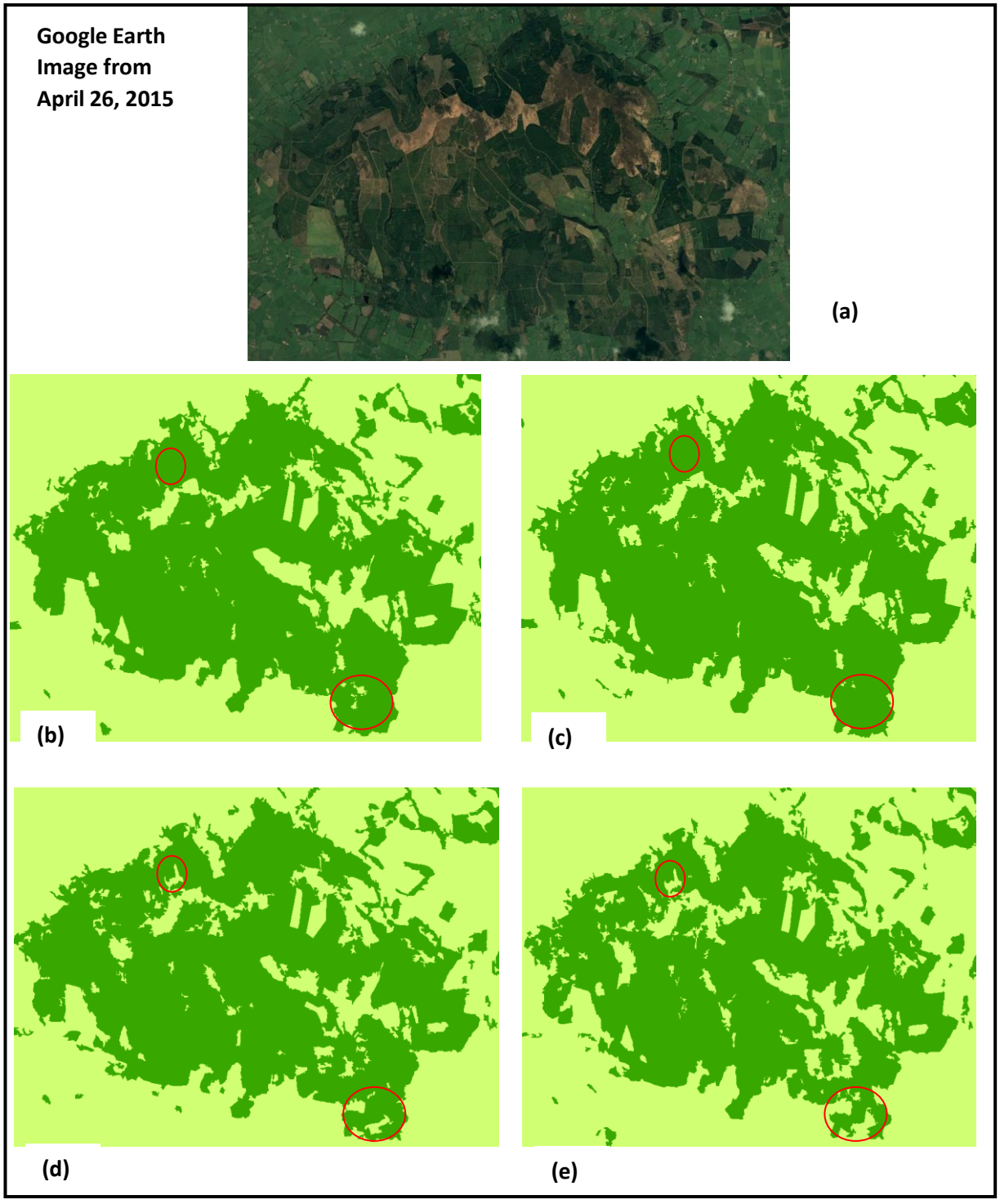

Figure 4.8: Zoomed-in extent of forest cover in area1 (b) 2007 (c) 2008 (d) 2009 (e) 2010; (a) is from Google Earth dated April 26, 2015; red circles highlight areas that undergo changes

A visual inspection was carried out between the Forestry12 polygons and the SAR derived forest polygons for the entire study area. An example from two different regions is shown in figure 4.9.

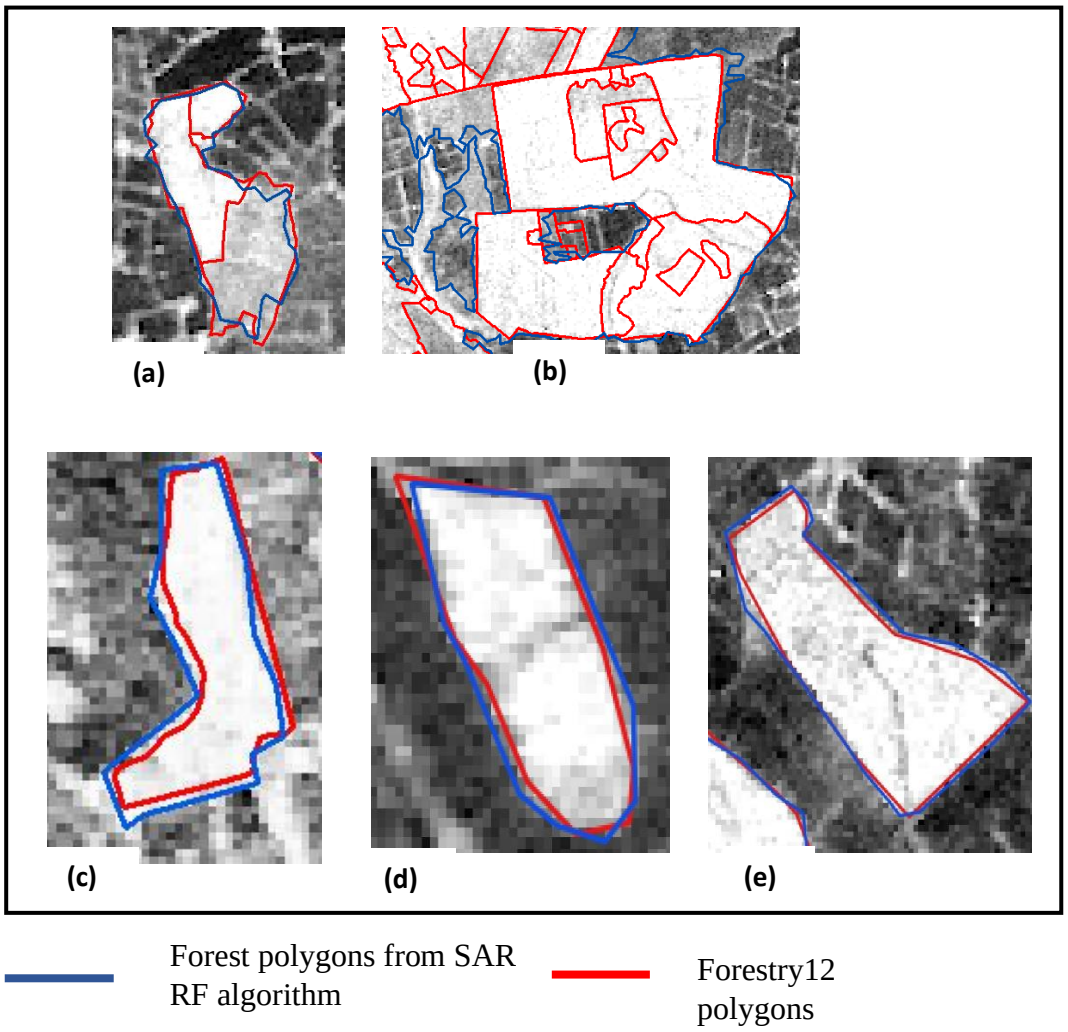

Figure 4.9: Zoomed-in extent of three regions displaying a visual comparison between Forestry12 polygons and SAR derived forest polygon outlines

The forest boundaries of both the datasets coincide visually – blue lines corresponding to SAR forest boundaries and red lines corresponding to Forestry12 polygons. Out of the 5035 SAR derived forest polygons, this visual analysis was performed for 55% of the total polygons and the boundaries were observed to be coincident between the two data sources. This percentage was a random choice which also gave a fair estimation as it covers more than half of the total percentage and was checked on polygons distributed spatially over the entire area. The examples in figure 4.9 are a typical representation of how well the two data sources match. The SAR image considers the entire forest polygon whereas the Forestry12 layer consists of compartments[7] and sub-

[7] A discrete forest area – can contain one or many forest parcels

compartments[8] and hence more polygons are seen. In the Forestry12 dataset, attributes such as Compartment numbers were missing for some polygons. For a simple and direct comparison, the Forestry12 internal polygons were dissolved and the comparison is explained in section 4.3.3.2 of this chapter. In figure 4.9(c), (d) and (e), the RF classifier for SAR image has generated a forest polygon that has a complete coverage of the forest parcel, while Forestry12 omits some of the boundary pixels, with over and under estimation of the boundaries a known problem within the Forestry12 dataset *(Department of Agriculture and Food and Forest Service, 2008)*.

4.3.2 Algorithm transferability to area2 and area3

The methodology developed for Area1 was applied to the other two study areas (Area2 and Area3). The training samples were collected from the stack of input variables and the locations of the samples are shown in figure 4.10.

[8] A homogenous forest unit with respect to forest class, area is at least 0.5ha, average width is greater than 40m.

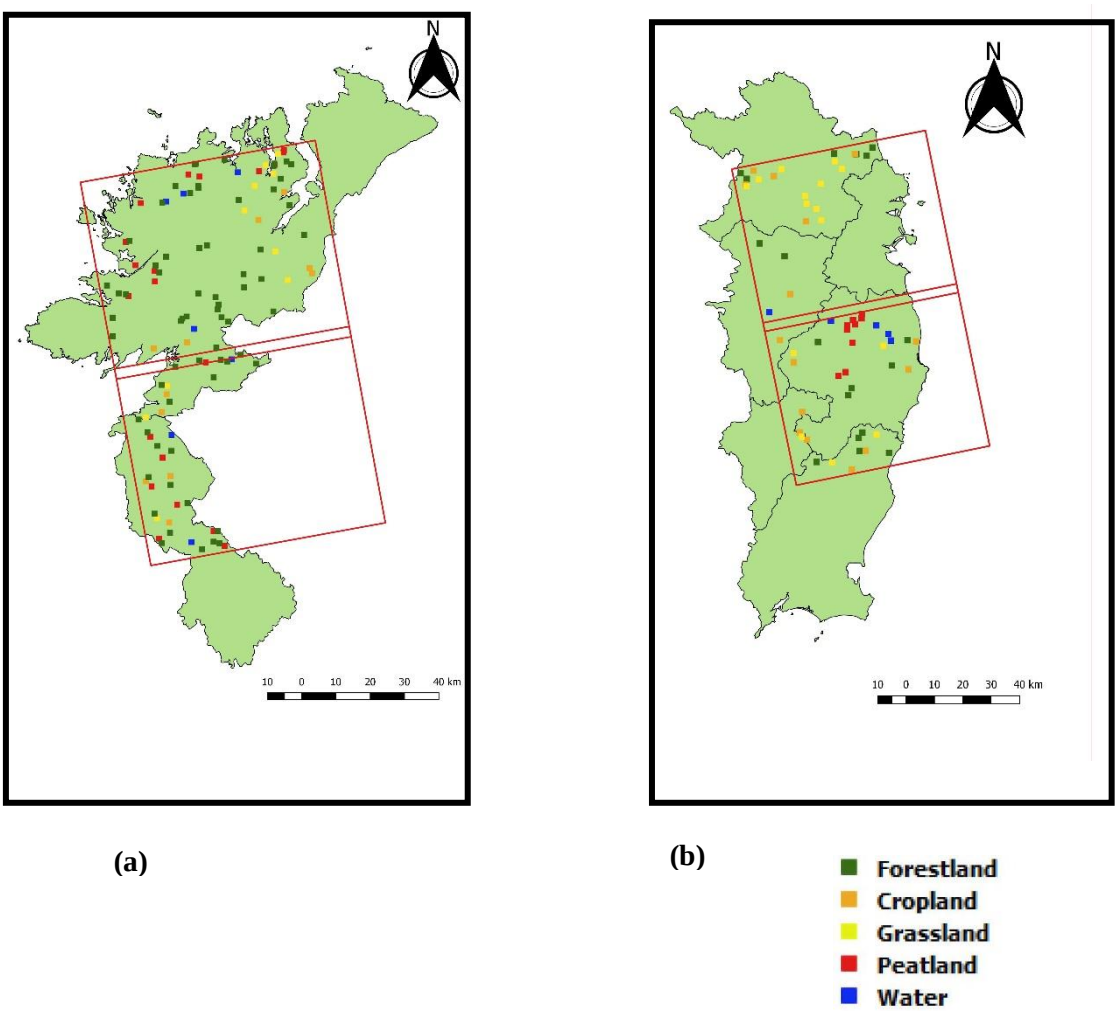

Figure 4.10: Location of training samples (a) Area2 (b) Area3

Using these training data from the 2010 image, 2007-2010 images of Area2 and Area3 were classified using the same approach followed for area1. The 2010 classified maps are given in figures 4.11 and 4.12 for both the study areas.

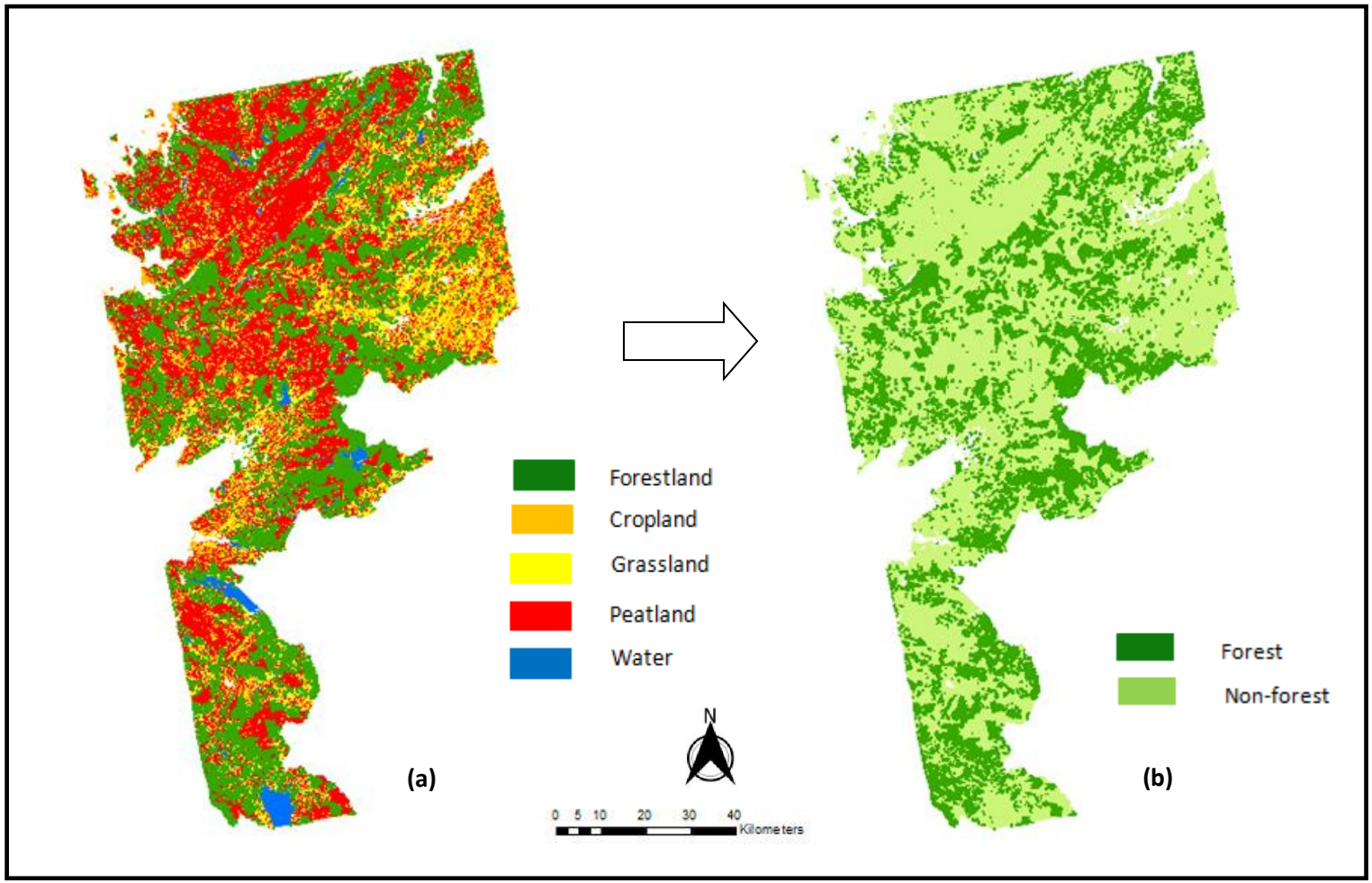

Figure 4.11: Land cover map (a) and forest/non-forest maps (b) derived from (a) from 2010 SAR image of Area2

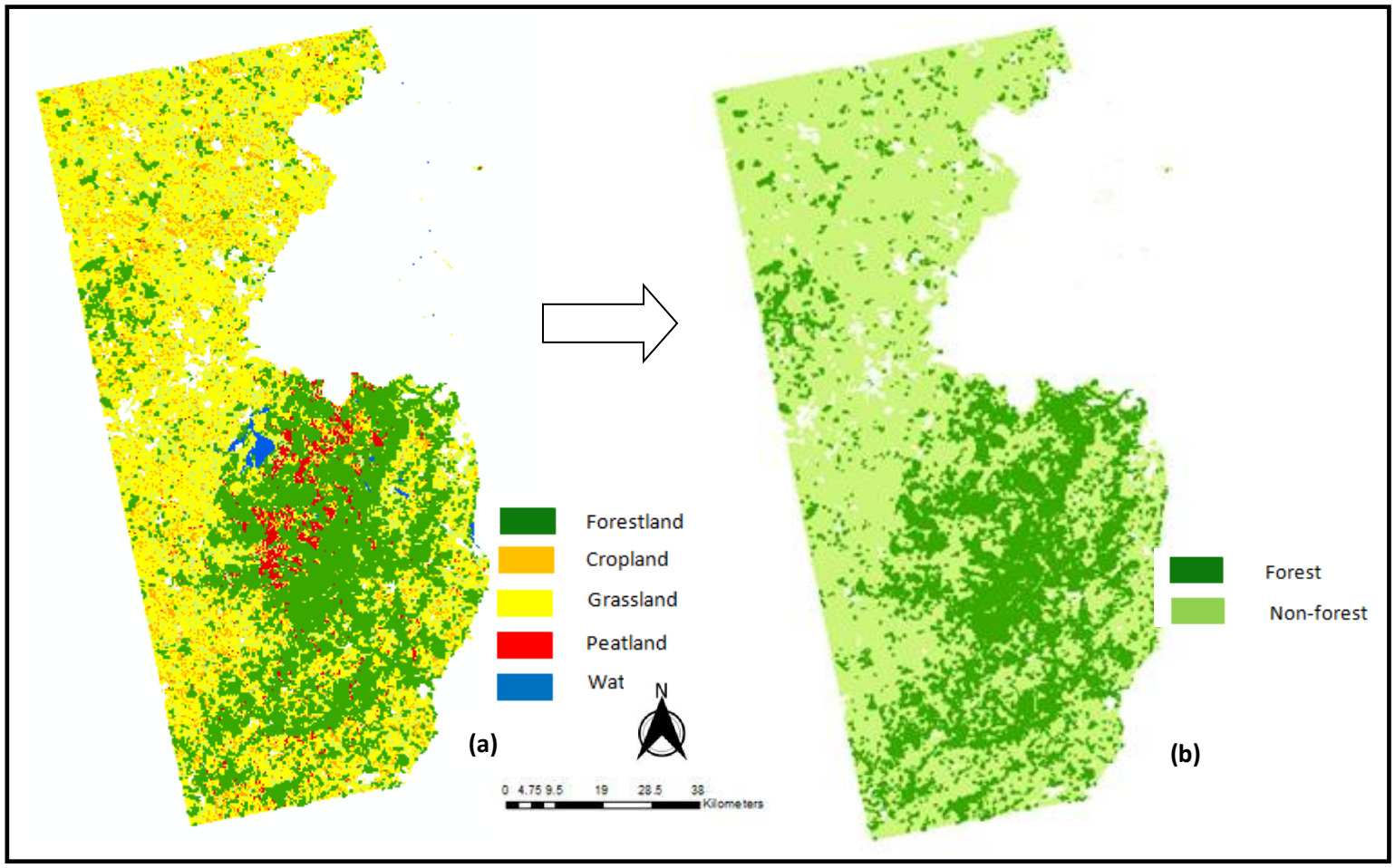

Figure 4.12: Land cover map (a) and forest/non-forest maps (b) derived from (a) from 2010 SAR image of Area3

Proceeding to the visual assessment of the forest polygons, figure 4.13 shows samples of forest areas (from four different regions) covered by the Forestry12 forest polygons and SAR derived forest polygons.

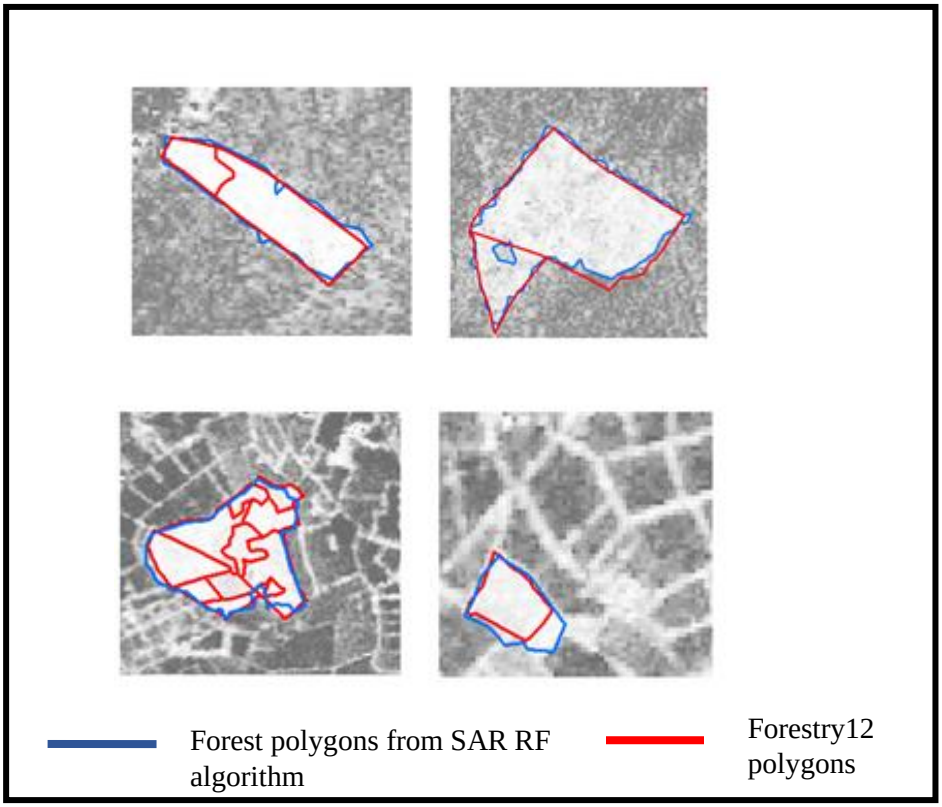

Figure 4.13: Zoomed in extent of selected regions in Area2 and Area3 displaying a visual comparison between Forestry12 polygons and SAR derived forest polygons

The forest edges and the shape of the forest areas shown in figure 4.13 visually appear to be consistent between the polygons from both the datasets. Interestingly in the lower right image (figure 4.13), the Forestry12 polygon has missed part of the forest area, but the SAR derived polygon has covered the entire forest patch. Out of the 3933 and 2987 polygons in Area2 and Area3 respectively, 55% of polygons were studied for visual analysis and the forest boundaries were consistently matching between the two datasets with some parts missing in Forestry12 due to the limitation explained in section 4.3.1.

4.3.3 Quantitative analysis

Three types of quantitative analysis were carried out for further analysis of the results obtained.

1) Classification accuracies
2) Count of number of forest polygons each dataset has identified – commission and omission errors
3) Forest area estimation from each dataset

4.3.3.1 Classification accuracies

When RF is run, one-third of the training data are held back for each tree to be used for testing accuracy and this gives the OOB error estimate. One caveat is that this approach will give results biased towards high accuracy when training data are correlated. Texture measures are also usually correlated with one another. Therefore, an independent accuracy assessment was performed on all land cover classes to obtain robust overall, user's and producer's accuracies based on the reference data used for training sample collection. This consisted of 750 points for forestland, 150 for cropland, 150 for grassland, 250 for peatland and 250 for water. The RF radar classification accuracies for Area1, Area2 and Area3 are presented in tables 4.3, 4.4 and 4.5.

Table 4.2: Classification accuracies for all land cover classes for Area1 where PA=Producer's Accuracy, UA=User's Accuracy, OA=Overall Accuracy

	2007		2008		2009		2010	
	PA	UA	PA	UA	PA	UA	PA	UA
Forestland	96.00	96.98	96.85	91.92	94.78	96.95	95.87	93.93
Cropland	79.01	82.03	79.99	98.11	85.97	90.12	85.99	95.03
Grassland	71.86	99.00	88.06	70.15	90.88	83.97	91.06	79.98
Peatland	91.00	70.99	81.02	79.15	85.21	94.12	85.00	76.99
Water	84.98	94.01	93.00	95.96	84.96	94.93	81.98	94.02
OA	87.72%		87.91%		89.62%		88.93%	
Kappa	0.83		0.84		0.86		0.85	

Table 4.3: Classification accuracies for all land cover classes for Area2 where PA=Producer's Accuracy, UA=User's Accuracy, OA=Overall Accuracy

	2007		2008		2009		2010	
	PA	UA	PA	UA	PA	UA	PA	UA
Forestland	95.97	97.99	94.78	96.99	97.03	94.86	97.98	98.16
Cropland	71.15	97.79	68.12	96.13	80.04	91.97	79.06	96.01
Grassland	90.99	71.96	93.89	65.03	89.99	76.05	80.19	75.02
Peatland	85.98	80.01	89.00	78.99	78.92	79.94	98.96	89.06
Water	94.96	95.07	93.04	94.06	92.96	93.89	87.84	92.88
OA	87.83%		87.18%		87.64%		88.75%	
Kappa	0.84		0.83		0.84		0.85	

Table 4.4: Classification accuracies for all land cover classes for Area3 where PA=Producer's Accuracy, UA=User's Accuracy, OA=Overall Accuracy

	2007		2008		2009		2010	
	PA	UA	PA	UA	PA	UA	PA	UA
Forestland	98.01	97.06	97.99	98.87	96.89	96.94	97.95	98.01
Cropland	88.69	77.86	88.97	77.07	89.10	81.17	87.99	88.76
Grassland	82.67	88.76	82.97	88.98	83.97	84.11	85.23	81.25
Peatland	84.13	86.11	83.06	85.09	84.00	86.99	84.89	83.06
Water	83.04	86.88	88.00	87.99	86.90	84.06	83.99	87.89
OA	87.53%		87.42%		87.15%		88.18%	
Kappa	0.84		0.84		0.84		0.85	

Overall accuracies between 87% and 89% were obtained for all study areas over all the data acquisition periods and the producer's and user's accuracies for the forest class are consistently higher than those of the rest of the classes. With respect to the outliers from table 4.3, cropland has a very high user accuracy of 98% in 2008 indicating the tendency of the algorithm to overestimate cropland class (classify more non-cropland class to cropland class). Similarly selecting the producer's accuracy from peatland class of year 2007 from table 4.3, 91% accuracy indicates underestimation of peatland classes in the classification.

An accuracy assessment was then conducted on the binary class forest and non-forest maps. The results are shown in tables 4.6, 4.7 and 4.8 for Area1, Area2 and Area3 respectively.

Table 4.5: Classification accuracies for forests and non-forest classes (area1) where PA=Producer's Accuracy, UA=User's Accuracy, OA=Overall Accuracy

	2007		2008		2009		2010	
	PA	UA	PA	UA	PA	UA	PA	UA
Forests	96.14	97.98	95.99	98.04	97.06	97.89	97.99	99.00
Non-forests	98.01	97.06	97.06	95.99	95.87	97.89	96.97	95.99
OA	97.23%		97.31%		97.22%		97.28%	
Kappa	0.98		0.99		0.97		0.98	

Table 4.6: Classification accuracies for forests and non-forest classes (area2) where PA=Producer's Accuracy, UA=User's Accuracy, OA=Overall Accuracy

	2007		2008		2009		2010	
	PA	UA	PA	UA	PA	UA	PA	UA
Forests	96.99	99.03	95.99	99.02	96.05	98.04	95.99	98.00
Non-forests	97.05	99.04	98.02	97.13	97.15	96.10	97.21	98.22
OA	97.51%		97.12%		97.03%		97.42%	
Kappa	0.99		0.98		0.97		0.99	

Table 4.7: Classification accuracies for forests and non-forest classes (area3) where PA=Producer's Accuracy, UA=User's Accuracy, OA=Overall Accuracy

	2007		2008		2009		2010	
	PA	UA	PA	UA	PA	UA	PA	UA
Forests	96.89	98.92	96.98	99.06	97.03	99.04	98.22	98.97
Non-forests	96.04	96.06	97.98	96.94	96.97	95.88	97.99	95.97
OA	97.62%		97.31%		97.22%		97.01%	
Kappa	0.99		0.98		0.97		0.97	

An increase in the overall accuracies can be observed for the forest and non-forest maps, compared to the full land cover map, as the confusion between the non-forest classes was removed. To understand the slight differences observed between the producer's accuracy and user's accuracy, the number of forest polygons identified by the SAR RF algorithm and Forestry12 dataset were compared. To simplify the investigation, and also due to the fact that the Forestry12 dataset becomes less reliable for the earlier years, this was only checked for 2010 over all the study sites.

4.3.3.2 Comparison of forest polygons from FIPS and SAR datasets – commission and omission errors

The SAR and Forestry12 (with dissolved sub-compartments) datasets were compared for three scenarios

1) Scenario 1: Forests coincident between SAR and Forestry12
2) Scenario 2: Forests in SAR shown as non-forests in Forestry12 (commission error)
3) Scenario 3: Non-forests in SAR shown as forests in Forestry12 (omission error)

Table 4.9 gives a summary of the polygon numbers for all three scenarios

Table 4.8: Summary of the number of forest polygons in SAR and Forestry12 dataset

	Agree	**Commission**	**Omission**
Area1	4995	37	3
Area2	3893	34	6
Area3	2953	29	5

As can be seen in table 4.9, more commission error is observed than omission error i.e. more forest polygons are identified by the SAR algorithm than that are not present in the Forestry12 data (commission), with 6 or fewer polygons identified by Forestry12 missed by the SAR RF algorithm (omission).

4.3.3.3 Forest area estimation

The results of comparative analysis of forest area estimates for the three study sites for the Forestry12 and SAR datasets are presented in table 4.10. In Area1, the total forest area

varied between 76,619.9 ha in 2007 to 81,795.0 ha in 2010; in Area2, the forest area is almost constant from 2007-2009 with a reduction of 3000 ha in 2010 amounting to an area of 63,640.5 ha; in Area3, the smallest area was observed in 2010 with 63,403.5 ha with the largest in 2009 of 67,989,7 ha. It can be noted from the table that the Forestry12 forest area is smaller than the SAR derived forest area in all three areas. More discussion on this is given in the following section.

Table 4.9: Forest area estimates from SAR and Forestry12 datasets

	Forest area from SAR RF classification (ha)				**Forestry12 forest area (ha)**
	2007	**2008**	**2009**	**2010**	**2012**
Area1	76,619.9	77,532.2	79,495.1	81,795.0	74,144.1
Area2	66,201.6	66,504.5	66,374.0	63,640.5	61,390.5
Area3	64,619.9	67,358.2	67,989.7	63,403.5	56,213.9

4.3.4 Discussion and conclusions

Quantitative analysis shows that the forest class consistently achieved higher producer's and user's accuracy ranging between 94% and 98% across all years and study areas when compared with the other classes (table 4.3-4.5). The overall accuracies achieved are between 87% and 89%, and one of the reasons is the similar backscatter responses that grassland and cropland tend to show *(Dusseux et al., 2014b)*. In this context, for monitoring other land cover classes such as grasslands and croplands, multi-temporal data with images from different stages of the phenological cycle are useful for inter- and intra-annual monitoring. But for this study, as forests are of the main interest, the classification of two classes (forests and non-forests) even with one image per year has resulted in high classification accuracies of 97% and the algorithm has been shown to work equally well in all study areas.

From a comparison of the number of forest polygons, it can be seen that the RF algorithm has identified more forest plots than are present in the Forestry12 dataset. The main reasons for the differences could be:

1) SAR derived forest maps might have identified some non-forest vegetation such as small shrubs as forest, leading to an over estimation of what is considered forest areas from a Forestry12 perspective and therefore forest polygon count. Upon verification with Google Earth images, among the 37, 34 and 29 extra forest polygons in SAR for the three areas respectively, 12, 15 and 16 polygons belong to shrubs misclassified as forests.
2) Privately owned woodlands might be missed by Forestry12 as it is a State forest company and does not record private grant aided forests.
3) In some instances, pre-approved afforested plots are digitized for FIPS but never actually planted on ground *(Department of Agriculture and Food and Forest Service, 2008)*

The SAR-2010 derived forest area estimate for Area1 is 9.35% greater than the Forestry12 estimate, with Area2 and Area3 3.53% and 11.00% greater respectively than the Forestry12 estimate. Figure 4.14 shows the inter-annual differences between SAR-derived estimates.

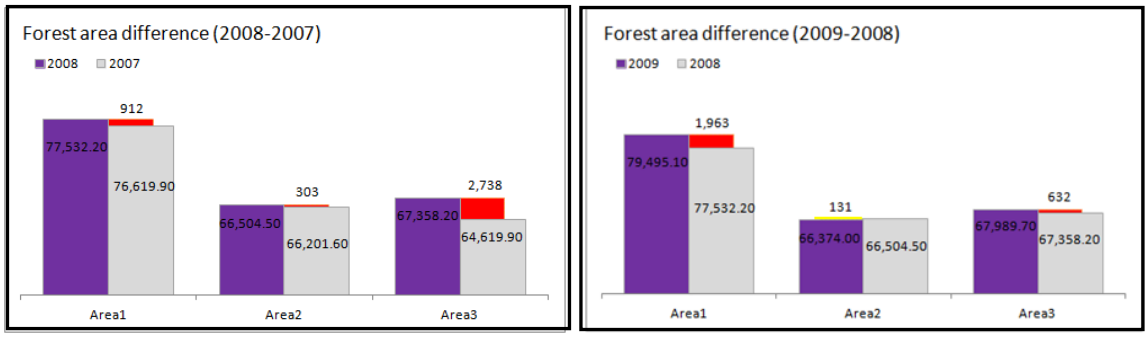

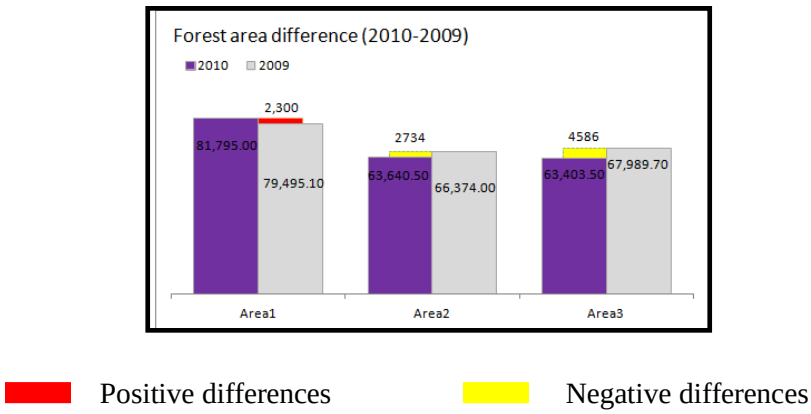

Figure 4.14: Inter-annual difference between SAR-derived forest estimates

Negative differences indicate a decrease in the forest area and positive differences indicate an increase. The spatial distribution of the differences was investigated to check if greater commission/omission errors were concentrated in one geographical location, for example due to the topography, or sensor near/far range, but the errors were well distributed throughout the study areas. These differences are expected as the classification has been run on each image set individually. To check if there are genuine errors such as presence of forest in 2007, absence in 2008 and presence again in 2009, time series analysis of these classified maps has been performed in Chapter 5. The nature and spatial location of such errors are then tracked. Other possible factors that can affect the radar backscatter from forests are changes in forest structure *(Dobson et al., 1995)*, environmental conditions at the time of image acquisition such as soil moisture, surface roughness, temperature and heavy wind/gusts *(Harrell et al., 1997; Kasischke et al., 2011; Lucas et al., 2010)*. Apart from the environmental parameters, the main changes in the forest area between each year are due to forest disturbances such as clear-felling and natural causes such as storm, fire, plant failure due to nutrient deficiency and also forest growth (increase in the forest biomass). The NFI carries out a systematic national assessment of forest damage in Irish forests and categorises the causes of forest damage into three classes - human induced (e.g. harvesting), abiotic (e.g. wind) and biotic (e.g. deer) *(Forest Service of Ireland, 2013)*. According to the NFI assessment, around 15 different types of forest damage are recorded each year which include human induced, windblow, frost, nutrient deficiency,

browsing, peeling, squirrel, defoliators, decay or canker fungi. These factors may be some contributors to the inter-annual changes in forests as shown in the quantitative analysis section (section 4.3.3).

The three study areas selected are situated in three different geographical locations representing different terrain types. While Area1 has a greater plain terrain, Area2 is more mountainous with Area3 having a mixed terrain. To account for all different terrain types, the algorithm uses slope and aspect variables which are useful for classification of non-flat areas. The three areas are also representative of different tree species and climatic conditions prevailing across Ireland. Given the high forest accuracies achieved using the methodology followed for the present study over the three study sites, this approach could be applied on a national scale to generate forest maps to obtain recent or updated information.

This method, when used for operational monitoring of forests, can support FIPS monitoring system from forest service in determining annual forest updates. As FIPS is updated only once in six years, the RF algorithm could complement it by providing annual updates, based on objective analysis of satellite imagery.

The processing time of the whole algorithm including SAR pre-processing of four image frames, using a 4GB RAM computer, is divided as per the following categories.

- SAR image pre-processing for a stack of four images: 3 hours
- GLCM texture measure extraction for one image: 1.5 hours
- RF classification of one image: 40 mins

As the classification was performed on R programming platform, it is important to be aware that R keeps all the data in RAM. As the size of the SAR images is 2GB, the processing requires memory to store all the processed data and sometimes R may crash if the internal memory of the computer is not sufficient. Therefore, it is beneficial to use a computer with a RAM minimum of 4 GB (the higher the better and lesser processing time).

The present work aims to map the discontinuous and sparse forests of Ireland using the FBD ALOS PALSAR data. As the forestland in Ireland consists of isolated fragments of

forests, the challenge here was to select variables and filter parameters that assist in producing high accuracy forest maps, eliminating small shrubs and hedgerows that are not forests and also retaining sharp forest edges/boundaries. The algorithm used random forests machine learning classifier by using the variables that are most influential to classification through the variable importance plot generated by the classifier. SAR backscatter coefficient, GLCM texture measures, DEM derived slope and aspect aided in producing forest and non-forest maps with overall classification accuracies of 97%. This chapter illustrates the use of L-band SAR images, the procedure to select the optimum variables necessary for classification, how the variables have an impact on the forest maps and a comparison between the SAR derived forest maps and the Forestry12 dataset in terms of classification accuracies, commission and omission errors and forest area.

In this work, one image per year was used which successfully resulted in high accuracy forest maps. To get intra annual forest updates, more images per year can be used. As more frequent ALOS PALSAR data were unavailable over Ireland, one image per year was chosen - ideally summer images have been used where trees have full canopy cover leading to volumetric scattering for the SAR sensor. One of the limitations of the study was that high classification accuracies for the rest of the land cover classes could not be achieved due to the confusion in the backscatter responses mainly between cropland and grassland. But as only forest mapping was the main objective of the study and as it resulted in higher accuracies, this did not impact on the subsequent analysis. For the end users who wish to use SAR data for land cover class mapping, multiple acquisitions per year of fully polarimetric ALOS PALSAR data is recommended which can distinguish different phenological aspects and different scattering mechanisms respectively.

The algorithm has been shown to be robust over three differing study sites and based on the evidence and understanding, this could be implemented on a national scale as part of a continuous forest monitoring system. In this chapter, the first objective of the thesis which is exploring the potential of microwave sensor in mapping Irish forests using a machine learning approach has been achieved. As ALOS PALSAR malfunctioned in 2011, ALOS-2 PALSAR-2 (L-band) can be used to provide contemporary forest monitoring operations. This algorithm can support Irish forest agencies, such as the Forest

Service, to provide updates on forests annually and hence support private foresters and other end users in making forest management decisions.

In the following chapter, the forest maps generated in this chapter are further used to characterize and monitor disturbances that have occurred within the forest areas mapped. An unsupervised approach has been presented to understand the nature and extent of change which is the second objective of this PhD work.

Chapter 5

Characterisation and Monitoring of Forest Disturbances in Ireland using Divergence-guided ISODATA Clustering Algorithm

"If not now, when?" – Hillel the Elder

5.1 Introduction

Measure, Monitor and Manage are the main aspects of an operational forestry industry to balance the forest carbon emissions and address climate change issues. Accurate and consistent information on forest area and its change is important given the carbon reporting requirements that countries are committed to. To comply with the carbon emission targets, countries are designing different strategies. To achieve the contracted targets, through forestry activities, four major strategies are available: (i) Reforestation and Afforestation: Increase the forest land area by planting trees; (ii) Increase the carbon stocks in existing forests by management activities such as forest fertilization, pest control, forest quantity and attention to soil health before planting; (iii) sustainable management of forest products to replace fossil-fuel CO_2 emissions; and (iv) to reduce emissions from human induced forest disturbances such as felling, deforestation and forest degradation *(Canadell and Raupach, 2008)*. Forests, being the largest terrestrial carbon sink, influence the future trajectory of atmospheric carbon dioxide *(Collalti et al., 2019)*. Monitoring forests on a global, national and regional scale is therefore important to understand the forest dynamics impacted by the changing environmental conditions and anthropogenic activities.

This chapter focuses on monitoring changes within the forest areas mapped in Chapter 4 by understanding their characteristics and labelling them depending on the nature of change. Following on Chapter 2, after exploring the various change detection approaches, the unsupervised ISODATA classification approach has been used. The signatures of the different clusters formed through the classification process are analyzed and labelled. Figure 5.1 shows the main steps of an unsupervised classification.

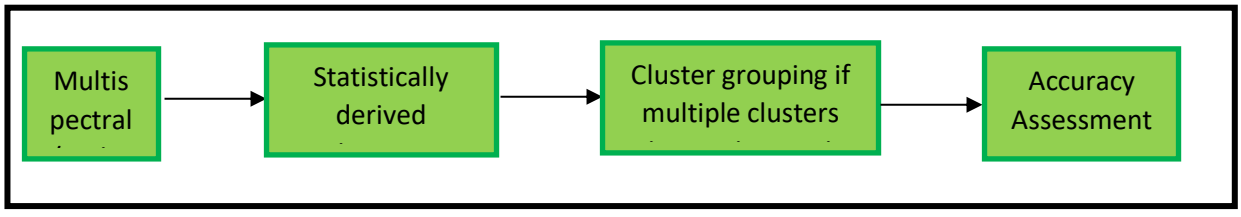

Figure 5.1: Main steps of an unsupervised classification

In this study, a modification was made to the classic ISODATA unsupervised clustering technique, illustrated in figure 5.2. The boxes in yellow are the new elements added to the standard ISODATA classification approach. This approach is guided by Divergence statistics to provide guidance on selecting the optimal number of clusters to be used, and hence the name Divergence guided ISODATA clustering algorithm. As the name suggests, it is a self-organizing algorithm that does not require any training data for classification; natural clusters are formed which are then grouped into various categories based on cluster similarities. The signatures of the cluster groups are studied and with the help of ground truth data, the groups are labelled.

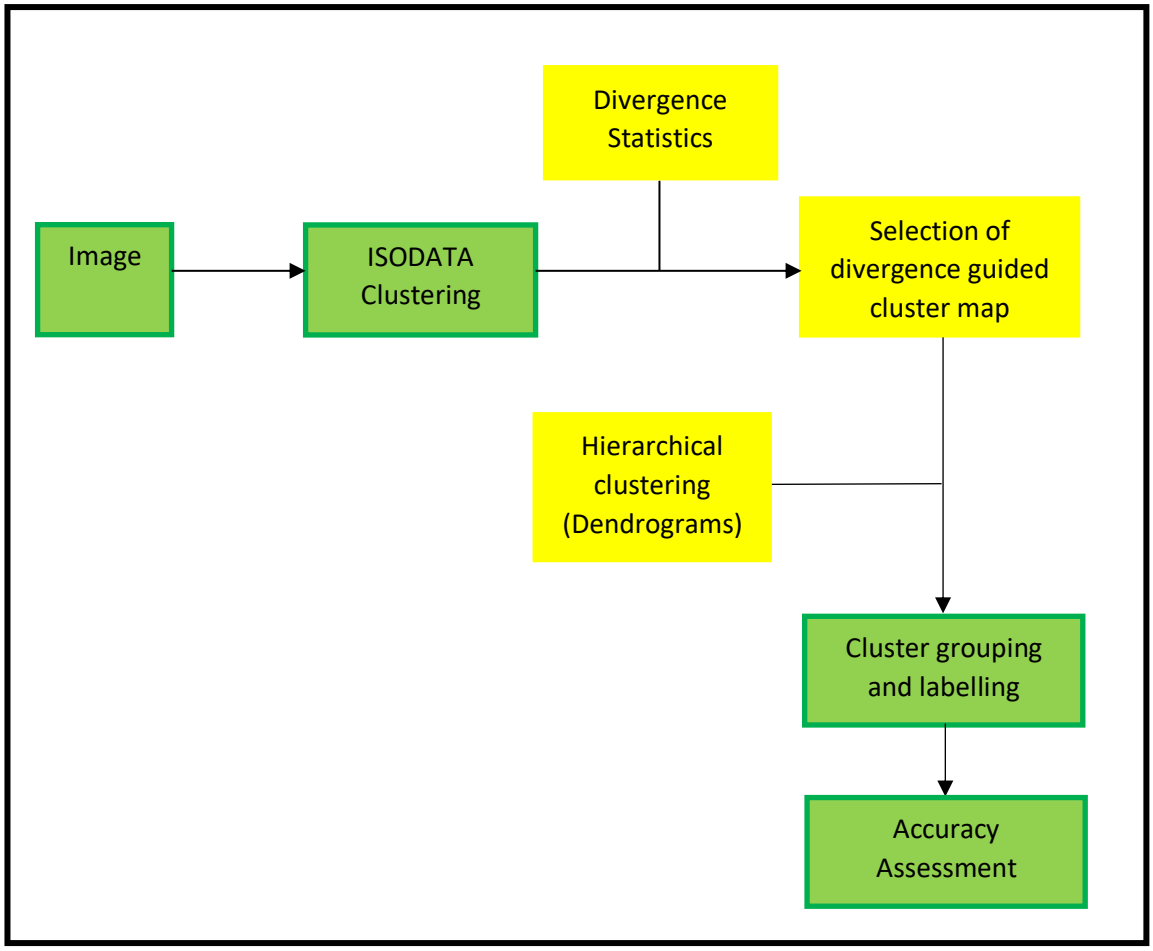

Figure 5.2: Modifications made to unsupervised classification

This methodology was adopted from the work by *de Bie et al., (2012*) and *Ali et al., (2013)* where hyper-temporal NDVI images were used to map land cover gradients. Application of this technique on SAR images to detect and characterize disturbances in Irish forests is

the main purpose of the current study, and is the first time such a study has been carried out for Irish forests.

5.1.1 Working principles of divergence guided ISODATA clustering algorithm

Understanding clustering: Dividing objects into groups (clustering) and assigning objects to groups (classification) is a skill that humans have developed. Conceptually meaningful groups of objects, or classes, sharing common characteristics play a critical role in how human beings generally analyse and describe the world. In the context of deriving information from data, clustering is an unsupervised classification of data items into different clusters or classes based on statistical similarity *(Jain et al., 2000)*. Given an unlabelled dataset, clustering separates the dataset into a finite and distinct set of natural data structures based on the similarity measure chosen to create relevant clusters *(Baraldi et al., 2005; Baraldi and Alpaydin, 2002; Backer and Jain, 1981)*. Deducing the optimal number of clusters which represent the variability in the dataset (in the present case – forest cover as represented on multiple satellite images) is a difficult task that most of the algorithms face *(Boudraa, 1999)*.

K-means and ISODATA are two unsupervised clustering algorithms that are iterative. They start by assigning an arbitrary initial cluster vector. In the second step, each pixel is classified to the closest cluster, and in the third step, new cluster means are calculated based on all the pixels in one cluster. The ISODATA clustering algorithm is derived from the K-means clustering technique with refinements such as splitting and merging of clusters. The ISODATA technique forms clusters of pixels through the "self-organizing" ability by minimizing the Euclidean[9] distances *(Swain, 1973)*. The clusters with a small distance between their centroids are merged into a single cluster and then the cluster with the largest variance is divided into two clusters *(Jain et al., 1999)*. During the iterations, the initial k centroids are updated and after a user-defined number of iterations, those k centroids represent the k clusters. The divergence separability index entails extracting statistical separability values which denote the average and minimum separability values for the set of clusters within each classification. "The average separability is a measure of the mean similarity between temporal signatures amongst all possible pairwise

[9] Square root of the sum of the squares of the distances between each pair of band mean values

combinations of output clusters, while the minimum divergence value expresses the similarity between the temporal signatures of the two most similar clusters" *(Ali et al., 2014, pg.no.178)*. According to the approach by *de Bie et al., (2012),* based on two conditions, the optimal number of clusters was chosen from the separability plot

- Coincident average and minimum divergence peak (both the clusters should be as high as possible to separate the clusters); D_{ij} is the statistical distance between two classes i and j, and a value below 24 indicates a poor separability *(Jensen, 2005; Mather, 2001)*
- Lowest possible number of clusters

The methodology was applied on Area1 initially, and is described in detail in section 5.2 and 5.3. Briefly, using cluster statistics and a hierarchical clustering approach (a method of cluster analysis which builds a hierarchy of clusters, or a cluster tree known as a dendrogram), similar clusters were merged into groups. By investigating the means and standard deviations of the cluster groups, and with the aid of the available ground truth data, the cluster groups were labelled, and the disturbance clusters were extracted. The algorithm was then transferred to the other two study areas and the signature profiles of the common cluster groups were compared and the transferability of the algorithm was assessed.

5.2 Methodology

The algorithm developed to achieve forest disturbance maps is divided into four main stages (Figure 5.3), The overall idea of the methodology can be gained from figure 5.2 which highlights the modifications made to the standard unsupervised classification procedure (figure 5.1) which lead to the final map of clusters with labels for each type of cluster group highlighting forest type and disturbances.

Stage 1: ISODATA clustering guided by Divergence statistics and selection of suitable bands to be used for clustering

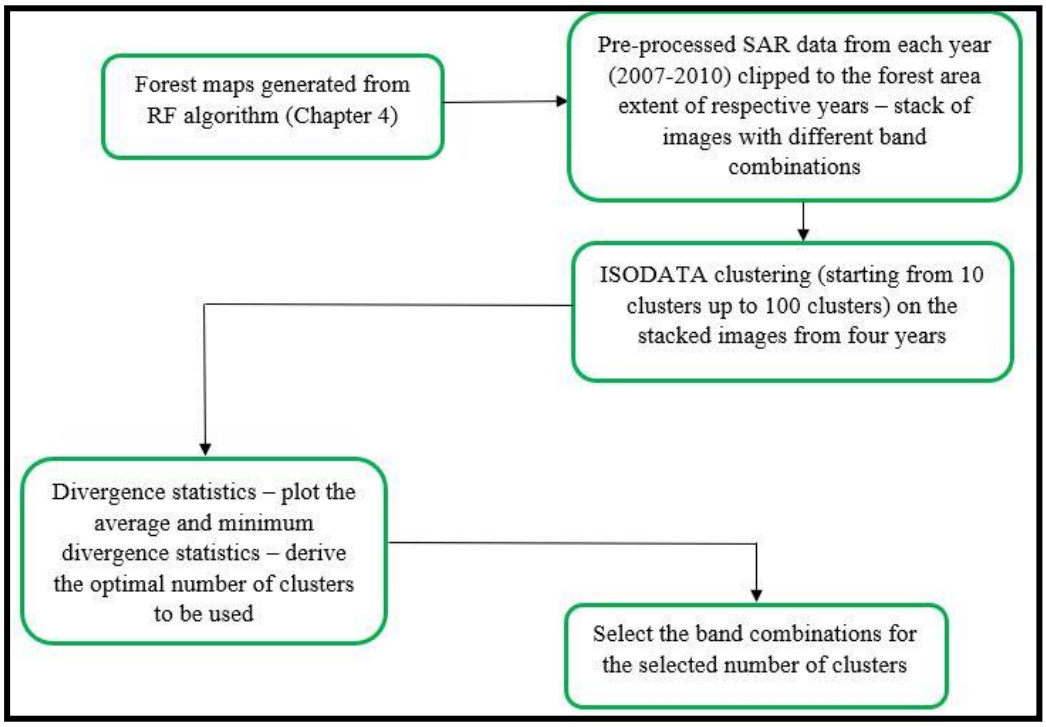

Stage 2: Cluster Grouping

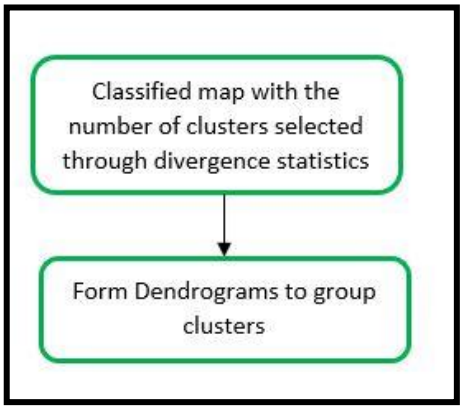

Stage 3: Signature Analysis and Labelling

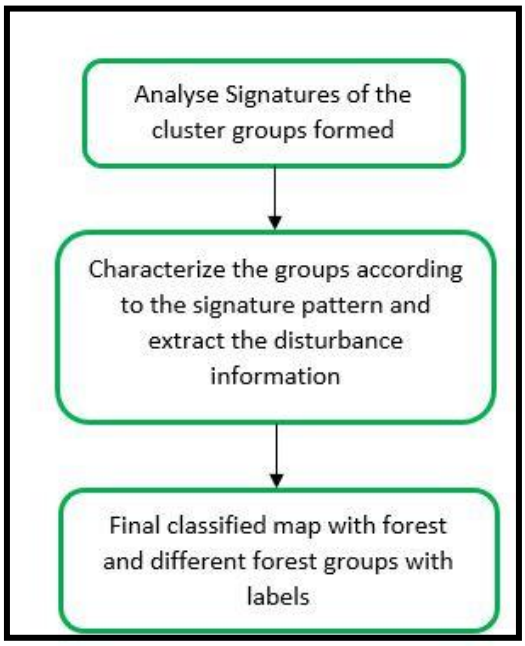

Stage 4: Quantitative Analysis

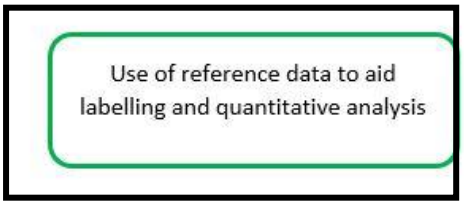

Figure 5.3: The four stages of methodology

5.3 Detailed Methodology and Results

This section presents a detailed methodology for each process, and the results obtained at each stage of the methodology for Area1.

5.3.1 Stage 1: Selection of bands to be used for clustering

The band combinations selected for different clustering trials are presented in table 5.1.

Table 5.1: Different band combinations used for clustering experiments

Combination 1	72 bands (bands from each individual year 2007-2010) • HV gamma nought • 8 GLCM texture measures derived from HV • HH gamma nought • 8 GLCM texture measures derived from HH
Combination 2	36 bands (bands from each individual year 2007-2010) • HV gamma nought • 8 GLCM texture measures derived from HV
Combination 3	36 bands (bands from each individual year 2007-2010) • HH gamma nought • 8 GLCM texture measures derived from HH
Combination 4	16 bands (bands from each individual year 2007-2010) • HV gamma nought • 1 GLCM image from each group: contract from contrast group, entropy from orderliness group, correlation from stats group derived from HV
Combination 5	16 bands (bands from each individual year 2007-2010) • HH gamma nought • 1 GLCM image from each group: contract from contrast group, entropy from orderliness group, correlation from stats group derived from HH
Combination 6	8 bands (bands from each individual year 2007-2010) • HV gamma nought • HH gamma nought

Each layer of the combinations presented in table 5.1 was clipped to the forest extent derived from RF classification in Chapter 4 (Chapter 4 - Forest maps figure 4.7). The products (HV and HH gamma nought and GLCM texture measures) used in the current

chapter were derived in chapters 2 (Study area and Datasets) and 4 (Mapping forests using RF classifier). These layers from each year were then stacked according to the different band combinations to form 1 image per combination to run the clustering algorithm.

5.3.1.1 Experiment parameters: All the experiments for ISODATA clustering were run on Erdas Imagine version 10

Number of clusters: Started with 10 clusters up to 100 clusters with an interval of 10 between each run (i.e. 10, 20, 30, 40, 50, 60, 70, 80, 90, 100 clusters each).

Standard Deviation (SD) and Minimum Distance (MD): Clusters that have a standard deviation greater than the specified value are split into two and clusters pairs with a Euclidean distance less than the specified value are merged into a single cluster *("ERDAS IMAGINE Ribbon Workspace" 2019)*. As an initial trial, these values were kept at the default value of 5.

Convergence Threshold: This is the maximum proportion of pixels that do not change classes between successive iterations. This was given a value of 0.95 (default value), which specifies that as soon as 95% or more of the pixels stay in the same cluster between one iteration and the next, the processing should stop.

Maximum iterations: A high number of 25 was set. This high number was chosen to ensure that the algorithm would run enough times to reach the convergence threshold.

With the above parameters, the experiment trials were run on the different band combinations. With combinations 1-5, certain issues were encountered as discussed below.

- Technological: Combinations 1-3, due to their higher file size (24GB and 12GB) could not be processed due to technical constraints (in a 4GB RAM processor) which eventually led to system crash.
- With combinations 4 and 5, it was observed that, the algorithm resulted in few empty classes. For example, if the classifier was instructed to generate 10 classes, only 6 classes would be filled, leaving the rest of the 4 classes empty. This was because clusters with a standard deviation greater than 5 (default value that the classifier was set to) were split into two clusters and clusters pairs with a Euclidean

distance less than 5 were merged into a single cluster indicating that the specified values were inappropriate for the experiment. However, after running various trials, the SD and MD values were set to 0.1 which then resolved the issue.

- With combinations 4 and 5, the different data ranges for the intensity and the texture bands required data normalisation. However this resulted in values suppressed between 0 and 1, making interpretation challenging. All cluster values in the time-series lied between 0 and 1 which made separating changed and unchanged clusters unreliable and insignificant.

These issues were avoided in combination 6 in which only HV and HH intensity bands from each year were stacked together.

With Combination 6 (8 bands):

The potential of HV in forest monitoring has been discussed in Chapter 2 in which studies such as *Pantze et al., (2010), Fransson et al., (2007), Tanase et al., (2018) and Haarpaintner et al., (2015)* proved the higher sensitivity of the HV channel to forest changes than the HH channel. Although the classification in this study was run on the combined HV and HH bands, the potential of HV to perform cluster grouping and most cluster analysis in stages 3 and 4 is demonstrated. The HH band is used primarily to aid the characterisation of cluster groups through investigating the signatures from the targets and understanding the scattering mechanism generating them.

Combination 6 comprised of the set of bands shown in table 5.2 which was subjected to ISODATA clustering.

Table 5.2: Final band combination used for clustering and characterising the clusters

Band1	HV ɣ° 2007
Band2	HH ɣ° 2007
Band3	HV ɣ° 2008
Band4	HH ɣ°2008
Band5	HV ɣ°2009
Band6	HH ɣ° 2009
Band7	HV ɣ° 2010
Band8	HH ɣ° 2010

Divergence statistics were calculated for each classification run for clusters from 10-100, and the minimum and average divergence were plotted against the number of clusters. Figure 5.4 shows the graph with average and minimum divergence statistics and the selection of the optimal number of clusters for this classification. A sharp peak in the minimum separability at a value of 1282, coinciding with a moderate peak in average separability at a value of 1969 at 80 clusters can be observed from the figure. The map generated from 80 clusters is shown in figure 5.5. The clusters in this map represent the variability within the mapped forest areas. SAR intensity profiles exhibiting similar temporal behaviour are then grouped through a hierarchical clustering approach aided by signature analysis.

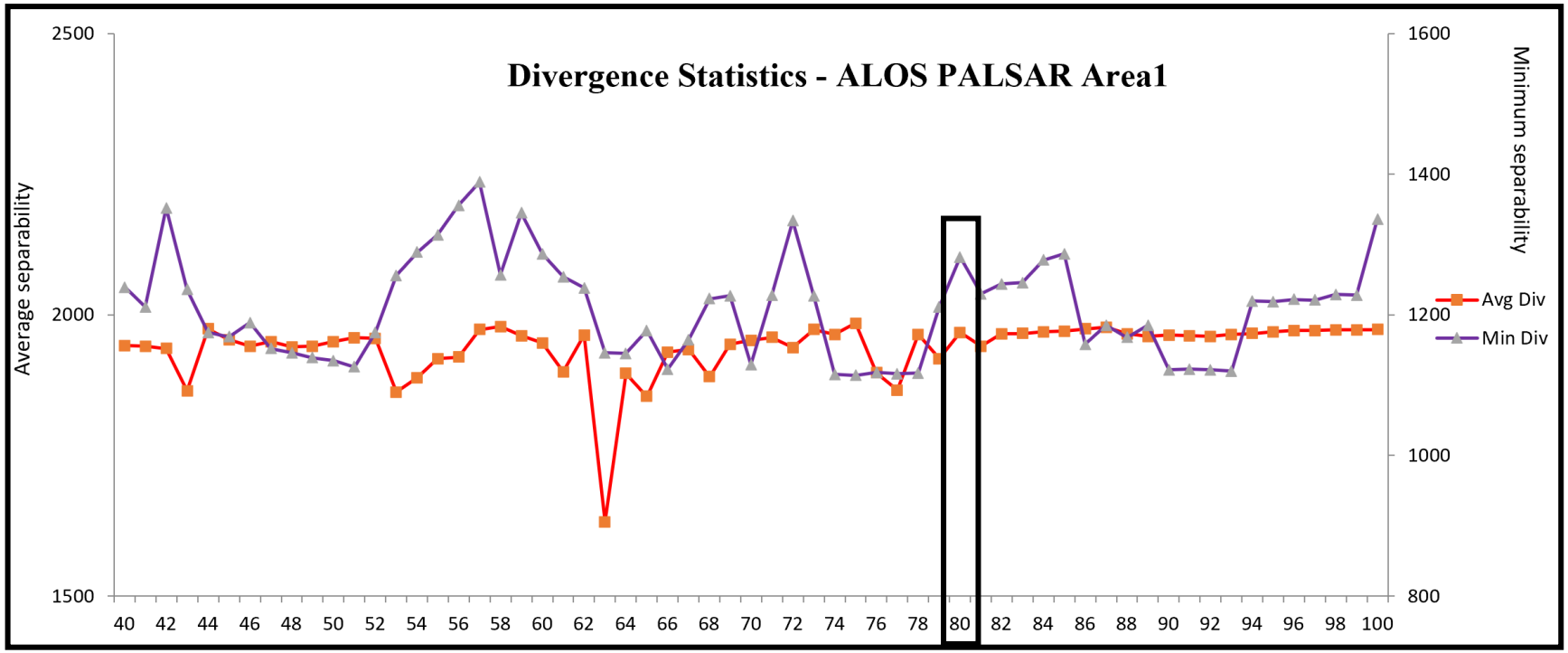

Figure 5.4: Divergence statistics plot derived on the 8 band raster stack for Area1 indicating 80 as the optimal number of clusters (with coincident average and minimum divergence peak) to be used for further analysis

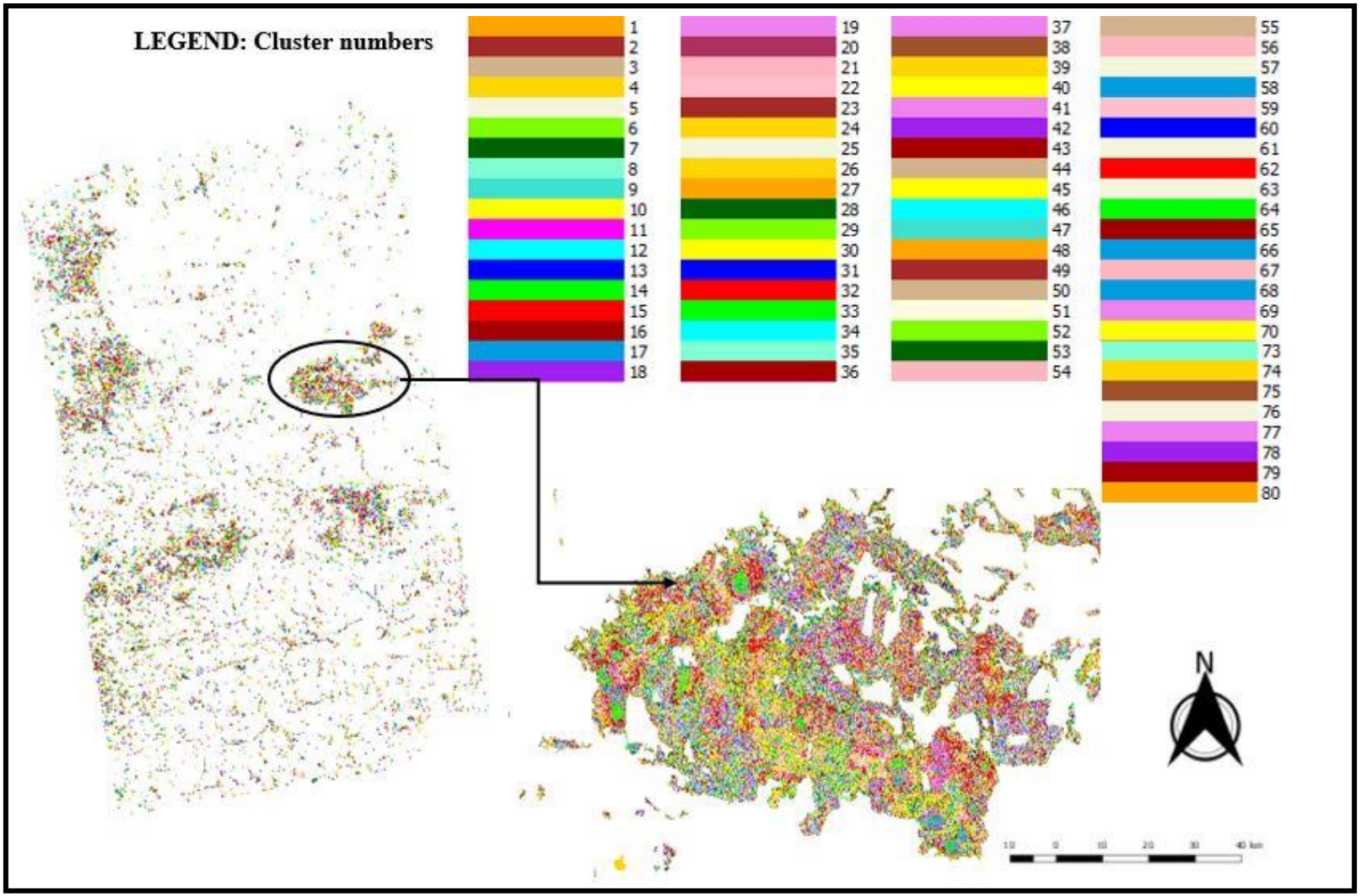

Figure 5.5: Spatial clusters generated using ISODATA unsupervised clustering algorithm on Area1 using ALOS PALSAR HV and HH intensity bands over the four year (2007-2010) time-series

5.3.2 Stage 2: Cluster Grouping

The next stage was to extract the cluster signatures, analyse their patterns and then assign clusters with similar characteristics into groups. For each cluster starting from 1 to 80, a signature file was derived. The signatures were examined carefully, and to facilitate the cluster grouping certain initial preparations were necessary.

Different patterns in the signatures of clusters were observed.

1) Pixel values remained constant to within 1 dB over the four years
2) A drop greater than 4dB occurred between two consecutive years
3) A drop of 2 dB occurred between two consecutive years
4) An increase of 4 dB occurred gradually over the years from 2007 to 2010
5) An unusual rise and fall of 6-8 dB occurred between 2 consecutive years
6) A gradual decrease of 2 dB from 2007 to 2010

As a first step, the 58 clusters whose pixel values remained the same to within 1 dB were segregated and grouped. These clusters were then grouped using the Hierarchical Clustering Analysis (HCA) approach, using the HV cluster means from 2007. This is an exploratory method which is designed to reveal natural groupings within a dataset *(Ali et al., 2013; Gauch and Whittaker, 1981; Sidorova, 2012; Marcal and Castro, 2005).* Hierarchical clustering produces dendrograms which represent branching, tree-like relationships. A cluster tree is formed with different branches and nodes. The x-axis shows the cluster numbers and the y-axis shows at which level fusion of clusters occur (it represents the distance of dissimilarity between clusters). In this study, agglomerative clustering as described by *Huang (2002)* is used as each object is a single cluster and the intention is to form groups of most similar clusters.

The next step is to calculate the similarity between the clusters. This has been calculated here using the Euclidean distance between two clusters. Among the many cluster agglomeration methods such as complete linkage, single linkage, average linkage and centroid linkage, the complete linkage hierarchical clustering has been used to merge the clusters.

Figure 5.6 shows dendrograms formed for the 58 clusters, whereby each node in the tree contains a group of data that are statistically similar to each other. The next crucial step was to decide when to stop merging the clusters, which is a somewhat subjective decision. Many trials were performed with different threshold values. Different thresholds were set starting from 1.25 to 15 as shown in figure 5.6. After much experimentation, it was observed that thresholds above 2.5 merged more clusters and led to lesser number of groups and thresholds below 2.5 resulted in more number of groups. For example, a step above 2.5 (3.75, indicated by the blue line in figure 5.6) formed 5 groups whereas a step below 2.5 (1.25, indicated by the green line in figure 5.6) formed 15 groups. Under-grouping resulted in information loss, and over-grouping resulted in too much information making the process of deciphering the cluster signatures complicated. In this case, the dendrogram tree was cut with a horizontal line at height 2.5 as shown in figure 5.6 in dotted red line. This resulted in 7 cluster groups shown by the green circles.

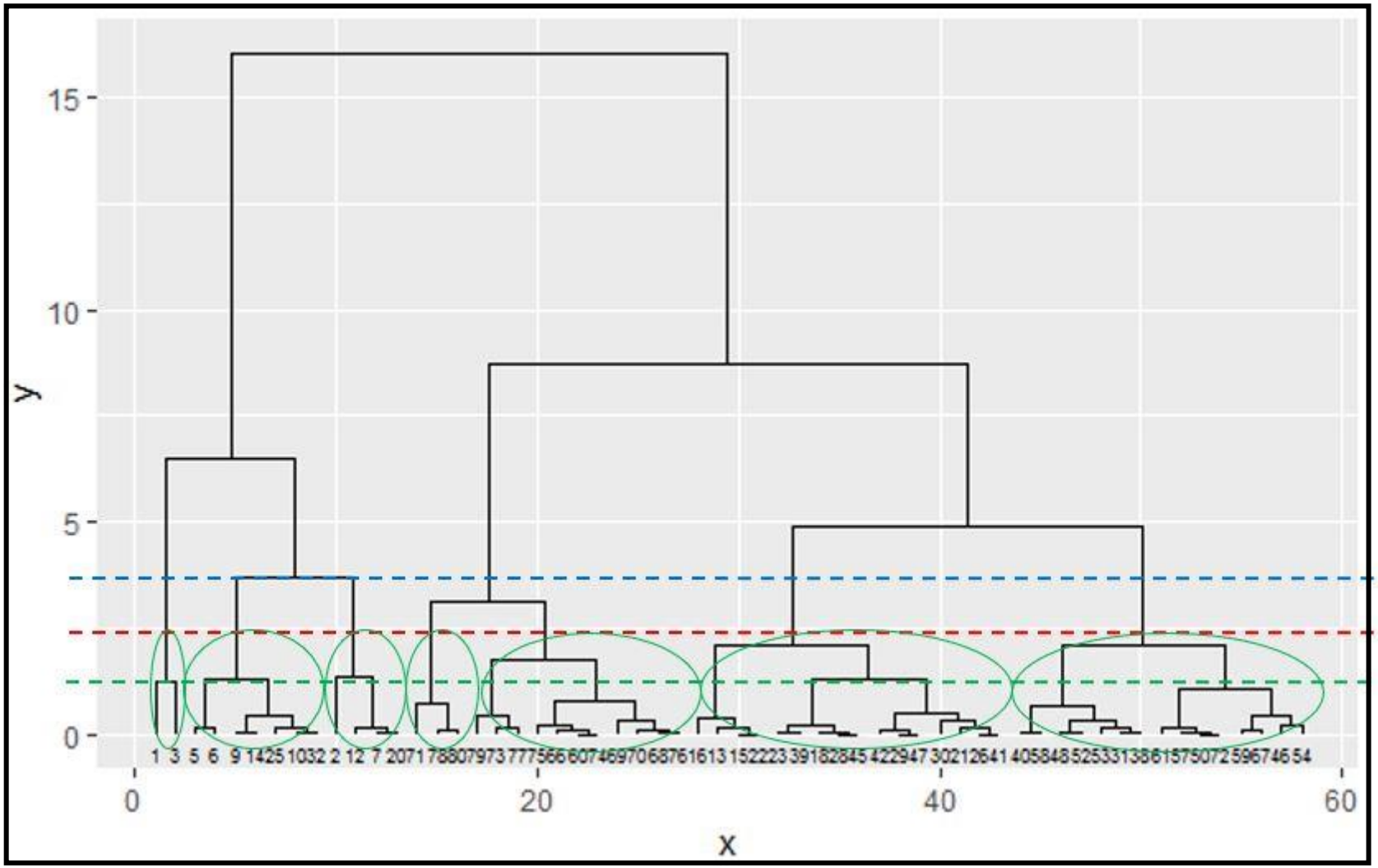

Figure 5.6: Dendrograms showing cluster merges at different Euclidean distances, highlighting the 7 groups formed within the green circles for a y-axis value of 2.5

To study clusters that exhibited a change greater than 1dB between the years, the clusters were manually seggregated based on the amount and year of change. The hierarchical clustering process as described above was applied for the remaining patterns. The extent and year of change and the number of groups formed for each case is given below.

- Drop greater than 4dB between 2009 and 2010: 1 group was formed with clusters 56 and 62 from the Dendrogram
- Drop greater than 4dB between 2008 and 2009: 1 group was formed with clusters 24, 17 and 33
- Drop of 2dB between 2008 and 2009: 1 group was formed with clusters 43, 51, 19, 36, 27, 37
- Increase of 4dB from 2007 to 2010: 3 groups were formed with 1 group containing cluster 11, another group containing clusters 63, 44, 55 and a third group containing clusters 34, 35 and 39
- Unusual raise and drop of 6-8 dB between 3? consecutive years: 1 group was formed containing cluster 14
- A decrease of 2 dB from 2007 to 2010: 1 group containing cluster 65 was formed.

In total, 15 groups were formed for Area1.

5.3.3 Stage 3 and Stage 4: Signature Analysis and Labelling; Use of reference data to aid labelling

Signatures from the cluster groups were plotted to understand the extent and year of change. Figure 5.7 shows the consolidated map with 15 groups formed in stage 2. This map was filtered to clean the map and eliminate isolated pixels as shown in figure 5.8. To aid labelling, reference data were used.

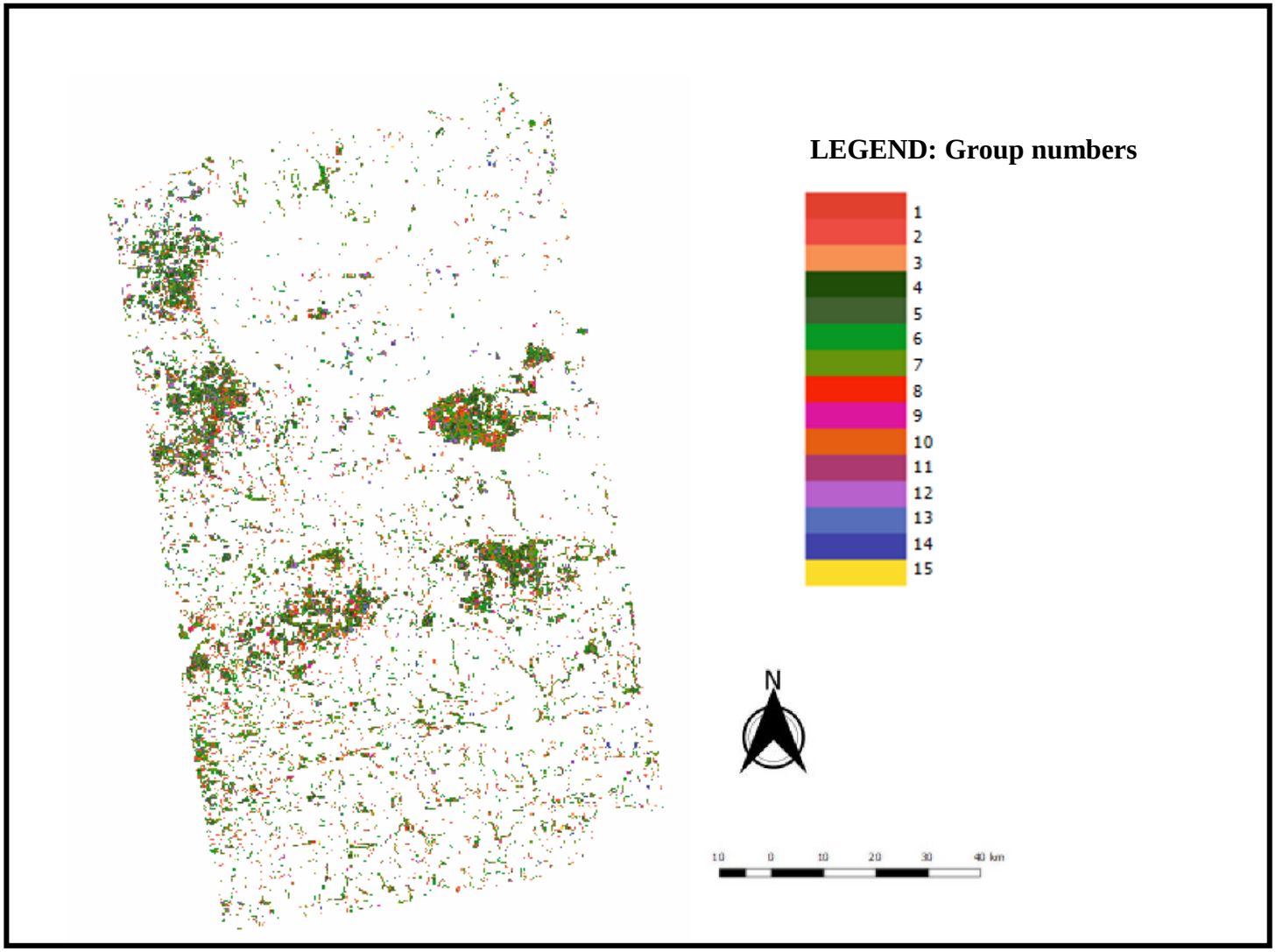

Figure 5.7: Final groups of clusters representing the different patterns within the previously mapped forest land

Once the clusters were assigned to their respective groups, the map was filtered using a sieve filter to remove noise and clean the map. After experimentation, the sieve size selected removed all areas less than or equal to 1.125 ha. Figure 5.8 shows the classified map before and after the application of sieve filter.

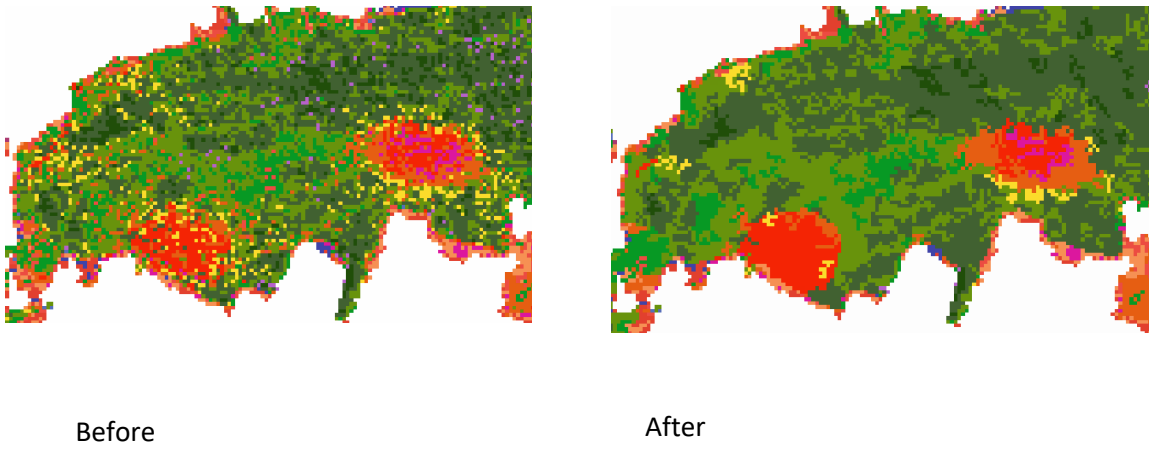

Figure 5.8: Application of sieve filter on the classified map

This resulted in omission of forestlands of area less than or equal to 1.125 ha from the final classified map. An example is shown in figure 5.9. Forest pixels under the red circle are missing from (b) which is a post sieved image.

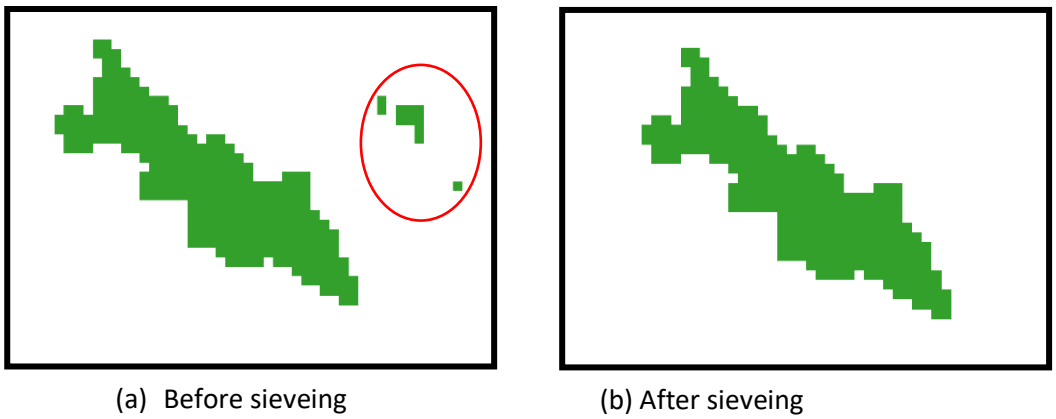

Figure 5.9: Removal of forest areas of less than 1.125 ha from classified map

When quantified with Forestry12 dataset, 52 ha of forestland were missing from the final classified map. This was the final classified map that was used for further analysis.

To support the analysis and characterization of cluster groups, ground truth information from Coillte, Forestry12, historic Google Earth imagery and Bing imagery were used. Data for the Coillte estate included compartment id, sub-compartment id, planting year, land cover type, and species, and polygons containing information referring to clear fells year and area. While clear fells were validated with these polygons, other cluster groups in this chapter have been discussed and labelled based on hypothesis as limited evidence was available.

5.3.3.1 Groups of clusters with less than 1 dB variation between the four years

Figure 5.10 shows the mean and standard deviation of all 58 cluster signatures assigned to the 7 groups. The shaded part of the graph shows the lower and upper bounds of one standard deviation. The cluster means of groups fall within the limits of the next similar cluster (validating the dendrograms). From the graphs it can be observed that groups 1, 2 and 3 have a lower mean backscatter of less than -24 dB. Group 4 clusters have the highest backscatter between -13 and -15 dB. Clusters within group 5 have mean backscatter signatures less than -15 dB up to -17 dB. While clusters within group 6 have values less than -20 dB and greater than -23 dB, group 7 clusters have values ranging between -17 dB and -20 dB. A certain level of overlap between the groups is apparent.

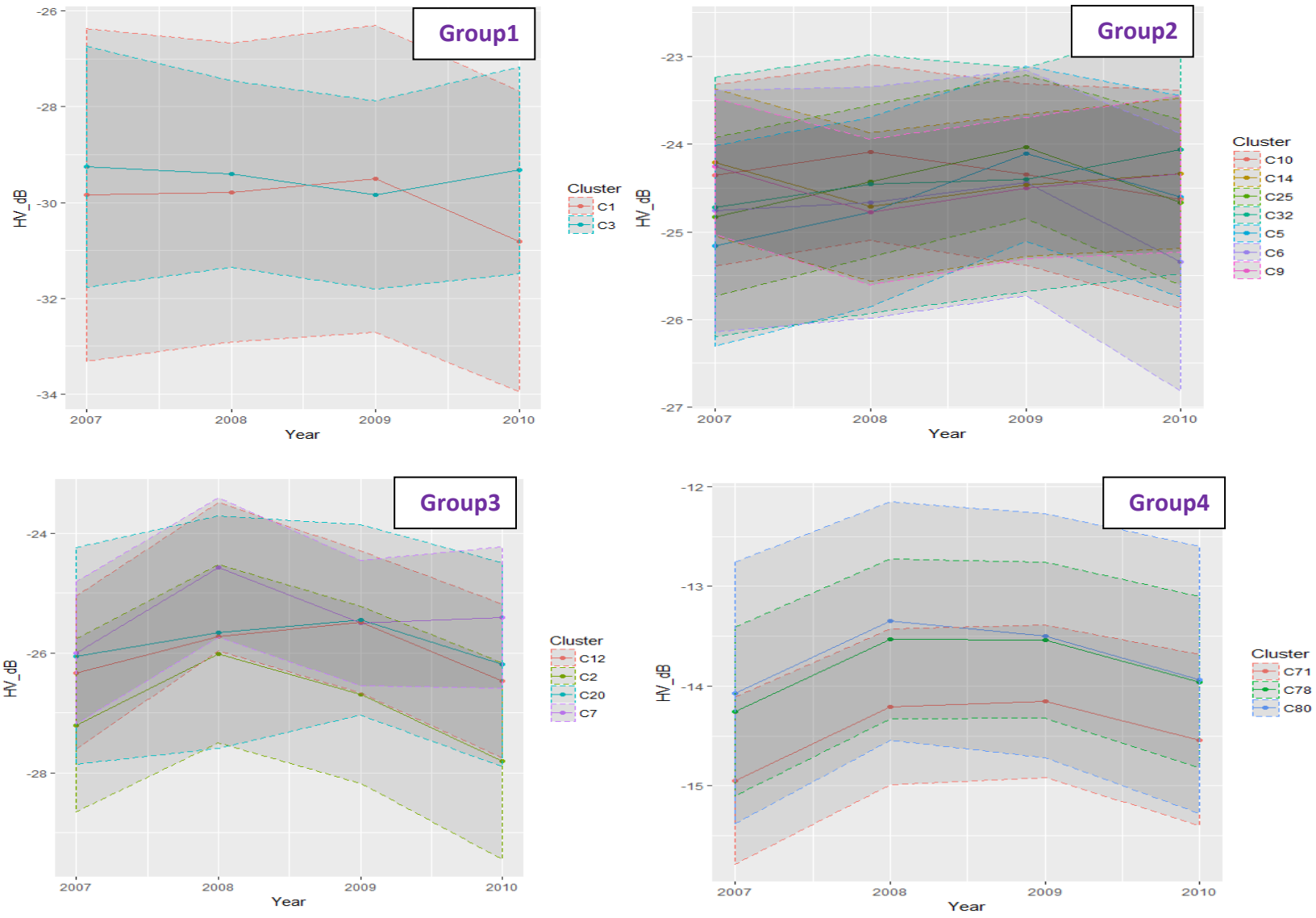
Group1
HV_dB
-26
-28
-30
-32
-34
2007
2008
2009
2010
Year
Cluster
C1
C3
Group2
HV_dB
-23
-24
-25
-26
-27
2007
2008
2009
2010
Year
Cluster
C10
C14
C25
C32
C5
C6
C9
Group3
HV_dB
-24
-26
-28
2007
2008
2009
2010
Year
Cluster
C12
C2
C20
C7
Group4
HV_dB
-12
-13
-14
-15
2007
2008
2009
2010
Year
Cluster
C71
C78
C80

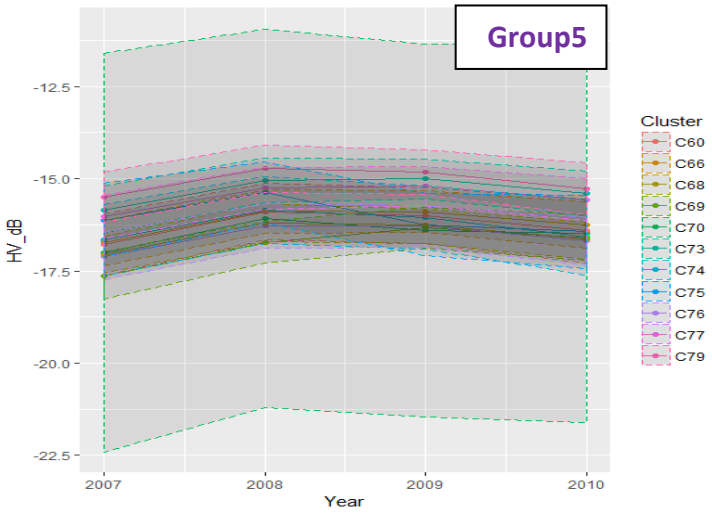

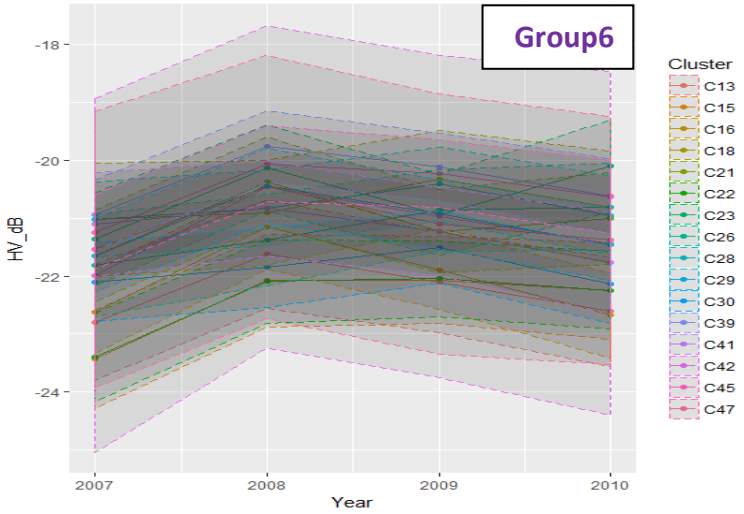

Figure 5.10: Signature patterns within cluster groups with less than 1 dB variation between consecutive years

5.3.3.1.1 Groups 1, 2 and 3: Misclassification

The clusters within these groups displayed a signature in which the mean HV backscatter values were very low relative to the other cluster groups. The spatial distribution of these clusters was inspected by overlaying them on BING imagery. These clusters appeared on non-forest lands and at forest edges. One example is shown in figure 5.11 which shows a ploughed field. The undulations on the land have caused a higher backscatter due to higher surface roughness and it is likely that the texture measures have detected these undulations on the ground and mapped them as a tree canopy.

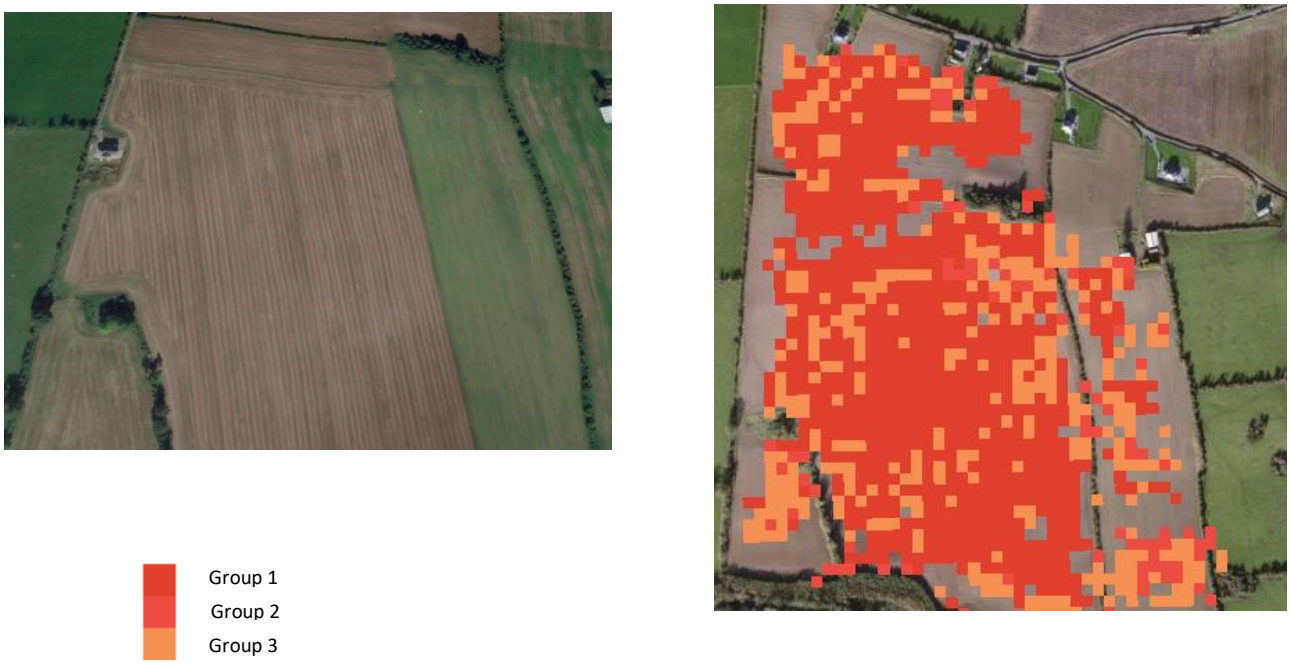

Figure 5.11: Example of an arable land represented by cluster groups 1, 2 and 3

Misclassifications were also observed at forest edges, where mixed pixels occurred. The clusters of these groups were assigned into 3 different groups by the dendrograms based on the HV means. This highlights the inter group variability and the properties of the land represented by the clusters. The HH signatures were examined due to their higher sensitivity to surface scattering. Clusters representing surface undulations displayed a higher backscatter of -8 dB and smoother surfaces showed a lower backscatter, as low as -23 dB, over the years. Based on these analyses, these classes were found to be misclassified pixels and hence, these groups were labelled as Misclassifications. These

groups together represent 4% of the land of Area1. These can be masked out of the classification map if necessary.

5.3.3.1.2 Groups 4, 5, 6, 7: Mature and Young forests

These groups have a HV backscatter range between -13.4 dB and -22 dB and a HH range of -8.1 dB and -15.2 dB. The spatial distribution of these groups were observed with the aid of BING maps and Forestry12 layer. An example is shown in figure 5.12.

Figure 5.12: An snippet of groups 4, 5, 6, 7 bound by FIPS polygon

These groups corresponded with the Forestry12 polygons representing forests, and the backscatter values are coherent to those expected over forest for both HH and HV channels as described in chapter 4. The difference in the range of backscatter returns is related to factors such as age of the trees, forest type and the tree species, amount of biomass and soil conditions.

The planting date information was useful to extract the age of the different groups of clusters and therefore label them accordingly. Only 34% of Forestry12 polygons contained the planting date information and hence the planting year (PY) information from Coillte was used for further analysis and labelling of these groups.

Upon investigation, it was found that for some polygons the PY information was not updated. With the aid of Google Earth imagery for visual inspection, Coillte polygons with updated PY were tested against these four groups of clusters. For mature and young looking forests appearing on Google Earth imagery, the PY information was checked and hence tallied. Through this approach, groups 4 and 5 were then assigned the label of mature trees (age: 10-30) and groups 6 and 7 were labelled as young trees (age: 0-9). The intra variability between these individual groups based on the tree species and other factors causing the difference in the energy return was beyond the scope of this project and this would require further analysis of the scattering mechanisms.

5.3.3.2 Groups of clusters with greater than 1dB variation between four years

This section presents the signatures and analysis of the remaining 22 clusters that were indicative of change within the forests.

5.3.3.2.1 Group 8 and Group 9 – Drop of 4dB between two consecutive years

Groups 8 and 9 exhibited a characteristic feature in which a difference of greater than 4 dB was observed between two consecutive years. This difference was apparent in both HV and HH bands. In group 8, this difference occurred between 2009 and 2010 and in group 9, this difference occurred between 2008 and 2009. Figures 5.13(a) and (b) show the annotated time series signatures

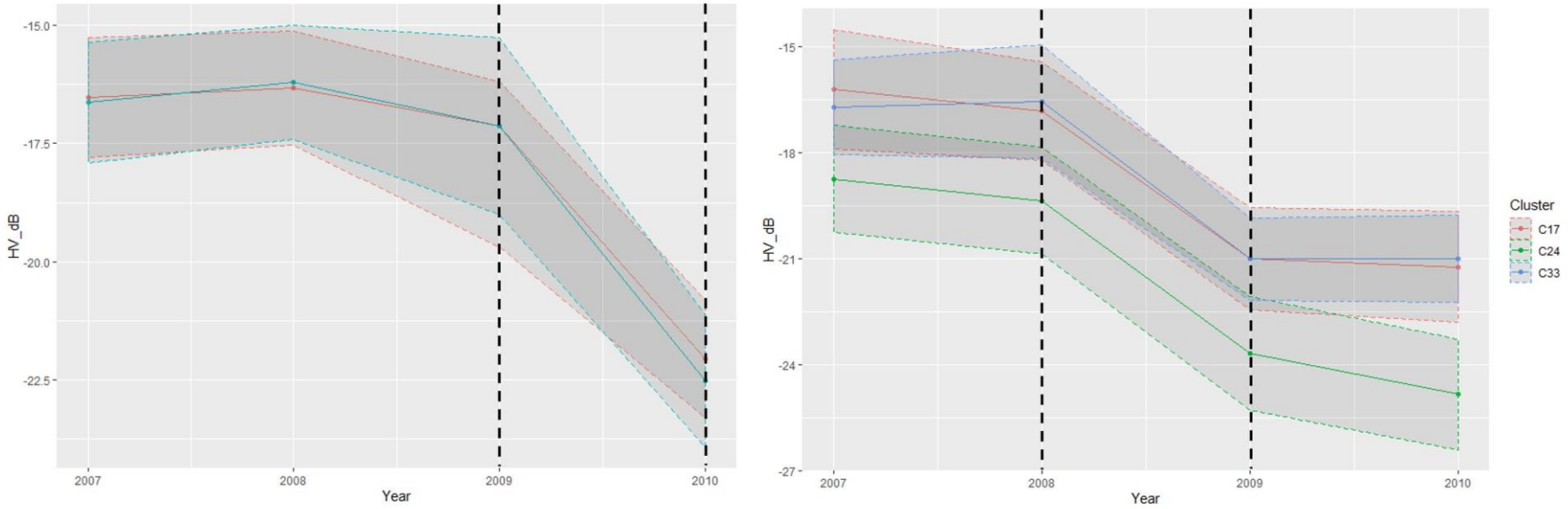

Figure 5.13: (a)left: Signature means of group 8 clusters for HV; (b)right: signature means of group 9 clusters for HV. The black dotted lines mark two years between which the change has occurred.

These groups were further examined spatially with the help of reference data obtained from Coillte. Upon examination it was found that these groups matched with the felled polygons representing clear-fells. Figures 5.14 (upper) and (lower) show examples of group 8 and group 9 clusters contained within the felled polygon. The PY as entered in the felled attributes is also shown. In the two example polygons in figure 5.14 (upper) with fell_year 2010, the felling has taken place in 2010 which is reflected in the SAR image. This indicates that the areas represented by group 8 clusters have been felled before 24 June 2010 which is the SAR image acquisition date. The two polygons in figure 5.14 (lower) have undergone felling in 2008 as per the fell_year record. The corresponding SAR clusters show this change in the year 2009 indicating that the felling has occurred between the SAR acquistion 03 May 2008 and before the start of the year 2009. To support this analysis, results from *Fransson et al., (2008), Santoro et al., (2010) and Pantze et al., (2014)* described similar backscatter returns from a felling event.

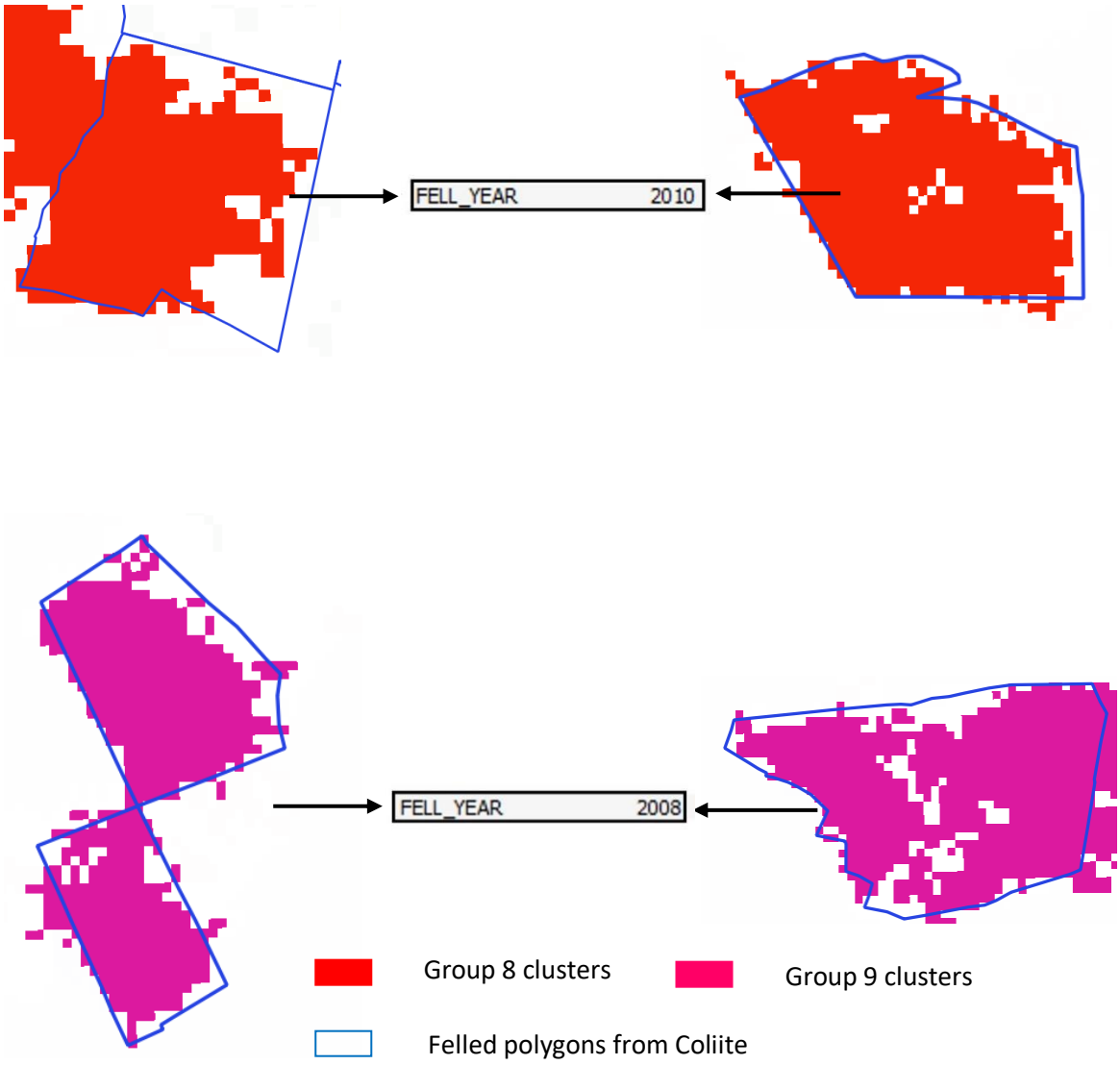

Figure 5.14: upper: Group 8 clusters (change between 2009-2010) representing change in 2010 as verified by the Felled polygon; lower: Group 9 clusters (change between 2008-2009) representing change in 2008 as verified by the Felled polygons

A quantitative analysis was performed and the groups were characterized. Before proceeding further, the following points were considered

- The felled polygons from Coillte contain only the year of felling information. The month/date of felling are not provided.

- Changes in SAR images occur between June(2007)-May(2008)-June(2009)-June(2010).

Because of this discrepancy between the datasets, it was not possible to do a yearly comparison of felling events between them. Therefore, the total number of group 8 and group 9 instances were compared against the entire felled dataset of Coillte and the number of matching cases were recorded. Table 5.3 sums up the number of felling events recorded in each dataset. Zonal statistics were retrieved for the Coillte felled polygons with respect to the group 8 and 9 pixels, and the count of pixels within each polygon was recorded. SAR pixel clumps greater than or equal to 6 contiguous pixels were considered.

Table 5.3: Comparison of number of felling instances between Coillte felled polygons and SAR image clusters

	Number of felled polygons from Coillte (2007-2010)	**Number of instances identified by SAR corresponding to the Coillte felled polygons**
Area1	145	94

The percentage agreement between the two datasets was 64.82%. The rest of the 51 Coillte felled polygons that the SAR based algorithm did not identify were next examined. The analysis involved checking these 51 polygons based on the polygon area and verifying each polygon with historic Google Earth imagery. Table 5.4 shows the polygon division based on their area.

Table 5.4: Polygon area based analysis

Polygon area	**Number of polygons**
<0.1ha	1
>0.1ha<1.0ha	7
>1ha<10ha	36
>10ha<15ha	7

From table 5.4, 44 polygons which are less than 10ha in size have been missed by the clustering algorithm,and 7 polygons of between 10ha and 15ha have been missed.

Another observation was that among the 145 Coillte felled polygons, 23 polygons had an area greater than 15ha and the rest were smaller than 15ha and all these 23 polygons have been identified by the SAR derived algorithm. The 51 missing polygons from table 5.4 were further investigated to understand the disparity between the two datasets.

Upon deeper investigation, six categories were defined for the 51 missing polygons as shown in table 5.5.

Table 5.5: Categories for missing polygons between the Coillte felled areas and SAR derived results

Category	Number of polygons
Linear polygons	6
Validated with GE and discovered not felled	25
Very close to buildings	3
Very small polygons (<0.1 ha; <1 ha)	8
Bare Upland (*Calluna* (Heather) cover)	1
No definite reason	8

The description of each category and key notes on the forest inventory system at Coillte is given in the section below.

1) Linear polygons

These are polygons with a diagonal width ranging between 20m and 30m as shown in figure 5.15 and of varying lengths. If the width is between 20 and 30m, the polygon would consist of 1 or 1.5 pixels. Given the smaller width of such polygons, these areas were not identifed by SAR as change pixels.

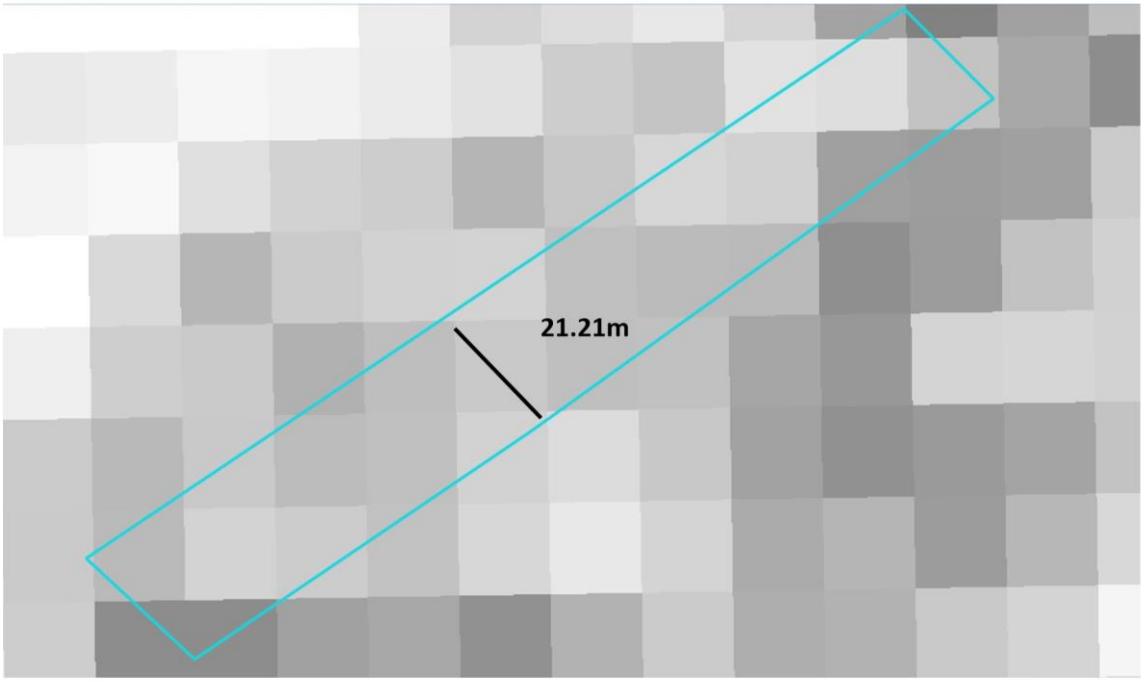

Figure 5.15: Illustration of a linear polygon

2) Validated with Google Earth and discovered not felled

Historic Google Earth images from 2003 – 2011 were checked as a means of validation to support this analysis. It was discovered that 25 polygons recorded as felled by Coillte were not felled on ground, and the SAR data has naturally not categorised these areas as disturbances. One example is shown in figure 5.16.

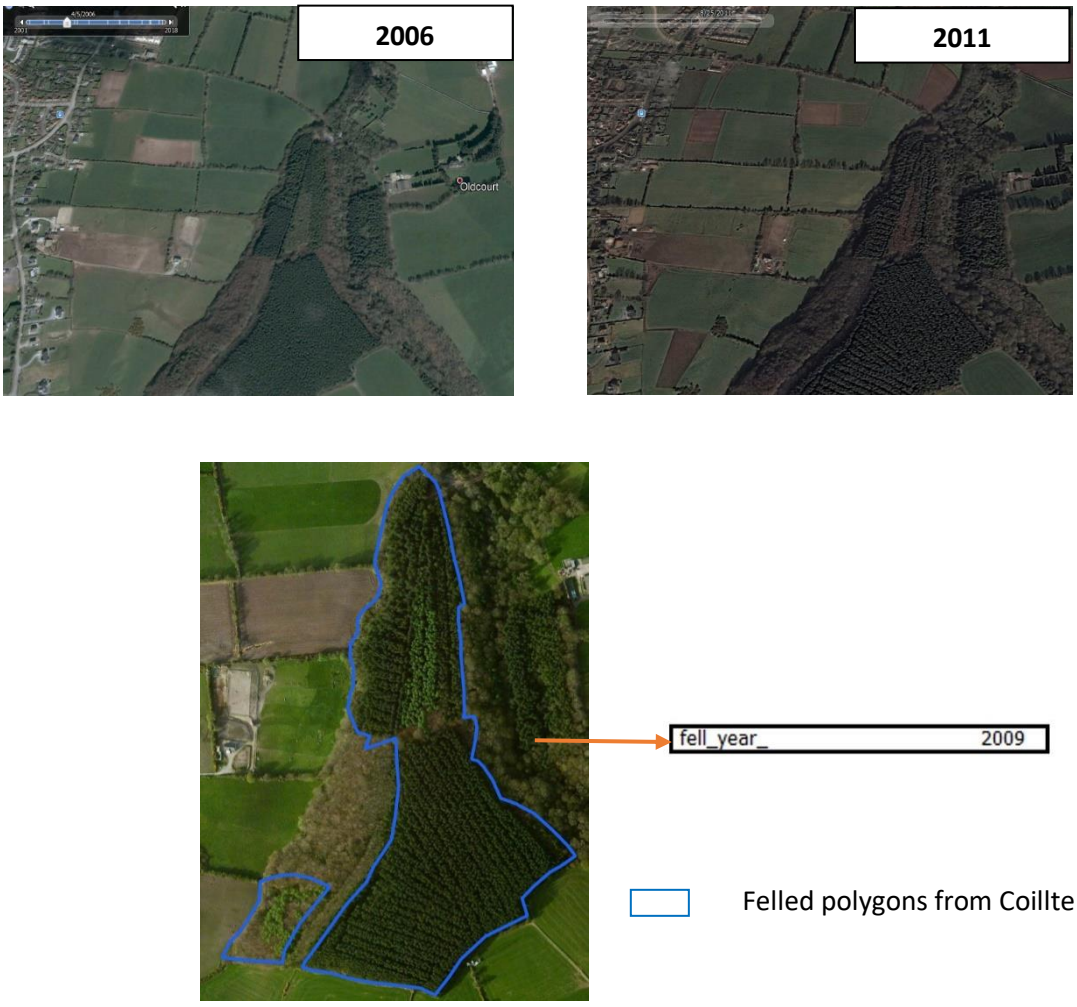

Figure 5.16: Example of a Google Earth image showing no change between 2006 and 2011-marked as felled in 2009 in the Coillte felled polygon database

3) Very close to buildings

Forests planted within a 60m buffer of buildings or monuments are left unfelled, however these polygons have not been updated in the database and they still appear as felled.

4) Very small polygons

Eight polygons were found to be less than 1ha in size, with one of them less than 0.1ha. These polygons correspond to less than 4 pixels. During the sieve operation, clumps

of 6 or fewer pixels were eliminated to make the results as coherent as possible. Due to this, these polygons were not idenitfied as change by SAR algorithm.

5) Bare Upland

A polygon of area 9.38ha was identifed as no change by SAR but categorised as felled by Coillte. When this was cross verified with Google Earth and Coillte Sub-compartment polygons, this polygon was found to be Bare Upland that was covered by *Calluna*, or Heather, which is abundant on acidic soils on mountains and bogs in Ireland. As this is clearly a non-forest land, occurrence of a felling event on this land is unlikelyand it has been incorrectly entered in the database as felled.

6) No definite reason

Eight polygons did not fall under any of the above categories and therefore no definite reason could be arrived at to address the question of why these are felled according to felled polygons of Coillte and not felled according to SAR. These polygons were spatially well distributed and they belonged to groups 4, 5, 6 and 7, indicating the presence of trees during the entire four year period.

Some possible reasons for the discrepancy between the two data sources are

From the perspective of the forest inventory process at Coillte

1) Once the felling license has been issued by the forest service, the foresters prepare to perform the felling operation for that particular compartment.
2) But in some places, trees marked as felled are not actually cut. A part of the polygon or the entire polygon is left unfelled leaving inconsistency between what has been recorded digitally and what has taken place on the ground. The exact area felled is not recorded in the database.
3) In areas with very poor ground (very soft and wet) where the timber is of limited value, and on very steep slopes where the machinery used for felling cannot operate, forests are left unfelled.
4) Biodiversity is one of the factors taken into account before any forest operation is performed. During the breeding season from April to July, forests with birds nesting are not felled.

From SAR perspective

1) The felling event might have occurred before or after the image acquisition period. As Coillte records the events throughout the calender year, there could be occurrences of felling events from 1 January – 16 June 2007 and 24 June – 31 December 2010.
2) Environmental effects and high dielectric constant of the ground

Taking into account the 26 polygons (25 validated with Google Earth and 1 Bare Upland) which are confirmed to be not felled, the percentage agreement between the two data sources now increased from 64.82% to 78.33%. Based on the analysis and evidence, this pattern exhibited by clusters within groups 8 and 9 were attributed to felling events and labelled as Clear Fells.

5.3.3.2.2 Group 10 – Drop of 2dB between two consecutive years

The signature pattern of this group of clusters showed a difference of 2dB between two consecutive years (2008 and 2009) in both the HV and HH channels (Figure 5.17).

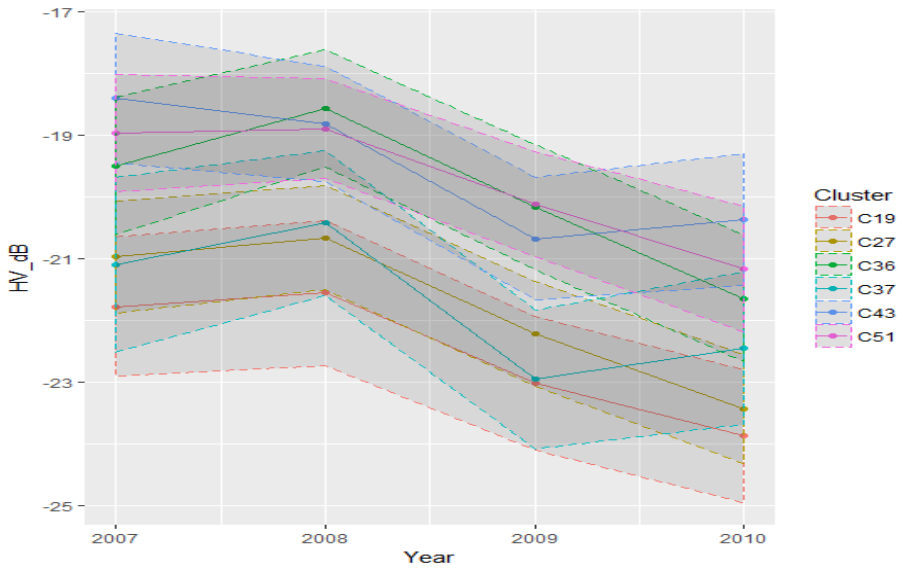

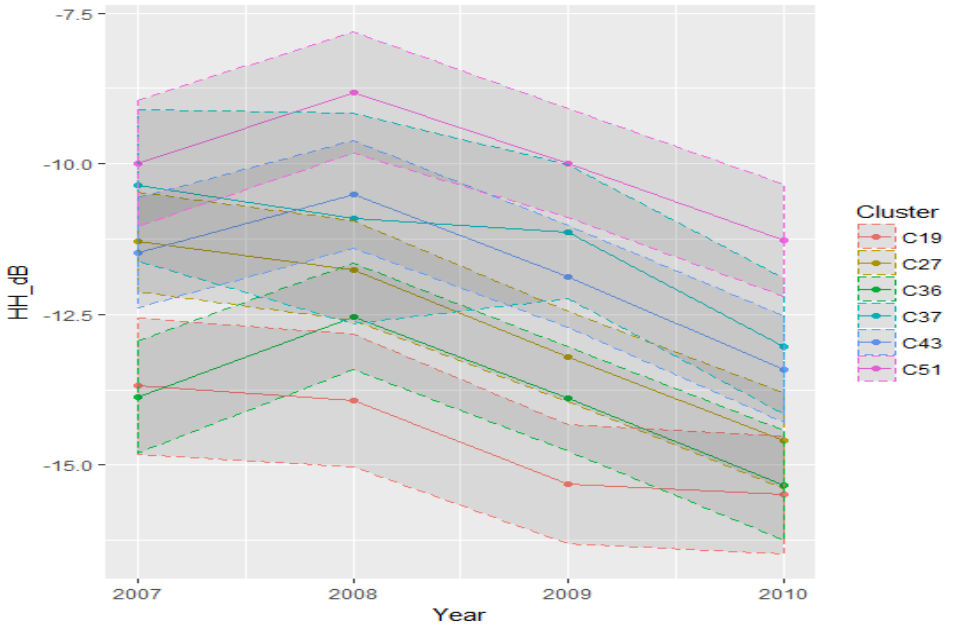

Figure 5.17: Signatures of Group 10 clusters

No reference data was available to understand the nature of this group of clusters. Investigation of the spatial distribuiton of this group revealed two observations

- 27 polygons from groups 8 and 9 (clear-fells) were found to contain pixels from this group near the edges as shown in figure 5.18

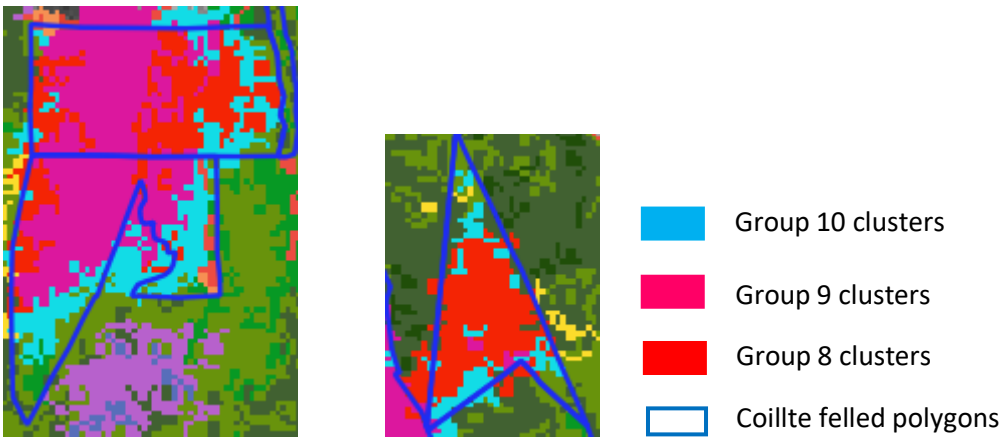

Figure 5.18: Examples of appearance of group 10 clusters within Coillte felled polygons

- Where reference data were unavailable, with the use of Google Earth imagery, it was found that these clusters represented areas with thinning lines in between indicating thinning event. One such example is shown in figure 5.19.

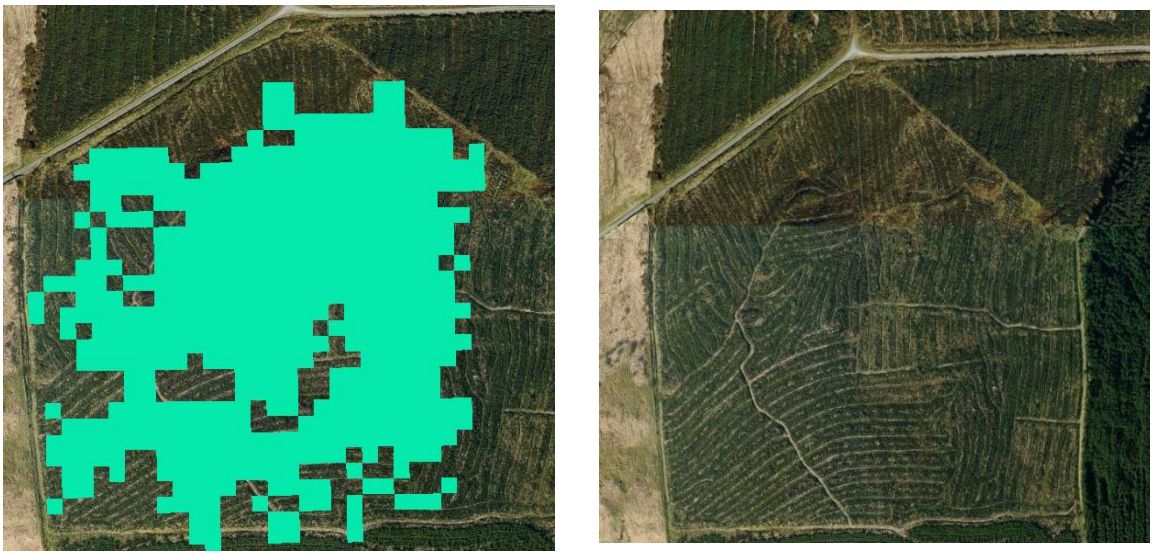

Figure 5.19: An example of group 10 clusters indicating the possibility of thinning event

Three theories were drawn from the many observations made

- The reason 27 polygons from groups 8 and 9 are found to contain a small percentage of group 10 clusters is the possibility of the presence of debris. After a felling event, the debris are completely removed or piled to form windrows. The surface roughness from this debris has caused a lower amount of decrease in the backscatter as compared to the actual felling.
- Young plants need utmost care otherwise they get subjected to nutrient deficieny or insect bites or animals such as deer eat them. Insects such as Weevils as shown in figure 5.20 attack pine trees when they are young and cause major loss for the forest company.

Figure 5.20: Weevils – a type of beetle that feed on young pine trees (taken during a field visit in April 2017)

- Thinning: Plantations that are heavily stocked are subjected to thinning at intervals of forest crop rotation. The sole purpose of thinning is to increase the overall timber revenue by providing a provisional income for the owner. The timing of thinning mainly depends on the yield class. Crops with a higher yield class are thinned earlier.

Based on the field visits and practical knowledge of the ground reality, these theories were drawn. This group was therefore categorised into one of the above groups and was given a generic label of Plant failure/Ground debris/Thinning.

5.3.3.2.3 Groups 11, 12, 13 - Increase in backscatter over the years

An increase in the backscatter was recorded from 2007-2010 as shown in figure 5.21. A gradual increase is seen starting at -26dB in 2007 and ending at -23dB by 2010.

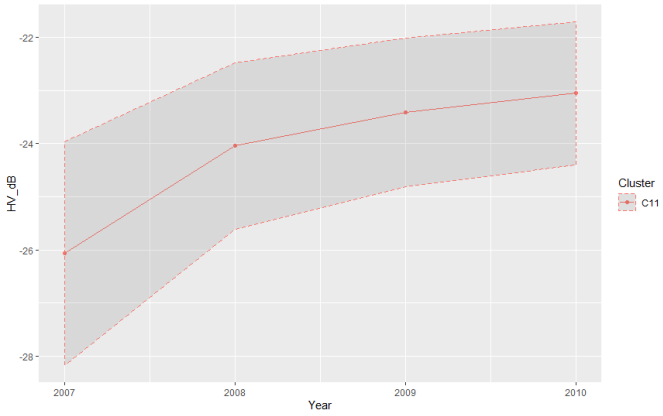

Figure 5.21: Signature pattern of group 11 cluster

Upon examining the spatial distribution of this group, two observations were drawn

a. This group represented mowed grasslands and bare forest areas which were prepared for replantation. These two areas give similar surface roughness with undulations on the ground. Mowed grasslands have tractor lines, and areas prepared for replantation have windrows to align the new trees that are going to be planted,both of which give the very low backscatter in 2007. These areas, upon replantation in the subsequent years, generate the higher backscatter recorded in 2010. Figure 5.22, taken during a field visit with Coillte in April 2017, shows an example of a felled area which has been replanted. .

Figure 5.22: A forest site showing recently planted trees under the red circles

The total area represented by this group was very low at 218 ha i.e., only 0.25% of Area1. Based on the observations, this group was labelled as Mowed grasslands/Replantation ready areas.

Group 12 with 4 clusters started with a backscatter of -19.9 dB in 2007 and showed an increase of 2 dB in 2010. Figure 5.23 shows the HV signatures of this group of clusters. There was also a similar pattern in HH signatures. This backscatter range, as explained for groups 6 and 7, was categorised as young trees. The gradual increasing pattern of backscatter in both HH and HV channels is indicative of growth in the tree structure leading to higher scattering.

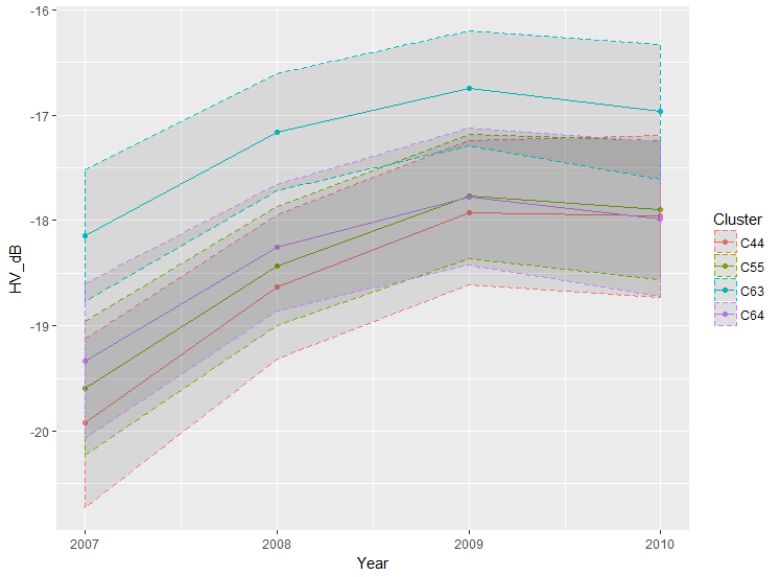

Figure 5.23: Signature pattern of group 12 cluster

Figure 5.23 shows an example of this group overlaid on BING imagery encapsulated by Forestry12 polygon. The planting date is 2002, indicating that this group of clusters belong to young forests. 40% of sub-compartment polygons were checked for planting year and these indicated a Planting year between 2000-2002 clearly indicating the presence of young trees. The increasing backscatter in the signatures indicate the growth of these young trees.

Group 13 also gave a similar pattern and by checking the PY, this group along with groups 11 and 12 were labelled as Tree Growth.

5.3.3.2.4 Group 14 – Increase and drop of 6-8 dB between two consecutive years

Figure 5.24 shows the cluster signatures of this group from both HV and HH channels. A large change was observed in the signatures between successive years.

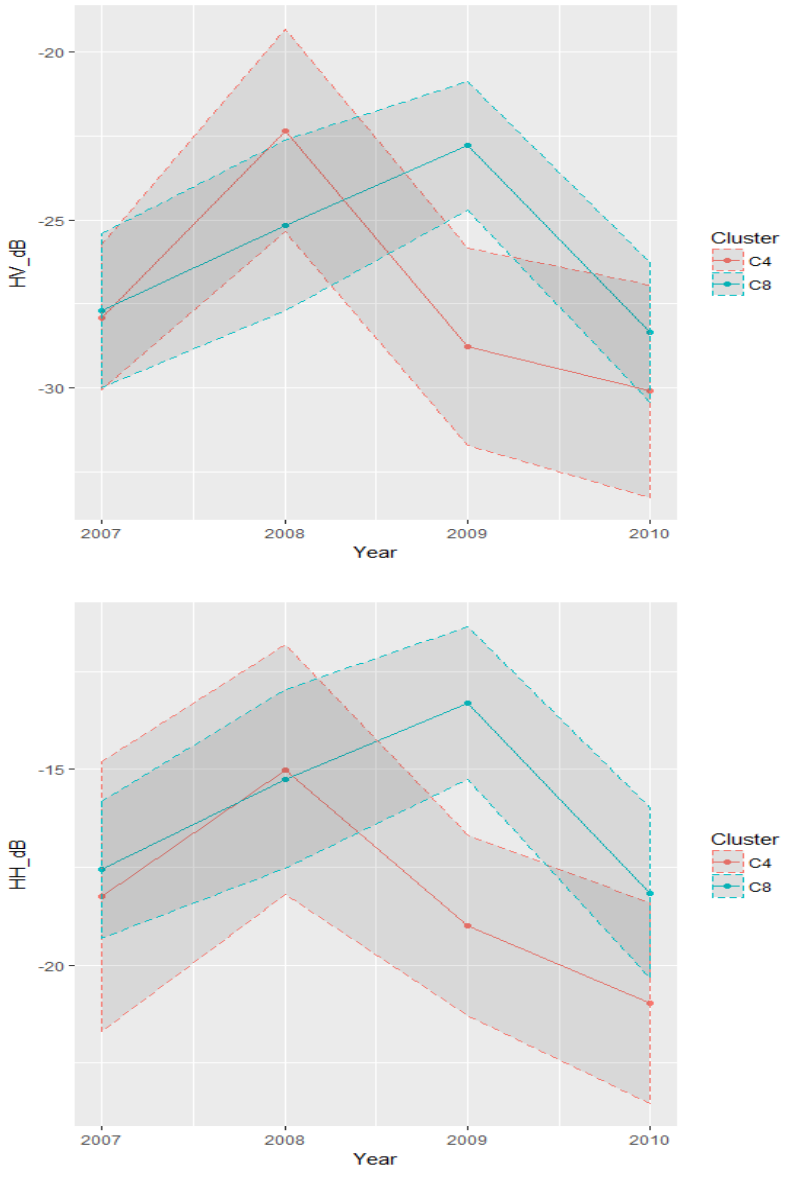

Figure 5.24: Signature pattern of group 14 clusters

In the HV bands of cluster 4, an increase from -27.9 dB to -22.3 dB was recorded between 2007 and 2008, and a drop from -22.3 dB to -28.7 dB was noted between 2008 and 2009. In HH, the magnitude of change was not as high as in HV, but a change

of 3 dB was recorded between 2007-2008-2009. Similar change was observed in cluster 8 in 2009 in both HH and HV bands.

Upon detailed investigation and examination, this group was labelled as anomalous because of the unexplainable characteristic of the signature pattern. Considering the role of environmental factors in the backscatter signal, this type of change is unusual. The spatial distribution of these clusters did not reveal any specific pattern. Only 818 ha of the entire Area1 was occupied by these clusters making less than 1% of Area1.

5.3.3.2.5 Group 15 – A decrease of 2dB from 2007-2010

A decrease from -16.8 dB to -18.3 dB was recorded from 2007 to 2010 in the HV bands as shown in figure 5.25. The HH signatures exhibited a similar pattern with different absolute values.

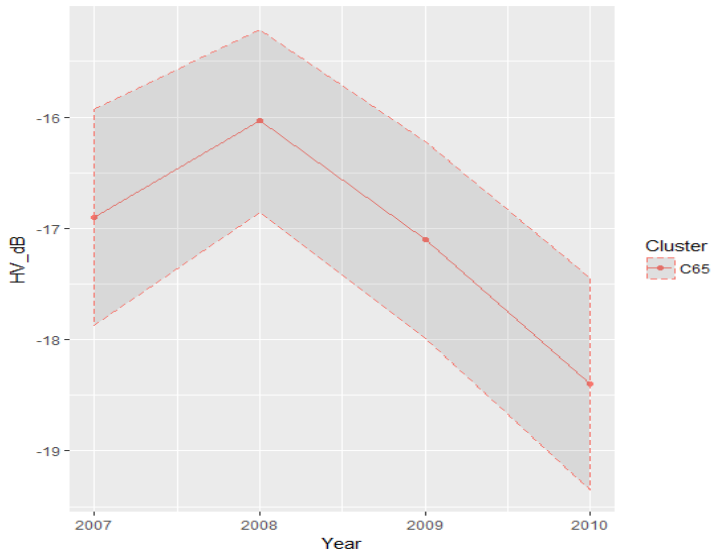

Figure 5.25: Signature pattern of group 15 cluster in both HV and HH band

The spatial distribution of this group was examined and it was found that this pattern appeared in random locations; only 0.11% of the entire Area1 was occupied by this group.This group was labelled Unknown.

5.3.3.3 Final groups of clusters

The final labels have been divided into three broad categories shown in figure 5.26.

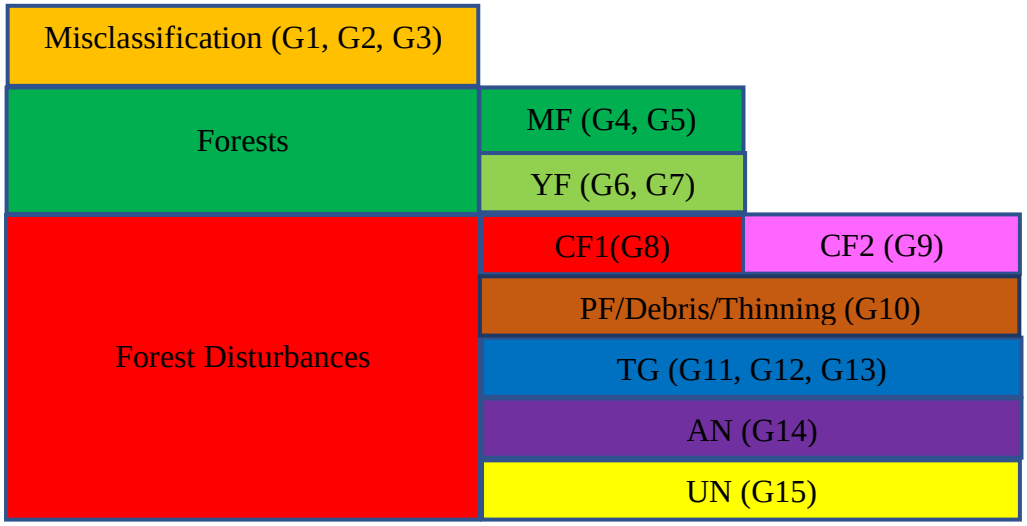

Figure 5.26: Final cluster groups and sub-divisions: G=Group; MF=Mature Forest; YF=Young Forest; CF1=Clear Fell (2009-2010); CF2=Clear Fell (2008-2009); PF=Plant Failure; TG=Tree Growth; AN=Anomaly; UN=Unknown

An extract of the final map taken from a small area of interest is presented in figure 5.27 representing the three broad categories and their sub-divisions. The disturbance events can be visualised spatially, and the exact area changed can also be derived. This can complement the forest inventory where discrepancies arise between the actual area felled and the fell area reported digitally.

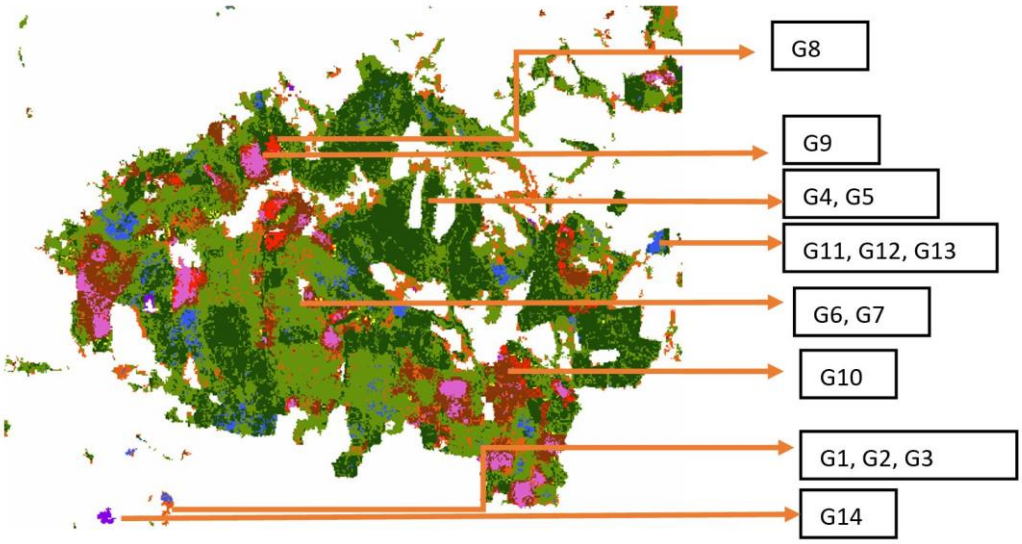

Figure 5.27: Extract from the final cluster map showing spatial locations of the final cluster groups

5.3.4 Transferring the algorithm on the other two study areas (Area2, Area3)

The algorithm with different experiment set up after being tested on Area1 was applied to Area2 and Area3. The data stack consisted of the HV and HH intensity bands from all four years forming an 8 band raster stack. The union of forest maps from each year generated from chapter 4 using the RF algorithm was used as a mask to ensure the clustering algorithm was appliede to the forest areas.

Due to the differences in the topography, forest types and weather conditions (as explained in chapter 3), the variations in the backscatter from the targets in the different areas were necessarily considered in making the algorithm robust. The initial step of the algorithm – deriving divergence statistics was applied to each of the study areas. In Area2, two peaks were found at 74 and 83 and in Area3, the peak was found at 80 clusters, as in Area1. As the smaller number of clusters were to be selected

according to the conditions outlined in section 5.1.1, 74 clusters were selected for Area2. Figures 5.28 and 5.29 show the divergence statistics derived for Area2 and Area3 respectively.

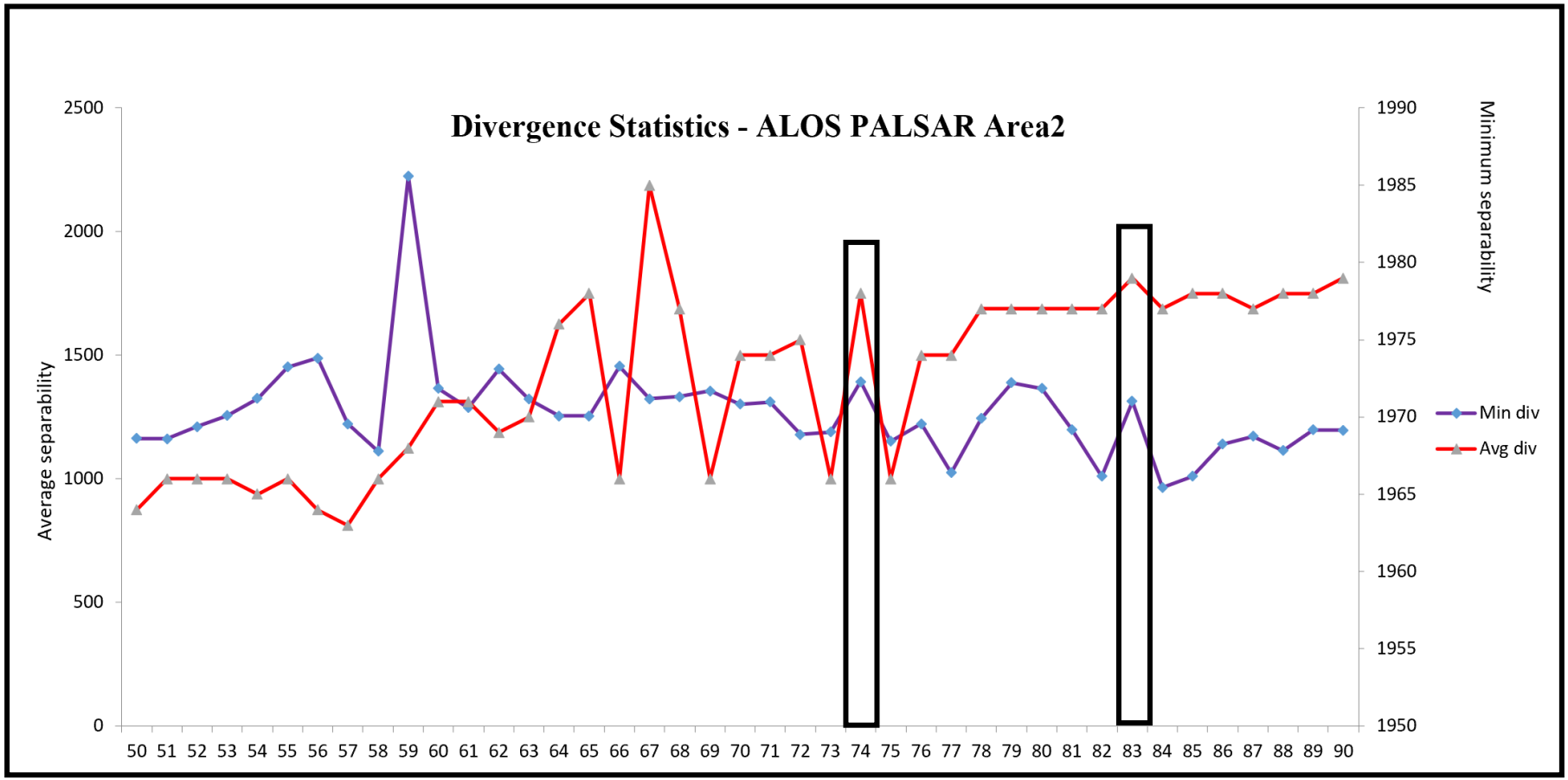

Figure 5.28: Divergence statistics plot dervied on Area2 indicating peaks at 74 and 83 clusters

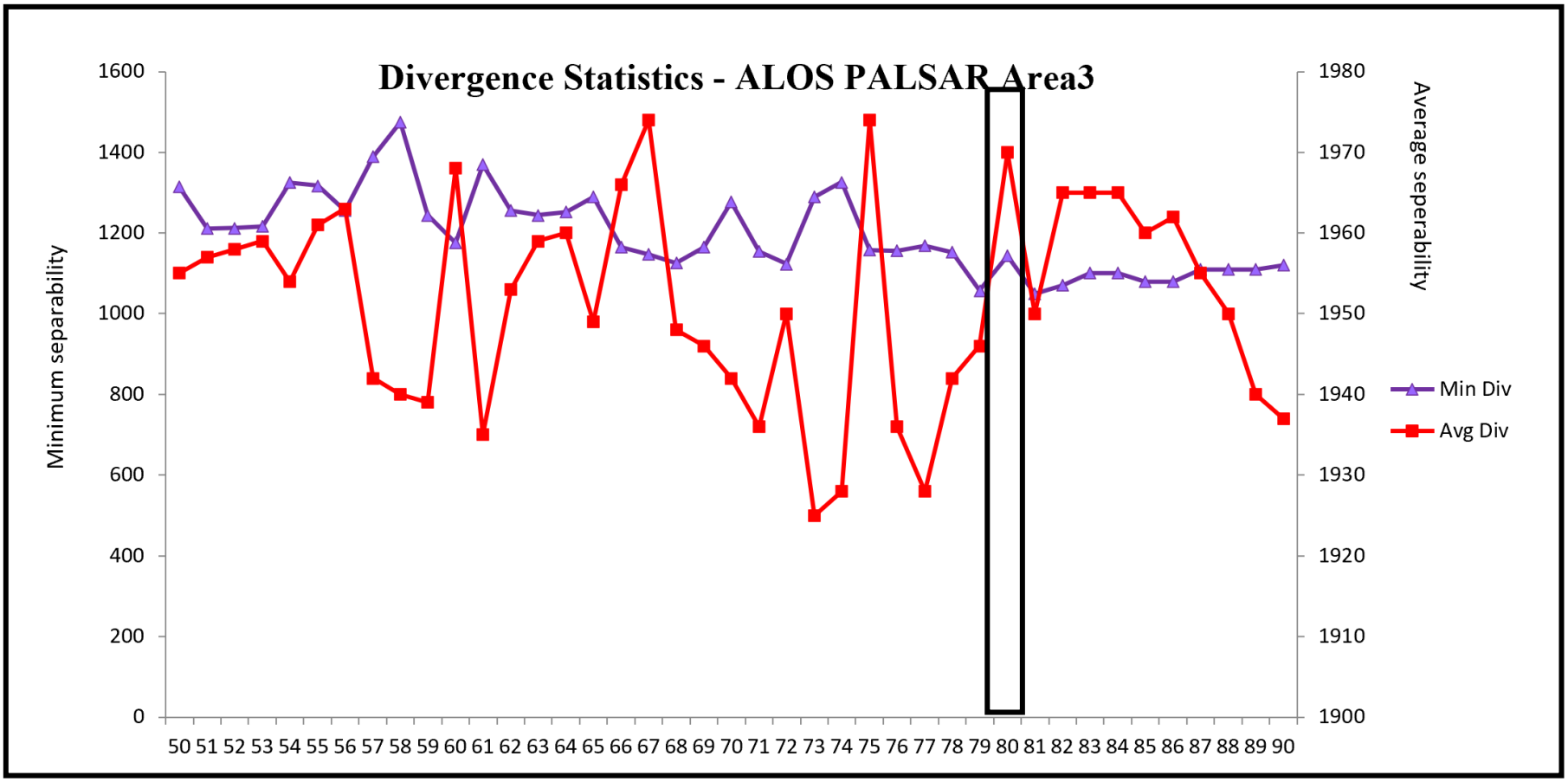

Figure 5.29: Divergence statistics plot dervied on Area3 indicating peak at 80 clusters

Dendrograms were used to group all the clusters to characterize the changes. Table 5.6 provides information on the different signature patterns observed for these two areas.

Table 5.6: Signature patterns observed in Area2 and Area3

Signature pattern	No. of groups in Area2	No. of groups in Area3
Pixel values remained the same to within 1 dB over the four years	7	7
A drop greater than 4dB between two consecutive years	2	3
A drop of 2 dB between two consecutive years	2	1
An increase of 4 dB over the years from 2007 to 2010	1	1
Increase and decrease of 6-8 dB in the backscatter between 2 consecutive years	1	1
A decrease of 2 dB from 2007 to 2010	1	1

In total 14 groups were formed in both Area2 and Area3. Similar patterns were noticeable between all the three study areas. One extra group was formed in Area3where a drop of greater than 4dB was recorded between two years in both the HV and HH bands. The pattern of this group was compared with that of Area1 and it showed similarity with the signatures of clear felling group of clusters. To analyse this further, the felled polygons from Coillte were used for validation.

Table 5.7: Comparison of number of felling instances between Coillte felled polygons and SAR image clusters

	Number of felled polygons from Coillte (2007-2010)	Number of instances identified by SAR corresponding to the felled polygons
Area2	67	43
Area3	154	98

From table 5.7, an agreement of 64.8% and 62.3% was obtained between the two datasets in Area2 and Area3 respectively. Similar investigations were undertaken as described in section 5.3.3.2, with Tables 5.8, 5.9, 5.10 and 5.11 showing the area based analysis and the categories defined for the missing polygons for both areas.

Table 5.8: Polygon based analysis for Area2 felling events

Polygon area	Number of polygons
<0.1ha	1
>0.1ha<1.0ha	9
>1ha<10ha	10
>10ha<15ha	2
>15ha<20ha	2

Table 5.9: Polygon based analysis for Area3 felling events

Polygon area	Number of polygons
<0.1ha	3
>0.1ha<1.0ha	19
>1ha<10ha	28
>10ha<15ha	3
>15ha<20ha	3

Table 5.10: Defined categories for missing polygons in Area2

Category	Number of polygons
Linear polygons	2
Validated with GE and discovered not felled	10
Very close to buildings	0
Very small polygons (<0.1 ha; <1 ha)	10
Bare Upland (*Mollinia*, Purple Blue grass)	1
No definite reason	1

Table 5.11: Defined categories for missing polygons in Area2

Category	Number of polygons
Linear polygons	4
Validated with GE and discovered not felled	17
Felled after June 2010	9
Very small polygons (<0.1 ha; <1 ha)	22
Not felled (recently planted in 2001)	1
Bare UpLand (Furze)	1
No definite reason	2

Similar to the results for Area1, in these two areas as well, there were polygons discovered that were actually not felled on ground but were incorrectly recorded as felled in the database which led to the discrepancies. In Area3, 9 polygons were checked and found to be felled after the date of SAR image acquisition which is not counted as a discrepancy in SAR results. In the undefined category, 3 polygons were Identified, possible reasons for this have been discussed in section 5.3.3.2.

The final agreements between the SAR and Coillte datasets were 75.43% and 74.67% for Area2 and Area3 respectively. Overall, in Area2 933 hectares were felled within the SAR derived forest areas based on the SAR results,with a slightly higher value in Area3 of 1029 hectares.

The same process for analysis of the cluster groups in Area1 was followed for Area2 and Area3 and the groups were labelled accordingly as presented in table 5.12. Classes with misclassifications and anomalies were apparent in these two areas as well. The algorithm has been successful in identifying signatures related to a generic group of mature and young forests (labelled based on the planting year information), and disturbances such as clear fells and tree growth within them. Similar to Area1, the dendrograms divided the higher backscatter into two groups of mature forests and the two of young forests. These have been marginally divided into different groups although the planting dates for group 4 and group 5 overlap. The different classes in each area have been compared and discussed in the discussion section 5.4 below. Figures 5.30 and 5.31 show the final maps of the different clusters.

Table 5.12: Cluster groups and their labels for Area2 and Area3

Group	Labels for Area2	Lables for Area3
1	Misclassification	Misclassification
2	Misclassification	Misclassification
3	Misclassification	Misclassification
4	Mature forests	Mature forests
5	Mature forests	Mature forests
6	Young forests	Young forests
7	Young forests	Young forests
8	Clear fells (2007 and 2008)	Clear fells (2007 and 2008)
9	Clear fells (2009 and 2010)	Clear fells (2008 and 2009)
10	PF/Debris/Thinning (2008 and 2009)	Clear fells (2009 and 2010)
11	PF/Debris/Thinning (2007 and 2008)	PF/Debris/Thinning (2007 and 2008)
12	Tree growth	Tree growth
13	Anomalies	Anomalies
14	Unknown	Unknown

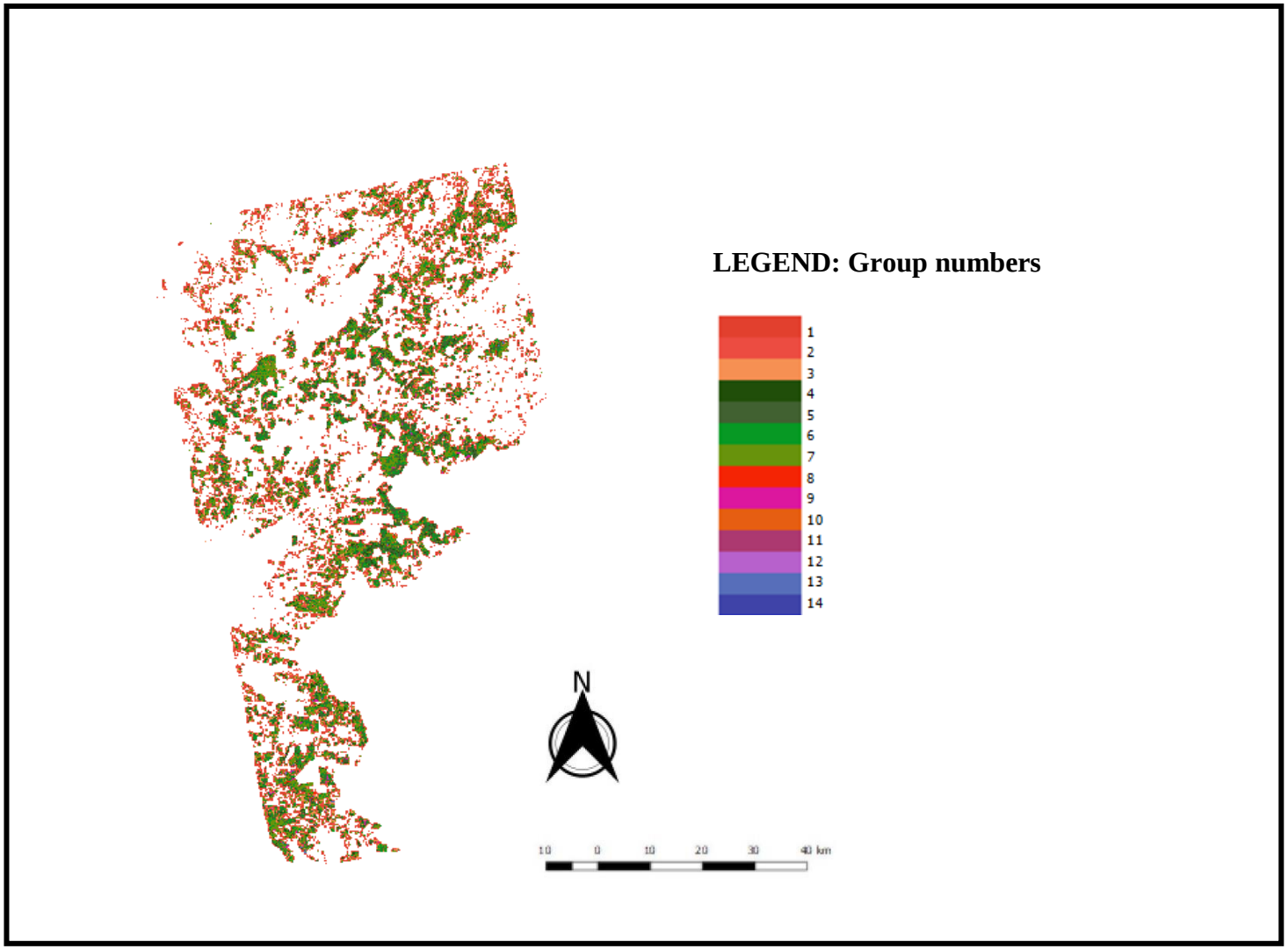

Figure 5.30: Map of final groups of clusters of Area2

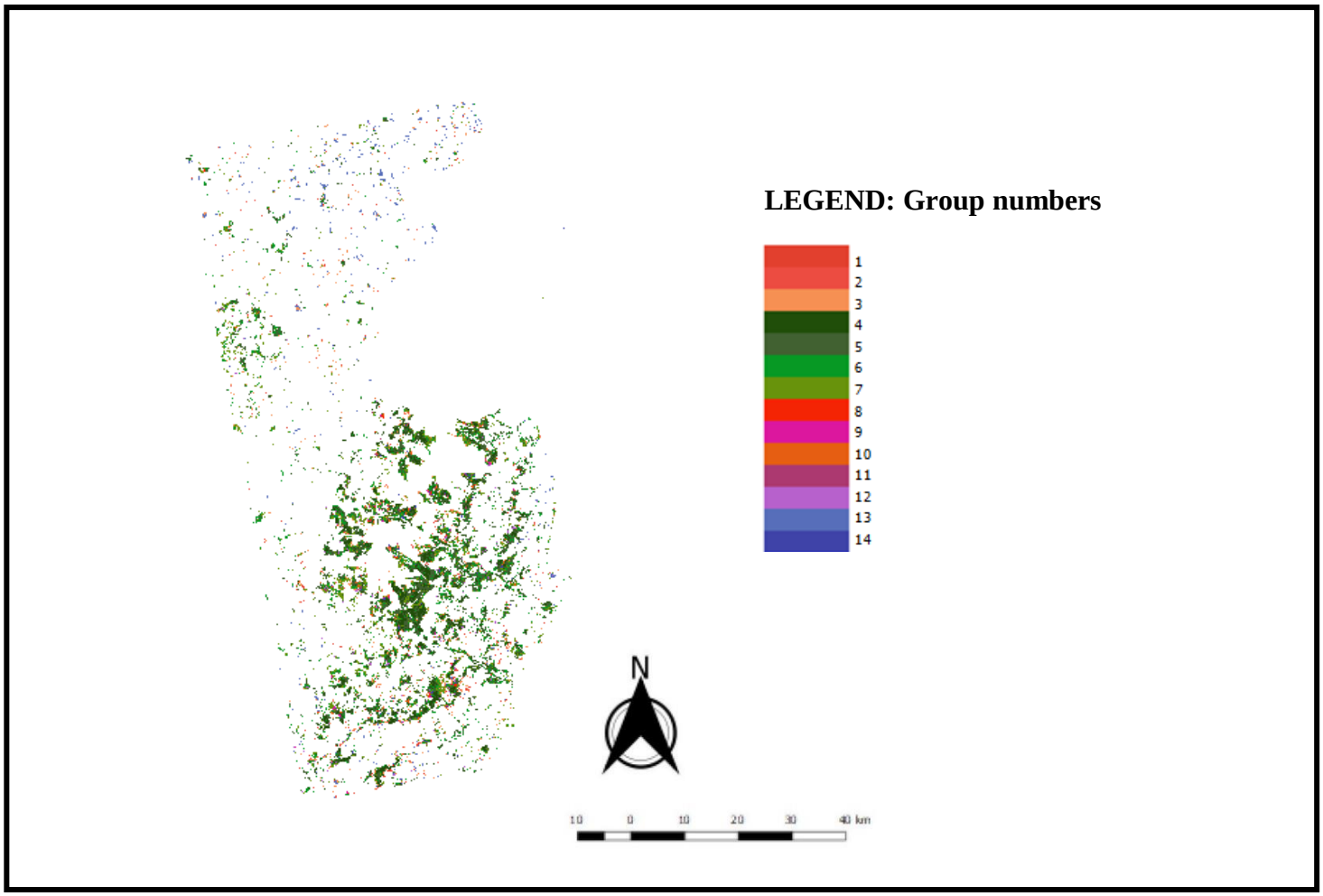

Figure 5.31: Map of final groups of clusters of Area3

5.3.4.1 Common groups identified by the algorithm across all study areas

Groups with a very low backscatter in HV (less than -25 dB) and HH (less than -23 dB) existed across all three areas. Considering classes related to misclassifications and anomalies, 4.25%, 2% and 6% of Area1, Area2 and Area3 was occupied. The cluster profiles pertaining to three classes common in all areas are discussed below.

1) **Clear felling:** This was unambiguously identified in all the areas with a distinct pattern. They were cross verified and validated with the available reference polygons and the occurrence of the events were confirmed. Clusters from all the years and from a representative site in each area which showed this change were plotted in Figure 5.32 for the HV band..

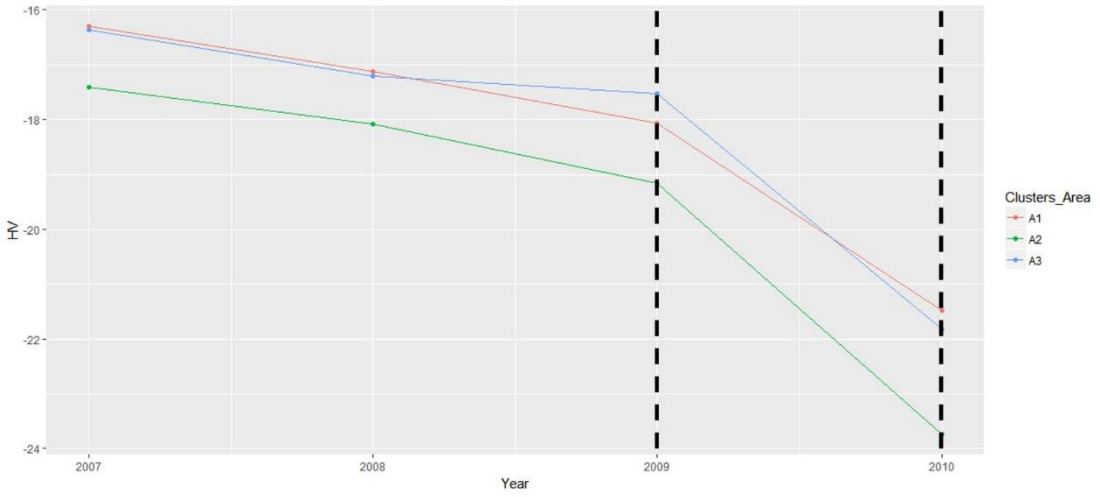

Figure 5.32: Signature profiles of clusters in HV representing clear fells across all three areas;A1=Area,A2=Area2,A3=Area3. The black lines mark the period of change on the graph

A significant change of greater than 4 dB can be seen in the figure for the HV band. The difference in the 2007 pixel values between the areas, depends on the tree species, the management approach, and the age of trees. A similar pattern was observed in the HH band of all three sitesirrespective of the area. This similarity between areas and bands suggests that the SAR algorithm can successfully distinguish areas of clear felling, which is one of the primary harvesting methods in Ireland.

2) **Forest group:** The profiles from each area for the mature and young trees groups were compared against each other. Figure 5.33 shows the boxplots showing the distribution range of backscatter values in HV band for these groups. Across all the areas, the backscatter values fall within the same range for this category of clusters, thus stressing on the fact that these groups belong to the same category (Mature and Young forests) across all study areas. In the figure, the groups of mature and young forests have been combined to understand the intensity range of forests that have not undergone any change within the four year period. This can also be compared with the boxplots of backscatter analysis in chapter 4, section 4.2.1 in which the boxplot for forests have the same range as specified in this section. Across all the study areas, the backscatter range for these groups fall within the range -10 to -22dB in HV and -8 dB and -16 dB in HH.

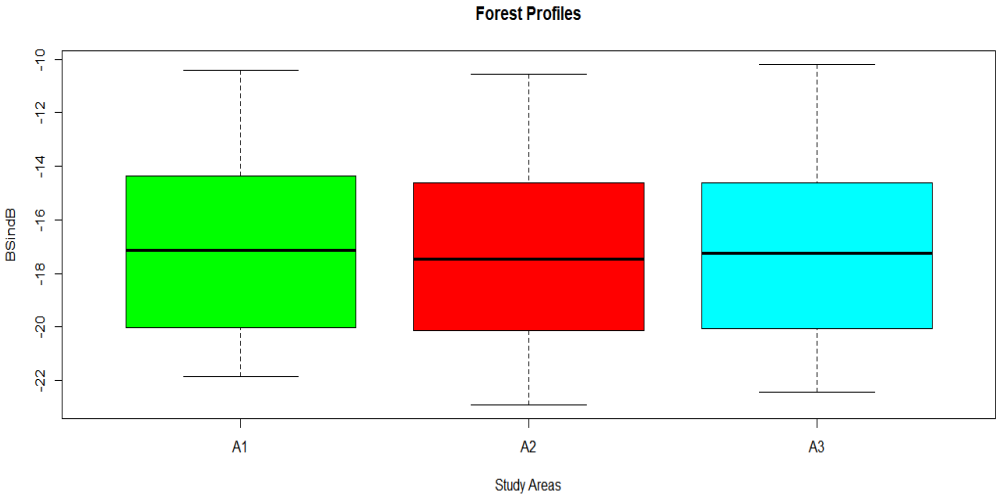

Figure 5.33: Boxplots for forest profiles across all areas of study for HV polarisation; A1 = Area1, A2 = Area2, A3 = Area3

3) **Tree growth:** Clusters representing growth in the trees from 2007 to 2010 have the same pattern across all areas. This is shown in figure 5.34. There is an increase in the backscatter towards 2010 in all the areas. The value range may differ but the pattern is similar. A total of 3986 ha, 837 ha and 432 ha were afforested between 2007 and 2010 in Cork (bigger part of Area1), Donegal (bigger part of Area2) and Wicklow (bigger part of Area3) according to (*DAFM, 2017)* with Sitka Spruce as the dominant tree species. The fast growth

of these trees is identified by the clusters with the increasing backscatter with the increasing tree biomass.

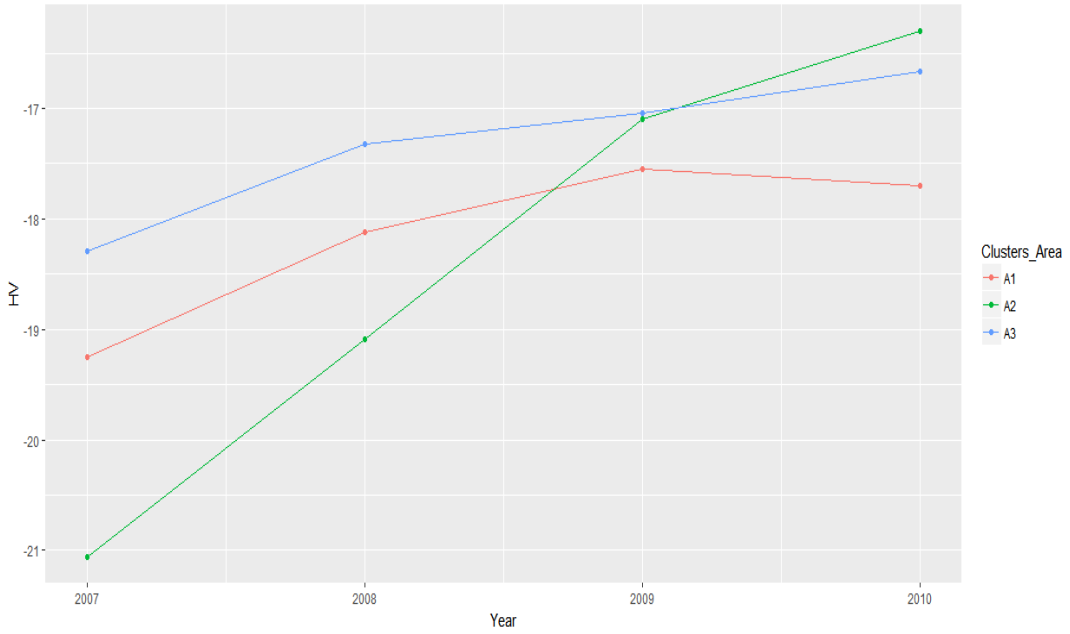

Figure 5.34: Signature profiles of clusters representing tree growth across all three areas ;A1=Area,A2=Area2,A3=Area3

These analysis support the fact that the algorithm has worked succesfully on all the three areas. Other classes such as plant failure/thinning/debris and unknown were also analysed and similar patterns were found. Due to the lack of evidence supporting these classes, they could not be used for further analysis. The unknown class across each site occupied a very little area of each study area – 0.25% of A1, 0.01% of A2 and 0.4% of A3 which was negligible.

The results presented in the current section have been discussed in section 5.4.

5.4 Discussion and conclusions

This chapter described an approach to track and label the different types of disturbances within the forests of Ireland that were initially mapped in Chapter 4. Using the HV and HH composites of ALOS PALSAR data over the period of four years, ISODATA clustering was performed. The advantage of using the divergence index for this clustering approach was the possibility of choosing the number of clusters in defining the different variabilities within the mapped forests. Due to indices such as the Transformed Divergence and Jeffries-Matusita distance suffering from saturation, especially for values above 1.9, divergence indices were used which work on the condition that D_{ij} must be > 24 *(de Bie et al., 2012)*. The self-organizing algorithm formed clusters based on the input bands following which natural cluster groups were formed using the hierarchical clustering approach. No training data or extensive prior knowledge of the area were required, which was practical for this study where the forest monitoring system is conducted once in six years causing a lag in forest updates. However, the ISODATA approach has its own limitations and requires attention before performing the clustering process. The ISODATA algorithm strongly depends on the distance threshold for the merge of clusters (MD) and deviation threshold for the split of clusters (SD) as described in section 5.3.1. Incorrect choice of these parameters could result in an incorrect number of. The parameters are dependent on range of the input band values, and the most suitable parameters for this study derived after conducting many trials.

By using only backscatter values, clear fell events have been identified with a definite pattern among all study areas. Inclusion of texture measures, and ancillary data such as slope and aspect, was not feasible due to the technical and data normalisation issues encountered as described in section 5.3.1. Improvements to this algorithm can be made by including polarimetric decomposition techniques to separate different scattering mechanisms – this is possible through fully polarimetric (quad-pol) SAR data on areas where these data are available. This will however limit the application of the algorithm to areas where fully polarimetric data are unavailable. This will hinder the forest monitoring application on a national level, however on a reginal scale specific to the availability of quad-pol data, forest monitoring is feasible. A recommendation is to modify the input bands depending on the specific application for example, choosing bands such as Radar Burn Ratio and Radar Burn Difference as input to the ISODATA

approach as shown in the study by *(Lasaponara and Tucci, 2019)* will enhance the potential of the algorithm in detecting burn scars in forests.

This approach has used one image per year depending on the availability of ALOS PALSAR images over the study areas. Most often classes from ISODATA or K-Means classification overlap and using more images per year will be better. However while monitoring forest changes, including imagery from different seasons will add seasonal influences leading to mixed signals which can be confused with the actual disturbance events. In this study one image per year acquired during the summer months has been used. One reason for choosing one image per year was the low frequency of data – only 3 ALOS PALSAR images were acquired per year over the study areas (two from winter and one from summer). The growth and rotation cycle of forests is very different when compared to other land cover types such as grasslands and cropland in which the latter undergo the entire cycle of seeding, growing and harvesting within the year. In Ireland, on average for Sitka spruce, the forest rotation cycle is 40 years – annual changes are not common provided the trees are healthy. To assess yearly changes in forests, a minimum of two images are required to evaluate the condition of forests before and after a disturbance. To assess changes such as deforestation, a minimum of three temporal observations are required, the first one of which must represent forest *(Hamunyela et al., 2016)*.

The Forestry12 polygons and Coillte felled polygons have been useful sources of data in interpreting the cluster signatures. Although concrete evidence for groups of clusters other than clear fells was unavailable, these data sources provided vital information such as planting year which were useful in understanding the growth cycle of forests. Through this information it was possible to understand and draw theories on certain groups of clusters such as mature/young forests and tree growth and hence labelled. The discrepancies that these data have in terms of forest area coverage and reporting disturbances, have been addressed by SAR data in the study. Disturbance events that occurred in forest estates that are not owned by Coillte have been identified by SAR providing updates on forests. This will also be useful to private forest owners in monitoring their forest estates. An additional value provided by this algorithm is the size of the forest area disturbed. In some forest inventory reports, the exact area disturbed is incorrect leading to confusion in further stages of monitoring. This information can be supported by the algorithm presented here by extracting the exact

forest changed and help in the next stages of monitoring. The annual and timely updates provided by SAR through this algorithm can also supplement forest inventory databases that have inconsistencies in their reporting systems. Keeping the databases up-to-date by updating the missing/outdated attributes is certainly a promising service that this algorithm will provide, especifically for clear felled events.

After the application of the ISODATA approach to Area1, its transferability to the other two areas was assessed. The approach used in this study was found to be robust in identifying clear fells over all study areas with a distinct pattern in the cluster signatures. The similar trends observed in each area demonstrated the consistency and robustness of the algorithm. A significant change of 4-5 dB was clearly observed in places where trees were felled. Both HV and HH bands showed a distinct difference in the backscatter after clear felling, with the HV band giving a better difference before and after change. The challenging part was to characterize the group of clusters with a decrease of 2dB between consecutive years. A limitation of this approach was it was unable to distinctly separate the signals coming these intra groups. No ground truth information was available to compare the results with and understand the type of behaviour the clusters exhibited. Based on the field knowledge and the PY from reference datasets, it was possible to gauge these disturbance types and categorise into one group. The signals for tree growth were visible with a gradual increase in the backscatter from 2007 to 2010. This type of change was assessed with the help of Google Earth imagery and the PY data from the reference datasets. Field visits were helpful in acquiring knowledge on what happens in the field which helped with the characterization of these cluster groups. The anomalies and unknown groups of clusters are also common in all areas with signatures unable to validate. This consistency in the algorithm across the study areas with slightly different geographic and topographic features is an indication of its applicability on a national scale. By testing the approach on three study areas, supporting local and regional scale forest monitoring is possible which will help local and regional forest owners/companies in making decisions. Ireland is supporting many forest monitoring programs as explained in chapter 1 of this thesis. The forest monitoring projects that use optical data can be supplemented with this algorithm which is beneficial for providing data on cloud covered areas. Supporting the NFI and providing forest updates on an annual basis is surely a foresight of this algorithm which will provide additional value to forest

monitoring in terms of providing weather unaffected images and identifying the nature, location and size of disturbed forests.

The ISODATA transferability has shown encouraging results. However, these are purely data driven. These clusters do not necessarily have a direct meaning according to the semantic definitions of land categories as used by IPCC. There is a risk involved in interpreting the clusters that are formed purely based on information content of the SAR image. While assigning meaningful labels to these clusters, the onus is on the interpreter to make the meticulous transition from indirect to direct meaningful labelling of the clusters.

The overall methodology of mapping forests and monitoring the disturbances within them presented in chapters 4 and 5 has shown to be consistent across all three study areas. The combination of supervised and unsupervised approaches for monitoring forests using SAR data carries the benefits and limitations of each approach. The power of machine learning has been presented in chapter 4 where, upon training a single image, other images can be classified without acquiring training data for each image. Running clustering algorithms on these images combined has helped enhance the algorithm by highlighting some of the misclassifications brought about by each individually image classified previously. The different misclassification groups, anomalies and unknown groups of clusters are either a result of the discrepancies between the two algorithms or SAR induced errors. Apart from this caveat, the overall methodology has been able to successfully map mature and young forests and identify changes such as clear fells, degradation and tree growth within the study areas.

Considering the big picture of the project which is providing consistent updates to CARBWARE in the light of reporting carbon emissions to Kyoto Protocol, the algorithm presented here can be used as a support tool. However this requires consistent data acquisition which is an issue given the lifespan of satellites. In order to establish a continuous forest monitoring platform, this algorithm was transferred on the existing ALOS-2 PALSAR-2 L-band SAR sensor. The next chapter desribes the transferability of the algorithm on this sensor and its consistency is assessed.

Chapter 6

ALOS PALSAR Based Algorithm Transferability to ALOS-2 PALSAR-2

"The important thing is not to stop questioning. Curiosity has its own reason for existence" – Albert Einstein

6.1 Introduction

The UNFCCC definition of deforestation refers to the "direct human-induced conversion of forested land to non-forested land" *(FAO, 2020)* and for most purposes, in Ireland, if replanting has not taken place within five years *(Devaney et al., 2017)*, this is considered to be a permanent land-use change (i.e. deforestation). If replanting occurs within this period, disturbances such as clear-felling do not constitute deforestation. For the four-year period of ALOS PALSAR data discussed in chapter 4, identifying deforestation events according to this definition was not feasible, but with the incorporation of ALOS-2 PALSAR-2 datasets from 2015-16, the window of five or more years provided an opportunity to monitor permanent loss of tree cover within the study areas. Monitoring forests and their short and long term changes in a robust, reliable and objective manner on an annual basis is crucial in understanding forest management operations and their implications, therefore, having a method that is applicable to more than one satellite sensor is important.

The ALOS PALSAR sensor operating between 2006 and 2011 provided data for many operational and research endeavours worldwide *(Almeida-Filho et al., 2009; Shimada et al., 2014; Baghdadi et al., 2015; Khati et al., 2018).* After reaching the end of its targeted life of 5 years, there was a gap before the launch of its successor ALOS-2 PALSAR-2 in 2014 with enhanced features including higher spatial resolution and radiometric senstivity and better observation repetition frequency (*Rosenqvist et al., 2014)*. This chapter aims to evaluate the potential of ALOS-2 PALSAR-2 data in mapping inter-annual and longer term forest disturbances in Ireland by applying the methodology developed in chapters 4 and 5. The specific objectives are to:

1) Evaluate the transferability of the algorithm to ALOS-2 PALSAR-2 datasets by assessing any inconsistencies identified during the process.
2) Identify forest areas that were removed between 2007 and 2010 and not replanted by 2015-2016, thus indicating permanent land-use change.

6.2 Methodology

The consolidated methodology developed in chapters 4 and 5 is shown in figure 6.1. The workflow consists of generating forest/non-forest maps using the Random Forests classifier and, from the resulting forest cover maps, using an ISODATA classification to characterize disturbances. Steps 1 and 2 of the workflow (figure 6.1), along with ALOS-2 PALSAR-2 data acquisition details have been discussed in chapter 3 (section 3.3.2). Steps 3, 4, 5 and 6 are discussed in sections 6.3, 6.4, 6.5, 6.6 and 6.7.

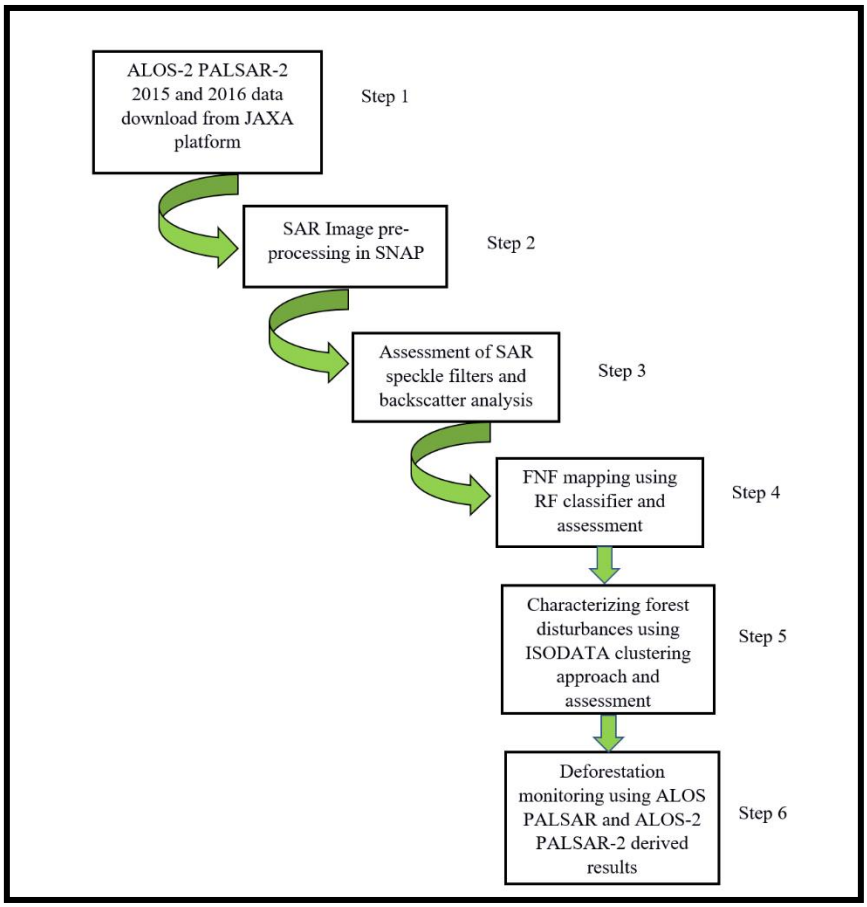

Figure 6.1: Workflow of the methodology used to generate forests and forest change maps using PALSAR-2 data

6.3 Transition in the SAR pre-processing software and assessment of SAR speckle filters to be used

Previously, in chapters 4 and 5, ALOS PALSAR datasets were pre-processed using the proprietary SARscape software. With a growing move towards open-source and freely available software, a transition was made to the ESA SNAP toolboxes to pre-process the ALOS-2 PALSAR-2 images. Both the software packages offer standard SAR pre-processing modules, however the speckle filters are exclusive to each software. The De Grandi multi-temporal filter was used for the ALOS PALSAR data, and in order to select the most comparable speckle filter available in SNAP, an image that had been pre-processed in SARscape was re-processed in SNAP and the data values were compared. Three assessments were conducted for the selection of the most appropriate filter.

- Based on literature: Many studies have proposed the Lee filter as the most standard speckle filter because this is superior in preserving prominent edges and texture information *(Qiu et al., 2004; Domg et al., 2001)*.
- Based on Equivalent Number of Looks (ENL): "The equivalent (or effective) number of looks (ENL) is a parameter of multilook synthetic aperture radar (SAR) images, which describes the degree of averaging applied to the SAR measurements during data formation and sometimes also postprocessing" *(Anfinsen et al., 2008, pg. no. 1)*. To assess the ability to suppress the speckle in a SAR image, the ENL is commonly calculated over a uniform area. Typically, the higher the ENL, the higher the efficiency of the filter in suppressing the speckle (*Gagnon and Jouan, (1997), Wang et al., (2012) and Xiao et al., (2003).* This was calculated over a large patch of homogeneous forest area, with the results shown in table 6.1. From table 6.1, the closest to De Grandi filter was Lee followed by frost, gammaMap, boxcar and IDAN filters.

Table 6.1: ENL for different speckle filters

	De Grandi	Lee	RLee	Frost	GammaMap	Boxcar	IDAN
ENL	30.2	32.2	9.9	28.5	28.5	28.5	28.5

- Based on visual assessment: It was found that the Lee filter worked well in achieving a balance between speckle reduction and preserving finer details. However, it was observed that the Lee filter blurs the image and does not retain

the edges to the same extent as the De Grandi filter. So, to minimise this, the window size was limited to 3×3. Figure 6.2 shows an ALOS PALSAR image before speckle filtering, the image filtered with the De Grandi filter in SARscape and the image filtered with the Lee filter in SNAP.

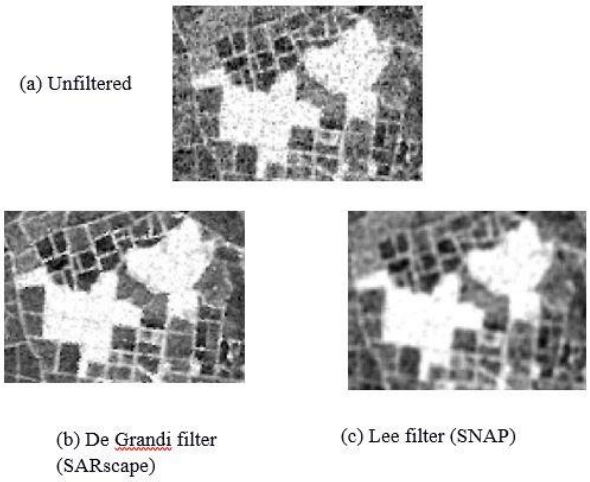

Figure 6.2: Viusal comparison between (a)unfiltered, (b) De Grandi and (c) Lee speckle filtered ALOS PALSAR image

6.4 Backscatter analysis

The backscatter values from ALOS-2 PALSAR-2 FBD HV and HH channels for the summer, autumn, and winter images of 2015 and 2016 were analysed to assess the response from various targets. Combining reference data from Forestry12 and PrivateForests2016 datasets, a single reference dataset (subsequently referred to as Forests12_16) was formed. Using this combined reference dataset, HV and HH backscatter (γ°) values from 500 forest pixels were collected; 500 non-forest (excluding urban) pixels were identified using Google Earth imagery and LPIS 2012, and, with the aid of CORINE 2018 data, 500 urban pixels were extracted from both HH and HV SAR images. The distribution of γ° values for forests, non-forests (excluding urban) and urban for all three areas and both acquisition years are shown in figure 6.3 and 6.4.

2015 HV

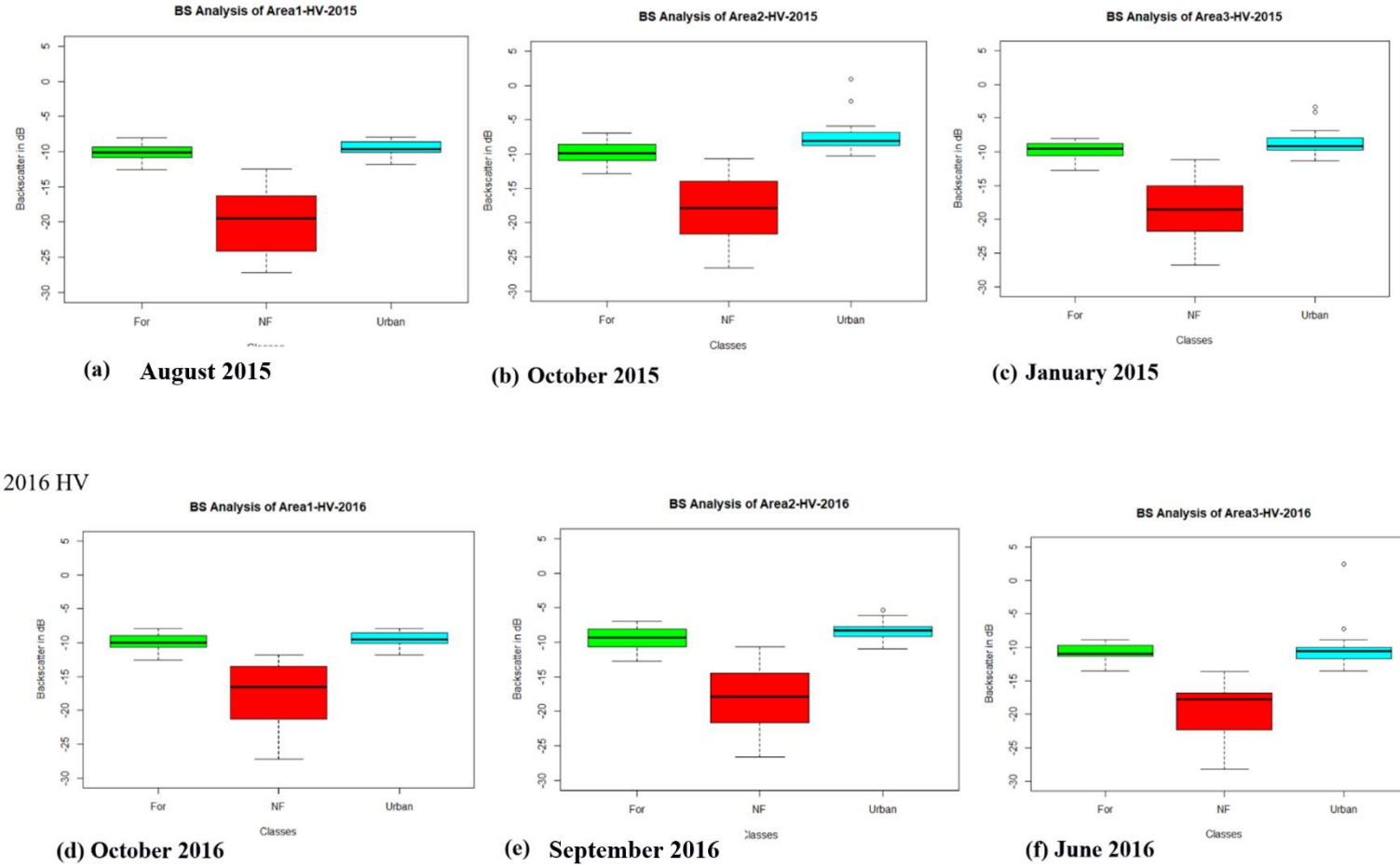

Figure 6.3: Distribution of ALOS-2 PALSAR-2 HV γ° values across all areas and classes (forests, non-forests and urban)

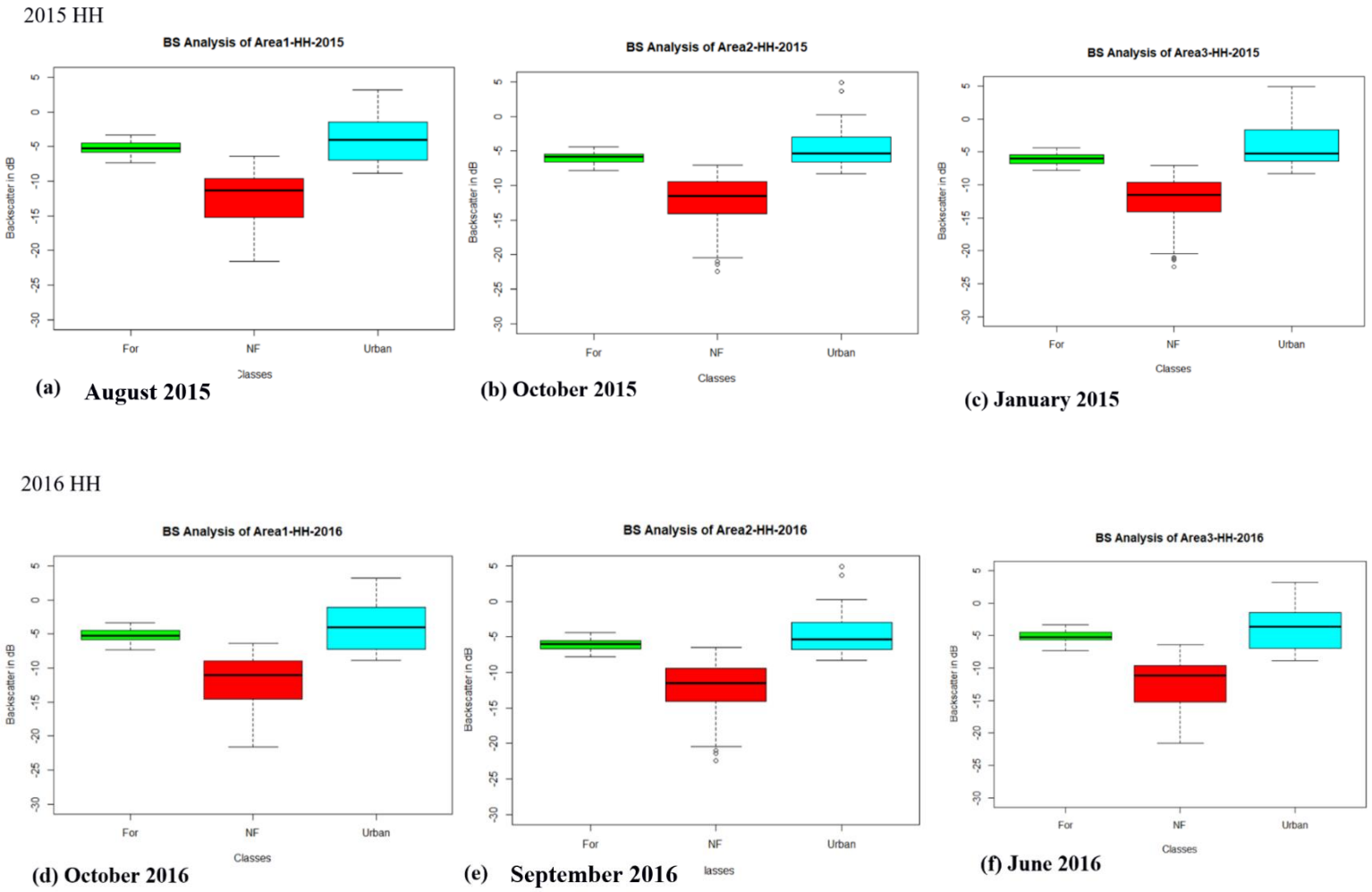

Figure 6.4: Distribution of ALOS-2 PALSAR-2 HH γ° values across all areas and classes (forests, non-forests and urban

As expected, a wider difference in the backscatter between forests and non-forest classes is observed in the HV channel, with an average difference of 10dB, compared to a 6dB difference in the HH channel. Within the samples chosen for this analysis, minimal overlap is observed between forests and non-forest classes for Area1-2015 (figure 6.3 (a)) and Area3-2016 (figure 6.3 (f)) which are summer acquired. The overlap between the forests and non-forest classes is apparent in the other boxplots in figure 6.3 (b, c, d, e), with the first quartile of the former containing the same range of values as the fourth quartile of the latter. Although summer images are ideal for the work, the impact of using non-summer images is studied in this chapter by considering autumn and winter images.

A summer image from ALOS-2 PALSAR-2 was compared with a summer image of ALOS PALSAR covering the exact same area to understand the distribution of γ° values in both sensors (see section 4.2.1 for more detail on the ALOS PALSAR values). Figure 6.5 shows the distribution of HV γ° values for ALOS PALSAR in June 2010 and ALOS-2 PALSAR-2 in August 2015 for Area1. The mean difference between forests and non-forests with ALOS-2 PALSAR-2 is -10dB while with ALOS PALSAR is -8dB which agrees with *Rosenqvist et al., (2014)* with the bigger difference between forests and non-forests in ALOS-2 PALSAR-2 image than ALOS PALSAR image.

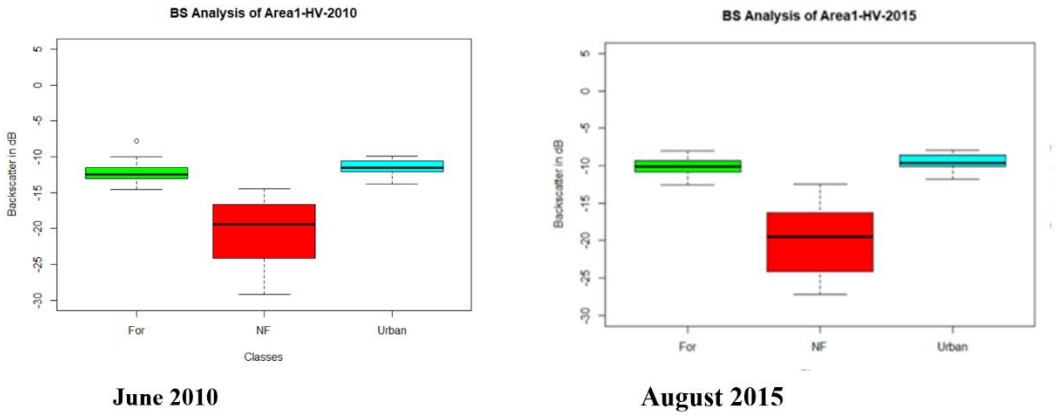

Figure 6.5: Distribution of ALOS PALSAR HV γ° values from Area1 - 2010 for forests, non-forests and urban classes

Another observation from the boxplots is that a higher power is received from the targets for ALOS-2 PALSAR-2 when compared with ALOS PALSAR. For example, in figure 6.5 the mean HV γ° value for forests from ALOS PALSAR is –13dB, while from ALOS-2 PALSAR-2 it is -11dB. Similar observations were found for the HH channel with a mean of -8dB for ALOS PALSAR and -6dB for ALOS-2 PALSAR-2 for the forest class. Given the similarity between the urban and forest classes, as described in chapter 4, section 4.2.1, urban/settlement classes were masked out from all the images using the CORINE 2018 data *(Copernicus, 2018)*.

6.5 Forest non-forest maps using RF classifier and evaluation

A new RF model was built for ALOS-2 PALSAR-2 images by collecting new training samples from the 2015 images of Area1 and Area2 and the 2016 image for Area3, in preference to the winter 2015 image in order to achieve optimum forest/non-forest discrimination. A total of 3100 training samples were collected (forestland=1800; cropland=300; grassland=400; peatland=400; water=200). Reference data included Forests12_16 data for forestland, LPIS 2012 for cropland and peatland, and Google Earth, BING imagery and CORINE 2018 for grassland and water. As described in chapter 4, section 4.2.2, the RF classifier was run on the stack of radar HV backscatter coefficient images (γ^0), seven GLCM texture measures (from window size 11×11 - variance, entropy, correlation, contrast, homogeneity, second moment and dissimilarity), slope and aspect.

The variable importance plot was examined, and, as shown in figure 6.6, it was found that the two most important variables for Area1 were GLCM variance and HV gamma. For Area2 and Area3, slope was the most important variable, with HV γ^0 and GLCM variance the next two most important variables. As these latter two areas are more mountainous than Area1, the classifier correctly identified that slope was a more important consideration for classification than the other GLCM texture measures, with slope taking a much lower importance value in classification for the flatter topography of Area1.

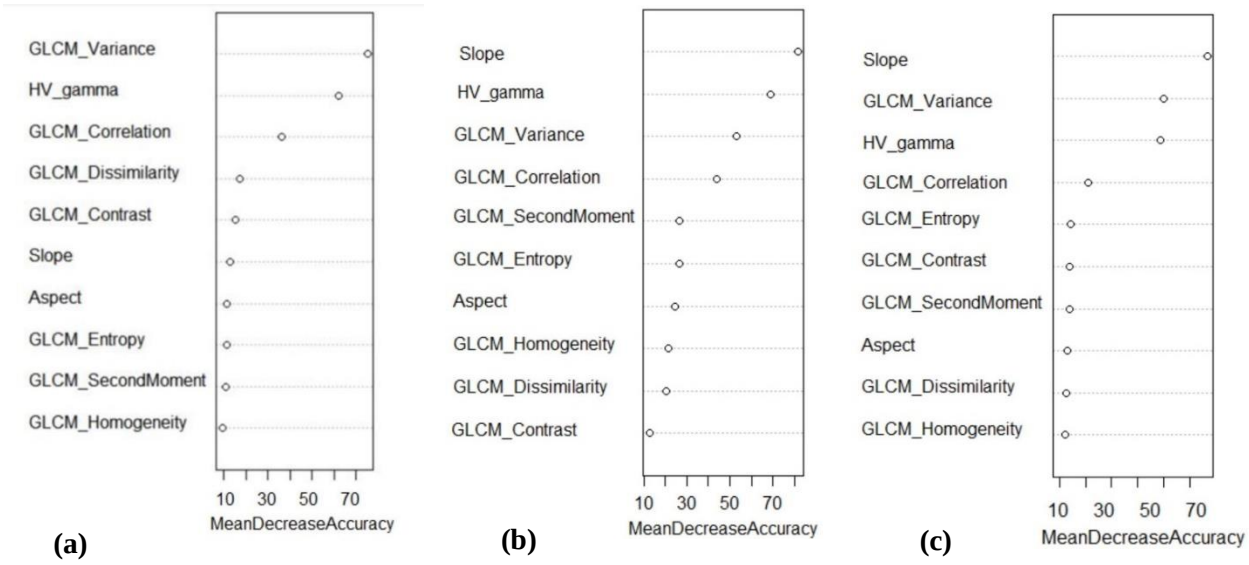

Figure 6.6: Variable Importance Plots generated by the RF classifier for (a)Area1, (b)Area2, (c)Area3 for ALOS-2 PALSAR-2 image classification

From chapter 4, section 4.2.4, the most influential input for classification of ALOS PALSAR for all the three areas, apart from slope, was HV γ^0 followed by different GLCM measures for each study site. From figure 6.6, for ALOS-2 PALSAR-2 classification, ignoring slope, GLCM variance and HV γ^0 are the most important variables across all three regions. For both the sensors, HV γ^0 plays an important role for RF classification followed by texture measures. GLCM variance represents the inter-class variations (abrupt changes in the DN values) which are more apparent in ALOS-2 PALSAR-2 images due to the enhanced radiometric difference between forests and non-forests.

6.5.1 Post-classification filtering (PCF)

For the ALOS PALSAR classified images, many single misclassified pixels were generated, and the result was unacceptably noisy. However, for the ALOS-2 PALSAR-2 images, the classification resulted in a cleaner and smoother appearance as shown in figure 6.7. One plausible explanation for this is the application of the Lee filter, which is better at speckle suppression than De Grandi filter and well known to produce a smoother appearance on the image. However, single pixels existed that required cleaning, and as with the ALOS PALSAR images, the majority filter was applied to the ALOS-2

PALSAR-2 classified outputs to remove the noise. Forest patches before and after PCF from both ALOS PALSAR and ALOS-2 PALSAR-2 are shown in figure 6.7.

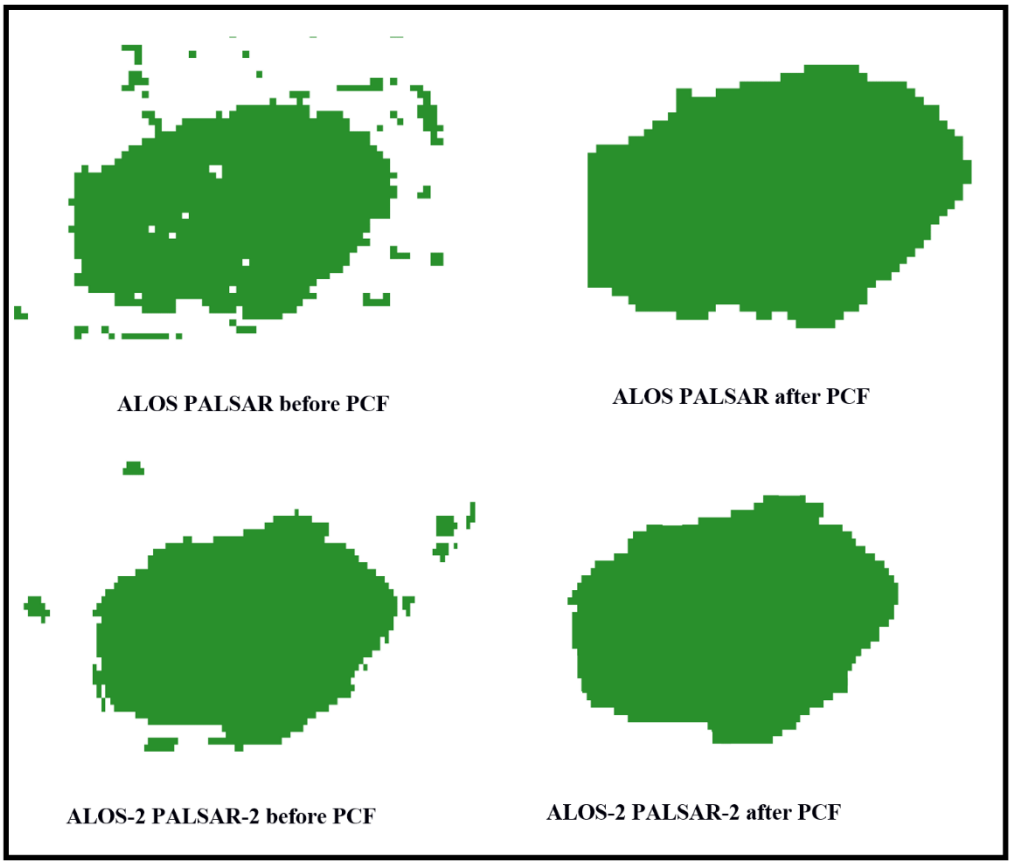

Figure 6.7: Comparison of a single forest patch derived from ALOS PALSR and ALOS-2 PALSAR-2 before and after PCF

The next stages of the filtering process for the ALOS PALSAR images involved removing areas smaller than a threshold of 82 pixels, equivalent to an area of 1.8 ha (chapter 4, table 4.2) resulting in the maximum overall accuracy of 87.7%. With the higher resolution of 8×8m, when an area-equivalent filter of 293 pixels was applied to the ALOS-2 PALSAR-2 data, lower accuracies of 76% were found for the classification. In an iterative process of reducing the value, filters with lower thresholds were applied, with the highest accuracies of 86% observed for a threshold of 175 pixels which equates to an area of 1.1 ha. With fewer mixed pixels in the higher spatial resolution images of ALOS-2 PALSAR-2 and the suppression of hedgerows and shrubs by the low pass Lee filter, cleaner result

has been obtained. This suggests that mapping with ALOS-2 PALSAR-2 is an improvement over ALOS PALSAR.

6.5.2 Comparing Forest/Non-Forest maps with ALOS PALSAR derived maps and reference data

6.5.2.1 Visual analysis

All the forest polygons from 2007-2016 were overlaid, as shown by examples in figure 6.8, to examine the consistencies/inconsistencies in the outlines over the years.

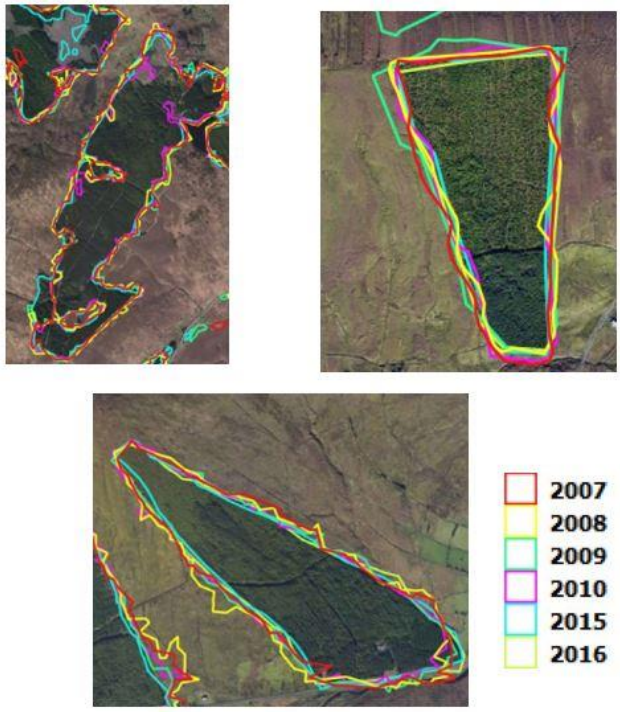

Figure 6.8: Visual analysis of selected SAR derived forest polygons from Area1 (2007-2016)

It can be seen from figure 6.8 that more regular boundaries were formed with ALOS-2 PALSAR-2 images when compared to ALOS PALSAR images. Due to the better radiometric separability between forests and non-forests for the ALOS-2 PALSAR-2 sensor, as well as the higher spatial resolution, there is clearer distinction between forests and non-forests, and hence the forest boundaries more closely match those on the ground. Although removal of the mean GLCM measure for the ALOS PALSAR image

classification (chapter 4, section 4.2.4) helped to constrain the forest boundaries and limit their over estimation, in comparison with ALOS-2 PALSAR-2 forest boundaries, they appear more irregular. It can also be observed that the boundaries from 2015 and 2016 appear much more similar to each other whereas boundaries from 2007-2010 have more irregularities between each other, which suggests that data from ALOS-2 PALSAR-2 are more stable than from ALOS PALSAR.

Comparing the ALOS-2 PALSAR-2 derived forest polygons with the Forests12_16 dataset as shown in figure 6.9, the boundary fit between the two datasets can be observed. Full area coverage is obtained by the ALOS-2 PALSAR-2 forest polygons in comparison with the reference datasets.

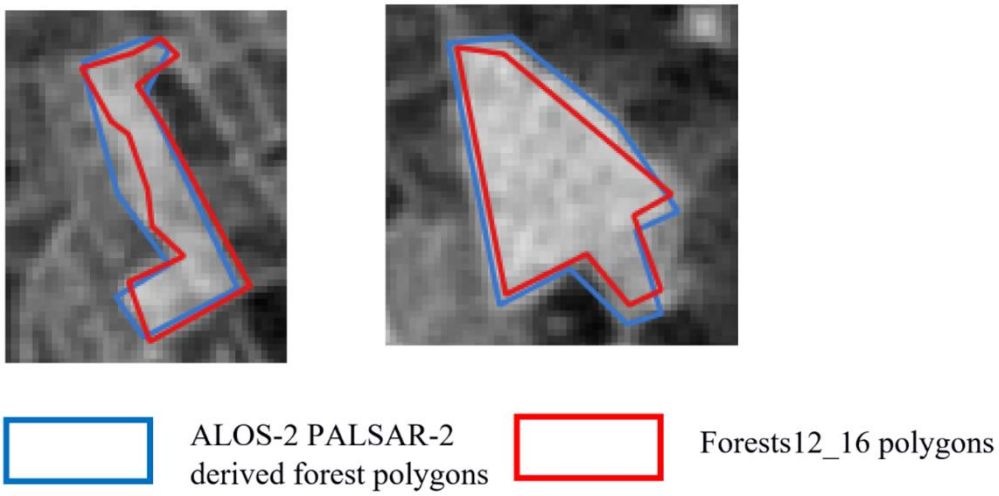

Figure 6.9: Visual analysis and comparison of ALOS-2 PALSAR-2 derived forest polygons with Forests12_16 dataset

6.5.2.2 Quantitative analysis

The classified maps were quantitatively compared to assess their accuracies and estimate the forest area from 2007-2010 and 2015-2016.

6.5.2.2.1 Classification accuracies

The overall accuracies for the land cover maps are shown in table 6.2. Maximum overall accuracies of 86.23% and 86.15% were achieved for Area1-2015 and Area3-2016

respectively which are summer acquired. The autumn and winter images have a lower accuracy.

Table 6.2: Overall accuracies of land cover maps derived from ALOS-2 PALSAR-2 images

Overall Accuracy	Area1		Area2		Area3	
	2015 (August)	**2016 (October)**	**2015 (October)**	**2016 (September)**	**2015 (January)**	**2016 (June)**
	86.23	83.90	83.82	82.72	79.65	86.15

The January 2015 image from Area3 produced the lowest overall accuracy among all the images, so precipitation, and wind effects for 2015 and 2016 from Met Éireann were examined. Average monthly precipitation from four weather stations in the vicinity of Area3 was derived (Glen Imaal, Hacketstown, Oldbridge and M.Sally Gap) for January 2015 (407.8mm) and June 2016 (151.8mm). The highest precipitation for all these stations was recorded between November 2014 and January 2015 *(Met Eireann, 2020).* Historic wind records were available for only two stations within Area3 – Naas and Osprey. The maximum wind speed recorded from these two stations on the day of image acquisition (January 23, 2015) was are 4km/h and 6km/h respectively. For June 10, 2016, the wind speed record was available from only Naas at 1.6km/h. From these records it was inferred that January 2015 was wetter and windier than June 2016 which could account for some of the difference in classification accuracies.

In Ireland, showers are commonly observed throughout the year irrespective of the season. However, prolonged periods of wet weather are observed from October- March. Such wetter conditions in winter increase the dielectric constant in the soil moisture, thus increasing the backsactter value. As explained in chapter 2, section 2.2.1, L-band is affected by soil mositure for low vegetation covers. Land cover such as bare soils on arable lands and peatlands absorb more water due to such wet conditions thus increasing the dielectric constant and giving a higher backscatter response to the SAR sensor. The increase in the vegetation water content is another factor to be considered that affects the

backscatter values. Very wet conditions might diminish SAR sensitivity to forest structure (Tanase et al., 2018). Concerning wind effects, generally, storm events in Ireland do not cause largescale damage in forests *(Department of Agriculture, 2014)*. However, prolonged period of storm events, cause waterlogged soils which leads to damage in the trees. Strong winds can also cause injury to trees by affecting their branches, stems and roots, specially among the young trees.

The forest and non-forest classes were assessed in more detail, with producer's and user's accuracies shown in table 6.3.

Table 6.3: Forests and Non-forests classification accuracies from ALOS-2 PALSAR-2 (PA= Producer's Accuracy, UA=User's Accuracy)

	Forests		**Non-Forests**		**OA**
2015	**PA**	**UA**	**PA**	**UA**	
Area1	94.91	97.98	91.96	96.99	94.91
Area2	88.96	85.01	89.98	91.97	89.21
Area3	86.89	80.01	79.91	85.78	86.76
2016					
Area1	88.85	86.11	88.74	91.98	90.81
Area2	90.15	91.88	92.18	93.89	89.33
Area3	94.92	97.05	92.02	96.67	94.72

With approximately 95% probability of being classified as forests and agreement with Forests12_16 dataset, the summer images prove the potential of ALOS-2 PALSAR-2 data in mapping forests. Along with high user's accuracies of 97%, these images are highly reliable for representing ground reality. Higher commission errors were observed than omission errors when compared with the Forests12_16 dataset, indicating potential over-estimation of forests by the SAR processing over these areas (table 6.4). Area2 shows the greatest number of such false positives, however in both 2015 and 2016 the additional forest patches identified represent less than 2% of the total number of agreed patches.

Table 6.4: Commission and omission errors from ALOS-2 PALSAR-2 datasets compared with the Forests12_16 reference dataset

2015	Agree	Commission	Omission
Area1	2995	12	8
Area2	3263	56	14
Area3	2343	24	8
2016			
Area1	2798	32	10
Area2	3250	58	17
Area3	2456	15	9

The classification of the ALOS PALSAR images resulted in higher overall accuracies of 97% for the forests/non-forests maps (section 4.3.3.1). The potential impact of the weather conditions has been already been considered as a possible cause of the lower accuracies for the ALOS-2 PALSAR-2 data, but a further limitation is the accuracy of the reference dataset. This dataset consists of all forests in 2012 but only private forests were updated to 2016, therefore changes in the much larger public forest sector have not been included and could be a cause for the potentially large number of commission errors.

6.5.2.2.2 Forest area estimation

The forest area estimates for the coincident areas from ALOS PALSAR and ALOS-2 PALSAR-2 derived products are shown in figure 6.10 for the period 2007-2010 and 2015-2016. The corresponding forest areas from the Forestry12 and Forests12_16 datasets are also presented.

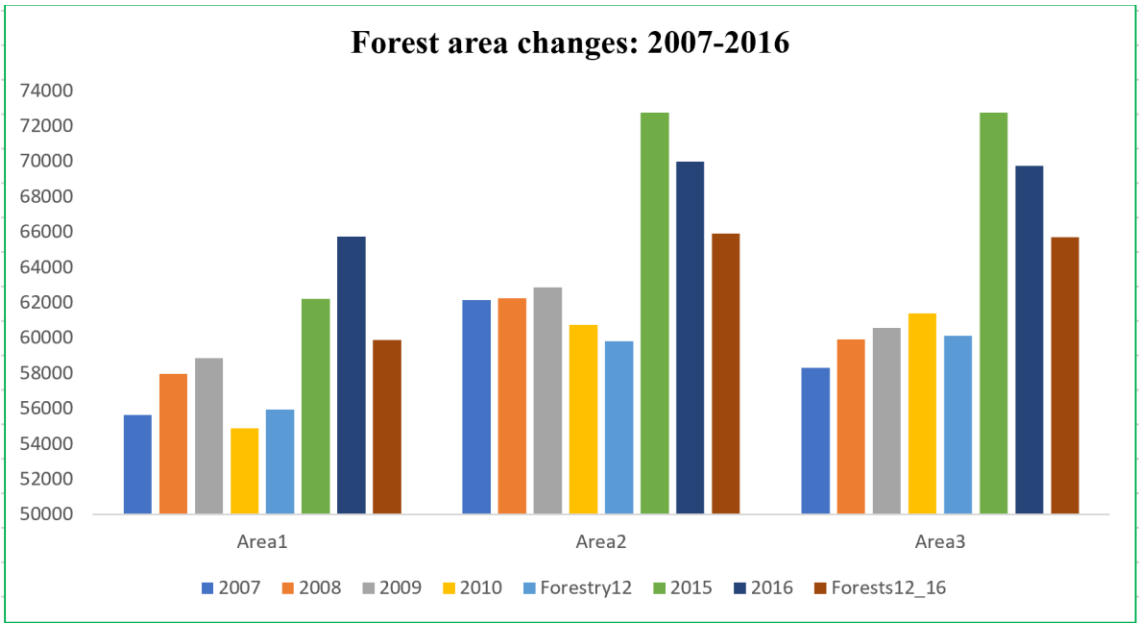

Figure 6.10: Forest area estimates as derived from SAR and reference datasets for the period 2007-2016 for the coincident ALOS PALSAR and ALOS-2 PALSAR-2 areas of Area1, Area2 and Area3

From figure 6.10, it can be observed that there is a generally increasing trend in the forest area between 2007 and 2016 across all the study areas. An increase of 13.3%, 19.8% and 18.5% has been observed between 2010 and 2015 in Area1, Area2 and Area3. Between the three year gap between Forestry12 and 2015, there is an increase of 10.0%, 17.7% and 17.34% in Area1, Area2 and Area3. However, due to the limitation within the Forests12_16 dataset as discussed above, there is a difference of 5,834 ha, 4,077 ha and 4,060 ha between the SAR derived and reference datasets for the year 2016. A key limitation of the current reference datasets is their infrequency, and this approach has demonstrated that where satellite imagery are available consistent results can be generated on an annual basis. To understand local and regional changes in the forest area estimates in response to forest policy and management as well as natural events, obtaining annual forest updates is critical.

6.6 Forest disturbance maps using divergence guided ISODATA clustering approach

Following the steps described in chapter 5, section 5.2 for ISODATA clustering, the algorithm was run on the stack of HV and HH γ^o bands for 2015 and 2016. The divergence statistics plotted for Area1 are shown in figure 6.11. The coincident peak of average and minimum divergence occurs at 80 clusters where the average separability is 1877 and the minimum separability is 328. For the corresponding ALOS PALSAR image (chapter 5, section 5.3.1.1), the average and minimum separability were observed at 1969 and 1282 respectively but the peak also occurred at 80 clusters. The drop in the minimum separability between the two datasets could be a response of the divergence statistics to the different lengths of the two time series resulting in a reduction in the number of bands from 8 for ALOS PALSAR to 4 for ALOS-2 PALSAR-2. Where ISODATA clustering guided by divergence statistics has been applied in previous studies it has primarily been for hyper-temporal time series *(Ali et al., 2014; Bie et al., 2012)* to obtain the best separability values.

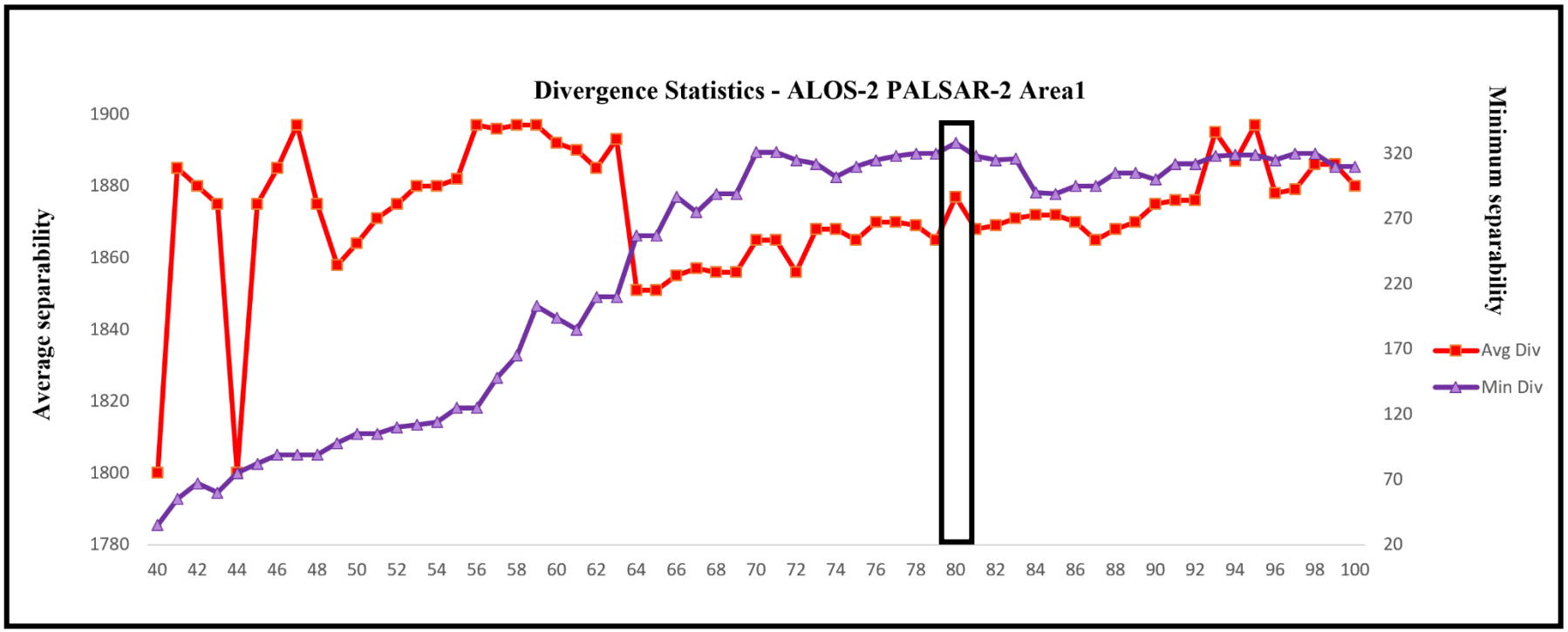

Figure 6.11: Divergence statistics plot for Area1 derived from the 4-band raster stack, indicating 80 as the optimal number of clusters (with coincident average and minimum divergence peak) to be used for further analysis

For Area2 and Area3, coincident peaks were observed at 78 and 86 clusters respectively, compared to 74 and 80 clusters for the ALOS PALSAR images. It is possible that for the more varied topographic landscapes of Area2 and Area3, the higher spatial resolution of ALOS-2 PALSAR-2 has led to the detection of more variability within these areas. Alternatively, using images from mixed seasons, different classes have been identified due to mixed temporal signals.

As described in chapter 5, after generation of the cluster map, the image was filtered using the sieve operation with a threshold of 6 pixels to eliminate fragmented and isolated pixels and make the interpretation more reliable.

6.6.1 Cluster groups

After examining the cluster signatures for each of the areas, they were grouped through the hierarchical clustering approach described in section 5.3.2. Groups common to both the ALOS PALSAR and ALOS-2 PALSAR-2 outputs were identified, as well as those that exhibited a signature different to those previously derived.

6.6.1.1 Groups formed in Area1

Signature patterns observed in ALOS-2 PALSAR-2 results that were also identifed for ALOS PALSAR.

1) Pixel values remained constant to within 1dB over the two years of 2015-2016– 43 clusters
2) A drop greater than 4dB between the two years – 9 clusters
3) A drop of 2±0.5dB between the two years – 9 clusters
4) Increase of 2±0.5dB in the backscatter between two years – 13 clusters
5) A drop of 13dB between the two years – 1 cluster

The characteristics of these common groups are given in table 6.5 below.

Table 6.5: Groups formed from ALOS-2 PALSAR-2, also found in ALOS PALSAR clustering results

Groups	Clusters within the group	Group labels	Characteristics	Percentage area covered by the group of clusters
G1	1	Misclassification/Forest edges	**Mean γ^o HV** -19±2.5 dB **Mean γ^o HH** -12±2.2 dB	1.5%
G2	2, 7	Misclassification/Forest edges	**Mean γ^o HV** -17±1.2 dB **Mean γ^o HH** -11±1.3 dB	
G3	73, 76, 79, 80	Mature trees (age 10-30 years)	**Mean γ^o HV** -7±0.5 dB **Mean γ^o HH** -4±0.5 dB	23%
G4	57, 70, 74, 63, 68, 69, 50, 71, 44, 65, 28, 54, 58, 59, 46, 75, 62	Mature trees (age 10-30 years)	**Mean γ^o HV** -9±1.1 dB **Mean γ^o HH** -5±0.5 dB	16%
G5	4, 6, 12, 13, 14, 15, 17, 43	Young trees (age 0-9 years)	**Mean γ^o HV** -13±1.2 dB **Mean γ^o HH** -8±0.7 dB	14%
G6	18, 19, 20, 22, 26, 32, 34, 42, 51, 33, 49	Young trees (age 0-9 years)	**Mean γ^o HV** -15±0.5 dB **Mean γ^o HH** -10±0.7 dB	8%
G7	8, 25, 30, 48, 53, 56, 27	Clear fells	Drop > 4 dB between 2015 and 2016	7%
G8	10, 21, 23, 35, 37, 39, 41, 61, 67, 72, 78	Storm/fire/insect/plant failure/leaf-off conditions	Drop of 2 dB ±0.5 between 2015 and 2016	10%
G9	5,11,16,31,36,38,40, 47,52,55,60,66,77	Afforestation/reforestation/Tree growth/seasonal influences	Increase of 2±0.5dB in 2016	11%
G10	3	Anomaly	Drop of 13dB between the two years	0.5%

The groups representing misclassification are a testament to the fact that the signatures from ISODATA clustering can be used to eliminate misclassified clusters that have resulted from the supervised classification. These groups were

also formed in the ALOS PALSAR classified outputs and also include the forest boundaries which have a mix of forests and other land cover classes within a pixel. Thus errors of commission that occurred following the RF classification (discussed in section 6.5.2.2.1) that are genuine errors can be eliminated at this stage.

The HV mean signatures of groups 3 and 4 were greater than -11dB, and thus combined as mature trees, while the HV mean signatures of groups 5 and 6 were below -11dB and combined as a class of young trees. This pattern was also observed in the ALOS PALSAR classification, with four forest groups representing different age groups of trees. These groups were characterized as mature and young trees respectively, but it was not possible to discriminate at species level.

Group 7, with a drop greater than 4dB, matched the clear fell pattern seen in ALOS PALSAR. A comparison of ALOS-2 PALSAR-2 group 7 clusters with Coillte clear felled polygons for both years (2015 and 2016) is shown in table 6.6. Additionally, 18 clear-felled instances were identified by the SAR data that were not identified in Coillte datasets. Among these 18 felling instances, 4 belonged to private non-grant aided owners, 11 cases belonged to Coillte estates and 3 more were private premium grant aided ownerships. This highlights that SAR can be used to identify felling events that do not show up in any database (Coillte or NFI or FIPS). Clear-felling requires licencing, therefore the identification of deforested areas by SAR can support forest monitoring and compliance.

Table 6.6: Comparing the number of clear-fell instances derived from ALOS-2 PALSAR-2 with Coillte data (2015-2016)

	Number of felled polygons from Coillte (2015-2016)	**Number of instances identified by ALOS-2 PALSAR-2 corresponding to the felled polygons**
Area1	298	175

From table 6.6, 123 clear-felling instances recorded in the Coillte dataset are missing from the ALOS-2 PALSAR-2 results. Some possible reasons for this are:

1. that the polygons were not felled: 8 polygons verified with Google Earth imagery (any available imagery within the time frame – 2013-2016) were discovered to be felled after 2016 or not felled at all. As explained in chapter 5, section 5.3.3.2.1, discrepancies in the database were observed that are highlighted by SAR data.
2. a temporal mismatch: as the SAR image acquisition period is between August 2015 and October 2016, records of felling events that have taken place before and after this period (January – August 2015 and October – December 2016) exist in the Coillte database and therefore lead to the difference in the numbers.
3. Seasonal impacts: Rainfall data from Met Éireann for four stations located in Area1 were examined. Most rainfall for 2016 in this area was recorded for January and February, followed by September and December. The Area1-2016 image was acquired on October 05, 2016, when the ground was wet following the September rainfall. Soil moisture effects may influence the backscatter values resulting in some misclassifications of the ALOS-2 PALSAR-2 data.

When the 8 polygons from (1) which were identified as having not been felled are included, the agreement between ALOS-2 PALSAR-2 and the Coillte dataset is 61.4%. For the same scenario and region, the agreement between ALOS PALSAR and the Coillte dataset was 78.3% (chapter 5, section 5.3.3.2.1). While the analysis for ALOS PALSAR was performed between June-June for the four-year period, for ALOS-2 PALSAR-2, the analysis was performed between August and October of two consecutive years. Reflecting on (2), most of the clear-fells in Ireland occur between June-August therefore a possible hypothesis is that the clear-fells recorded in the Coillte database have not been detected in the SAR due to the inappropriate timing of the image acquisitions.

The signature pattern of group 8 clusters was also observed with ALOS PALSAR results (chapter 5, section 5.3.3.2.2) with a drop of 2±0.5dB between the two years. The potential reasons, as discussed previously in section 5.3.3.2.2., include:

1) Presence of debris after felling
2) Insect attack
3) Animals such as deer feeding on the young planted trees
4) Thinning
5) Plant failure
6) Storm/wind damage
7) Fire

However, an additional reason of relevance here is the seasonal impact as the image was from the autumn (October). Part of this area contains deciduous trees which will have lost their leaves in October 2016 when compared to leaf-on conditions in summer, and this will cause changes in the backscatter response.

An increase of 2dB in the backscatter between two years represented tree growth in the ALOS PALSAR clusters, which showed this increasing pattern over the four years. For ALOS-2 PALSAR-2, there is an increase of 2dB in 2016 in group 9 clusters suggesting afforestation, reforestation, tree growth or seasonal influences. Planting date information was not available from the recently updated PrivateForests2016 dataset and therefore further analysis could not be conducted for this group. However, FNF maps from the RF classifier were used to assist labelling of this group which is discussed in section 6.6.1.1.1 below.

Anomalies were also found in the ALOS PALSAR clustering with an increase and fall of 6-8dB between three years. Within the two-year period of ALOS-2 PALSAR-2 clustering, a drop greater than 13dB was found in 2016. This only concerned one cluster (cluster 3) in one Group (G10) and covered only 0.5% of the total area of Area1. Therefore, this was labelled as an anomaly.

6.6.1.1.1 New signature pattern formed in Area1

A new signature pattern of an increase of more than 3dB between 2015 and 2016 was identified. Figure 6.12 illustrates this increase in HV for these clusters that covered 8% of the total area of Area1. This suggests either new plantings or seasonal induced responses similar to the group 9 clusters (table 6.5) with a greater increase of backscatter in the time series. A similar increase was also observed in the HH signatures. Therefore, considering the similarities of signature patterns, these clusters were combined with group 9 clusters essentially indicating either afforestation, reforestation, tree growth or seasonal induced variations. The PrivateForests2016 dataset was checked for the year of planting or species information for these clusters, however none was available.

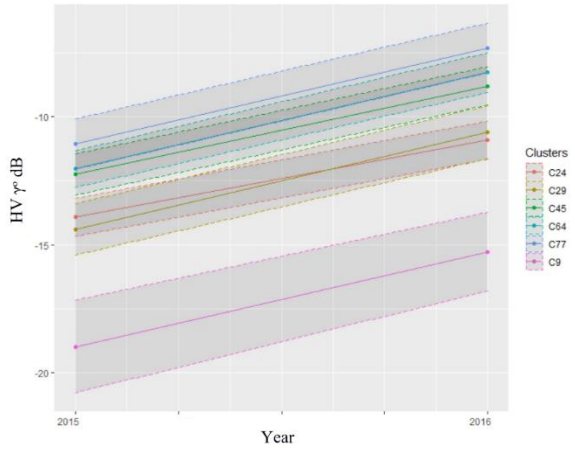

Figure 6.12: New cluster signatures identified from ALOS-2 PALSAR-2 clustering process

These clusters cover 19% of Area1 with an increasing trend in the backscatter. In order to determine if afforestation/reforestation had taken place the FNF maps were examined. From this analysis only 1% of the area was deemed to have been afforested between the two years. Therefore tree growth is the predominant characteristic of these clusters.

A comparison of cluster groups formed between ALOS PALSAR and ALOS-2 PALSAR-2 for Area1 is given in table 6.7 along with the percentage area covered by each group.

Table 6.7: Groups formed through the clustering process in Area1 from ALOS PALSAR and ALOS-2 PALSAR-2 datasets and percentage area

Groups	ALOS PALSAR (4-year period): 80 clusters	ALOS-2 PALSAR-2 (2-year period): 80 clusters
Misclassification/Forest edges	G1, G2, G3 **(4%)**	G1, G2 **(1.5%)**
Forests (mature and young)	G4, G5, G6, G7 **(66%)**	G3, G4, G5, G6 **(61%)**
Clear-felling	G8, G9 **(11%)**	G7 **(7%)**
Storm/Fire/Plant failure/Thinning/plant debris/Insect or animal attack/leaf-off/seasonal conditions	G10 **(8%)**	G8 **(10%)**
Afforestation/reforestation/tree growth/seasonal influence	G11, G12, G13 **(9%)**	G9 **(19%)**
Anomaly	G14 **(1%)**	G10 **(0.5%)**
Unknown	G15 **(0.1%)**	-

For the four-year period of ALOS PALSAR, 15 groups of forest character were formed, and for the two-year period of ALOS-2 PALSAR-2, 10 groups were formed.

6.6.1.2 Groups formed in Area2 and Area3

Similar to table 6.7, table 6.8 shows a comparison of groups formed in Area2 from ALOS PALSAR and ALOS-2 PALSAR-2 datasets, along with the percentage area covered by each cluster group.

Table 6.8: Groups formed through clustering process in Area2 from ALOS PALSAR and ALOS-2 PALSAR-2 datasets and percentage area

Groups	ALOS PALSAR (4-year period): 74 clusters	ALOS-2 PALSAR-2 (2-year period): 78 clusters
Misclassification/Forest edges	G1, G2, G3 **(0.8%)**	G1, G2 **(0.8%)**
Forests (mature and young)	G4, G5, G6, G7 **(67%)**	G3, G4, G5, G6 **(73%)**
Clear-felling	G8, G9 **(14%)**	G7 **(8%)**
Storm/Fire/Plant failure/Thinning/plant debris/Insect or animal attack/leaf-off/seasonal conditions	G10, G11 **(7%)**	G8 **(5%)**
Afforestation/reforestation/tree growth/seasonal influence	G12 **(10%)**	G9, G10 **(13%)**
Anomaly	G13 **(0.7%)**	G11 (0.2%)
Unknown	G14 **(0.5%)**	-

A total of 14 groups were formed for ALOS PALSAR with 74 clusters, and 11 groups for ALOS-2 PALSAR-2 with 78 clusters for Area2. Contrary to the comparison done to Area1 presented above, the clear-felling comparison between SAR data and Coillte database was performed for only 2016 clear-fells. As most clear-fells would have happened before October 2015 (which is the 2015 SAR image), and the reference database captures clear-fells for 2015, the comparison would be misleading. Therefore, comparing all 2016 clear-fells, an agreement of 57% was found between the two datasets.

Table 6.9 shows the groups formed in Area3 between both the sensor datasets.

Table 6.9: Groups formed through the clustering process in Area3 from ALOS PALSAR and ALOS-2 PALSAR-2 datasets and percentage area

Groups	ALOS PALSAR (4-year period): 80 clusters	ALOS-2 PALSAR-2 (2-year period): 86 clusters
Misclassification/Forest edges	G1, G2, G3 **(0.5%)**	G1, G2 **(1.2%)**
Forests (mature and young)	G4, G5, G6, G7 **(66%)**	G3, G4, G5, G6 **(76%)**
Clear-felling	G8, G9, G10 **(12%)**	G7**(12%)**
Storm/Fire/Plant failure/Thinning/plant debris/Insect or animal attack/leaf-off/seasonal conditions	G11 **(9%)**	G8 **(4.7%)**
Afforestation/reforestation/tree growth/seasonal influence	G12 **(12%)**	G9 **(6%)**
Anomaly	G13 **(0.3%)**	G10 **(0.1%)**
Unknown	G14 **(0.2%)**	-

The clear-felling group (G7) of Area3 showed a signature pattern with a decrease greater than 6.5dB from 2015 to 2016 with an agreement of 65% with Coillte datasets. Considering the wet soil and leaf-off conditions due to the winter image in 2015, such large difference must have occurred in this area.

6.7 Deforestation monitoring

In addition to identifying disturbance events such as clear fells, the ALOS-2 PALSAR-2 datasets were explored to identify permanent deforestation events within the study areas. Permanent land-use changes constituting deforestation may be due to construction of wind turbines, roads, human settlements on forest land, and conversion of forest to agricultural land.

If a clear-felled patch identified between 2007-2010 remains non-forested in 2015-2016, then it is considered as deforested. The ALOS-PALSAR clear-fellings between 2007-2010 were compared with FNF maps from 2015-2016 to locate areas that were felled anytime between 2007 and 2010 and appeared as

non-forest in 2015 and 2016. This process was assisted by Google Earth imagery in an attempt to determine the reason for the change. Table 6.10 provides details of deforested areas identified across all the three study areas.

Table 6.10: Details of deforested areas between ALOS PALSAR and ALOS-2 PALSAR-2 image acquisitions (2007-2016)

Study area	**Clear-felled Year**	**Reasons for deforestation**	**Total Area deforested in hectare (ha)**
Area1	2009-2010	Construction of wind turbines	164.29
		Conversion to agricultural land	49.01
Area2	2007-2008	Conversion to agricultural land	5.13
	2009-2010	Construction of wind turbines	33
		Conversion to agricultural land	20.75
Area3	2007-2008	Construction of wind turbines	12.6
	2008-2009	Conversion to agricultural land	106.74
	2009-2010	Conversion to agricultural land	55.13
	After 2011	Construction of wind turbines	11.56

With respect to the final row of table 6.10, an area of 11.56 ha was found to be non-forest in the 2015/2016 images, although was forested up to June 2010 and

was therefore felled after this date. Inspection of Google Earth images, as shown in figure 6.13, confirmed that the land-use transition was permanent with construction of a wind turbine complex.

(a) Image from Google Earth

(b) 2010

(c) 2015

Figure 6.13: Conversion of forest patches to wind turbines (a) Google Earth image – wind turbines highlighted by red circles – image from Area1-2012(b) forest patch as mapped from ALOS PALSAR image in 2010 (c) forest patch as mapped from ALOS-2 PALSAR-2 image with red diamonds highlighting location of forest patches converted to wind turbines

Further analysis revealed that:

- Deforestation was identified at 40 locations from all three sites combined
- The smallest deforested area identified was 1.13 ha in Area3 where forests have been removed to construct wind turbines
- The largest deforested area was 121.21 ha in Area1 which was converted to windfarms
- A total of 213.3 ha, 58.8 ha and 174.47 ha of forests have been deforested in Area1, Area2 and Area3 respectively between 2007 and 2016
- The greatest amount of deforestation occurred in Area1, with majority of the converted area becoming wind turbine parks
- Among the deforested areas, a high proportion of approximately 85% was attributed to conifer mature spruce planted in 1998
- Out of the total deforested area, 30% was in private ownership and was converted to agricultural land

6.8 Discussions and conclusions

With a growing need for robust, reliable and objective forest monitoring, developing techniques using existing remote sensing data to obtain up-to-date and reliable forest estimates is important. It is also important to be able to apply equivalent and comparable techniques between different datasets for historic comparisons. The potential for ALOS PALSAR data to be used for mapping forests and forest disturbances from a combination of RF classification and ISODATA clustering was demonstrated in chapters 4 and 5. This chapter aims to evaluate the capabilities of ALOS-2 PALSAR-2 (operational from 2014 to the present day in June 2020) by transferring the forest monitoring algorithm previously developed for ALOS PALSAR.

Three key issues need to be addressed in this chapter. First, the transferability of the methodology to ALOS-2 PALSAR-2 datasets to operationalise forest monitoring; second, SAR image selection for forest monitoring in Ireland; and third, deforestation monitoring between the ALOS PALSAR and ALOS-2 PALSAR-2 time periods for three regions of Ireland.

To address the transferability of the algorithm to ALOS-2 PALSAR-2 datasets by assessing any inconsistencies identified during the process, results from sections 6.5, 6.6 and 6.7 were reviewed. Visual and quantitative analysis from the RF classification, based on the comparison with ALOS PALSAR results, reveal that the methodology can successfully be applied to ALOS-2 PALSAR-2 datasets. Forest polygon boundaries which match with those from the ALOS PALSAR and Forests12_16 reference datasets were successfully generated, which confirms the ability to transfer the forest mapping methodology. Quantitative analysis shows that 95% classification accuracies for summer images were achieved, with slightly lower values of between 86% and 90% achieved for the images from the for the images from the autumn and winter months. The lowest producer's and user's accuracies were achieved for Area3, but these still show that there is 86% probability of forests being classified as forests and the maps are 80% reliable for the user on the ground. Additionally, the variable importance plot from the RF classification re-emphasizes the importance of GLCM texture measures for classification, as shown for ALOS PALSAR datasets. While there is a reduction of approximately 60% accuracy upon eliminating HV γ^o, eliminating the most important GLCM measure from ALOS PALSAR (figure 4.5) and ALOS-2 PALSAR-2 (figure 6.6) reduces the accuracy by 35% in the former case and 70% in the latter case. This suggests that GLCM texture measures are more valuable for ALOS-2 PALSAR-2 classification than for ALOS PALSAR classification. As a caveat however, due to the shorter time series in this case, skew in the most important variables is also expected. For the more topographically rugged areas, as the plot suggests, slope is an important ancilliary data.

Transferability of the second part of the methodology with the ISODATA clustering can be evaluated based on the signature patterns and cluster groups formed. Across all the study areas, irrespective of the seasons, the dendrograms formed groups representing misclassification/forest edges, mature and young forests, clear-felling, possibilities of other disturbances such as storm /fire /plant failure /thinning /insect or animal attack /leaf-off conditions /seasonal influences,

afforestation /reforestation /tree growth, and small regions of unidentifiable behaviour, confirming the success of the transferability process. Some variations within the cluster groups were observed which can be attributed to the resolution and seasonalities of the ALOS-2 PALSAR-2 images. The algorithm has statistically identified similar number of clusters in each region which showed comparable behaviour between the two sensors. For both sensors, among the disturbance groups, only clear-felling could be validated due to a lack of detailed ground information on other disturbances. For both datasets, clear-felling showed a clear signature that was evident across all the study sites. The consistency in the signature patterns from both the sensors confirmed that this part of the algorithm was transferable.

Some improvements were evident in the ALOS-2 PALSAR-2 results, most importantly that due to its higher spatial resolution, more regular, and more stable forest boundaries were delineated, and areas as small as 1.1 ha were mapped. Nonetheless, it is worth noting that new behaviours can occur between the different time periods and therefore clusters from one image cannot necessarily be mapped directly onto another image.

A second issue to be addressed is the selection of SAR images for forest monitoring. With the higher spatial and radiometric resolution of ALOS-2 PALSAR-2 data, higher classification accuracies could be anticipated. However, slightly lower classification accuracies than those achieved with the ALOS PALSAR data were observed. It is suggested that this is largely due to the combination of ALOS-2 PALSAR-2 images being acquired from different seasons, and the full potential of the enhanced sensor could only be explored if images from June were available. Given the number of wet days for the months of September and January across all areas, and the mix of leaf-on and leaf-off image dates which affect the broadleaved species covering 25% of forests in Ireland, the seasonal influences on the SAR images are apparent from the results achieved. Due to constraints with the ALOS-2 satellite scheduling, only one image per year was available and most of these images were from autumn and

winter. Although summer images are the most appropriate for forest monitoring, making the best use of available data is important to avoid gaps between the ongoing annual updates. If the images are of different dates, it can be very challenging to calculate annual disturbance events such as felling. For example, January 2015 to June 2016 is an 18 month period that fully captures the 2015 felling season but almost entirely excludes the 2016 season. This is very difficult to compare with October 2015 to September 2015 (Area2) which is less than 12 months and only really covers the 2016 felling season. Therefore, the minimum requirement is to have images that are from the same months for all regions.

With the clear-felling patterns successfully identified by both the sensors, the second key aim of this chapter i.e. identifying forest areas that were removed between 2007 and 2010 and not replanted by 2015-2016 indicating permanent land-use change, could be addressed. The current system in Ireland does not capture deforestation and it is important to track this kind of disturbance from forest management and carbon reporting perspective. Given the definition of deforestation in Ireland requiring no planting within five years of felling, differentiating clear-felling events from deforestation can only be achieved with time series in excess of five years. Therefore, annual forest datasets over time are essential if longer term, as well as shorter term, changes in land cover are to be monitored. In this study, a comparison of ALOS PALSAR and ALOS-2 PALSAR-2 derived products show areas of permanent loss of forest ranging from as large as 121 ha to as small as 1.13 ha. High resolution Google Earth images were able to confirm the nature of the change, with the majority involving transition from forests to wind turbine complexes.

From the evidence of this chapter, it can be concluded that ALOS-2 PALSAR-2 can be used to monitor forest disturbances in Ireland. These forest disturbances include clear-felling and deforestation that were identified, quantified, and validated with ancillary data.

PART III

CONCLUSIONS

Chapter 7

Conclusions and Recommendations

"When you really want something, the whole Universe conspires in helping you to achieve it" – Paulo Coelho

7.1 Conclusions

The overall objective of this work was to investigate the capability of L-band SAR to map and monitor forest stands and forest disturbances in Ireland over the period 2007-2016 to support national forest monitoring operations. The specific objectives were: (i) to produce forest maps for three geographically varied regions by using a machine learning classifier; (ii) to explore the possibilities of a data-driven unsupervised classifier to identify the occurrence of different disturbances and characterize them; and (iii) to transfer the approach developed for a historic dataset to a more recent L-band SAR dataset and explore the prospects of continuing this monitoring operation in Ireland.

According to IPCC guidelines, a mix of land use and land cover categories have been used (section 4.2.2.1) in this study to develop a classification system representing land area. While landcover describes the land in terms of natural surface type present on land, information on land use is of particular interest for carbon reporting. Land use change is often associated with a change in land cover (for example conversion of forestland to agriculture) and associated change in carbon stocks. Forestland is a landcover which is being managed according to land use needs. For example, forests have been managed as land use by humans from carbon reporting point of view – by planting fast growing, high carbon sequestering trees. Depending on the type of land cover associated with the new land use, carbon stocks in aboverground biomass varies after a clearing event. Alterations in both land cover and land use lead to far-reaching environmental changes impacting carbon stocks and reporting. Land use is not always discernible from satellite images and therefore, it requires additional ground truth information to fully determine the landuse of a particular land area. Therefore, IPCC strongly recommends the use of ground survey data or conventional forest inventories while interpreting land use categories and their changes.

Forest monitoring in Ireland is currently carried out systematically every six years as part of the National Forestry Inventory process. However, given the mix of public and private ownership there are challenges in carrying out the monitoring because of the different forest stand characteristics and management practices. More frequent monitoring, for example on an annual basis, would permit better quantification of change, allow more

timely updates of the forest inventory, provide spatial information on biomass, and better inform national carbon budgets through integration with the national carbon reporting system, CARBWARE. Disturbances due to more intensive forest management practices, weather events, fires, and insect attacks are changing forest resources at an increasing rate. Monitoring these changes over time in an effective and transparent way requires timely and objective information which can be obtained through remote sensing. In order to be efficient and cost-effective, such an approach requires automation. To date, most work on forest monitoring using remote sensing in Ireland has relied on optical satellite and airborne imagery, and LiDAR, with a growing use of unmanned aerial vehicles at a local level in recent years. A few examples of such work include the creation of the FIPS datasets which was the largest national remote sensing project when it was carried out in 1998 using aerial photography and medium resolution optical satellite imagery, forest parameter estimation by *McInerney and Nieuwenhuis, (2009)* using optical imagery, and estimating tree height using LiDAR by *Clifford et al., (2009).* In an operational context, the cost per unit area of LiDAR and difficulty of acquiring cloud free optical satellite imagery limit their use. The sensitivity of active microwave systems to forest scattering, irrespective of cloud cover, has made radar remote sensing an attractive technique to address the problem of forest monitoring. One such application of SAR data for Irish forests is described in the study conducted by *Black et al., (2017)* to predict changes in biomass and volume due to forest disturbances. Backscatter values from ALOS PALSAR datasets for the study areas from this PhD work were used as inputs to the backscatter-biomass model. Due to the saturation of L-band SAR backscatter at 100Mg ha^{-1}, the developed biomass model was limited to immature forest stands. However, for forest mapping and monitoring events such as change detection, L-band SAR is suitable as has been demonstrated in the present work.

This chapter summarises the key insights arising from this PhD study, research constraints and recommendations for future work and enhancements.

7.1.1 Contributions of this work

7.1.1.1 Machine learning classifiers for forest mapping

After reviewing the various machine learning algorithms, the RF classifier was selected for this study because it consistently demonstrated an ability to map tree cover using both satellite and ancillary data as shown by authors such as *Gislason et al., (2006)* and *Devaney et al., (2015)*. Because of its ability to handle several input variables of different data ranges, it was possible to improve classification accuracies by assessing the influence of input bands. The performance of the classifier was strongly impacted by the GLCM texture measures – for example with the removal of GLCM variance, which was shown to be the most important input variable among the texture measures, the classifier performance decreased by up to 35%. Using 10 input variables - HV γ^{o}, seven GLCM texture measures, slope and aspect, maximum overall accuracies of 97% were achieved for forest/non-forest classification. With the ability by ALOS PALSAR to map a minimum forest area of 1.8 ha across three study areas, this work has shown an improvement from the current NFI mapping system in which each circular plot measures a diameter of 25.24m. Thus objective (i) i.e. to produce forest maps for three geographically varied regions by using a machine learning classifier, was accomplished.

7.1.1.2 ISODATA clustering and dendrograms for signature definition

In this study, ISODATA clustering guided by divergence statistics was successfully applied to SAR imagery to monitor forest disturbances. The ISODATA approach supported by analysis of the divergence statistics has been mainly used on optical hypertemporal NDVI datasets such as in the work by *Ali et al., (2013)* and *Bie et al., (2012)*, and there is no evidence in the published literature of it being applied to a multi-temporal SAR dataset. This work has demonstrated however that it is possible to achieve cluster separability within forest areas of SAR imagery above the defined threshold for divergence. Describing the ground characteristics that matched the large number of clusters with various differing signature patterns was a significant challenge. To resolve this, along with manual interpretation and segregation of groups, dendrograms were used through which clusters were grouped based on the Euclidean distance between two cluster

means. Dendrograms represent a cluster hierarchy as a tree diagram with a threshold set to define the grouping levels of the clusters. In this study, a threshold of 2.5 was selected, such that clusters below the threshold value were merged into a single group, and the clusters above the threshold were grouped at a higher level within the hierarchy. The key point here is that the groups are comparable between the different study areas. Issues arise when a group is present in one region but not in another. Therefore, at a national scale, it is important to identify all groups within the training areas and recognise that some groups may not be apparent in some regions.

From the signatures derived from the ISODATA clustering, disturbance patterns were evident. With well-defined signatures common to all three regions, clear-fellings were identified and validated using reference data. Additional clusters indicated the occurrence of disturbance events such as storms, fire, insect attack and plant failure, however these could not be conclusively validated due to the unavailability of reference data. Therefore, objective (ii) i.e. to explore the possibilities of a data-driven unsupervised classifier to identify the occurrence of different disturbances and characterize them was only partially fulfilled.

7.1.1.3 Transferability of algorithm between ALOS PALSAR and ALOS-2 PALSAR-2 sensors

Objective (iii) i.e. to transfer the approach developed for a historic dataset to a recent L-band SAR dataset and explore the prospects of continuing this monitoring operation in Ireland has been achieved by applying the methodology developed for ALOS PALSAR to the more recent ALOS-2 PALSAR-2 datasets. Forest/non-forest classification accuracies of up to 95% were achieved for summer images. The seasonal effects were reflected in the RF classification which resulted in relatively lower accuracies of 92% and 89% for autumn and winter images of ALOS-2 PALSAR-2 respectively. With its higher spatial and radiometric resolution, an improvement in the ability to map small areas of forest was achieved, with a minimum mapping unit of 1.1 ha. The transferability of the ISODATA algorithm was demonstrated by the similarity in the signature patterns of the common groups identified by both the sensors, and, as with the ALOS PALSAR results, clear-fells were successfully validated. However, considering the different time periods

and seasons of the ALOS-2 PALSAR-2 imagery, new signature patterns in the clusters were discovered, and therefore clusters from one image cannot be unequivocally mapped directly onto another image.

This study illustrated the potential for identification of deforestation between two different sensors. With the successful transferability of the algorithm between the sensors deforested areas as large as 121 ha to as small as 1.13 ha were mapped over the period 2007-2016.

7.1.2 Research constraints

The main constraints encountered in this study were caused by SAR data availability and reference data limitations. Because of the 'systematic observation restrictions' operated by the Japanese Space Agency, JAXA, only 1-2 FBD ALOS PALSAR and ALOS-2 PALSAR-2 images over Ireland were available over the study areas each year. Although summer images were available for ALOS PALSAR, which were ideal for the work, only autumn and winter images were available in some years for ALOS-2 PALSAR-2. This resulted in two major limitations in this study – (i) non-optimal conditions for forest classification due to seasonal influences; and (ii) inaccuracies in quantification of felling events.

This work initially hoped to characterise different disturbance events that can cause forest loss such as windthrow, fires, insect attack, plant failure and weather events. Although signatures other than those of clear-fells suggested such responses in the time-series, defining the nature of that change could not be achieved. One of the reasons for this was the lack of reference data with no systematic reporting of events such as forest fires, and spatial information only available following occasional large-scale events such as after Storm Darwin in February 2014. These signature patterns were observed for all three areas indicating significant forest loss of 8%, 7% and 9% over Area1, Area2 and Area3 respectively between the period 2007-2010 as mapped by ALOS PALSAR. For the period 2015-2016 as mapped by ALOS-2 PALSAR-2, these clusters represented forest loss of 10%, 4% and 5% in Area1, Area2 and Area3, respectively. Due to the limitation arising from the image acquisition dates, having one image per year precluded precise dating of such events. From the viewpoint of forest management, and biomass and carbon

estimation, identifying the causes of such forest loss is essential. These clusters exhibited the same pattern of a decrease of 2±0.5dB between consecutive years across all the sites but further investigation would be required to determine if these changes were caused due to a single or multiple forms of disturbance. If multiple events are responsible for such cluster behaviour, a more challenging task will be to differentiate those events, which requires a much denser time series of imagery.

Discrepancies in the reference datasets existed, such as inconsistencies between field work and digital records, missing entries of planting year of forests, and incorrect entries of the actual area felled. Additionally, reference datasets were available only for Coillte owned forests, which is 50.8% of the total forest area. However, the approach used in this study can potentially help in clarifying some of these discrepancies. For example, the exact area felled can be identified by its multi-temporal signature, which can be used to annually confirm areas that have been felled. Irrespective of forest ownership, the felling areas can be identified through this approach, which can subsequently inform overall tree area and carbon potential.

The single image per year approach precluded species level classification, and mapping disturbances below 1ha could not be achieved with this approach. However, by matching the available planting year information with the mean backscatter values of the signatures, forest age was retrieved and hence clusters were grouped into mature (age:10-30 years) and young (age:0-9 years) trees. With the availability of more images at different seasons of the year, and also combining information from optical imagery with the SAR dataset, more valuable information can be extracted through this approach.

7.1.3 Recommendations for future work

This research has identified new possibilities for forest monitoring operations in Ireland. A national systematic reporting procedure, which can be a common platform for both field measurements and those derived from imagery and other secondary sources, is essential for a robust and reliable inventory. For example, PastureBase operated by Teagasc *(Teagasc, 2020)* in Ireland is a tool that enables a subset of farmers to upload data on grassland production and utilization, which can be enhanced with imagery and other management information. Similarly, establishing a common platform for forests would

help bridge the gap between foresters and analysts, allowing some of the discrepancies in the reference datasets, as discussed in section 7.1.2, to be reduced. Recording the nature, location and extent of disturbances such as clear-felling, deforestation, fire, storms, insect attacks and nutrient deficiency in plants will help in maintaining up-to-date records on the database, which can be retrieved at any point in time and used to validate national image datasets.

Synergies between multiple SAR, or SAR and optical, datasets to improve the quality of disturbance information should be explored. Combining the high temporal resolution of freely available satellite data such as C-band Sentinel-1 with L-band SAR systems will help to understand better the nature of change. Upcoming satellites such as ALOS-4 with PALSAR-3 onboard, Tandem-L and the P-band Biomass satellite to be launched in 2022 will also provide more research opportunities for forest monitoring with sensors that have been developed specifically for such activities. The methods developed in this study can be expanded by combining data from the existing and upcoming satellites to enhance the clustering process by incorporating additional backscatter information. As discussed in *McInerney et al., (2011),* one of the main limitations of using optical images in operational contexts in Ireland is the difficulty in obtaining cloud-free satellite imagery, particularly over northern and western parts of the country where it is cloudier. But while SAR data can overcome this limitation, as this work has shown it cannot provide a comprehensive inventory of, for example, tree species. Sentinel-2 and WorldView imagery, for example, can successfully identify tree species in countries such as Poland *(Grabska et al., 2019),* Sweden *(Persson et al., 2018)* and Austria *(Immitzer et al., 2012)*. So, a similar approach in Ireland could provide baseline information that would vary little from one year to the next. Disturbance events from SAR data could then be integrated with this baseline information to better understand the implications of a change in tree cover.

To operationalise the algorithm, some factors must be considered. To begin with, a fully automated end-to-end programming script to execute the entire processing steps of the algorithm would be required. The script would draw on the relevant freely available programming and software packages such as the graph processing tool from the SNAP software to pre-process SAR images, the R programming language for RF classification

or Python for running ISODATA clustering. Other options such as Google Earth Engine and the Orfeo toolbox can also be considered for SAR pre-processing and classification as these enable faster processing and avoid software licensing issues. Using the RF classifier for national forest mapping is feasible given that it was successfully used in three different geographical areas in this work. However, the efficiency of the classifier lies in the consistency of the images used. Using images from different seasons has significant impacts on classification accuracies, and therefore the choice of sensor needs to consider the long term continuity and image acquisition plans of the agency managing the satellites. Implementing ISODATA clustering nationally presents more of a challenge given the different types of forest system, management processes and disturbance events across the country. As seen from the results in this study, selection of the optimal number of clusters through divergence separability indices varied across the areas and between sensors, and although common cluster groups were formed, the cluster numbers within each group differed. Adopting a regional approach for disturbance monitoring could be a solution to this.

The approach presented in this work can support the ongoing and envisioned future forest monitoring requirements by forest companies and government agencies charged with detecting clear-fells, disturbance events and deforestation. While, this work with radar remote sensing cannot replace ground-based methods, the advantage lies in its ability to monitor forests and their changes over large areas on an annual basis. Its capability in adding value to mapping distinct forest areas compensates for some of the discrepancies and omissions in the existing datasets such as FIPS and PrivateForests2016. As the 6th ALOS-2 Research Announcement by JAXA is open for all the principal investigators (PI) until the end of the sensor life, data from 2017 onwards can be acquired to extend the existing datasets for the regions studied in this thesis, and also complete the spatial gaps for national coverage. Nonetheless, the most important requirement is a commitment to long-term operational missions from space agencies, especially in the light of the international climate change treaties to which Ireland and other countries subscribe. The upcoming ESA BIOMASS mission offers the potential for a step change in forest mapping and monitoring globally and should be carefully evaluated by Irish research and operational organisations and agencies once its data become available.

Bibliography

Aalen, F.H.A., Whelan, K., Stout, M., 1997. Atlas of the Irish Rural Landscape. University of Toronto Press.

Abbas, A.W., Minallh, N., Ahmad, N., Abid, S.A.R., Khan, M.A.A., 2016. K-Means and ISODATA Clustering Algorithms for Landcover Classification Using Remote Sensing.

Abdelrahman, M., Ali, A., Farag, A.A., 2011. Precise change detection in multi-spectral remote sensing imagery using SIFT-based registration, in: 2011 International Conference on Multimedia Technology. Presented at the 2011 International Conference on Multimedia Technology, pp. 6238–6242. https://doi.org/10.1109/ICMT.2011.6003099

Abramovitz, J.N., Starke, L., Worldwatch Institute, 1998. State of the world 1998: a Worldwatch Institute report on progress toward a sustainable society. W.W. Norton, New York; London.

Achard, F., Eva, H., Mayaux, P., 2001. Tropical forest mapping from coarse spatial resolution satellite data: Production and accuracy assessment issues. Int. J. Remote Sens. 22, 2741–2762. https://doi.org/10.1080/01431160120548

Ajadi, O., Meyer, F., Webley, P., 2016. Change Detection in Synthetic Aperture Radar Images Using a Multiscale-Driven Approach. Remote Sens. 8, 482. https://doi.org/10.3390/rs8060482

Albregtsen, F., 2008. Statistical Texture Measures Computed from Gray Level Coocurrence Matrices. Image processing laboratory, department of informatics, University of Oslo.

Albright, T.P., Painter, T.H., Roberts, D.A., Shi, J., Dozier, J., Fielding, E., 1998. Classification of surface types using SIR-C/X-SAR, Mount Everest Area, Tibet. J. Geophys. Res. Planets 103, 25823–25837. https://doi.org/10.1029/98JE01893

Ali, A., de Bie, C.A.J.M., Skidmore, A.K., Scarrott, R.G., Hamad, A., Venus, V., Lymberakis, P., 2013. Mapping land cover gradients through analysis of hyper-temporal NDVI imagery. Int. J. Appl. Earth Obs. Geoinformation 23, 301–312. https://doi.org/10.1016/j.jag.2012.10.001

Ali, A., de Bie, C.A.J.M., Skidmore, A.K., Scarrott, R.G., Lymberakis, P., 2014. Mapping the heterogeneity of natural and semi-natural landscapes. Int. J. Appl. Earth Obs. Geoinformation 26, 176–183. https://doi.org/10.1016/j.jag.2013.06.007

Almeida-Filho, R., Rosenqvist, A., Shimabukuro, Y.E., Silva-Gomez, R., 2007. Detecting deforestation with multitemporal L-band SAR imagery: a case study in western Brazilian Amazônia. Int. J. Remote Sens. 28, 1383–1390. https://doi.org/10.1080/01431160600754591

Almeida-Filho, R., Shimabukuro, Y.E., Rosenqvist, A., Sánchez, G.A., 2009. Using dual-polarized ALOS PALSAR data for detecting new fronts of deforestation in the Brazilian Amazônia. Int. J. Remote Sens. 30, 3735–3743. https://doi.org/10.1080/01431160902777175

Amazon fires [WWW Document], 2019. . Environment. URL https://www.nationalgeographic.com/environment/2019/08/amazon-fires-cause-deforestation-graphic-map/ (accessed 3.5.20).

Anfinsen, S.N., Doulgeris, A.P., Eltoft, T., 2008. Estimation of the Equivalent Number of Looks in Polarimetric SAR Imagery, in: IGARSS 2008 - 2008 IEEE International Geoscience and Remote Sensing Symposium. Presented at the IGARSS 2008 - 2008 IEEE International

Geoscience and Remote Sensing Symposium, p. IV-487-IV–490. https://doi.org/10.1109/IGARSS.2008.4779764
Arbelaitz, O., Gurrutxaga, I., Muguerza, J., Pérez, J.M., Perona, I., 2013. An extensive comparative study of cluster validity indices. Pattern Recognit. 46, 243–256. https://doi.org/10.1016/j.patcog.2012.07.021
Archer, K.J., Kimes, R.V., 2008. Empirical characterization of random forest variable importance measures. Comput. Stat. Data Anal. 52, 2249–2260. https://doi.org/10.1016/j.csda.2007.08.015
Ari Sambodo, K., Indriasari, N., 2013. Land Cover Classification of ALOS PALSAR Data Using Suppor Vector Machine. Int. J. Remote Sens. Earth Sci., 1 10, 9–18.
Askne, J.I.H., Dammert, P.B.G., Ulander, L.M.H., Smith, G., 1997. C-band repeat-pass interferometric SAR observations of the forest. IEEE Trans. Geosci. Remote Sens. 35, 25–35. https://doi.org/10.1109/36.551931
Attarchi, S., Gloaguen, R., 2014a. Classifying Complex Mountainous Forests with L-Band SAR and Landsat Data Integration: A Comparison among Different Machine Learning Methods in the Hyrcanian Forest. Remote Sens. 6, 3624–3647. https://doi.org/10.3390/rs6053624
Attarchi, S., Gloaguen, R., 2014b. Classifying Complex Mountainous Forests with L-Band SAR and Landsat Data Integration: A Comparison among Different Machine Learning Methods in the Hyrcanian Forest. Remote Sens. 6, 3624–3647. https://doi.org/10.3390/rs6053624
Backer, E., Jain, A.K., 1981. A clustering performance measure based on fuzzy set decomposition. IEEE Trans. Pattern Anal. Mach. Intell. 3, 66–75.
Baghdadi, N., Le Maire, G., Bailly, J.-S., Ose, K., Nouvellon, Y., Zribi, M., Lemos, C., Hakamada, R., 2015. Evaluation of ALOS/PALSAR L-Band Data for the Estimation of Eucalyptus Plantations Aboveground Biomass in Brazil. IEEE J. Sel. Top. Appl. Earth Obs. Remote Sens. 8, 3802–3811. https://doi.org/10.1109/JSTARS.2014.2353661
Balzter, H., 2001. Forest mapping and monitoring with interferometric synthetic aperture radar (InSAR). Prog. Phys. Geogr. 25, 159–177. https://doi.org/10.1177/030913330102500201
Balzter, H., Cole, B., Thiel, C., Schmullius, C., 2015. Mapping CORINE Land Cover from Sentinel-1A SAR and SRTM Digital Elevation Model Data using Random Forests. Remote Sens. 7, 14876–14898. https://doi.org/10.3390/rs71114876
Ban, Y., Yousif, O.A., 2012. Multitemporal Spaceborne SAR Data for Urban Change Detection in China. IEEE J. Sel. Top. Appl. Earth Obs. Remote Sens. 5, 1087–1094. https://doi.org/10.1109/JSTARS.2012.2201135
Banskota, A., Kayastha, N., Falkowski, M.J., Wulder, M.A., Froese, R.E., White, J.C., 2014. Forest Monitoring Using Landsat Time Series Data: A Review. Can. J. Remote Sens. 40, 362–384. https://doi.org/10.1080/07038992.2014.987376
Baraldi, A., Alpaydin, E., 2002. Constructive Feedforward ART Clustering Networks. II. Trans Neur Netw 13, 662–677. https://doi.org/10.1109/TNN.2002.1000131
Baraldi, A., Bruzzone, L., Blonda, P., 2005. Quality assessment of classification and cluster maps without ground truth knowledge. IEEE Trans. Geosci. Remote Sens. 43, 857–873. https://doi.org/10.1109/TGRS.2004.843074
Baraldi, A., Parmiggiani, F., 1995. An investigation of the textural characteristics associated with gray level cooccurrence matrix statistical parameters. IEEE Trans. Geosci. Remote Sens. 33, 293–304. https://doi.org/10.1109/36.377929

Baronti, S., Carla, R., Sigismondi, S., Alparone, L., 1994. Principal component analysis for change detection on polarimetric multitemporal SAR data, in: Proceedings of IGARSS '94 - 1994 IEEE International Geoscience and Remote Sensing Symposium. Presented at the Proceedings of IGARSS '94 - 1994 IEEE International Geoscience and Remote Sensing Symposium, pp. 2152–2154 vol.4. https://doi.org/10.1109/IGARSS.1994.399678

Bartholome, E., `Belward, A.S., 2005. GLC2000: a new approach to global land cover mapping from Earth observation data. Int. J. Remote Sens. 26, 1959–1977. https://doi.org/10.1080/01431160412331291297

Bazi, Y., Bruzzone, L., Melgani, F., 2005. An unsupervised approach based on the generalized Gaussian model to automatic change detection in multitemporal SAR images. IEEE Trans. Geosci. Remote Sens. 43, 874–887. https://doi.org/10.1109/TGRS.2004.842441

Belenguer-Plomer, M.A., Fernandez-Carrillo, A., McCaw, L., Tanase, M.A., 2018. L-band SAR sensitivity to prescribed burning effects in eucalypt forests of Western Australia, in: Notarnicola, C., Pierdicca, N., Bovenga, F., Santi, E. (Eds.), Active and Passive Microwave Remote Sensing for Environmental Monitoring II. Presented at the Active and Passive Microwave Remote Sensing for Environmental Monitoring, SPIE, Berlin, Germany, p. 31. https://doi.org/10.1117/12.2325669

Belgiu, M., Drăguţ, L., 2016. Random forest in remote sensing: A review of applications and future directions. ISPRS J. Photogramm. Remote Sens. 114, 24–31. https://doi.org/10.1016/j.isprsjprs.2016.01.011

Benelcadi, H., Frison, P.-L., Lardeux, C., Mercier, G., Rudant, J.-P., 2014. Using texture from high resolution Terrasar-X images for tropical forest mapping. Presented at the International Geoscience and Remote Sensing Symposium (IGARSS), pp. 2328–2331. https://doi.org/10.1109/IGARSS.2014.6946937

Bie, C.A.J.M. de, Nguyen, T.T.H., Ali, A., Scarrott, R., Skidmore, A.K., 2012. LaHMa: a landscape heterogeneity mapping method using hyper-temporal datasets. Int. J. Geogr. Inf. Sci. 26, 2177–2192. https://doi.org/10.1080/13658816.2012.712126

Bindel, M., Hese, S., Berger, C., 2011. Feature selection from high resolution remote sensing data for biotope mapping. Presented at the High-Resolution Earth Imaging for Geospatial Information, Hannover, pp. 14–17.

Black, K., Gallagher, G., Connelly, J., Hawkins, M., Tarleton, M., Hamel, J., 2011. CARBWARE - Development of tools and systems for reporting on forest carbon stocks and stock change under the Kyoto protocol and the UNFCCC.

Black, K., Nieuwenhuis, M., Cawkwell, F., Balaji, P., 2017. Estimation of forest biomass using L-band backscatter microwave satellite data. Ir. For.

Bosch, A., Zisserman, A., Munoz, X., 2007. Image Classification using Random Forests and Ferns, in: 2007 IEEE 11th International Conference on Computer Vision. Presented at the 2007 IEEE 11th International Conference on Computer Vision, pp. 1–8. https://doi.org/10.1109/ICCV.2007.4409066

Bossard, M., Feranec, J., Otahel, J., 2000. CORINE Land cover technical guide - Addendum 2000 (Technical Report No. 40).

Boudraa, A.O., 1999. Dynamic estimation of number of clusters in data sets. Electron. Lett. 35, 1606–1608. https://doi.org/10.1049/el:19991151

Bovolo, F., Bruzzone, L., 2005. A detail-preserving scale-driven approach to change detection in multitemporal SAR images. IEEE Trans. Geosci. Remote Sens. 43, 2963–2972. https://doi.org/10.1109/TGRS.2005.857987

Breiman, L., 2001. Random Forests. Mach. Learn. 45, 5–32. https://doi.org/10.1023/A:1010933404324

Bujor, F., Trouve, E., Valet, L., Nicolas, J.-M., Rudant, J.-P., 2004. Application of log-cumulants to the detection of spatiotemporal discontinuities in multitemporal SAR images. IEEE Trans. Geosci. Remote Sens. 42, 2073–2084. https://doi.org/10.1109/TGRS.2004.835304

Cable, J., Kovacs, J., Shang, J., Jiao, X., 2014. Multi-Temporal Polarimetric RADARSAT-2 for Land Cover Monitoring in Northeastern Ontario, Canada. Remote Sens. 6, 2372–2392. https://doi.org/10.3390/rs6032372

Caccetta, P., Furby, S., Wallace, J., Wu, X., Richards, G., Waterworth, R., 2012. Long-Term Monitoring of Australian Land Cover Change Using Landsat Data, in: Global Forest Monitoring from Earth Observation, Earth Observation of Global Changes. CRC Press, pp. 243–258. https://doi.org/10.1201/b13040-14

Camps-Valls, G., 2009. Machine learning in remote sensing data processing, in: 2009 IEEE International Workshop on Machine Learning for Signal Processing. Presented at the 2009 IEEE International Workshop on Machine Learning for Signal Processing, pp. 1–6. https://doi.org/10.1109/MLSP.2009.5306233

Canadell, J.G., Raupach, M.R., 2008. Managing Forests for Climate Change Mitigation. Science 320, 1456–1457. https://doi.org/10.1126/science.1155458

Cannell, M.G.R., 1996. Forests as carbon sinks mitigating the greehouse effect. Commonw. For. Rev. 75, 92–99.

Carincotte, C., Derrode, S., Bourennane, S., 2006. Unsupervised change detection on SAR images using fuzzy hidden Markov chains. IEEE Trans. Geosci. Remote Sens. 44, 432–441. https://doi.org/10.1109/TGRS.2005.861007

CCRS, 2006. Fundamentals of Remote Sensing [WWW Document]. URL http://www.nrcan.gc.ca/earth-sciences/resource/tutor/fundam/pdf/fundamentals_e.pdf (accessed 12.18.14).

Celik, T., 2010. A Bayesian approach to unsupervised multiscale change detection in synthetic aperture radar images. Signal Process. 90, 1471–1485. https://doi.org/10.1016/j.sigpro.2009.10.018

Chen, C., Huang, K., Gao, G., 2019. Small-Target Detection between SAR Images Based on Statistical Modeling of Log-Ratio Operator. Sensors 19, 1431. https://doi.org/10.3390/s19061431

Chen*, D., Stow, D.A., Gong, P., 2004. Examining the effect of spatial resolution and texture window size on classification accuracy: an urban environment case. Int. J. Remote Sens. 25, 2177–2192. https://doi.org/10.1080/01431160310001618464

Chen, H., Cloude, S.R., Goodenough, D.G., 2016. Forest Canopy Height Estimation Using Tandem-X Coherence Data. IEEE J. Sel. Top. Appl. Earth Obs. Remote Sens. 9, 3177–3188. https://doi.org/10.1109/JSTARS.2016.2582722

Chen, L., Cui, X., Li, Z., Yuan, Z., Xing, J., Xing, X., Jia, Z., 2019. A New Deep Learning Algorithm for SAR Scene Classification Based on Spatial Statistical Modeling and Features Re-Calibration. Sensors 19, 2479. https://doi.org/10.3390/s19112479

Clausi, D., Zhao, Y., 2002. Rapid extraction of image texture by co-occurrence using a hybrid data structure. Comput. Amp Geosci. 28, 763–774. https://doi.org/DOI: 10.1016/S0098-3004(01)00108-X

Clifford, B., Farrelly, N., Green, S., 2009. A preliminary evaluation of the application of multi-return LiDAR for forestry in Ireland (No. COFORD Connects-Silviculture / Management No. 18).

Cloude, S.R., Papathanassiou, K.P., 1998. Polarimetric SAR interferometry. IEEE Trans. Geosci. Remote Sens. 36, 1551–1565. https://doi.org/10.1109/36.718859
COFORD, 2014. Irish Forests and Biodiversity.
Collalti, A., Thornton, P.E., Cescatti, A., Rita, A., Borghetti, M., Nolè, A., Trotta, C., Ciais, P., Matteucci, G., 2019. The sensitivity of the forest carbon budget shifts across processes along with stand development and climate change. Ecol. Appl. 29, e01837. https://doi.org/10.1002/eap.1837
COMMISSION OF THE EUROPEAN COMMUNITIES, 2007. COMMUNICATION FROM THE COMMISSION TO THE COUNCIL, THE EUROPEAN PARLIAMENT, THE EUROPEAN ECONOMIC AND SOCIAL COMMITTEE AND THE COMMITTEE OF THE REGIONS. Brussels, Belgium.
Copernicus, 2018. CLC 2018 — Copernicus Land Monitoring Service [WWW Document]. URL https://land.copernicus.eu/pan-european/corine-land-cover/clc2018 (accessed 6.16.20).
Coulibaly, L., Tlili, A., Hervet, E., Adegbidi, K., 2012. Mapping forest stands using RADARSAT-2 quad-polarization SAR images: A combination of polarimetric and spatial information, in: Geoscience and Remote Sensing Symposium (IGARSS), 2012 IEEE International. Presented at the Geoscience and Remote Sensing Symposium (IGARSS), 2012 IEEE International, pp. 3359–3362. https://doi.org/10.1109/IGARSS.2012.6350701
Criminisi, A., Shotton, J., Konukoglu, E., 2012. Decision Forests: A Unified Framework for Classification, Regression, Density Estimation, Manifold Learning and Semi-Supervised Learning. Found. Trends® Comput. Graph. Vis. 7, 81–227. https://doi.org/10.1561/0600000035
Cross, J., 2012. Ireland's Woodland Heritage - A guide to Ireland's Native Woodlands. Ireland.
Cui, B., Zhang, Y., Yan, L., Wei, J., Wu, H., 2019. An Unsupervised SAR Change Detection Method Based on Stochastic Subspace Ensemble Learning. Remote Sens. 11, 1314. https://doi.org/10.3390/rs11111314
Cutler, D.R., Edwards, T.C., Beard, K.H., Cutler, A., Hess, K.T., Gibson, J., Lawler, J.J., 2007. Random Forests for Classification in Ecology. Ecology 88, 2783–2792. https://doi.org/10.1890/07-0539.1
DAFM, 2017. Forest Statistics Ireland, 2017.
Davies, H., Image, M., 2014. Ireland's Forestry Programme 2014-2020. Leeds.
Davis, L.S., Johns, S.A., Aggarwal, J.K., 1979. Texture Analysis Using Generalized Co-Occurrence Matrices. IEEE Trans. Pattern Anal. Mach. Intell. PAMI-1, 251–259. https://doi.org/10.1109/TPAMI.1979.4766921
De Alban, J., Connette, G., Oswald, P., Webb, E., 2018. Combined Landsat and L-Band SAR Data Improves Land Cover Classification and Change Detection in Dynamic Tropical Landscapes. Remote Sens. 10, 306. https://doi.org/10.3390/rs10020306
De Bie, C.A., R.Khan, M., Toxopeus, A.G., Venus, V., Skidmore, A.K., 2008. Hypertemporal image analysis for crop mapping and change detection, in: Proceedings of the XXI Congress: Silk Road for Information from Imagery. Presented at the International Society for Photogrammetry and Remote Sensing, Beijing, China, pp. 803–812.
de Bie, C.A.J.M., Nguyen, T.T.H., Ali, A., Scarrott, R., Skidmore, A.K., 2012. LaHMa: a landscape heterogeneity mapping method using hyper-temporal datasets. Int. J. Geogr. Inf. Sci. 26, 2177–2192. https://doi.org/10.1080/13658816.2012.712126
De Grandi, G.F., Leysen, M., Lee, J.S., Schuler, D., 1997. Radar reflectivity estimation using multiple SAR scenes of the same target: technique and applications, in: IGARSS'97. 1997 IEEE International Geoscience and Remote Sensing Symposium Proceedings.

Remote Sensing - A Scientific Vision for Sustainable Development. Presented at the IGARSS'97. 1997 IEEE International Geoscience and Remote Sensing Symposium Proceedings. Remote Sensing - A Scientific Vision for Sustainable Development, IEEE, Singapore, pp. 1047–1050. https://doi.org/10.1109/IGARSS.1997.615338

Dekker, R.J., 2003. Texture analysis and classification of ERS SAR images for map updating of urban areas in the netherlands. IEEE Trans. Geosci. Remote Sens. 41, 1950–1958. https://doi.org/10.1109/TGRS.2003.814628

Deng, H., Clausi, D.A., 2005. Unsupervised segmentation of synthetic aperture Radar sea ice imagery using a novel Markov random field model. IEEE Trans. Geosci. Remote Sens. 43, 528–538. https://doi.org/10.1109/TGRS.2004.839589

Deng, H., Clausi, D.A., 2004. Gaussian MRF rotation-invariant features for image classification. IEEE Trans. Pattern Anal. Mach. Intell. 26, 951–955. https://doi.org/10.1109/TPAMI.2004.30

Department of Agriculture and Food, Forest Service, 2008. Derivation of the Forestry2007 forest cover spatial database.

Department of Agriculture, F.& the M., 2014. Storm Darwin 2014 - Department of Agriculture, Food & the Marine [WWW Document]. URL https://www.agriculture.gov.ie/forestservice/forestservicegeneralinformation/foreststatisticsandmapping/stormdarwin2014/ (accessed 7.2.20).

Department of Agriculture, Food and the Marine, 2019. Forest Statistics - Ireland 2019. Wexford, Ireland.

Department of Agriculture, Food and the Marine, 2018. Forest Statistics - Ireland 2017. Wexford, Ireland.

Department of Communications, Climate Action and Environment, 2018. Sectoral Planning Guidelines for Climate Change Adaptation.

Department of Fisheries and Forestry, 1973. Inventory of private forests-1973.

Devaney, J., Barrett, B., Barrett, F., Redmond, J., O`Halloran, J., 2015a. Forest Cover Estimation in Ireland Using Radar Remote Sensing: A Comparative Analysis of Forest Cover Assessment Methodologies. PLOS ONE 10, e0133583. https://doi.org/10.1371/journal.pone.0133583

Devaney, J., Barrett, B., Barrett, F., Redmond, J., O`Halloran, J., 2015b. Forest Cover Estimation in Ireland Using Radar Remote Sensing: A Comparative Analysis of Forest Cover Assessment Methodologies. PLOS ONE 10, e0133583. https://doi.org/10.1371/journal.pone.0133583

Devaney, J., Redmond, J., Barrett, B., Cott, G., O'Halloran, J., 2017. 21st Century Deforestation in Ireland (EPA Research report No. 221). Wexford.

Devaney, J.L., Redmond, J.J., Cott, G.M., Halloran, J.O., 2016. Deforestation in Ireland 2000 – 2012. Ir. For. 2016 73.

Devaney, J.L., Redmond, J.J., O'Halloran, J., 2015. Contemporary forest loss in Ireland; quantifying rare deforestation events in a fragmented forest landscape. Appl. Geogr. 63, 346–356. https://doi.org/10.1016/j.apgeog.2015.07.008

Dobson, M.C., Ulaby, F.T., Pierce, L.E., Sharik, T.L., Bergen, K.M., Kellndorfer, J., Kendra, J.R., Li, E., Lin, Y.C., Nashashibi, A., Sarabandi, K., Siqueira, P., 1995. Estimation of forest biophysical characteristics in Northern Michigan with SIR-C/X-SAR. IEEE Trans. Geosci. Remote Sens. 33, 877–895. https://doi.org/10.1109/36.406674

Domg, Y., Milne, A.K., forster, B.C., 2001. Toward edge sharpening: a SAR speckle filtering algorithm. IEEE Trans. Geosci. Remote Sens. 39, 851–863. https://doi.org/10.1109/36.917910

Dorren, L.K.A., Maier, B., Seijmonsbergen, A.C., 2003. Improved Landsat-based forest mapping in steep mountainous terrain using object-based classification. For. Ecol. Manag. 183, 31–46. https://doi.org/10.1016/S0378-1127(03)00113-0

Dostálová, A., Hollaus, M., Milenković, M., Wagner, W., 2016. Forest Area Derivation from SENTINEL-1 Data. ISPRS Ann. Photogramm. Remote Sens. Spat. Inf. Sci. 7, 227–233. https://doi.org/10.5194/isprs-annals-III-7-227-2016

Du, P., Samat, A., Waske, B., Liu, S., Li, Z., 2015. Random Forest and Rotation Forest for fully polarized SAR image classification using polarimetric and spatial features. ISPRS J. Photogramm. Remote Sens. 105, 38–53. https://doi.org/10.1016/j.isprsjprs.2015.03.002

Duffy, P., Hanley, E., Hyde, B., O'Brien, P., Ponzi, J., Cotter, E., Black, K., 2012. National Inventory Report 2012 - Ireland. Environmental Protection Agency.

Durden, S.L., van Zyl, J.J., Zebker, H.A., 1989. Modeling and observation of the radar polarization signature of forested areas. IEEE Trans. Geosci. Remote Sens. 27, 290–301. https://doi.org/10.1109/36.17670

Durieux, A.M., Calef, M.T., Arko, S., Chartrand, R., Kontgis, C., Keisler, R., Warren, M.S., 2019. Monitoring forest disturbance using change detection on synthetic aperture radar imagery, in: Zelinski, M.E., Taha, T.M., Howe, J., Awwal, A.A., Iftekharuddin, K.M. (Eds.), Applications of Machine Learning. Presented at the Applications of Machine Learning, SPIE, San Diego, United States, p. 39. https://doi.org/10.1117/12.2528945

Dusseux, P., Corpetti, T., Hubert-Moy, L., Corgne, S., 2014a. Combined Use of Multi-Temporal Optical and Radar Satellite Images for Grassland Monitoring. Remote Sens. 6, 6163–6182. https://doi.org/10.3390/rs6076163

Dusseux, P., Corpetti, T., Hubert-Moy, L., Corgne, S., 2014b. Combined Use of Multi-Temporal Optical and Radar Satellite Images for Grassland Monitoring. Remote Sens. 6, 6163–6182. https://doi.org/10.3390/rs6076163

Dwyer, N., 2013. The Status of Ireland's Climate. Environmental Protection Agency, Johnstown Castle, Ireland.

Dwyer, N., Monaco, S., Pasquali, P., 2000. An operational forest monitoring tool using spaceborne SAR data. Presented at the ERS-ENVISAT Symposium, Göteborg, Sweden.

Elsharkawy, A., Elhabiby, M., El-Sheimy, N., 2012. Improvement in the detection of land cover classes using the WorldView-2 imagery. Presented at the ASPRS 2012 Annual Conference, Sacramento, California.

ERDAS IMAGINE Ribbon Workspace - Getting Started [ERDAS IMAGINE Help] (16.00) [WWW Document], n.d. URL https://hexagongeospatial.fluidtopics.net/book#!book;uri=adc685a3d751eb77be1765d568f7b6d3;breadcrumb=b16542a22ade5a8ec685f108f2ec915d (accessed 2.5.17).

European Commission, 2012. Kyoto 1st Commitment Period (2008-12).

European Commission, 2010. Communication from the commission - Europe 2020 - A strategy for smart, sustainable and inclusive growth. Brussels, Belgium.

European Environment Agency, 2017. Climate change, impacts and vulnerability in Europe 2016: An indicator-based report. European Environment Agency, Denmark.

FAO, 2020. Definitional issues related to reducing emissions from deforestation in developing countries [WWW Document]. URL http://www.fao.org/3/j9345e/j9345e07.htm (accessed 7.2.20).

FAO (Ed.), 2018. Forests pathways to sustainable development, State of the world's forests. FAO, Rome.

FAO, 2015. FAO assessment of forests and carbon stocks, 1990-2015.

FAO, 2001. Forests and Climate Change Working Paper 1.
Ferretti, A., Prati, C., Rocca, F., 2001. Permanent scatterers in SAR interferometry. IEEE Trans. Geosci. Remote Sens. 39, 8–20. https://doi.org/10.1109/36.898661
Ferro, Christopher.J., Warner, Timothy.A., 2002. Scale and texture in digital image classification. Photogramm. Eng. Remote Sens. 68, 51–63.
Food and Agriculture Organization of the United Nations, 2016. Global forest resources assessment 2015: how are the world's forests changing?
Forest Service, 2018a. Ireland's national forest inventory 2017: main findings. Forest Service, Department of Agriculture, Food and the Marine, Co. Wexford, Ireland.
Forest Service, 2018b. Ireland's National Forest Inventory 2017 - Results.
Forest Service (Ed.), 2013. The Second National Forest Inventory, Republic of Ireland: main findings: covering the National Forestinventory, 2009 to 2012. Forest Service, Department of Agriculture, Food and the Marine, Johnstown Castle Estate, Co. Wexford, Ireland.
Forest Service of Ireland, 2013. The Second National Forest Inventory of Ireland-Field procedures and methodology. Department of Agriculture, Food and the Marine, Johnstown castle. Co.Wexford, Ireland.
Fransson, J.E.S., 1999. Estimation of stem volume in boreal forests using ERS-1 C- and JERS-1 L-band SAR data. Int. J. Remote Sens. 20, 123–137. https://doi.org/10.1080/014311699213640
Fransson, J.E.S., Magnusson, M., Olsson, H., Eriksson, L.E.B., Folkesson, K., Sandberg, G., Santoro, M., Ulander, L.M.H., 2008. Detection of Clear-Cuts Using ALOS PALSAR Satellite Images, in: 2008 7th European Conference on Synthetic Aperture Radar (EUSAR). Presented at the 2008 7th European Conference on Synthetic Aperture Radar (EUSAR), pp. 1–4.
Fransson, Johan E.S., Magnusson, M., Olsson, H., Eriksson, L.E.B., Sandberg, G., Smith-Jonforsen, G., Ulander, L.M.H., 2007. Detection of forest changes using ALOS PALSAR satellite images. IEEE, pp. 2330–2333. https://doi.org/10.1109/IGARSS.2007.4423308
Fransson, J. E S, Magnusson, M., Olsson, H., Eriksson, L.E.B., Sandberg, G., Smith-Jonforsen, G., Ulander, L.M.H., 2007. Detection of forest changes using ALOS PALSAR satellite images, in: Geoscience and Remote Sensing Symposium, 2007. IGARSS 2007. IEEE International. Presented at the Geoscience and Remote Sensing Symposium, 2007. IGARSS 2007. IEEE International, pp. 2330–2333. https://doi.org/10.1109/IGARSS.2007.4423308
Freudenberg, M., Nölke, N., Agostini, A., Urban, K., Wörgötter, F., Kleinn, C., 2019. Large Scale Palm Tree Detection In High Resolution Satellite Images Using U-Net. Remote Sens. 11, 312. https://doi.org/10.3390/rs11030312
Frost, V.S., Stiles, J.A., Shanmugan, K.S., Holtzman, J.C., 1982. A Model for Radar Images and Its Application to Adaptive Digital Filtering of Multiplicative Noise. IEEE Trans. Pattern Anal. Mach. Intell. PAMI-4, 157–166. https://doi.org/10.1109/TPAMI.1982.4767223
Fung, T., LeDrew, E., 1987. Application of principal components analysis to change detection.
Gagnon, L., Jouan, A., 1997. Speckle filtering of SAR images: a comparative study between complex-wavelet-based and standard filters, in: Aldroubi, A., Laine, A.F., Unser, M.A. (Eds.), . Presented at the Optical Science, Engineering and Instrumentation '97, San Diego, CA, pp. 80–91. https://doi.org/10.1117/12.279681
Gallagher, G., Dunne, S., Jordan, P., Stanley, B., 1999. Ireland's Forest Inventory and Planning System.
Gauch, Hugh.G., Whittaker, Robert.H., 1981. Hierarchical Classification of Community Data. ResearchGate. http://dx.doi.org/10.2307/2259682

Gebejes, A., Huertas, R., 2013. Texture Characterization based on Grey-Level Co-occurrence Matrix. Proc. Conf. Inform. Manag. Sci.

Ghimire, B., Rogan, J., Miller, J., 2010. Contextual land-cover classification: incorporating spatial dependence in land-cover classification models using random forests and the Getis statistic. Remote Sens. Lett. 1, 45–54. https://doi.org/10.1080/01431160903252327

Gimeno, M., San-Miguel Ayanz, J., Barbosa, P.M., Schmuck, G., 2003. Burnt area mapping from ERS-SAR time series using the principal components transformation, in: Posa, F. (Ed.), . pp. 171–180. https://doi.org/10.1117/12.475850

Gislason, P.O., Benediktsson, J.A., Sveinsson, J.R., 2006a. Random Forests for land cover classification. Pattern Recognit. Lett. 27, 294–300. https://doi.org/10.1016/j.patrec.2005.08.011

Gislason, P.O., Benediktsson, J.A., Sveinsson, J.R., 2006b. Random Forests for land cover classification. Pattern Recognit. Lett., Pattern Recognition in Remote Sensing (PRRS 2004) 27, 294–300. https://doi.org/10.1016/j.patrec.2005.08.011

Gong, M., Li, Y., Jiao, L., Jia, M., Su, L., 2014. SAR change detection based on intensity and texture changes. ISPRS J. Photogramm. Remote Sens. 93, 123–135. https://doi.org/10.1016/j.isprsjprs.2014.04.010

Gong, M., Zhou, Z., Ma, J., 2012. Change Detection in Synthetic Aperture Radar Images based on Image Fusion and Fuzzy Clustering. IEEE Trans. Image Process. 21, 2141–2151. https://doi.org/10.1109/TIP.2011.2170702

Goodenough, D.G., Narendra, P.M., O'Neill, K., 1978. Feature Subset Selection in Remote Sensing. Can. J. Remote Sens. 4, 143–148. https://doi.org/10.1080/07038992.1978.10854976

Goodman, J.W., 1976. Some fundamental properties of speckle. https://doi.org/10.1364/JOSA.66.001145

Grabska, E., Hostert, P., Pflugmacher, D., Ostapowicz, K., 2019. Forest Stand Species Mapping Using the Sentinel-2 Time Series. Remote Sens. 11, 1197. https://doi.org/10.3390/rs11101197

Grebner, D.L., Bettinger, P., Siry, J.P., 2013. Forest Regions of the World, in: Introduction to Forestry and Natural Resources. Elsevier, pp. 21–76. https://doi.org/10.1016/B978-0-12-386901-2.00002-6

Haarpaintner, J., Almeida-Filho, R., Edemir Shimabukuro, Y., Malnes, E., Lauknes, I., 2009. Comparison of Envisat ASAR deforestation monitoring in Amazônia with Landsat-TM and ALOS PALSAR images, in: Anais XIV Simposio Brazileiro de Sensoriamento Remoto. Presented at the INPE, Natal, Brazil, pp. 5857–5864.

Haarpaintner, J., Davids, C., Hindberg, H., Zahabu, E., Malimbwi, R.E., 2015. Forest and Forest Change Mapping with C- and L-band SAR in Liwale, Tanzania. ISPRS - Int. Arch. Photogramm. Remote Sens. Spat. Inf. Sci. XL-7/W3, 391–395. https://doi.org/10.5194/isprsarchives-XL-7-W3-391-2015

Hagg, W., Sties, M., 1994. Efficient speckle filtering of SAR images, in: Proceedings of IGARSS '94 - 1994 IEEE International Geoscience and Remote Sensing Symposium. Presented at the Proceedings of IGARSS '94 - 1994 IEEE International Geoscience and Remote Sensing Symposium, pp. 2140–2142 vol.4. https://doi.org/10.1109/IGARSS.1994.399674

Halls, P.J. (Ed.), 2001. Spatial information and the environment, Innovations in GIS. Taylor & Francis, London ; New York.

Hamdi, Z.M., Brandmeier, M., Straub, C., 2019. Forest Damage Assessment Using Deep Learning on High Resolution Remote Sensing Data. Remote Sens. 11, 1976. https://doi.org/10.3390/rs11171976

Hamunyela, E., Verbesselt, J., de Bruin, S., Herold, M., 2016. Monitoring Deforestation at Sub-Annual Scales as Extreme Events in Landsat Data Cubes. Remote Sens. 8, 651. https://doi.org/10.3390/rs8080651

Han, C., Guo, H., Shao, Y., Liao, J., 2005. Classification of ASAR images based on texture. Presented at the International Geoscience and Remote Sensing Symposium (IGARSS), pp. 3849–3851. https://doi.org/10.1109/IGARSS.2005.1525749

Han, H., Guo, X., Yu, H., 2016. Variable selection using Mean Decrease Accuracy and Mean Decrease Gini based on Random Forest, in: 2016 7th IEEE International Conference on Software Engineering and Service Science (ICSESS). Presented at the 2016 7th IEEE International Conference on Software Engineering and Service Science (ICSESS), pp. 219–224. https://doi.org/10.1109/ICSESS.2016.7883053

Hansen, M.C., Potapov, P.V., Moore, R., Hancher, M., Turubanova, S.A., Tyukavina, A., Thau, D., Stehman, S.V., Goetz, S.J., Loveland, T.R., Kommareddy, A., Egorov, A., Chini, L., Justice, C.O., Townshend, J.R.G., 2013a. High-Resolution Global Maps of 21st-Century Forest Cover Change. Science 342, 850–853. https://doi.org/10.1126/science.1244693

Hansen, M.C., Potapov, P.V., Moore, R., Hancher, M., Turubanova, S.A., Tyukavina, A., Thau, D., Stehman, S.V., Goetz, S.J., Loveland, T.R., Kommareddy, A., Egorov, A., Chini, L., Justice, C.O., Townshend, J.R.G., 2013b. High-Resolution Global Maps of 21st-Century Forest Cover Change. Science 342, 850–853. https://doi.org/10.1126/science.1244693

Hansen, M.C., Stehman, S.V., Potapov, P.V., 2010. Quantification of global gross forest cover loss. Proc. Natl. Acad. Sci. 107, 8650–8655. https://doi.org/10.1073/pnas.0912668107

Haralick, R.M., Shanmugam, K., Dinstein, I., 1973. Textural Features for Image Classification. IEEE Trans. Syst. Man Cybern. SMC-3, 610–621. https://doi.org/10.1109/TSMC.1973.4309314

Haralick, R. M., Shanmugam, K., Dinstein, I., 1973. Textural Features for Image Classification. IEEE Trans. Syst. Man Cybern. SMC-3, 610–621. https://doi.org/10.1109/TSMC.1973.4309314

Harrell, P.A., Kasischke, E.S., Bourgeau-Chavez, L.L., Haney, E.M., Christensen, N.L., 1997. Evaluation of approaches to estimating aboveground biomass in Southern pine forests using SIR-C data. Remote Sens. Environ. 59, 223–233. https://doi.org/10.1016/S0034-4257(96)00155-1

He, C., Zhao, Y., Wei, A., 2010. Land-use/land-cover change detection by using the extended change-vector analysis, in: 2010 2nd International Conference on Information Science and Engineering (ICISE). Presented at the 2010 2nd International Conference on Information Science and Engineering (ICISE), pp. 3809–3812. https://doi.org/10.1109/ICISE.2010.5691699

Hecheltjen, A., Thonfeld, F., Menz, G., 2014. Recent Advances in Remote Sensing Change Detection – A Review, in: Manakos, I., Braun, M. (Eds.), Land Use and Land Cover Mapping in Europe. Springer Netherlands, Dordrecht, pp. 145–178. https://doi.org/10.1007/978-94-007-7969-3_10

Hendrick, E., Black, K., 2009. Climate change and Irish forestry (Environment No. 9). COFORD, Dublin.

Henebry, G.M., 1997. Advantages of principal components analysis for land cover segmentation from SAR image series [WWW Document].

Hirschmugl, M., Sobe, C., Deutscher, J., Schardt, M., 2018. Combined Use of Optical and Synthetic Aperture Radar Data for REDD+ Applications in Malawi. Land 7, 116. https://doi.org/10.3390/land7040116

Hoekman, D.H., 1987. Multiband-scatterometer data analysis of forests. Int. J. Remote Sens. 8, 1695–1707. https://doi.org/10.1080/01431168708954809

Hu, H., Ban, Y., 2014. Unsupervised Change Detection in Multitemporal SAR Images Over Large Urban Areas. IEEE J. Sel. Top. Appl. Earth Obs. Remote Sens. 7, 3248–3261. https://doi.org/10.1109/JSTARS.2014.2344017

Hu, T., Su, Y., Xue, B., Liu, J., Zhao, X., Fang, J., Guo, Q., 2016. Mapping Global Forest Aboveground Biomass with Spaceborne LiDAR, Optical Imagery, and Forest Inventory Data. Remote Sens. 8, 565. https://doi.org/10.3390/rs8070565

ICOS - Integrated Carbon Observation System [WWW Document], n.d. . ICOS RI. URL http://www.icos-ri.eu/home (accessed 3.5.20).

Immitzer, M., Atzberger, C., Koukal, T., 2012. Tree Species Classification with Random Forest Using Very High Spatial Resolution 8-Band WorldView-2 Satellite Data. Remote Sens. 4, 2661–2693. https://doi.org/10.3390/rs4092661

Intergovernmental Panel on Climate Change, 2018. Global warming of 1.5°C.

IPCC, 2000. IPCC - Intergovernmental Panel on Climate Change: Land use, land-use change, and forestry.

IPCC, Penman, J., IPPC National Greenhouse Gas Inventories Programme (Eds.), 2003. Good practice guidance for land use, land-use change and forestry /The Intergovernmental Panel on Climate Change. Ed. by Jim Penman. Hayama, Kanagawa.

Isola, M., Cloude, S.R., 2001. Forest height mapping using space-borne polarimetric SAR interferometry, in: IGARSS 2001. Scanning the Present and Resolving the Future. Proceedings. IEEE 2001 International Geoscience and Remote Sensing Symposium (Cat. No.01CH37217). Presented at the IGARSS 2001. Scanning the Present and Resolving the Future. Proceedings. IEEE 2001 International Geoscience and Remote Sensing Symposium (Cat. No.01CH37217), pp. 1095–1097 vol.3. https://doi.org/10.1109/IGARSS.2001.976757

Jain, A.K., Duin, R.P.W., Mao, J., 2000. Statistical Pattern Recognition: A Review. IEEE Trans Pattern Anal Mach Intell 22, 4–37. https://doi.org/10.1109/34.824819

Jain, A.K., Farrokhnia, F., 1990. Unsupervised texture segmentation using Gabor filters, in: , IEEE International Conference on Systems, Man and Cybernetics, 1990. Conference Proceedings. Presented at the , IEEE International Conference on Systems, Man and Cybernetics, 1990. Conference Proceedings, pp. 14–19. https://doi.org/10.1109/ICSMC.1990.142050

Jain, A.K., Murty, M.N., Flynn, P.J., 1999. Data Clustering: A Review. ACM Comput Surv 31, 264–323. https://doi.org/10.1145/331499.331504

Jawak, S.D., Devliyal, P., Luis, A.J., 2015. A Comprehensive Review on Pixel Oriented and Object Oriented Methods for Information Extraction from Remotely Sensed Satellite Images with a Special Emphasis on Cryospheric Applications. Adv. Remote Sens. 04, 177–195. https://doi.org/10.4236/ars.2015.43015

Jensen, J.R., 2005. Introductory Digital Image Processing: A Remote Sensing Perspective. Prentice Hall.

Jolliffe, I.T., Cadima, J., 2016. Principal component analysis: a review and recent developments. Philos. Trans. R. Soc. Math. Phys. Eng. Sci. 374, 20150202. https://doi.org/10.1098/rsta.2015.0202

Jones, H.G., Vaughan, R.A., 2010. Remote sensing of vegetation principles, techniques, and applications. Oxford Univ. Press, Oxford [u.a.].

Jong-Sen Lee, Jen-Hung Wen, Ainsworth, T.L., Kun-Shan Chen, Chen, A.J., 2009. Improved Sigma Filter for Speckle Filtering of SAR Imagery. IEEE Trans. Geosci. Remote Sens. 47, 202–213. https://doi.org/10.1109/TGRS.2008.2002881

Joshi, N., Mitchard, E.T., Woo, N., Torres, J., Moll-Rocek, J., Ehammer, A., Collins, M., Jepsen, M.R., Fensholt, R., 2015. Mapping dynamics of deforestation and forest degradation in tropical forests using radar satellite data. Environ. Res. Lett. 10, 034014. https://doi.org/10.1088/1748-9326/10/3/034014

Kaasalainen, S., Holopainen, M., Karjalainen, M., Vastaranta, M., Kankare, V., Karila, K., Osmanoglu, B., 2015. Combining Lidar and Synthetic Aperture Radar Data to Estimate Forest Biomass: Status and Prospects. Forests 6, 252–270. https://doi.org/10.3390/f6010252

Kandaswamy, U., Adjeroh, D.A., Lee, M.C., 2005. Efficient Texture Analysis of SAR Imagery. IEEE Trans. Geosci. Remote Sens. 43, 2075–2083. https://doi.org/10.1109/TGRS.2005.852768

Kasischke, E.S., Tanase, M.A., Bourgeau-Chavez, L.L., Borr, M., 2011. Soil moisture limitations on monitoring boreal forest regrowth using spaceborne L-band SAR data. Remote Sens. Environ. 115, 227–232. https://doi.org/10.1016/j.rse.2010.08.022

Kellndorfer, J.M., Walker, W.S., LaPoint, E., Kirsch, K., Bishop, J., Fiske, G., 2010. Statistical fusion of lidar, InSAR, and optical remote sensing data for forest stand height characterization: A regional-scale method based on LVIS, SRTM, Landsat ETM+, and ancillary data sets: LIDAR/INSAR DATA FUSION FOR VEGETATION HEIGHT. J. Geophys. Res. Biogeosciences 115, n/a-n/a. https://doi.org/10.1029/2009JG000997

Kempeneers, P., McInerney, D., Sedano, F., Gallego, J., Strobl, P., Kay, S., Korhonen, K.T., San-Miguel-Ayanz, J., 2013. Accuracy Assessment of a Remote Sensing-Based, Pan-European Forest Cover Map Using Multi-Country National Forest Inventory Data. IEEE J. Sel. Top. Appl. Earth Obs. Remote Sens. 6, 54–65. https://doi.org/10.1109/JSTARS.2012.2236079

Keshk, H.M., Yin, X.-C., 2019. Change Detection in SAR Images Based on Deep Learning. Int. J. Aeronaut. Space Sci. https://doi.org/10.1007/s42405-019-00222-0

Khan, M.R., de Bie, C.A.J.M., van Keulen, H., Smaling, E.M.A., Real, R., 2010. Disaggregating and mapping crop statistics using hypertemporal remote sensing. Int. J. Appl. Earth Obs. Geoinformation 12, 36–46. https://doi.org/10.1016/j.jag.2009.09.010

Khati, U., Kumar, V., Bandyopadhyay, D., Musthafa, M., Singh, G., 2018. Identification of forest cutting in managed forest of Haldwani, India using ALOS-2/PALSAR-2 SAR data. J. Environ. Manage. 213, 503–512. https://doi.org/10.1016/j.jenvman.2018.02.025

Koppad, A.G., Janagoudar, B.S., 2017. VEGETATION ANALYSIS AND LAND USE LAND COVER CLASSIFICATION OF FOREST IN UTTARA KANNADA DISTRICT INDIA THROUGH GEO-INFORMATICS APPROACH. ISPRS - Int. Arch. Photogramm. Remote Sens. Spat. Inf. Sci. XLII-1/W1, 219–223. https://doi.org/10.5194/isprs-archives-XLII-1-W1-219-2017

Krizhevsky, A., Sutskever, I., Hinton, G.E., 2012. ImageNet Classification with Deep Convolutional Neural Networks, in: Pereira, F., Burges, C.J.C., Bottou, L., Weinberger, K.Q. (Eds.), Advances in Neural Information Processing Systems 25. Curran Associates, Inc., pp. 1097–1105.

Kuan, D.T., Sawchuk, A.A., Strand, T.C., Chavel, P., 1985. Adaptive Noise Smoothing Filter for Images with Signal-Dependent Noise. IEEE Trans. Pattern Anal. Mach. Intell. PAMI-7, 165–177. https://doi.org/10.1109/TPAMI.1985.4767641

Kugler, F., Schulze, D., Hajnsek, I., Pretzsch, H., Papathanassiou, K.P., 2014. TanDEM-X Pol-InSAR Performance for Forest Height Estimation. IEEE Trans. Geosci. Remote Sens. 52, 6404–6422. https://doi.org/10.1109/TGRS.2013.2296533

Kulkarni, S., Kedar, M., Rege, P.P., 2018. Comparison of Different Speckle Noise Reduction Filters for RISAT -1 SAR Imagery, in: 2018 International Conference on Communication and Signal Processing (ICCSP). Presented at the 2018 International Conference on Communication and Signal Processing (ICCSP), pp. 0537–0541. https://doi.org/10.1109/ICCSP.2018.8524250

Kumar, S., Melkani, N., Awasthi, N., Prakash, R., 2015. Texture analysis and classification of polarimetric SAR images using histogram measures. IEEE, pp. 506–511. https://doi.org/10.1109/SPIN.2015.7095365

Landsberg, J., Waring, R., 2014. Forest Types around the World, in: Forests in Our Changing World. Island Press/Center for Resource Economics, Washington, DC, pp. 21–46. https://doi.org/10.5822/978-1-61091-497-0_2

Lasaponara, R., Tucci, B., 2019. Identification of Burned Areas and Severity Using SAR Sentinel-1. IEEE Geosci. Remote Sens. Lett. 16, 917–921. https://doi.org/10.1109/LGRS.2018.2888641

Le Quéré, C., Andrew, R.M., Friedlingstein, P., Sitch, S., Hauck, J., Pongratz, J., Pickers, P.A., Korsbakken, J.I., Peters, G.P., Canadell, J.G., Arneth, A., Arora, V.K., Barbero, L., Bastos, A., Bopp, L., Chevallier, F., Chini, L.P., Ciais, P., Doney, S.C., Gkritzalis, T., Goll, D.S., Harris, I., Haverd, V., Hoffman, F.M., Hoppema, M., Houghton, R.A., Hurtt, G., Ilyina, T., Jain, A.K., Johannessen, T., Jones, C.D., Kato, E., Keeling, R.F., Goldewijk, K.K., Landschützer, P., Lefèvre, N., Lienert, S., Liu, Z., Lombardozzi, D., Metzl, N., Munro, D.R., Nabel, J.E.M.S., Nakaoka, S., Neill, C., Olsen, A., Ono, T., Patra, P., Peregon, A., Peters, W., Peylin, P., Pfeil, B., Pierrot, D., Poulter, B., Rehder, G., Resplandy, L., Robertson, E., Rocher, M., Rödenbeck, C., Schuster, U., Schwinger, J., Séférian, R., Skjelvan, I., Steinhoff, T., Sutton, A., Tans, P.P., Tian, H., Tilbrook, B., Tubiello, F.N., van der Laan-Luijkx, I.T., van der Werf, G.R., Viovy, N., Walker, A.P., Wiltshire, A.J., Wright, R., Zaehle, S., Zheng, B., 2018. Global Carbon Budget 2018. Earth Syst. Sci. Data 10, 2141–2194. https://doi.org/10.5194/essd-10-2141-2018

Lee, J.-S., 1983a. Digital image smoothing and the sigma filter. Comput. Vis. Graph. Image Process. 24, 255–269. https://doi.org/10.1016/0734-189X(83)90047-6

Lee, J.-S., 1983b. A simple speckle smoothing algorithm for synthetic aperture radar images. IEEE Trans. Syst. Man Cybern. SMC-13, 85–89. https://doi.org/10.1109/TSMC.1983.6313036

Lee, J.-S., 1980. Digital Image Enhancement and Noise Filtering by Use of Local Statistics. IEEE Trans. Pattern Anal. Mach. Intell. PAMI-2, 165–168. https://doi.org/10.1109/TPAMI.1980.4766994

Lee, J.-S., Grunes, M.R., Mango, S.A., 1991. Speckle reduction in multipolarization, multifrequency SAR imagery. IEEE Trans. Geosci. Remote Sens. 29, 535–544. https://doi.org/10.1109/36.135815

Lee, J.-S., Hoppel, K., 1992. Principal components transformation of multifrequency polarimetric SAR imagery. IEEE Trans. Geosci. Remote Sens. 30, 686–696. https://doi.org/10.1109/36.158862

Lee, S.-K., Fatoyinbo, T.E., Lagomasino, D., Feliciano, E., Trettin, C., 2018. Multibaseline TanDEM-X Mangrove Height Estimation: The Selection of the Vertical Wavenumber. IEEE J. Sel. Top. Appl. Earth Obs. Remote Sens. 11, 3434–3442. https://doi.org/10.1109/JSTARS.2018.2835647

Lehmann, E.A., Caccetta, P., Lowell, K., Mitchell, A., Zhou, Z.-S., Held, A., Milne, T., Tapley, I., 2015. SAR and optical remote sensing: Assessment of complementarity and interoperability in the context of a large-scale operational forest monitoring system. Remote Sens. Environ. 156, 335–348. https://doi.org/10.1016/j.rse.2014.09.034

Lehmann, E.A., Caccetta, P., Zhou, Z., Mitchell, A.L., Tapley, I., Milne, A.K., Held, A., Lowell, K., McNeill, S.R., 2011. Forest Discrimination Analysis of Combined Landsat TM and ALOS-PALSAR Data.

Lehmann, E.A., Caccetta, P.A., Zhou, Z.-S., McNeill, S.J., Wu, X., Mitchell, A.L., 2012. Joint Processing of Landsat and ALOS-PALSAR Data for Forest Mapping and Monitoring. IEEE Trans. Geosci. Remote Sens. 50, 55–67. https://doi.org/10.1109/TGRS.2011.2171495

Lei, Y., Lucas, R., Siqueira, P., Schmidt, M., Treuhaft, R., 2018a. Detection of Forest Disturbance With Spaceborne Repeat-Pass SAR Interferometry. IEEE Trans. Geosci. Remote Sens. 56, 2424–2439. https://doi.org/10.1109/TGRS.2017.2780158

Lei, Y., Treuhaft, R., Keller, M., dos-Santos, M., Gonçalves, F., Neumann, M., 2018b. Quantification of selective logging in tropical forest with spaceborne SAR interferometry. Remote Sens. Environ. 211, 167–183. https://doi.org/10.1016/j.rse.2018.04.009

Li, G., Lu, D., Moran, E., Dutra, L., Batistella, M., 2012. A comparative analysis of ALOS PALSAR L-band and RADARSAT-2 C-band data for land-cover classification in a tropical moist region. ISPRS J. Photogramm. Remote Sens. 70, 26–38. https://doi.org/10.1016/j.isprsjprs.2012.03.010

Li, J., Wang, S., 2018. Using SAR-Derived Vegetation Descriptors in a Water Cloud Model to Improve Soil Moisture Retrieval. Remote Sens. 10, 1370. https://doi.org/10.3390/rs10091370

Li, M., Zang, S., Zhang, B., Li, S., Wu, C., 2014. A Review of Remote Sensing Image Classification Techniques: the Role of Spatio-contextual Information. Eur. J. Remote Sens. 47, 389–411. https://doi.org/10.5721/EuJRS20144723

Liesenberg, V., Gloaguen, R., 2013. Evaluating SAR polarization modes at L-band for forest classification purposes in Eastern Amazon, Brazil. Int. J. Appl. Earth Obs. Geoinformation 21, 122–135. https://doi.org/10.1016/j.jag.2012.08.016

Long, D., Singh, V.P., 2013. An Entropy-Based Multispectral Image Classification Algorithm. IEEE Trans. Geosci. Remote Sens. 51, 5225–5238. https://doi.org/10.1109/TGRS.2013.2272560

Longepe, N., Rakwatin, P., Isoguchi, O., Shimada, M., Uryu, Y., Yulianto, K., 2011a. Assessment of ALOS PALSAR 50 m Orthorectified FBD Data for Regional Land Cover Classification by Support Vector Machines. IEEE Trans. Geosci. Remote Sens. 49, 2135–2150. https://doi.org/10.1109/TGRS.2010.2102041

Longepe, N., Rakwatin, P., Isoguchi, O., Shimada, M., Uryu, Y., Yulianto, K., 2011b. Assessment of ALOS PALSAR 50 m Orthorectified FBD Data for Regional Land Cover Classification by Support Vector Machines. IEEE Trans. Geosci. Remote Sens. 49, 2135–2150. https://doi.org/10.1109/TGRS.2010.2102041

Lopes, A., Touzi, R., Nezry, E., 1990. Adaptive speckle filters and scene heterogeneity. IEEE Trans. Geosci. Remote Sens. 28, 992–1000. https://doi.org/10.1109/36.62623

Lou, X., Jia, Z., Yang, J., Kasabov, N., 2019. Change Detection in SAR Images Based on the ROF Model Semi-Implicit Denoising Method. Sensors 19, 1179. https://doi.org/10.3390/s19051179

Lu, D., Batistella, M., Moran, E., 2007. Land-cover classification in the Brazilian Amazon with the integration of Landsat ETM+ and Radarsat data. Int. J. Remote Sens. 28, 5447–5459. https://doi.org/10.1080/01431160701227596
Lu, D., Mausel, P., Brondízio, E., Moran, E., 2004. Change detection techniques. Int. J. Remote Sens. 25, 2365–2401. https://doi.org/10.1080/0143116031000139863
Lu, D., Weng, Q., 2007. A survey of image classification methods and techniques for improving classification performance. Int. J. Remote Sens. 28, 823–870. https://doi.org/10.1080/01431160600746456
Lucas, R., Armston, J., Fairfax, R., Fensham, R., Accad, A., Carreiras, J., Kelley, J., Bunting, P., Clewley, D., Bray, S., Metcalfe, D., Dwyer, J., Bowen, M., Eyre, T., Laidlaw, M., Shimada, M., 2010. An Evaluation of the ALOS PALSAR L-Band Backscatter—Above Ground Biomass Relationship Queensland, Australia: Impacts of Surface Moisture Condition and Vegetation Structure. IEEE J. Sel. Top. Appl. Earth Obs. Remote Sens. 3, 576–593. https://doi.org/10.1109/JSTARS.2010.2086436
Lucas, R.M., Mitchell, A.L., Rosenqvist, A., Proisy, C., Melius, A., Ticehurst, C., 2007. The potential of L-band SAR for quantifying mangrove characteristics and change: case studies from the tropics. Aquat. Conserv. Mar. Freshw. Ecosyst. 17, 245–264. https://doi.org/10.1002/aqc.833
Lynch, J., Maslin, M., Balzter, H., Sweeting, M., 2013. Sustainability: Choose satellites to monitor deforestation. Nature 496, 293–294. https://doi.org/10.1038/496293a
Maguire, B., COFORD, 2001. A review of legislation that impacts on Irish forestry.
Marcal, A.R.S., Castro, L., 2005. Hierarchical Clustering of Multispectral Images Using Combined Spectral and Spatial Criteria. IEEE Geosci. Remote Sens. Lett. 2, 59–63. https://doi.org/10.1109/LGRS.2004.839646
Marshak, C., Simard, M., Denbina, M., 2019. Monitoring Forest Loss in ALOS/PALSAR Time-Series with Superpixels. Remote Sens. 11, 556. https://doi.org/10.3390/rs11050556
Martone, M., Rizzoli, P., Brautigam, B., Krieger, G., 2015. A method for generating forest/non-forest maps from TanDEM-X interferometric data, in: 2015 IEEE International Geoscience and Remote Sensing Symposium (IGARSS). Presented at the IGARSS 2015 - 2015 IEEE International Geoscience and Remote Sensing Symposium, IEEE, Milan, Italy, pp. 2634–2637. https://doi.org/10.1109/IGARSS.2015.7326353
Martone, M., Rizzoli, P., Wecklich, C., González, C., Bueso-Bello, J.-L., Valdo, P., Schulze, D., Zink, M., Krieger, G., Moreira, A., 2018. The global forest/non-forest map from TanDEM-X interferometric SAR data. Remote Sens. Environ. 205, 352–373. https://doi.org/10.1016/j.rse.2017.12.002
Mascaro, J., Asner, G.P., Knapp, D.E., Kennedy-Bowdoin, T., Martin, R.E., Anderson, C., Higgins, M., Chadwick, K.D., 2014. A Tale of Two "Forests": Random Forest Machine Learning Aids Tropical Forest Carbon Mapping. PLoS ONE 9, e85993. https://doi.org/10.1371/journal.pone.0085993
Mather, B.T. and P.M., 2001. Classification Methods for Remotely Sensed Data, 1 edition. ed. CRC, London ; New York.
Mather, P., Tso, B., 2016. Classification Methods for Remotely Sensed Data. CRC Press.
McInerney, D., Barrett, F., Landy, J., McDonagh, M., 2016. A rapid assessment using remote sensing of windblow damage in Irish forests following Storm Darwin. Ir. For. 73, 161–179.
McInerney, D.O., Nieuwenhuis, M., 2009. A comparative analysis of *k* NN and decision tree methods for the Irish National Forest Inventory. Int. J. Remote Sens. 30, 4937–4955. https://doi.org/10.1080/01431160903022936

Mellor, A., Haywood, A., Stone, C., Jones, S., 2013. The Performance of Random Forests in an Operational Setting for Large Area Sclerophyll Forest Classification. Remote Sens. 5, 2838–2856. https://doi.org/10.3390/rs5062838

Mermoz, S., Le Toan, T., 2016. Forest Disturbances and Regrowth Assessment Using ALOS PALSAR Data from 2007 to 2010 in Vietnam, Cambodia and Lao PDR. Remote Sens. 8, 217. https://doi.org/10.3390/rs8030217

Met Eireann, 2020. Historical Data - Met Éireann - The Irish Meteorological Service [WWW Document]. URL https://www.met.ie/climate/available-data/historical-data (accessed 6.16.20).

Mishra, V.N., Kumar, P., Gupta, D.K., Prasad, R., 2014. Classification of various land features using RISAT-1 dual polarimetric data. ISPRS - Int. Arch. Photogramm. Remote Sens. Spat. Inf. Sci. 8, 833–837. https://doi.org/10.5194/isprsarchives-XL-8-833-2014

Mohri, M., Rostamizadeh, A., Talwalkar, A., 2018. Foundations of Machine Learning. MIT Press.

Moser, G., Serpico, S.B., 2006. Generalized minimum-error thresholding for unsupervised change detection from SAR amplitude imagery. IEEE Trans. Geosci. Remote Sens. 44, 2972–2982. https://doi.org/10.1109/TGRS.2006.876288

Motohka, T., Shimada, M., Uryu, Y., Setiabudi, B., 2014. Using time series PALSAR gamma nought mosaics for automatic detection of tropical deforestation: A test study in Riau, Indonesia. Remote Sens. Environ. 155, 79–88. https://doi.org/10.1016/j.rse.2014.04.012

Murphy, D., n.d. Ireland's Native woodlands [WWW Document]. Ir. Times. URL https://www.irishtimes.com/culture/heritage/ireland-s-native-woodlands-are-quietly-disappearing-1.3529317 (accessed 3.5.20).

Nabuurs, G.J., Dolman, A.J., Verkaik, E., Kuikman, P.J., van Diepen, C.A., Whitmore, A.P., Daamen, W.P., Oenema, O., Kabat, P., Mohren, G.M.J., 2000. Article 3.3 and 3.4 of the Kyoto Protocol: consequences for industrialised countries' commitment, the monitoring needs, and possible side effects. Environ. Sci. Policy 3, 123–134. https://doi.org/10.1016/S1462-9011(00)00006-X

Naeimi, V., Wagner, W., 2010. C-band Scatterometers and Their Applications, in: Imperatore, P., Riccio, D. (Eds.), Geoscience and Remote Sensing New Achievements. InTech. https://doi.org/10.5772/9102

Nezry, E., Lopes, A., Touzi, R., 1991. Detection of structural and textural features for SAR images filtering 2169–2172.

Nguyen, T.T.H., De Bie, C.A.J.M., Ali, A., Smaling, E.M.A., Chu, T.H., 2012. Mapping the irrigated rice cropping patterns of the Mekong delta, Vietnam, through hyper-temporal SPOT NDVI image analysis. Int. J. Remote Sens. 33, 415–434. https://doi.org/10.1080/01431161.2010.532826

Olesk, A., Voormansik, K., Põhjala, M., Noorma, M., 2015. Forest change detection from Sentinel-1 and ALOS-2 satellite images, in: 2015 IEEE 5th Asia-Pacific Conference on Synthetic Aperture Radar (APSAR). Presented at the 2015 IEEE 5th Asia-Pacific Conference on Synthetic Aperture Radar (APSAR), pp. 522–527. https://doi.org/10.1109/APSAR.2015.7306263

Onishi, M., Ise, T., 2018. Automatic classification of trees using a UAV onboard camera and deep learning. ArXiv180410390 Cs Stat.

Pal, M., Mather, P.M., 2005. Support vector machines for classification in remote sensing. Int. J. Remote Sens. 26, 1007–1011. https://doi.org/10.1080/01431160512331314083

Pantze, A., Fransson, J.E.S., Santoro, M., 2010. Forest change detection from L-band satellite SAR images using iterative histogram matching and thresholding together with data fusion. IEEE, pp. 1226–1229. https://doi.org/10.1109/IGARSS.2010.5650677

Pantze, A., Santoro, M., Fransson, J.E.S., 2014. Change detection of boreal forest using bi-temporal ALOS PALSAR backscatter data. Remote Sens. Environ. 155, 120–128. https://doi.org/10.1016/j.rse.2013.08.050

Pardini, M., Torano Caicoya, A., Kugler, F., Lee, S.-K., Hajnsek, I., Papathanassiou, K., 2012. On the estimation of forest vertical structure from multibaseline polarimetric SAR data, in: Geoscience and Remote Sensing Symposium (IGARSS), 2012 IEEE International. Presented at the Geoscience and Remote Sensing Symposium (IGARSS), 2012 IEEE International, pp. 3443–3446. https://doi.org/10.1109/IGARSS.2012.6350680

Park, S.-E., Moon, W.M., Pottier, E., 2012. Assessment of Scattering Mechanism of Polarimetric SAR Signal From Mountainous Forest Areas. IEEE Trans. Geosci. Remote Sens. 50, 4711–4719. https://doi.org/10.1109/TGRS.2012.2194153

Patel, P., Srivastava, H.S., Panigrahy, S., Parihar, J.S., 2006. Comparative evaluation of the sensitivity of multi-polarized multi-frequency SAR backscatter to plant density. Int. J. Remote Sens. 27, 293–305. https://doi.org/10.1080/01431160500214050

Pekkarinen, A., Reithmaier, L., Strobl, P., 2009. Pan-European forest/non-forest mapping with Landsat ETM+ and CORINE Land Cover 2000 data. ISPRS J. Photogramm. Remote Sens. 64, 171–183. https://doi.org/10.1016/j.isprsjprs.2008.09.004

Peng, X., Wang, J., Zhang, Q., 2005. Deriving terrain and textural information from stereo RADARSAT data for mountainous land cover mapping. Int. J. Remote Sens. 26, 5029–5049. https://doi.org/10.1080/01431160500180699

Persson, M., Lindberg, E., Reese, H., 2018. Tree Species Classification with Multi-Temporal Sentinel-2 Data. Remote Sens. 10, 1794. https://doi.org/10.3390/rs10111794

Philippe, C., Sabine, C., Bala, G., Bopp, L., Brovkin, V., Canadell, J., Chhabra, A., DeFries, R., Galloway, J., Heimann, M., Jones, C., Le Quéré, C., Myneni, R., Piao, S., Thornton, P., 2013. Carbon and Other Biogeochemical Cycles: In:Climate Change 2013: The Physical Science Basis. Contribution of Working Group I to the Fifth Assessment Report of the Intergovernmental Panel on Climate Change. Cambridge University Press, Cambridge, UK, New York, USA.

Pierce, L., Liang, P., Dobson, M.C., 2003. Texture Estimation in SAR Images of Forests. Presented at the International Geoscience and Remote Sensing Symposium (IGARSS), pp. 4010–4012.

Pierce, L.E., Bergen, K.M., Dobson, M.C., Ulaby, F.T., 1998. Multitemporal Land-Cover Classification Using SIR-C/X-SAR Imagery. Remote Sens. Environ. 64, 20–33. https://doi.org/10.1016/S0034-4257(97)00165-X

Poulain, V., Inglada, J., Spigai, M., Tourneret, J.-Y., Marthon, P., 2011. High-Resolution Optical and SAR Image Fusion for Building Database Updating. IEEE Trans. Geosci. Remote Sens. 49, 2900–2910. https://doi.org/10.1109/TGRS.2011.2113351

Pourshamsi, M., Garcia, M., Lavalle, M., Balzter, H., 2018. A Machine-Learning Approach to PolInSAR and LiDAR Data Fusion for Improved Tropical Forest Canopy Height Estimation Using NASA AfriSAR Campaign Data. IEEE J. Sel. Top. Appl. Earth Obs. Remote Sens. 11, 3453–3463. https://doi.org/10.1109/JSTARS.2018.2868119

Qiu, F., Berglund, J., Jensen, J.R., Thakkar, P., Ren, D., 2004. Speckle Noise Reduction in SAR Imagery Using a Local Adaptive Median Filter. GIScience Remote Sens. 41, 244–266. https://doi.org/10.2747/1548-1603.41.3.244

Quegan, S., Le Toan, T., Skriver, H., Gomez-Dans, J., 2003. Crop classification with multi temporal polarimetric SAR data, in: Applications of SAR Polarimetry and Polarimetric Interferometry.

Quegan, S., Toan, T.L., Yu, J.J., Ribbes, F., Floury, N., 2000. Multitemporal ERS SAR analysis applied to forest mapping. IEEE Trans. Geosci. Remote Sens. 38, 741–753. https://doi.org/10.1109/36.842003

Rahman, M.T., 2016. LAND USE AND LAND COVER CHANGES AND URBAN SPRAWL IN RIYADH, SAUDI ARABIA: AN ANALYSIS USING MULTI-TEMPORAL LANDSAT DATA AND SHANNON'S ENTROPY INDEX. ISPRS - Int. Arch. Photogramm. Remote Sens. Spat. Inf. Sci. XLI-B8, 1017–1021. https://doi.org/10.5194/isprs-archives-XLI-B8-1017-2016

Ramze Rezaee, M., Lelieveldt, B.P.F., Reiber, J.H.C., 1998. A new cluster validity index for the fuzzy c-mean. Pattern Recognit. Lett. 19, 237–246. https://doi.org/10.1016/S0167-8655(97)00168-2

Rauste, Y., 1990. Incidence-angle dependence in forested and non-forested areas in Seasat SAR data. Int. J. Remote Sens. 11, 1267–1276. https://doi.org/10.1080/01431169008955092

Reiche, J., Hamunyela, E., Verbesselt, J., Hoekman, D., Herold, M., 2018. Improving near-real time deforestation monitoring in tropical dry forests by combining dense Sentinel-1 time series with Landsat and ALOS-2 PALSAR-2. Remote Sens. Environ. 204, 147–161. https://doi.org/10.1016/j.rse.2017.10.034

Reis, M.S., Sant'Anna, S.J.S., Pantaleão, E., 2017. Change detection using polarimetric L band synthetic aperture radar data, in: 2017 IEEE International Geoscience and Remote Sensing Symposium (IGARSS). Presented at the 2017 IEEE International Geoscience and Remote Sensing Symposium (IGARSS), pp. 5354–5357. https://doi.org/10.1109/IGARSS.2017.8128213

Rignot, E., Chellappa, R., Dubois, P., 1992. Unsupervised segmentation of polarimetric SAR data using the covariance matrix. IEEE Trans. Geosci. Remote Sens. 30, 697–705. https://doi.org/10.1109/36.158863

Rignot, E.J.M., van Zyl, J.J., 1993. Change detection techniques for ERS-1 SAR data. IEEE Trans. Geosci. Remote Sens. 31, 896–906. https://doi.org/10.1109/36.239913

Rignot, E.J.M., Williams, C.L., Way, J., Viereck, L.A., 1994. Mapping of forest types in Alaskan boreal forests using SAR imagery. IEEE Trans. Geosci. Remote Sens. 32, 1051–1059. https://doi.org/10.1109/36.312893

Rodríguez-Galiano, V.F., Abarca-Hernández, F., Ghimire, B., Chica-Olmo, M., Atkinson, P.M., Jeganathan, C., 2011. Incorporating Spatial Variability Measures in Land-cover Classification using Random Forest. Procedia Environ. Sci., 1st Conference on Spatial Statistics 2011 – Mapping Global Change 3, 44–49. https://doi.org/10.1016/j.proenv.2011.02.009

Rodriguez-Galiano, V.F., Ghimire, B., Rogan, J., Chica-Olmo, M., Rigol-Sanchez, J.P., 2012. An assessment of the effectiveness of a random forest classifier for land-cover classification. ISPRS J. Photogramm. Remote Sens. 67, 93–104. https://doi.org/10.1016/j.isprsjprs.2011.11.002

Rosenqvist, A., Shimada, M., Chapman, B., Freeman, A., Grandi, G.D., Saatchi, S., Rauste, Y., 2000. The Global Rain Forest Mapping project - A review. Int. J. Remote Sens. 21, 1375–1387. https://doi.org/10.1080/014311600210227

Rosenqvist, A., Shimada, M., Chapman, B., McDonald, K., Grandi, G.D., Jonsson, H., Williams, C., Rauste, Y., Nilsson, M., Sango, D., Matsumoto, M., 2004. An overview of the JERS-1 SAR Global Boreal Forest Mapping (GBFM) project, in: IGARSS 2004. 2004 IEEE International

Geoscience and Remote Sensing Symposium. Presented at the IGARSS 2004. 2004 IEEE International Geoscience and Remote Sensing Symposium, pp. 1033–1036 vol.2. https://doi.org/10.1109/IGARSS.2004.1368587

Rosenqvist, A., Shimada, M., Ito, N., Watanabe, M., 2007. ALOS PALSAR: A Pathfinder Mission for Global-Scale Monitoring of the Environment. IEEE Trans. Geosci. Remote Sens. 45, 3307–3316. https://doi.org/10.1109/TGRS.2007.901027

Rosenqvist, A., Shimada, M., Suzuki, S., Ohgushi, F., Tadono, T., Watanabe, M., Tsuzuku, K., Watanabe, T., Kamijo, S., Aoki, E., 2014. Operational performance of the ALOS global systematic acquisition strategy and observation plans for ALOS-2 PALSAR-2. Remote Sens. Environ. 155, 3–12. https://doi.org/10.1016/j.rse.2014.04.011

Ryan, C.M., Hill, T., Woollen, E., Ghee, C., Mitchard, E., Cassells, G., Grace, J., Woodhouse, I.H., Williams, M., 2012. Quantifying small-scale deforestation and forest degradation in African woodlands using radar imagery. Glob. Change Biol. 18, 243–257. https://doi.org/10.1111/j.1365-2486.2011.02551.x

Saatchi, S.S., Rignot, E., 1997. Classification of boreal forest cover types using SAR images. Remote Sens. Environ. 60, 270–281. https://doi.org/10.1016/S0034-4257(96)00181-2

Saatchi, S.S., Soares, J.V., Alves, D.S., 1997. Mapping deforestation and land use in amazon rainforest by using SIR-C imagery. Remote Sens. Environ. 59, 191–202. https://doi.org/10.1016/S0034-4257(96)00153-8

Santoro, M., Fransson, J.E.S., Eriksson, L.E.B., Ulander, L.M.H., 2010. Clear-Cut Detection in Swedish Boreal Forest Using Multi-Temporal ALOS PALSAR Backscatter Data. IEEE J. Sel. Top. Appl. Earth Obs. Remote Sens. 3, 618–631. https://doi.org/10.1109/JSTARS.2010.2048201

Santoro, M., Pantze, A., Fransson, J.E.S., Dahlgren, J., Persson, A., 2012. Nation-Wide Clear-Cut Mapping in Sweden Using ALOS PALSAR Strip Images. Remote Sens. 4, 1693–1715. https://doi.org/10.3390/rs4061693

Sarmap, 2009. Synthetic Aperture Radar and SARscape - Tutorial.

Schlund, M., von Poncet, F., Hoekman, D.H., Kuntz, S., Schmullius, C., 2013. Importance of bistatic SAR features from TanDEM-X for forest mapping and monitoring. Remote Sens. Environ. https://doi.org/10.1016/j.rse.2013.08.024

Schlund, M., von Poncet, F., Kuntz, S., Schmullius, C., Hoekman, D.H., 2015. TanDEM-X data for aboveground biomass retrieval in a tropical peat swamp forest. Remote Sens. Environ. 158, 255–266. https://doi.org/10.1016/j.rse.2014.11.016

Schmitt, A., Wessel, B., Roth, A., 2010. Curvelet-based Change Detection on SAR Images for Natural Disaster Mapping. Photogramm. - Fernerkund. - Geoinformation 2010, 463–474. https://doi.org/10.1127/1432-8364/2010/0068

SÉAMUS, W., 2012. A Summary of Climate Averages 1981-2010 for Ireland (Climatological Note No. 14). MET ÉIREANN.

Sedano, F., Kempeneers, P., Strobl, P., McInerney, D., San Miguel, J., 2012. Increasing Spatial Detail of Burned Scar Maps Using IRS-AWiFS Data for Mediterranean Europe. Remote Sens. 4, 726–744. https://doi.org/10.3390/rs4030726

Sgrenzaroli, M., De Grandi, G.F., Eva, H., Achard, F., 2002. Tropical forest cover monitoring: Estimates from the GRFM JERS-1 radar mosaics using wavelet zooming techniques and validation. Int. J. Remote Sens. 23, 1329–1355. https://doi.org/10.1080/01431160110092920

Shang, R., Qi, L., Jiao, L., Stolkin, R., Li, Y., 2014. Change detection in SAR images by artificial immune multi-objective clustering. Eng. Appl. Artif. Intell. 31, 53–67. https://doi.org/10.1016/j.engappai.2014.02.004

Shanmugan, K.S., Narayanan, V., Frost, V.S., Stiles, J.A., Holtzman, J., 1981. Textural Features for Radar Image Analysis. IEEE Trans. Geosci. Remote Sens. GE-19, 153–156. https://doi.org/10.1109/TGRS.1981.350344

Shimada, M., Isoguchi, O., 2002. JERS-1 SAR mosaics of Southeast Asia using calibrated path images. Int. J. Remote Sens. 23, 1507–1526. https://doi.org/10.1080/01431160110092678

Shimada, M., Itoh, T., Motooka, T., Watanabe, M., Shiraishi, T., Thapa, R., Lucas, R., 2014a. New global forest/non-forest maps from ALOS PALSAR data (2007–2010). Remote Sens. Environ. 155, 13–31. https://doi.org/10.1016/j.rse.2014.04.014

Shimada, M., Itoh, T., Motooka, T., Watanabe, M., Shiraishi, T., Thapa, R., Lucas, R., 2014b. New global forest/non-forest maps from ALOS PALSAR data (2007–2010). Remote Sens. Environ. 155, 13–31. https://doi.org/10.1016/j.rse.2014.04.014

Shrestha, D.P., Zinck, J.A., 2001. Land use classification in mountainous areas: integration of image processing, digital elevation data and field knowledge (application to Nepal). Int. J. Appl. Earth Obs. Geoinformation 3, 78–85. https://doi.org/10.1016/S0303-2434(01)85024-8

Sidorova, V.S., 2012. Hierarchical cluster algorithm for remote sensing data of earth. Pattern Recognit. Image Anal. 22, 373–379. https://doi.org/10.1134/S1054661812020149

Simard, M., Saatchi, S.S., De Grandi, G., 2000. The use of decision tree and multiscale texture for classification of JERS-1 SAR data over tropical forest. IEEE Trans. Geosci. Remote Sens. 38, 2310–2321. https://doi.org/10.1109/36.868888

Singh, A., 1989. Review Article Digital change detection techniques using remotely-sensed data. Int. J. Remote Sens. 10, 989–1003. https://doi.org/10.1080/01431168908903939

Soh, L.-K., Tsatsoulis, C., 1999. Texture analysis of SAR sea ice imagery using gray level co-occurrence matrices. IEEE Trans. Geosci. Remote Sens. 37, 780–795. https://doi.org/10.1109/36.752194

Solomon, S, Qin, D., Manning, M., Chen, Z., Marquis, M., Averyt, K., B., Tignor, M., Miller, H.L., 2007. Contribution of working group I to the fourth assessment report of the intergovernmental panel on climate change. Cambridge, UK, New York, USA:Cambridge University Press.

Solomon, Susan, Quin, D., Manning, M., Zhenlin, C., Marquis, M., Averyt, K., Tignor, M., Miller, H.L. (Eds.), 2007. IPCC 2007:Climate change 2007: the physical science basis: contribution of Working Group I to the Fourth Assessment Report of the Intergovernmental Panel on Climate Change. Cambridge University Press, Cambridge ; New York.

Strobl, C., Boulesteix, A.-L., Zeileis, A., Hothorn, T., 2007. Bias in random forest variable importance measures: Illustrations, sources and a solution. BMC Bioinformatics 8, 25. https://doi.org/10.1186/1471-2105-8-25

Suga, Y., Takeuchi, S., 2000. Application of JERS-1 InSAR for monitoring deforestation of tropical rain forest, in: IGARSS 2000. IEEE 2000 International Geoscience and Remote Sensing Symposium. Taking the Pulse of the Planet: The Role of Remote Sensing in Managing the Environment. Proceedings (Cat. No.00CH37120). Presented at the IGARSS 2000. IEEE 2000 International Geoscience and Remote Sensing Symposium. Taking the Pulse of the Planet: The Role of Remote Sensing in Managing the Environment, IEEE, Honolulu, HI, USA, pp. 432–434. https://doi.org/10.1109/IGARSS.2000.860555

Swain, P.H., King, R.C., 1973. Two effective feature selection criteria for multispectral remote sensing, in: Proceedings of the 1st International Joint Conference on Pattern Recognition. Presented at the IEEE 73 CHO821-9 C, pp. 536–540.

Swain, Philip.H., 1973. Pattern Recognition: A Basis for Remote Sensing Data Analysis. ResearchGate.

Tanase, M.A., Aponte, C., Mermoz, S., Bouvet, A., Le Toan, T., Heurich, M., 2018. Detection of windthrows and insect outbreaks by L-band SAR: A case study in the Bavarian Forest National Park. Remote Sens. Environ. 209, 700–711. https://doi.org/10.1016/j.rse.2018.03.009

Tanase, M.A., Ismail, I., Lowell, K., Karyanto, O., Santoro, M., 2015. Detecting and Quantifying Forest Change: The Potential of Existing C- and X-Band Radar Datasets. PLOS ONE 10, e0131079. https://doi.org/10.1371/journal.pone.0131079

Teagasc, 2020. PastureBase Ireland - Teagasc | Agriculture and Food Development Authority [WWW Document]. URL https://www.teagasc.ie/crops/grassland/pasturebase-ireland/ (accessed 7.1.20).

Tempfli, K., Huurneman, G.C., Bakker, W.H., Janssen, L.L.F., Feringa, W.F., Gieske, A.S.M., Grabmaier, K.A., Hecker, C.A., Horn, J.A. van der, 2009. Principles of remote sensing: an introductory textbook. ITC, Enschede.

Tewkesbury, A., Comber, A., Tate, N., Lamb, A., Fisher, P., 2015. A critical synthesis of remotely sensed optical image change detection techniques. Remote Sens. Environ. 160. https://doi.org/10.1016/j.rse.2015.01.006

THÉAU, J., 2007. Change Detection Encyclopedia. GIS Training and Research Center, USA.

Tomppo, E., Antropov, O., Praks, J., 2019. Boreal Forest Snow Damage Mapping Using Multi-Temporal Sentinel-1 Data. Remote Sens. 11, 384. https://doi.org/10.3390/rs11040384

Toraño Caicoya, A., Kugler, F., Hajnsek, I., Papathanassiou, K.P., 2016. Large-Scale Biomass Classification in Boreal Forests With TanDEM-X Data. IEEE Trans. Geosci. Remote Sens. 54, 5935–5951. https://doi.org/10.1109/TGRS.2016.2575542

Trisasongko, B.H., 2015a. Evaluating compact SAR polarimetry for tropical forest monitoring, in: Nasution, A. (Ed.), . Presented at the International Seminar on Photonics, Optics, and Applications 2014, Sanur, Bali, Indonesia, p. 94440B. https://doi.org/10.1117/12.2075177

Trisasongko, B.H., 2015b. Evaluating compact SAR polarimetry for tropical forest monitoring. pp. 94440B-94440B–5. https://doi.org/10.1117/12.2075177

Trisasongko, B.H., 2010. The Use of Polarimetric SAR Data for Forest Disturbance Monitoring. Sens. Imaging Int. J. 11, 1–13. https://doi.org/10.1007/s11220-010-0048-8

Trisasongko, B.H., Panuju, D.R., Paull, D.J., Jia, X., Griffin, A.L., 2017. Comparing six pixel-wise classifiers for tropical rural land cover mapping using four forms of fully polarimetric SAR data. Int. J. Remote Sens. 38, 3274–3293. https://doi.org/10.1080/01431161.2017.1292072

Trisasongko, B.H., Trisasongko, B.H., Panuju, D.R., 2010. Performance of Wishart Classification Algorithm to Map Mangrove Forest Using Fully Polarimetric Synthetic Aperture Radar at C-, L- and P-bands. Int. J. Electr. Eng. Inform. 4, 474--482.

Turkar, V., Deo, R., Rao, Y.S., Mohan, S., Das, A., 2012. Classification Accuracy of Multi-Frequency and Multi-Polarization SAR Images for Various Land Covers. IEEE J. Sel. Top. Appl. Earth Obs. Remote Sens. 5, 936–941. https://doi.org/10.1109/JSTARS.2012.2192915

Tusa, E., Laybros, A., Monnet, J.-M., Dalla Mura, M., Barré, J.-B., Vincent, G., Dalponte, M., Féret, J.-B., Chanussot, J., 2020. Chapter 2.11 - Fusion of hyperspectral imaging and LiDAR for forest monitoring, in: Amigo, J.M. (Ed.), Data Handling in Science and Technology, Hyperspectral Imaging. Elsevier, pp. 281–303. https://doi.org/10.1016/B978-0-444-63977-6.00013-4

Ulaby, Fawwaz.T., Moore, Richard.K., Fung, Adrian.K., 1981. Microwave Remote Sensing - Active and Passive - Volume I - Microwave Remote Sensing Fundamentals and Radiometry (v. 1).

Urbazaev, M., Cremer, F., Migliavacca, M., Reichstein, M., Schmullius, C., Thiel, C., 2018. Potential of Multi-Temporal ALOS-2 PALSAR-2 ScanSAR Data for Vegetation Height Estimation in Tropical Forests of Mexico. Remote Sens. 10, 1277. https://doi.org/10.3390/rs10081277

Wagner, W., 2003. Large-scale mapping of boreal forest in SIBERIA using ERS tandem coherence and JERS backscatter data. Remote Sens. Environ. 85, 125–144. https://doi.org/10.1016/S0034-4257(02)00198-0

Wagner, W., Luckman, A., Vietmeier, J., Tansey, K., Balzter, H., Schmullius, C., Davidson, M., Gaveau, D., Gluck, M., Le Toan, T., Quegan, S., Shvidenko, A., Wiesmann, A., Yu, J.J., 2003. Large-scale mapping of boreal forest in SIBERIA using ERS tandem coherence and JERS backscatter data. Remote Sens. Environ. 85, 125–144. https://doi.org/10.1016/S0034-4257(02)00198-0

Walker, Wayne S., Stickler, C.M., Kellndorfer, J.M., Kirsch, K.M., Nepstad, D.C., 2010. Large-Area Classification and Mapping of Forest and Land Cover in the Brazilian Amazon: A Comparative Analysis of ALOS/PALSAR and Landsat Data Sources. IEEE J. Sel. Top. Appl. Earth Obs. Remote Sens. 3, 594–604. https://doi.org/10.1109/JSTARS.2010.2076398

Walker, W. S., Stickler, C.M., Kellndorfer, J.M., Kirsch, K.M., Nepstad, D.C., 2010. Large-Area Classification and Mapping of Forest and Land Cover in the Brazilian Amazon: A Comparative Analysis of ALOS/PALSAR and Landsat Data Sources. IEEE J. Sel. Top. Appl. Earth Obs. Remote Sens. 3, 594–604. https://doi.org/10.1109/JSTARS.2010.2076398

Wang, H., Xue, X., 2014. Classification of Regional Land Cover in ALOS PALSAR's FBD Data Based on Support Vector Machines. J. Chem. Pharm. Res. 6, 443–447.

Wang, H., Zhao, Y., Pu, R., Zhang, Z., 2015. Mapping Robinia Pseudoacacia Forest Health Conditions by Using Combined Spectral, Spatial, and Textural Information Extracted from IKONOS Imagery and Random Forest Classifier. Remote Sens. 7, 9020–9044. https://doi.org/10.3390/rs70709020

Wang, L., Sousa, W.P., Gong, P., 2004. Integration of object-based and pixel-based classification for mapping mangroves with IKONOS imagery. Int. J. Remote Sens. 25, 5655–5668. https://doi.org/10.1080/014311602331291215

Wang, W., Zhang, Y., 2007. On fuzzy cluster validity indices. Fuzzy Sets Syst. 158, 2095–2117. https://doi.org/10.1016/j.fss.2007.03.004

Wang, X., Ge, L., Li, X., 2012. EVALUATION OF FILTERS FOR ENVISAT ASAR SPECKLE SUPPRESSION IN PASTURE AREA. ISPRS Ann. Photogramm. Remote Sens. Spat. Inf. Sci. I–7, 341–346. https://doi.org/10.5194/isprsannals-I-7-341-2012

Warner, T.A., Foody, G.M., Nellis, M.D., 2009. The SAGE Handbook of Remote Sensing. SAGE Publications.

Waske, B., Braun, M., 2009. Classifier ensembles for land cover mapping using multitemporal SAR imagery. ISPRS J. Photogramm. Remote Sens., Theme Issue: Mapping with SAR: Techniques and Applications 64, 450–457. https://doi.org/10.1016/j.isprsjprs.2009.01.003

Watanabe, M., Koyama, C.N., Hayashi, M., Nagatani, I., Shimada, M., 2018. Early-Stage Deforestation Detection in the Tropics With L-band SAR. IEEE J. Sel. Top. Appl. Earth Obs. Remote Sens. 11, 2127–2133. https://doi.org/10.1109/JSTARS.2018.2810857

Weaver, A.J., Zickfeld, K., Montenegro, A., Eby, M., 2007. Long term climate implications of 2050 emission reduction targets. Geophys. Res. Lett. 34, L19703. https://doi.org/10.1029/2007GL031018

Wen, C., Zhang, Y., Deng, K., 2009. Urban Area Classification in High Resolution SAR based on texture Features, in: 50th Anniversary of the Chinese Academy of Surveying and Mapping. Presented at the International Conference on Geo-Spatial Solutions for Emergency Management.

Wheeler, J., Rodriguez-Veiga, P., Balzter, H., Tansey, K., Tate, N.J., 2017. Forest Mapping of the Congo Basin using Synthetic Aperture Radar (SAR), in: Balzter, H. (Ed.), Earth Observation for Land and Emergency Monitoring. John Wiley & Sons, Ltd, Chichester, UK, pp. 57–74. https://doi.org/10.1002/9781118793787.ch4

Wiemker, R., 1997. An iterative spectral-spatial Bayesian labeling approach for unsupervised robust change detection on remotely sensed multispectral imagery, in: Sommer, G., Daniilidis, K., Pauli, J. (Eds.), Computer Analysis of Images and Patterns. Springer Berlin Heidelberg, Berlin, Heidelberg, pp. 263–270. https://doi.org/10.1007/3-540-63460-6_126

Wijaya, A., Marpu, P.R., Gloaguen, R., 2010. Discrimination of peatlands in tropical swamp forests using dual-polarimetric SAR and Landsat ETM data. Int. J. Image Data Fusion 1, 257–270. https://doi.org/10.1080/19479832.2010.495323

Wilkinson, G.G., Folving, S., Kanellopoulos, I., McCormick, N., Fullerton, K., Mégier, J., 1995. Forest mapping from multi-source satellite data using neural network classifiers—an experiment in Portugal. Remote Sens. Rev. 12, 83–106. https://doi.org/10.1080/02757259509532277

Woodhouse, I.H., 2005. Introduction to Microwave Remote Sensing. CRC Press.

Wulder, M., 1998. Optical remote-sensing techniques for the assessment of forest inventory and biophysical parameters. Prog. Phys. Geogr. Earth Environ. 22, 449–476. https://doi.org/10.1177/030913339802200402

Wulder, M.A., White, J.C., Nelson, R.F., Næsset, E., Ørka, H.O., Coops, N.C., Hilker, T., Bater, C.W., Gobakken, T., 2012. Lidar sampling for large-area forest characterization: A review. Remote Sens. Environ. 121, 196–209. https://doi.org/10.1016/j.rse.2012.02.001

Xiao, J., Li, J., Moody, A., 2003. A detail-preserving and flexible adaptive filter for speckle suppression in SAR imagery. Int. J. Remote Sens. 24, 2451–2465. https://doi.org/10.1080/01431160210154885

Yousif, O., Ban, Y., 2015. Object-based urban change detection using high resolution SAR images, in: 2015 Joint Urban Remote Sensing Event (JURSE). Presented at the 2015 Joint Urban Remote Sensing Event (JURSE), IEEE, Lausanne, Switzerland, pp. 1–4. https://doi.org/10.1109/JURSE.2015.7120502

Yu, Y., Saatchi, S., 2016. Sensitivity of L-Band SAR Backscatter to Aboveground Biomass of Global Forests. Remote Sens. 8, 522. https://doi.org/10.3390/rs8060522

Yun, H.-W., Kim, J.-R., Choi, Y.-S., Lin, S.-Y., 2019. Analyses of Time Series InSAR Signatures for Land Cover Classification: Case Studies over Dense Forestry Areas with L-Band SAR Images. Sensors 19, 2830. https://doi.org/10.3390/s19122830

Zebker, H.A., Villasenor, J., 1992. Decorrelation in interferometric radar echoes. IEEE Trans. Geosci. Remote Sens. 30, 950–959. https://doi.org/10.1109/36.175330

Zhang, A., Yang, X., Jia, L., Ai, J., Dong, Z., 2019. SAR image classification using adaptive neighborhood-based convolutional neural network. Eur. J. Remote Sens. 52, 178–193. https://doi.org/10.1080/22797254.2019.1579616

Zhang, W., Hu, B., Woods, M., Brown, G., 2017. Characterizing Forest Succession Stages for Wildlife Habitat Assessment Using Multispectral Airborne Imagery. Forests 8, 234. https://doi.org/10.3390/f8070234

Zhou, X., Chang, N.-B., Li, S., 2009. Applications of SAR Interferometry in Earth and Environmental Science Research. Sensors 9, 1876–1912. https://doi.org/10.3390/s90301876

Zhuang, H., Fan, H., Deng, K., Yao, G., 2018a. A Spatial-Temporal Adaptive Neighborhood-Based Ratio Approach for Change Detection in SAR Images. Remote Sens. 10, 1295. https://doi.org/10.3390/rs10081295

Zhuang, H., Fan, H., Deng, K., Yu, Y., 2018b. An improved neighborhood-based ratio approach for change detection in SAR images. Eur. J. Remote Sens. 51, 723–738. https://doi.org/10.1080/22797254.2018.1482523

Zhuang, H., Tan, Z., Deng, K., Fan, H., 2019. It is a misunderstanding that log ratio outperforms ratio in change detection of SAR images. Eur. J. Remote Sens. 52, 484–492. https://doi.org/10.1080/22797254.2019.1653226

Appendix

ALOS PALSAR data characteristics

Date	Orbit	Track	Frame
Area1			
2007-06-16	7423	4	1030
2007-06-16	7423	4	1040
2008-05-03	12120	4	1030
2008-05-03	12120	4	1040
2009-06-21	18159	4	1030
2009-06-21	18159	4	1040
2010-06-24	23527	4	1030
2010-06-24	23527	4	1040
Area2			
2007-06-11	7350	1	1080
2007-06-11	7350	1	1090
2008-06-13	12718	1	1080
2008-06-13	12718	1	1090
2009-06-16	18086	1	1080
2009-06-16	18086	1	1090
2010-06-19	23454	1	1080
2010-06-19	23454	1	1090
Area3			
2007-06-23	7525	670	1050
2007-06-23	7525	670	1060
2008-06-25	12893	670	1050
2008-06-25	12893	670	1060
2009-06-28	18261	670	1050
2009-06-28	18261	670	1060
2010-07-01	23629	670	1050
2010-07-01	23629	670	1060

ALOS-2 PALSAR-2 data characteristics

Date	Orbit accumulation number	Path
Area1		
2015-08-26	06785	1030
2015-08-26	06785	1040
2016-10-05	09062	1030
2016-10-05	09062	1040
Area2		
2015-10-02	07332	1080
2015-10-02	07332	1090
2016-10-30	12714	1080
2016-10-30	12714	1090
Area3		
2015-01-23	03606	1050
2015-01-23	03606	1060
2016-06-10	11058	1050
2016-06-10	11058	1060